Assessment of the effects of plaques and glia on synaptic transmission in *App* knock-in models of Alzheimer's disease

Karina Vitanova

UCL

Thesis submitted for the degree of
Doctor of Philosophy

September 2021

Declaration

I, Karina Vitanova, confirm that the work presented in this thesis is my own. Where information has been derived from other sources, I confirm that this has been indicated in the thesis.

Acknowledgments

First, I would like to express my sincere gratitude to my supervisor, Prof Frances Edwards, for her support during my PhD, for the great discussions about my work during my years in her lab, as well as the invaluable input and help she gave during the write-up of this thesis.

Second, I would like to thank Dr Damian Cummings for his continuous support during my PhD. Damian, your help has really been invaluable and I am very thankful for everything you have taught me, from electrophysiology to critical scientific thinking. Your support and knowledge have helped me push through this PhD and I am very happy to have found someone like you, not just a supervisor, but a friend, during my time in the Edwards lab. You were always there to help me, even if my questions were slightly silly, and I am incredibly thankful for this!

Third, I would like to thank all of the members of the Edwards lab. I have met some amazing people during my time there who have all made my time more enjoyable. I would like to specifically thank Katie and Diana for their continuous support and numerous discussions, not all of which were related to science, yet they have all made my days brighter. The friends I have found in you I know will be there for life. I would also like to thank other members, especially Jon, Jack, Mila, Tashu, Dervis, as well as the many BSc and MSc students who have passed through the Edwards lab. It has been great to meet so many interesting people during my time here.

I would like to thank Ryan for his incredible support during my PhD. It has not been the easiest of journeys, but your motivation has been an integral part of it and I am forever thankful. We all need someone to support us, and you have played that role like no one else.

Lastly, I would like to thank my friends and family whose support and love have been so important during my PhD. My family has never stopped believing in me and have helped me during my whole university journey and beyond, something I will be forever grateful for.

Abstract

Alzheimer's disease (AD) is a neurodegenerative disorder associated with the formation of extracellular amyloid plaques and intracellular neurofibrillary tangles, coupled to extensive synaptic denervation and gliosis. The role of microglia in disease progression has become a central focus for AD research with studies showing that they cluster around amyloid plaques and some indications that plaque-associated microglia phagocytose synapses in these regions. The present work aimed to explore if this is a protective mechanism to limit plaque-associated toxicity by examining the hippocampus of *App*$^{NL-F}$ and *App*$^{NL-G-F}$ using patch-clamp electrophysiology and immunohistochemistry. This work also explored *App*$^{NL-F}$/*Trem2*^{R47H} mice to determine how a compromised microglial response affects synaptic activity.

I found that *App*$^{NL-G-F}$ mice exhibit heavier plaque pathology with age and a larger number of smaller-sized plaques, similar to what I observed in *App*$^{NL-F}$/*Trem2*^{R47H} mice in comparison to *App*$^{NL-F}$ mice. *App*$^{NL-G-F}$ mice also showed increased microglial density compared to wild-types, regardless of age, and no changes in astrocyte density. In comparison, the presence of the *Trem2*^{R47H} mutation in *App*$^{NL-F}$ mice led to reduced microglial density in the SLM region, where the plaque load in these mice was the heaviest, and also reversed the increased astrocytic density which was observed in *App*$^{NL-F}$ mice.

In terms of electrophysiological changes, I found alterations in the kinetics of the postsynaptic response and changes in the failure rate in both models. Exploring electrophysiological changes in plaque-associated regions revealed that both *App*$^{NL-G-F}$ and *App*$^{NL-F}$ mice exhibit lower amplitudes in plaque compared to no-plaque conditions, while this effect was lost in *App*$^{NL-F}$/*Trem2*^{R47H} mice. Furthermore, both *App*$^{NL-F}$ and *App*$^{NL-F}$/*Trem2*^{R47H} mice showed enhanced release probability in plaque conditions. Altogether, these results illustrate the dual effects of plaque presence around axons which are driven by the effects of soluble Aβ and microglia on the presynapse and postsynapse, respectively.

Impact statement

Alzheimer's disease (AD) is the most common type of dementia which is characterised by the progressive loss of memory and cognitive impairment. Currently, one in 14 people in the UK over the age of 65 has AD, and this has exerted great pressures both on the healthcare and economics sectors, illustrating the urgent need for current research to understand the main mechanisms leading to disease development. The two main hallmarks of AD are amyloid-β (Aβ) plaques and neurofibrillary tangles, however advances in recent research have demonstrated the multifactoriality of the disease, with many synergistic processes leading to its development. In fact, synaptic denervation, which results in the loss of communication between the brain cells, and gliosis are one of the earliest hallmarks of disease pathogenesis. Understanding the interaction between these is crucial to elucidating potential treatments and preventative measures against AD development.

The work presented in this thesis directly contributes to the understanding of how the immune cells of the brain – microglia – interact with synapses and Aβ, and provides important insights into what clinical research can use as potential targets for disease detection, and also highlights their therapeutic potential. I have suggested that the microglial response at moderate stages of Aβ pathology is protective in plaque-associated regions. In particular, microglia act as important regulators of the hyperactivity induced by Aβ plaques, reducing neuronal activity to basal levels through potential phagocytosis of postsynaptic regions. Thus, although Aβ increases synaptic activity which might result in subsequent excitotoxicity, the response of microglia is hereby suggested to be protective of this hyperactivity. The role of microglia in AD has been widely researched in recent years, with many studies reaching contradictory conclusions. By using the new *App* knock-in models, as well as models with perturbed microglial response, this study was able to provide one of the first insights into the role of microglia into models which are more relevant to human disease. This will hopefully help future clinical research in the design of targeted treatments for AD.

The results in this study will be written for a publication which will thus share with the scientific community the above insights into the role of microglia in modulating synaptic activity in early AD. I have and will be presenting the work from this thesis at five different conferences and one training workshop through poster material. I was also selected to give a talk at the ARUK conference this year (2021) for which I was awarded a prize for best presentation by an early career researcher. All of these events have been integral to my development as a scientist as discussions with peers and other researchers have helped me shape and guide the work in this thesis. I have participated in several outreach events for AD research, including Soapbox Science UK (2019), as well as events held by ARUK in 2018 and 2019, all of which have helped spread awareness of current AD research with the public.

Table of contents

List of figures

Chapter 1

Chapter 2

Chapter 3

Chapter 4

Chapter 5

Chapter 6

List of tables

Chapter 1

Chapter 2

Chapter 6

Abbreviations

AD	Alzheimer's disease
AMPA	α-amino-3-hydroxy-5-methyl-4-isoxazolepropionic
AMPAR	AMPA receptors
AP	Action potential
APOE	Apolipoprotein E
APP	Amyloid precursor protein
Aβ	Amyloid-β
BAC	Bacterial artificial chormosome
BDNF	Brain-derived neurotrophic factor
CaMKII	Ca2+/calmodulin-dependent protein kinase II
CD47	Cluster of differentiation-47
CLU	Clusterin
CR1	Complement receptor 1
CR3	Complement receptor 3
CSF	Cerebrospinal fluid
CSF1R	Colony-stimulating factor 1 receptor
DAM	Disease-associated microglia
DAP12	DNAX-activation protein 12
EC	Entorhinal cortex
EGTA	Ethylene glycol-bis(β-aminoethyl ether)-N,N,N′,N′-tetraacetic acid
EOAD	Early-onset Alzheimer's disease
GAP43	Growth associated protein 43
GFAP	Glial fibrillary acidic protein
HEPES	4-(2-hydroxyethyl)-1-piperazineethanesulfonic acid
IBA1	Ionized calcium binding adaptor molecule 1
IGF-1	Insulin-like growth factor-1
IL-1β	Interleukin-1 beta
IL6	Interleukin-6
LOAD	Late-onset Alzheimer's disease
LTD	Long term depression
LTP	Long-term potentiation
MAP	Mitogen-activated protein
MCI	Mild cognitive impairment
mEPSC	Miniature excitatory postsynaptic current
MRI	Magnetic resonance imaging

NFkB	Nuclear factor k-light-chain-enhancer of activated B cells
NFTs	Neurofibrillary tangles
NMDA	N-methyl-D-aspartate
NMDAR	NMDA receptors
NRGN	Neurogranin
oAβ	Oligomeric Aβ
OHSC	Organotypic hippocampal slice cultures
PDGF-β	Platelet-derived growth factor-β
PI3K	Phosphatidylinositol 3-kinase
PIP2	Phosphatidylinositol-4,5-biphosphate
PIP3	Phosphatidylinositol-3,4,5-triphosphate
PLCG2	1-phosphatidylinositol 4,5-bisphosphate phosphodiesterase gamma-2
PPD	Paired-pulse depression
PPF	Paired-pulse facilitation
PSD95	Postsynaptic density protein-95
PSEN-1	Presenilin 1
PSEN-2	Presenilin 2
PV	Parvalbumin
sEPSCs	Spontaneous excitatory postsynaptic currents
Siglec-3	Siglec-3
sIPSCs	Spontaneous inhibitory postsynaptic currents
SLM	Stratum lacunosum moleculare
SNAP25	Synaptosomal associated protein
SR	Stratum radiatum
STX1B	Syntaxin-1B
TGFβ	Transforming growth factor-beta
TLR	Toll-like receptor
TNFα	Tumour necrosis factor alpha
TREM2	Triggering receptor expressed on myeloid cells 2
TSPO	18-kDa translocator
VAMP1	Vesicle-associated membrane protein-1, Vesicle-associated membrane protein-1
VLUT2	Vesicular glutamate transporter-2
YKL-40	Chitinase 3-like 1
α7nAChRs	α7 nicotinic acetylcholine receptors

Chapter 1: Literature Review

Dementias are multisystem neurodegenerative disorders that can be influenced by both genetic and environmental factors. They have been shown to have profound effects on both the physiology and psychology of individuals and because of their multifaceted effects, they have exerted great emotional pressures on caregivers and patients, as well as economic pressures on health sectors when dealing with these diseases. Currently, there are over 50 million cases of dementia worldwide, with more than 850,000 individuals in the UK diagnosed with dementia (Alzheimer's Society, 2019). Globally, it is expected that 10 million cases will arise every year, reaching more than 150 million cases by the year 2050 (Patterson, 2018). The high prevalence of these diseases highlights the urgency for research to understand the underlying mechanisms leading to disease development, as well as to develop appropriate tools for disease diagnosis, as together these can help find a way to slow down or ultimately halt and even reverse disease progression.

1.1 Alzheimer's disease

Alzheimer's Disease (AD) is the most common type of dementia, contributing to between 60 and 70% of all dementia cases. Clinically, AD is initially characterised by a progressive cognitive decline known as mild cognitive impairment (MCI), with around 10-15% of people exhibiting MCI progressing to develop AD every year (Farias et al., 2009; Varatharajah et al., 2019). With AD development, patients begin to exhibit accelerated cognitive decline, changes in mood and behaviour, and memory impairment, coupled to extensive neuronal and synaptic denervation in the cortex and the hippocampus (Mattson, 2004; Rogan and Lippa, 2002). Despite increasing efforts and advances in current research to understand the pathology of this disease, as well as improve its diagnosis, currently there are no successful treatments for AD.

The majority of AD cases occur after the age of 65 and constitute late-onset AD (LOAD). However, there exists a small subset of AD cases (2-5%) which is primarily early onset (EOAD), occurring between the ages of 45-60 (Campion et al., 1999), and, in most cases, results from inherited autosomal mutations (Mattson, 2004). The pathology of these two types of AD is characterised by the accumulation of

extracellular senile plaques made up of the amyloid-β (Aβ) peptide and intracellular neurofibrillary tangles (NFTs) made up of hyperphosphorylated tau. In addition to these two hallmarks, neuronal and synapse loss, as well as gliosis are all characteristic of AD pathology (see Figure 1.1) (Hyman et al., 2012; Jack et al., 2013). The accumulation of Aβ plaques has been demonstrated to occur around 20 years prior to the detection of the first clinical symptoms, illustrating a large period of time during which the disease goes undetected. This has led to the idea that Aβ accumulation and plaque formation are the driving factors for disease progression (Long and Holtzman, 2019). In accordance with this, several studies have demonstrated that mutations in genes which are involved in the regulation of Aβ production and clearance, and specifically, that amyloid precursor protein (APP), from which Aβ is produced, and presenilins-1 (PSEN-1) and -2 (PSEN-2), which are involved in the cleavage of APP, play a central role in disease pathogenesis in EOAD cases (Berezovska et al., 2005; Jonsson et al., 2012; Scheuner et al., 1996; Verheijen and Sleegers, 2018). The discovery of these three genes has allowed for early AD research to shed light on the underlying mechanisms leading to disease development. However, given that the majority of AD cases are late onset in nature and that there are no specific mutations associated with disease development, although the findings from these studies are useful, they cannot be generalised to all cases, prompting research to explore specific factors which might increase the risk of developing the disease.

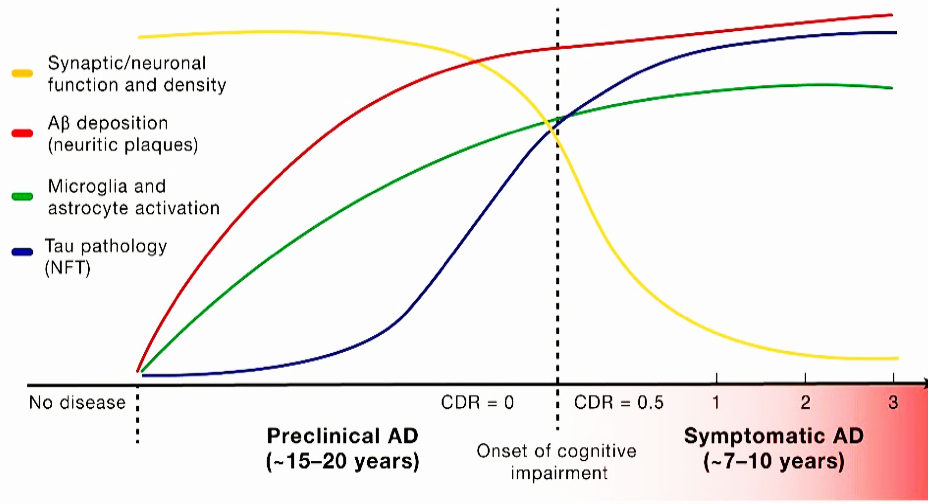

Figure 1.1. Timeline of the progression of Alzheimer's disease pathology.
The earliest pathophysiological event occurring in AD is Aβ plaque deposition. Concurrently, neuroinflammation begins in the brain, which is mediated by the activation of microglia and astrocytes. As a result, NFT pathology begins to spread which is accompanied by synaptic dysfunction, denervation, and neurodegeneration. Together these then trigger the onset of cognitive impairment, at which point detectable symptoms begin to emerge. Cognitive impairment is found to correlate well with tau accumulation and but not amyloid deposition (taken from Long and Holtzman (2019)).

In contrast to EOAD cases, the more common type of AD – LOAD – is primarily not genetically predetermined and is therefore termed sporadic (although it is largely explained by the involvement of genetic factors), with Aβ accumulation in these cases suggested to be caused by a mixture of environmental and genetic factors. Ageing has been highlighted as the biggest risk factor of AD (Guerreiro and Bras, 2015), although other environmental factors, including obesity, diabetes, depression, and cognitive inactivity have all been linked to AD (Barnes and Yaffe, 2011; Killin et al., 2016; Norton et al., 2014). Furthermore, several GWAS (genome-wide association studies) have demonstrated a number of genes which can increase the risk of developing AD, albeit not directly causing its occurrence (Karch et al., 2014; Lambert et al., 2013). Similarly to in EOAD, there are several indications of the role of Aβ in the sporadic form of AD. In particular, apolipoprotein E (APOE), a protein involved in lipid transport and maintenance of neuronal growth and repair, has been identified as one of the strongest risk factors for LOAD (Corder et al., 1993; Sanan et al., 1994; Sassi et al., 2016). APOE has three variants in humans – APOEε2, APOEε3, and APOEε4. While most people carry two copies of APOEε3, those carrying the ε4 variant exhibit increased risk of developing AD, possibly due to the high binding affinity of APOEε4

to Aβ which could in turn preclude Aβ clearance, from its role in promoting Aβ deposition into plaques, or through its effects on synaptic function (Huang et al., 2017; Lin et al., 2018; Liu et al., 2013; Selkoe, 2002). On the other hand, the ε2 variant reduces the risk of developing AD (Reiman et al., 2020), illustrating that understanding the pathway in which APOE is involved in is key for elucidating the disease mechanisms in AD. Furthermore, mutations in a number of genes, such as *TREM2* (triggering receptor expressed on myeloid cells 2), *CD33* (or Siglec-3), *PLCG2* (1-phosphatidylinositol 4,5-bisphosphate phosphodiesterase gamma-2), *CR1* (complement receptor 1), or *CLU* (clusterin), which are either associated with the innate immune cells of the brain, that is microglia, or the complement system, have also been shown to increase the risk of developing AD (Guerreiro et al., 2013c; Jansen et al., 2019; Ulland et al., 2017). Interestingly, APOE is highly expressed in disease-associated microglia (DAM) which constitute a specific subset of microglia shown to cluster around Aβ plaques, further corroborating an important role for the immune cells in the brain in disease pathogenesis (Keren-Shaul et al., 2017; Krasemann et al., 2017).

1.2 APP processing and its role in AD

APP can be cleaved by either α- and β-secretase, followed by the cleavage of γ-secretase, and this represents the canonical processing pathway of APP. α-Secretase cleaves APP within its Aβ domain, leading to the production of non-amyloidogenic fragments which have neurotrophic and neuroprotective properties (Mattson et al., 1993). On the other hand, β-secretase cleavage of APP, followed by that of γ-secretase, results in the release of 38, 40, and 42- amino acids long Aβ fragments, amongst others, into the cytoplasm (Figure 1.2). Although they have a physiological function in the healthy brain, such as regulating presynaptic release, in AD, these fragments can build up and subsequently result in the formation of hydrophobic Aβ oligomers which are the toxic species positioned as central to AD pathogenesis. These in turn impair synaptic transmission, disrupt mitochondrial function, and ultimately result in neuronal death (De Felice et al., 2008; Esch et al., 1990; Meyer-Luehmann et al., 2008).

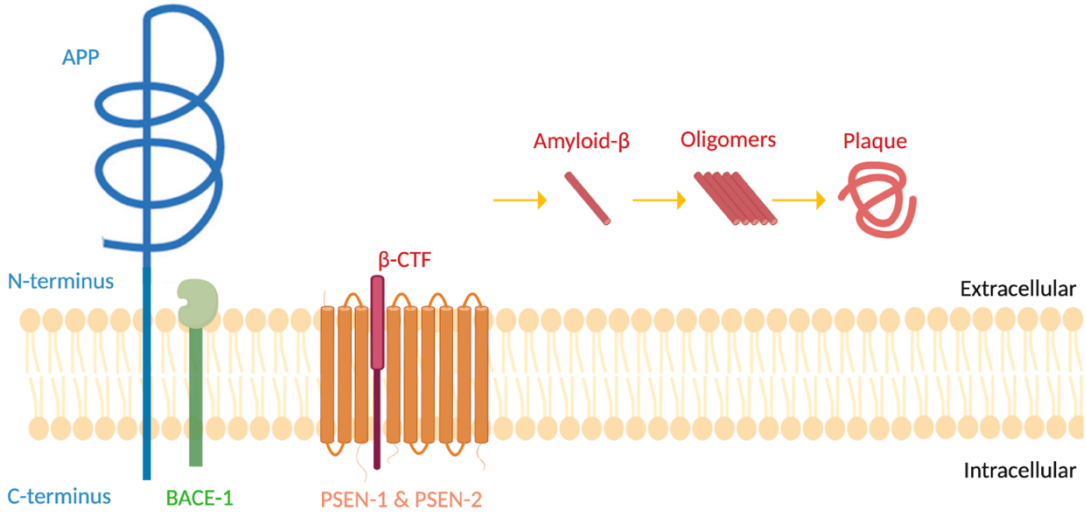

Figure 1.2. APP processing in AD.
APP gets cleaved at its N-terminus by β-secretase (BACE1) to generate the C-terminal fragment (β-CTF). Further cleavage by presenilin-1 and -2 transforms the β-CTF into the Aβ fragment which is released into the cytoplasm. 38, 40, and 42-long Aβ fragments are generated, with the former two having a strong tendency for oligomerization and fibrillation. Aβ gets transformed into oligomers and ultimately gets accumulated into plaques (figure adapted from Heneka et al. (2015)).

Given the important role of APP and the secretases involved in its proteolytic processing and Aβ production, it is not surprising that more than 30 mutations in these have been associated with EOAD (Jonsson et al., 2012). Studies in overexpressing transgenic mouse models have demonstrated that animals with such mutations exhibit many of the pathological hallmarks of AD, including amyloid plaques, synaptic denervation, gliosis, hyperphosphorylation of tau, some, although limited neurodegeneration, loss of synaptic mitochondria, and mitochondrial dysfunction (Chin et al., 2005; Cummings et al., 2015; Du et al., 2010; Games et al., 1995; Sasaguri et al., 2017). These animals demonstrate an increase in Aβ production and thus reveal a shift from the non-amyloidogenic to amyloidogenic pathway. Interestingly, mutations associated with the secretases and presenilin-1 and -2 specifically, have also been shown to enhance the protein's interaction with APP, leading to altered $A\beta_{42}/A\beta_{40}$ ratios, a finding in support of the critical role of APP processing in AD pathogenesis (Berezovska et al., 2005; Scheuner et al., 1996).

The above studies have led to the idea that Aβ production serves as an initiating step in AD which leads to the subsequent hyperphosphorylation and deposition of tau,

neuronal loss, and ultimately, cognitive decline – an idea known as the amyloid cascade hypothesis first described by Hardy and Higgins in 1992. However, although this hypothesis provides an important insight into the mechanisms involved in early AD, it has several shortcomings when it comes to explaining the mechanisms in LOAD. Perhaps the biggest limitation of positioning Aβ plaques or any form of Aβ in the centre of AD pathology is the fact that plaque burden is not correlated well with cognitive decline (Josephs et al., 2008; Morris et al., 2014), while tau has been pinpointed as a better predictor of cognitive decay and atrophy in patients (Cavedo et al., 2020; Mattsson et al., 2016a; Mattsson et al., 2016b). Furthermore, the fact that plaques can be found in cognitively normal individuals (Aizenstein et al., 2008; Katzman et al., 1988; Serrano-Pozo et al., 2011) also questions the applicability of the amyloid cascade hypothesis. Therefore, to address these issues, explain the involvement of newly-found mutations associated with an increased risk of AD, and include a role for the non-neuronal cells – microglia and astrocytes – as a way of linking Aβ and tau pathology in early AD pathogenesis, this hypothesis has been adapted over the past 30 years (Hardy and Salih, 2021; Hardy and Higgins, 1992; Karran and De Strooper, 2016; Selkoe and Hardy, 2016). These extensions have been triggered by the increasing number of studies demonstrating that mutations in microglial proteins are associated with an increased risk of developing AD, as a result of which glial cells have become a central focus of recent AD research (Jansen et al., 2019).

1.3 Diagnosis of AD

Recent research has made great efforts to develop ways in which early AD diagnosis could be accomplished as this can allow for earlier and potentially more effective treatments for this devastating disease. Until recently, the majority of AD diagnoses were based on clinical measures, such as cognitive decline not associated with neurological conditions other than AD (McKhann et al., 1984). This is because accurate diagnosis of AD could only be achieved upon the inspection of post-mortem brain tissue and the presence of Aβ plaque deposition and NFTs (Braak et al., 2006; Braak and Braak, 1991). In fact, through the evaluation of brain tissue from suspected AD patients, a six-stage system based on the distribution pattern of NFT was introduced. In particular, in stages I-II, NFT pathology is limited to trans entorhinal

regions; in stages III and IV NFT pathology extends to limbic regions including the hippocampus; in stages V-VI NFT pathology is substantial and has spread to isocortical structures, with brain tissue exhibiting extensive atrophy (Braak and Braak, 1995). Although this staging is useful in understanding pathology progression, it is based on evidence from post-mortem tissue and hence does not provide clinicians with a way of determining the stage at which AD patients are at during their life. This has been supported by the fact that one study found that there are at least four different trajectories of AD, each with distinct tau progression, further suggesting that the staging does not account for heterogenous differences between individuals and does not explain all AD cases (Vogel et al., 2021). Furthermore, given that changes in cognitive ability occur much later than any structural changes have occurred in the brain (Jack et al., 2004; Petrella et al., 2003), research has been urged to find measures allowing for earlier diagnosis to allow for more targeted treatment approaches. In the past decade, technological advances in diagnostic measures, as well as the discovery of specific biomarkers associated with AD, have both helped elucidate important biological measures for the early diagnosis of AD (Albert et al., 2011; Dubois et al., 2014; Frisoni et al., 2017).

There are three main ways in which AD diagnosis can be accomplished: through the use of magnetic resonance imaging (MRI), positron emission tomography (PET) imaging, or through cerebrospinal fluid (CSF) measures. MRI is primarily used for determining reductions in the volume of different medial temporal brain regions associated with AD, such as the hippocampus (Henneman et al., 2009; Jack et al., 2000) and entorhinal cortex (Du et al., 2001; Killiany et al., 2002). Brain atrophy measures have been correlated to the NFT stage introduced by Braak and Braak (2006; 1991), providing important insights into the effectiveness of this measure for early diagnosis and for distinguishing between MCI patients and those who progress onto developing AD (Fox et al., 1999; Josephs et al., 2008). However, structural changes solely identified using MRI could be misleading due to natural variations in brain volume which is why functional PET imaging is another tool used by clinicians. The most commonly used radiotracers are the ^{11}C-labelled Pittsburgh Compound-B, [^{18}F]FDDNP, and [^{18}F]Florbetapir, all of which bind to amyloid fibrils in AD patients and hence serve as useful measures for detecting AD (Klunk et al., 2004; Rowe and Villemagne, 2013). In addition to these amyloid-binding tracers, radiotracers targeting

the TSPO compound (18-kDa translocator), whose expression in microglia and astrocytes increases as they become activated and hence serves as a marker for inflammation (Cosenza-Nashat et al., 2009), have also been shown to be useful in detecting AD in patients. Several studies have demonstrated that TSPO binding is positively correlated to the degree of amyloid pathology in both animal models and AD patients relatively early in disease (Hamelin et al., 2016; Mirzaei et al., 2016; Tondo et al., 2020). Interestingly, the study by Hamelin et al. (2016) noted that AD patients who had higher scores on the clinical dementia rating 2 years after initial examination (slow decliners) exhibited higher TSPO binding, suggesting that, at least in the early stages of disease progression, microglial activation appears to play a protective role, slowing down cognitive decline. This link between gliosis and AD progression has also been confirmed in studies using CSF biomarkers, which have demonstrated that increased levels of chitinase 3-like 1 (YKL-40), which is secreted by both microglia and astrocytes, correlate well with CSF levels of total tau, as well as cognitive decline (Janelidze et al., 2018; Llorens et al., 2017). Interestingly, the levels of several pre- and post-synaptic markers, including neuragranin and synaptosomal-associated protein 25 (SNAP25), are also elevated in early AD and this is associated with greater amyloid pathology and worsened memory performance (Mila-Aloma et al., 2020; Pereira et al., 2021). This illustrates that gliosis and synaptic changes are early events in AD which might be tightly interlinked with disease progression.

1.4 The synapse in health and AD

1.4.1 The hippocampus

The hippocampus is a complex brain structure which has been associated with a number of different functions, the most prominent of which is memory formation and learning. However, the hippocampus has also been shown to have a role in olfaction (Soudry et al., 2011), spatial navigation (Stella et al., 2012), and emotional behaviour (Toyoda et al., 2011), illustrating the importance of its normal functioning for normal

brain activity. In humans, the hippocampus is situated deep into the temporal lobe and is well connected to surrounding brain regions. The hippocampal formation comprises of several distinct regions including the dentate gyrus (DG), the CA3, CA2, and CA1 pyramidal layers, the subiculum, presubiculum and parasubiculum. The hippocampal circuit and particularly, the trisynaptic loop, has been very well studied throughout the years and it consists of unidirectional neuronal activity flowing across three pathways. The trisynaptic loop begins at cells in layer II of the entorhinal cortex (EC) which form excitatory projections onto granule cells in the DG via the medial and lateral perforant paths. Following this, DG cells synapse onto pyramidal cells in the CA3 layer via the mossy fibre pathway and CA3 pyramidal cells then send axonal projections to CA1 pyramidal cells through the Schaffer collateral pathway. CA1 cells then either synapse onto cells in the subiculum which then project to the deep layers of the EC, or they project directly onto those layers (see Figure 1.3) (van Groen et al., 2003). In addition to the trisynaptic loop, there are also other connections in the hippocampus, such as EC projections directly onto CA3 pyramidal cells, as well as recurrent collaterals in the CA3 layer. Studies examining this trisynaptic loop have provided valuable insight into how synaptic activity can lead to memory formation and learning, but have also raised important questions in what ways the hippocampus becomes impaired under disease conditions.

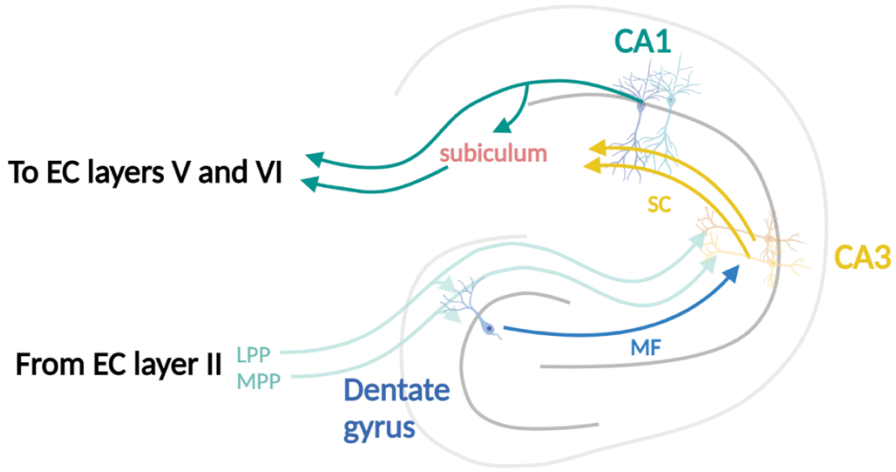

Figure 1.3. A simplified version of the hippocampal circuit.
The trisynaptic loop of the hippocampus is unidirectional and begins with inputs from layer II of the entorhinal cortex (EC) to the granule cells in the dentate gyrus via the medial and lateral perforant paths (MPP and LPP). Granule cells then project onto pyramidal cells in the CA3 layer via the mossy fibre pathway (MF) which then form connections to CA1 pyramidal cells via the Schaffer collateral pathway. CA1 cells then provide input to the deep layers of the EC (V and VI) or indirectly via the subiculum.

1.4.2 The synapse in the AD brain

Alterations in synaptic activity are one of the hallmarks of AD and are one of the most closely related factors to the speed of cognitive decline in AD (DeKosky and Scheff, 1990; Jackson et al., 2019a; Terry et al., 1991). In fact, fMRI studies have demonstrated abnormal hyperactivity in the hippocampus of AD patients before apparent cognitive changes, followed by hypoactivity once symptoms emerge (Bookheimer et al., 2000; Dickerson et al., 2005; Quiroz et al., 2010). This hippocampal hypoactivity is shown to be very closely related to the degree of cognitive decline (O'Brien et al., 2010). Since the hippocampus is essential for the formation of new memories and learning (Whitlock et al., 2006), and is in fact one of the first regions affected in AD (Braak and Braak, 1993), understanding the reason for the early changes in this brain region is crucial for understanding disease development.

1.4.3 Aβ and the synapse

In the healthy brain, APP and the different Aβ fragments produced from it have a physiological role in synaptic transmission. In particular, research has demonstrated that Aβ released in an activity-dependent manner promotes APP-APP interactions in presynaptic terminals. This in turn leads to enhanced presynaptic Ca^{2+} influx and thereby, glutamate release (Abramov et al., 2009; Fogel et al., 2014). A study by Lee et al. (2020) has also shown that the APP family is required for normal synaptic functioning. Its inactivation was shown to lead to impaired hippocampal synaptic plasticity and spatial memory resulting from neuronal hyperexcitability, as determined by a lowered actional potential (AP) threshold and increased frequency of firing. Another study showed that when applied exogenously, nanomolar levels of Aβ can inhibit long-term potentiation (LTP) formation through excessive activation of N-methyl-D-aspartate receptors (NMDARs) (Li et al., 2011). The opposite effect was observed in another study, which argued that endogenous Aβ is necessary for normal LTP, with antibodies against Aβ resulting in its reduction (Puzzo et al., 2011). The contrasting effects of these two studies could be due to the much younger mice used in the study by Li et al. or the different stimulation paradigms used for LTP induction, with Puzzo et al. using theta-burst stimulation, while Li et al. used two trains of stimuli. Nonetheless, altogether these studies demonstrate an important physiological

role of APP and its fragments in synaptic activity and raise the question as to what causes the shift from this normal functioning of Aβ to its toxic effects on synapses and neurons seen in AD.

Importantly, however, a growing number of evidence suggests that most of the synaptic toxicity imparted by Aβ arises from the soluble oligomeric Aβ species, rather than from the plaque formations themselves (Busche et al., 2012; Selkoe, 2008; Townsend et al., 2006; Walsh et al., 2002). This is supported by the finding that plaques may occur in cognitively normal elderly individuals without any sign of AD-associated manifestations (Aizenstein et al., 2008; Katzman et al., 1988; Serrano-Pozo et al., 2011). It is possible that early in AD pathology, amyloid plaques serve a somewhat protective role wherein they attract free-floating soluble Aβ oligomers, keeping the damage associated with them fairly local. As more and more soluble Aβ becomes produced, plaques become bigger, in turn increasing the toxic effects of Aβ on neighbouring structures like synapses.

The above has been supported by studies in mice which have demonstrated that changes in neuronal activity can occur before evident pathology and hence, during soluble Aβ oligomers accumulation. Most studies on animal models agree that with increased soluble Aβ levels, there is an increased probability of glutamate release and hence, increased excitability. For instance, our lab has demonstrated that CA3 pyramidal cells in the hippocampus of transgenic TASTPM mice (carrying the Swedish mutation in APP and the M146V mutation in PSEN1) exhibit increased release probability even before plaque formation (Cummings et al., 2015). More recently, we demonstrated the same effect in *App* knock-in models of AD which avoid some of the problems associated with overexpression (discussed in more detail later in this chapter). In this study, $App^{NL\text{-}F}$ and $App^{NL\text{-}G\text{-}F}$ mice exhibited increased release probability at 7 and 2 months of age, respectively, which is before or at very minimal plaque accumulation in these models, suggesting that it is due to the effects of the soluble oligomeric Aβ (oAβ) species (Benitez et al., 2021; Saito et al., 2014). The effect of Aβ on synaptic activity has also been confirmed in *in vivo* studies which have shown that neurons in the vicinity of soluble Aβ are hyperactive and become silent after plaque formation (Busche, 2018; Busche et al., 2012; Busche et al., 2008; Busche et al., 2015; Busche and Konnerth, 2016). The 2012 study by Busche et al. showed

hippocampal hyperactivity in the APP23xPS45 transgenic model which was reduced upon the addition of a gamma-secretase inhibitor and hence after a reduction of soluble Aβ in these mice.

Studies in AD models have demonstrated that Aβ can have prominent effects on both the presynapse and postsynapse which can ultimately result in altered synaptic transmission in these models (summarised below in Figure 1.4). For example, given that Aβ release is activity dependent (Abramov et al., 2009; Dolev et al., 2013; Palop and Mucke, 2010), it has been suggested that as Aβ is released from synapses more substantially in AD conditions due to either mutations in the *APP* gene or other risk factors, a positive feedback loop occurs, wherein more and more soluble Aβ becomes released and begins aggregating into amyloid plaques (Edwards, 2019). In fact, one study by Russell et al. (2012) demonstrated that exogenously applied $A\beta_{42}$ localises to presynaptic terminals where it disrupts the complex formed between VAMP2 and Synaptophysin, in turn increasing the number of vesicles primed for exocytosis. Furthermore, another study by Ovsepian et al. (2017) has shown that cells which are in the vicinity of plaques exhibit activity-dependent hyperactivity evidenced by increased frequencies of spontaneous excitatory postsynaptic currents (sEPSCs). The authors argue that this is due to the enhanced presynaptic glutamate release from dystrophic axons as a result of enhanced Ca^{2+}-induced Ca^{2+} release induced by presynaptic mGluR activation due to impaired glutamate reuptake, although the origin of the synaptic inputs was not examined specifically in this study (see Figure 1.4). Nonetheless, this work demonstrates an important role for Aβ and Aβ plaques in modulating synaptic activity in disease contexts.

The same was observed more recently in another study which demonstrated that both the *in vitro* and *in vivo* application of a synthetic Aβ compound ($[A\beta S26C]_2$) in wild-type mice enhances the hyperactivity in neurons with pre-existing baseline activity (Zott et al., 2019). The authors argued that this was due to the Aβ-mediated suppression of glutamate reuptake and specifically, through its effects on the astrocytic glutamate transporter GLT-1. They found that both TBOA (glutamate reuptake blocker) and GLT-1 antibodies mimicked the above effects in wild-type mice, while TBOA had no additional effect on hyperactivity in APP23/PS45 mice at a stage when levels of soluble Aβ are high (Zott et al., 2019). Disrupted glutamate

reuptake has also been suggested previously, with studies showing that pathological elevations in Aβ could reduce neuronal glutamate reuptake at the synapse, contributing to long-term depression (LTD) in disease contexts (Li et al., 2009; Li et al., 2011). These results demonstrate the important role of soluble Aβ in early neuronal dysfunction in AD, highlighting the need to understand its specific effects on synaptic activity early in the disease.

Exogenously applied oligomeric Aβ has on multiple occasions been shown to lead to alterations in presynaptic activity. In particular, a number of studies have shown the presence of oAβ to reduce the frequency of miniature excitatory postsynaptic currents (mEPSCs), which represent currents in response to spontaneously released glutamate vesicles in the absence of APs (Kamenetz et al., 2003; Nimmrich et al., 2008; Shankar et al., 2007; Talantova et al., 2013). Aβ derived from extracts from AD patients has been shown to block LTP, impair memory performance, and alter synaptic structures in the hippocampus (Barry et al., 2011; Borlikova et al., 2013; Li et al., 2011), with one study demonstrating that the addition of AD-derived Aβ to wild-type mice blocks LTP and enhances the presynaptic release of glutamate, an effect which was dependent on the presence of endogenous APP (Wang et al., 2017). The same work further demonstrated that Aβ also leads to enhanced frequency of sEPSCs and reduced frequency of spontaneous inhibitory postsynaptic currents (sIPSCs), and also accumulates in presynaptic compartments, showing the excitation/inhibition imbalance which could be induced by Aβ through its effect on the presynapse.

The above effects on synaptic transmission could also be driven by the decreased number of postsynaptic α-amino-3-hydroxy-5-methyl-4-isoxazolepropionic (AMPA) and NMDA receptors shown to occur as a result of elevated Aβ (which also leads to the loss of dendritic spines (Cirrito et al., 2005; Hsieh et al., 2006)), enhanced presynaptic glutamate release, reduced glutamate reuptake (Li et al., 2009), or a decrease in synaptic inhibition (Busche et al., 2012; Verret et al., 2012). In fact, oAβ has multiple binding partners at both the pre- and post-synapse, including NMDARs, NaKα3, α7nAChR, APOE, Clusterin, EphA4, and p75NTR (Jarosz-Griffiths et al., 2016). Therefore, it has been suggested that in early AD, the rising levels of Aβ promote its binding to multiple receptors in the synaptic space, in turn creating an imbalance between synaptic excitation and inhibition. This idea has more recently

been demonstrated in acute hippocampal slices from 5xFAD mice, where CA1 cells exhibited attenuated inhibitory postsynaptic currents, and hence hyperactivity, at a stage prior to Aβ plaque development, which was reversed upon the addition of $GABA_A$ receptor agonists (Li et al., 2021). The same reduced inhibitory activity was also reported in the lateral entorhinal cortex in $App^{NL\text{-}F}$ mice again prior to plaque accumulation, suggesting that the observed effects are due to soluble Aβ (Petrache et al., 2019). Although reducing inhibition, Aβ has additionally been shown to enhance excitation. For instance, work in acute hippocampal slices in rats has shown that the intracellular injection of oligomeric forms of Aβ can result in the insertion of GluA1-expressin AMPARs (Whitcomb et al., 2015). On the other hand, Aβ has also been shown to bind to GluA2- and GluA3-expressing AMPARs, in turn triggering their internalisation and disrupting synaptic transmission (Reinders et al., 2016; Zhao et al., 2010). Therefore, by altering the receptor makeup at the postsynapse, Aβ can result in abnormal synaptic activity in AD models. Furthermore, previous work has also highlighted an important interaction between Aβ and NMDARs which can lead to further alterations in synaptic transmission. In particular, it has been shown that Aβ can reduce NMDAR-mediated Ca^{2+} transients at the postsynapse (Bloodgood and Sabatini, 2007). Further work in knock-out mice aiming to delineate the specific mechanisms through which Aβ leads to altered NMDAR activity demonstrated that Aβ decreases the surface expression of NMDARs in 5xFAD mice, in turn reducing the number of functional synapses (Muller et al., 2018). Additionally, it has also been demonstrated that the binding of Aβ to NMDARs can lead to spine loss in a calcineurin-dependent manner (Rammes et al., 2018; Shankar et al., 2007; Wei et al., 2010). Therefore, it appears the physiological role of Aβ becomes dysregulated in AD conditions, in turn leading to altered properties of synaptic transmission, disturbing both pre- and postsynaptic mechanisms and impairing network activity (summarised in Figure 1.4 below) (Gulisano et al., 2019).

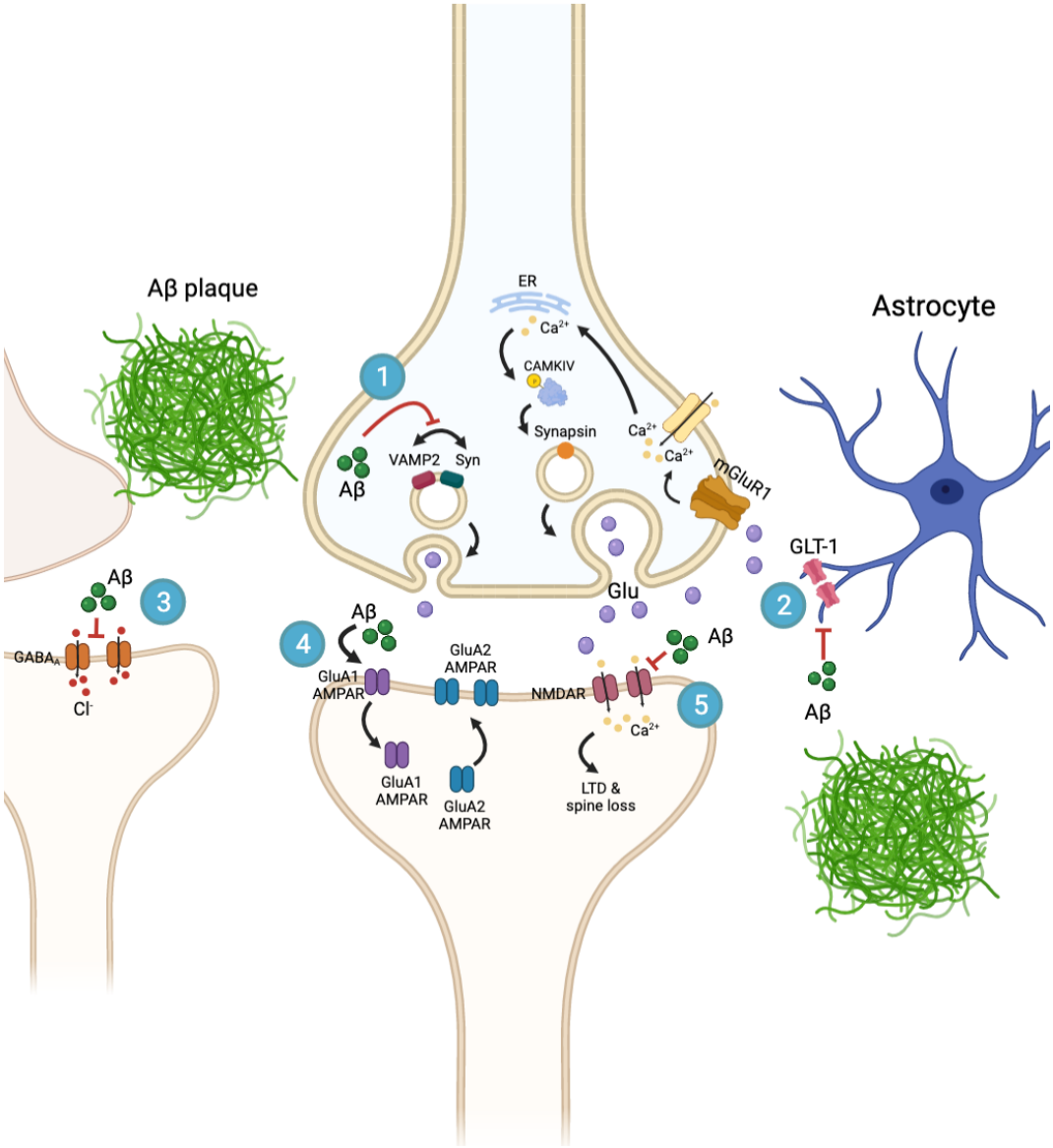

Figure 1.4. The effects of Aβ on the pre- and postsynapse and synaptic transmission in AD mouse models.

Presynapse: Aβ can increase the release probability in AD models through two main mechanisms: (1) Aβ is able to enhance synaptic vesicle docking and neurotransmitter release by disrupting the interaction between VAMP2 and Synaptophysin, allowing for VAMP2 to participate in the formation of the SNARE complex. (2) Additionally, Aβ can also inhibit glutamate reuptake via GLT-1 transporters on astrocytes, in turn resulting in presynaptic mGluR1 activation, Ca^{2+}-induced Ca^{2+} release from ER stores, CaMKIV and synapsin phosphorylation, ultimately increasing the number of synaptic vesicles available for docking.

Postsynapse: Aβ can also affect the excitatory/inhibitory balance by altering the receptor make-up at the postsynapse: (3) Aβ has been shown to inhibit $GABA_A$ receptors at the postsynapse, in turn resulting in reduced inhibitory transmission. (4) Aβ can also affect the composition of excitatory receptors at the presynapse by increasing the endocytosis of GluA1-expressing AMPARs and enhancing the exocytosis of GluA2-expressing AMPARs. (5) Aβ can also inhibit NMDAR-mediated Ca^{2+} influx, in turn resulting in calcineurin activation and impaired LTD and spine loss.

In addition to its effects on synaptic transmission, previous research has shown that soluble Aβ can also result in synaptic loss. In fact, a number of studies have shown a significant decrease in dendritic spines in AD patients, indicating a potential link between Aβ and synaptic health (Fiala et al., 2002; Knobloch and Mansuy, 2008; Koffie et al., 2012; Penzes et al., 2011). This finding has been very well established in mouse models with studies showing that synapses within a certain radius of a plaque are lost, although synapses outside this region also show some abnormalities (Spires et al., 2005). For instance, evidence from J20 mice, which overexpress *App* with two mutations linked to AD (Swedish and Iberian mutations), has shown a decreased number of synaptic puncta which is tightly correlated with soluble Aβ and, interestingly, not plaque load (Mucke et al., 2000). This is in accordance with other work on APP/PS1 transgenic mice which has indicated that that the halo of oAβ around plaques is what contributes to the reduction of excitatory postsynaptic densities, evidenced by a reduction of PSD95 staining around plaques (Koffie et al., 2012; Koffie et al., 2009). In fact, the same studies further demonstrated that the number of synapses returns to control levels at around 50 μm away from the plaque region, suggesting the region-specific toxic effects of the oAβ halo. The mechanisms for these effects are presently unknown, although it has been suggested that oligomeric Aβ may bind to NMDARs, in turn enhancing their endocytosis in the postsynaptic density (Snyder et al., 2005).

More recent research has corroborated the above findings in *App* knock-in mice and specifically, App^{NL-F} mice, with a study by Sauerbeck et al. (2020) showing reduced excitatory synaptic densities in the vicinity of plaques in the cortex. These effects were limited to up to approximately 25μm away from the plaque region, again illustrating that they are highly dependent on plaque presence and the toxicity associated with it. Opposite effects on the inhibitory postsynaptic density in pyramidal cells in the hippocampus have also been observed. Specifically, the synapse density of the CA3 axon initial segment established by PV-(parvalbumin)-positive axon-axonic inhibitory neurons was found to be enlarged, and therefore dystrophic, in 18-month App^{NL-F} mice compared to wild-type controls (Sos et al., 2020). The authors suggest that this could be a compensatory mechanism designed to counteract the enhanced synaptic activity observed in pyramidal cells, however how this is achieved remains to be determined. Interestingly, the same study also showed that PV-expressing inhibitory neurons,

which show no alterations in receptor makeup, nor synapse density despite moderate plaque pathology, occasionally exhibit dystrophic axons near amyloid plaques (Sos et al., 2020), highlighting the presynaptic compartment as especially vulnerable to Aβ pathology.

Therefore, in addition to its effects on postsynaptic densities, research has shown that Aβ can also have profound effects on presynaptic compartments. For instance, Sadleir et al. (2016) have demonstrated that microtubules are disrupted in peri-plaque regions. By looking at tissue from both AD patients and 5xFAD mice, their work shows that despite expressing normal levels of synaptophysin, axons around plaques exhibit reduced expression of the active zone protein bassoon, as well as reduced expression of the microtubule marker tubulin and aberrant accumulation of microtubule-associated proteins such as dynein, dynamitin, and kinesin (Sadleir et al., 2016). Their work shows that the reduction of tubulin occurs within 20μm of the plaque region, providing further support for plaque-specific toxicity. More recent work on AD patients has further shown using MRI and diffusion-tensor imaging that both pre- and post-synaptic markers (SNAP25; growth associated protein 43, GAP43; and neurogranin, NRGN) are differentially upregulated in early AD prior to tau pathology (Pereira et al., 2021). Changes in these markers are associated with greater amyloid pathology and worsened memory performance, indicating an important link between Aβ and synaptic mechanisms. Interestingly, through the use of pulse-chase proteomics, which allows the tracking of the dynamics of different proteins over time, Hark et al. (2021) also demonstrated that in the early stages of Aβ accumulation in *App* knock-in mice ($App^{NL\text{-}F}$ and $App^{NL\text{-}G\text{-}F}$), there is an impaired turnover of presynaptic proteins (including SNAP25; vesicle-associated membrane protein-1, VAMP1; and syntaxin-1B, STX1B), resulting in elevated levels of presynaptic vesicle proteins and enhanced synaptic vesicle pool density. This study highlights that the presynaptic compartment is particularly vulnerable to early Aβ accumulation, positioning the presynapse as critical for the early synaptic effects seen in AD.

Neurites themselves also become damaged as a result of plaque accumulation, with this phenomenon shown to be directly caused by newly-formed plaques or the soluble Aβ build-up prior to and during plaque development (Meyer-Luehmann et al., 2008; Spires et al., 2005). Furthermore, axons near plaques also display an interesting

anatomical feature, wherein they bend around plaques they pass nearby, perhaps because they are physically displaced by plaques' presence or possibly to avoid plaques-associated toxicity and maintain their own functionality (Spires et al., 2005). Given the effects of plaques on the activity and morphology of surrounding synapses and the importance of mitochondria and Ca^{2+} homeostasis on synaptic transmission, the finding that Aβ can disrupt mitochondrial functioning and Ca^{2+} buffering is not surprising. In fact, extracellular Aβ can be internalized and taken up by mitochondria (Hansson Petersen et al., 2008; Hedskog et al., 2013), where it can bind to several mitochondrial proteins, including ABAD (amyloid-binding alcohol dehydrogenase) and Cyclophilin D, in turn resulting in mitochondrial toxicity (Du et al., 2008; Lustbader et al., 2004). Interestingly, mitochondrial damage, lysosomal accumulation, and axonal dysfunction in both AD models and AD post-mortem tissue has been shown to occur predominantly in mitochondria in the vicinity plaques, a finding highlighting the importance of plaque toxicity in AD pathology (Cai and Tammineni, 2017; Sos et al., 2020).

1.5 Glial cells

1.5.1 Microglia in the healthy brain

Microglia are the brain-resident immune cells and they have increasingly been recognised as essential regulators of development, homeostasis, as well as disease mechanisms in the central nervous system. Microglia are derived from the myeloid progenitor cells in the embryonic yolk sac and they migrate to the brain early in embryonic development at approximately day 9.5 before growing into immature microglia, where they constitute 5-10% of all brain cells (Ginhoux et al., 2010; Ginhoux and Guilliams, 2016; Hoeffel and Ginhoux, 2015; Li and Barres, 2018). Using local signals, they adopt tissue-specific signatures and functions, creating vastly heterogeneous populations across the brain (Gautier et al., 2012; Hickman et al., 2013; Li et al., 2019). Microglia are able to quickly adapt to their surrounding environment and adopt a number of different functions, evidenced by the existence of different microglial activation states, as well as different transcriptional profiles (Gosselin et al., 2014; Gosselin et al., 2017; Lavin et al., 2014). Microglia are known to support neurons by clearing extracellular debris, as well as by releasing extracellular growth

factors, such as brain-derived neurotrophic factor (BDNF) and insulin-like growth factor-1 (IGF-1) (Gomes et al., 2013; Parkhurst et al., 2013; Ueno et al., 2013), and cytokines, such as tumour necrosis factor-α (TNFα) and interleukin-1β (IL-1β) (York et al., 2018). This release is achieved through the activation of their numerous receptors, which include purinergic receptors (Haynes et al., 2006), metabotropic glutamate receptors (Taylor et al., 2002; Taylor et al., 2003), GABA receptors, and acetylcholine receptors (reviewed extensively by Domercq et al. (2013)). Both during development and, as demonstrated more recently, in the adult brain, microglia have a crucial role in a number of processes, including neurogenesis (Aarum et al., 2003; Cunningham et al., 2013; Diaz-Aparicio et al., 2020; Ueno et al., 2013), synaptic maturation (Schafer et al., 2012; Stevens et al., 2007), and the establishment and regulation of neuronal circuits (Hoshiko et al., 2012; Pont-Lezica et al., 2014).

Microglia are incredibly mobile and *in vivo* imaging studies in the mouse brain have demonstrated that they continuously scan the local environment and contact neural components and synapses with their highly motile processes (Nimmerjahn et al., 2005; Wake et al., 2009). These microglia-synapse interactions have been suggested to be important in regulating synaptic maturation. In fact, there have been numerous reports of the extensive pruning of neurons and their respective synapses by microglia during development in different regions, including the hippocampus and the olfactory bulb (Lehrman et al., 2018; Stevens et al., 2007; Wallace et al., 2019; Wilton et al., 2019). This process has been shown to be dependent on the classical complement cascade, with the complement components C1q and C3 marking synapses for elimination, which are then recognised by the microglial receptor complement receptor 3 (CR3) (Schafer et al., 2012; Stevens et al., 2007). Interestingly, three-dimensional reconstructions acquired using correlative light and electron microscopy of organotypic hippocampal slice cultures (OHSCs) from mice have also demonstrated that microglia are able to trogocytose – or 'nibble' – presynaptic boutons and axons – a process which was not dependent on CR3 (Weinhard et al., 2018). Microglial pruning has also been shown to be regulated through cluster of differentiation-47 (CD47) signalling and its microglial receptor, SIRPα, with CD47 deletion resulting in enhanced engulfment, thereby suggesting that it constitutes a synaptic "don't eat me" signal for microglia to recognise (Lehrman et al., 2018). CD47 was shown to be

primarily localised to active synapses, suggesting that its expression is used as a tag to limit microglial phagocytosis of necessary inputs during synaptic pruning.

A similar function of microglia has also been reported to occur as a normal process throughout life, with studies showing that microglia actively and constantly regulate the number of functional synapses in the nervous system (Ji et al., 2013; Paolicelli et al., 2011; Peretti et al., 2015; Zhan et al., 2014). A recent study has also shown that microglial pruning of postsynaptic density protein-95 (PSD95) synapses could occur in the adult hippocampus, positioning microglia as important players for mediating the forgetting of contextual fear memory (Wang et al., 2020). Similarly to during development, microglial pruning in this context was shown to be dependent on the use of the complement pathway and was targeted to weakly activated neurons. It appears that, in the healthy brain and throughout life, microglial reorganisation of hippocampal synapses is important for normal functioning.

In addition to affecting the structure of synaptic elements, microglia have also been shown to have profound effects on synaptic function. This idea was brought forward by the fact that a number of studies have shown that microglial motility is dependent on changes in neuronal activity (Cserep et al., 2020; Liu et al., 2019; Stowell et al., 2019). In particular, one study demonstrated that reduced microglial branching and motility observed in *Cx3cr1* knock-out mice resulted in altered glutamatergic transmission at CA3-CA1 synapses and specifically, a defective AMPA component of EPSCs, defective functional connectivity, as well as reduced release probability (Basilico et al., 2019). Moreover, several studies have shown that upon enhanced neuronal activity and NMDAR activation, ATP is released from neurons which in turn stimulates the outgrowth of microglial processes towards synaptic compartments (Dissing-Olesen et al., 2014; Eyo et al., 2014). A study by Ji et al. (2013) also demonstrated that microglial removal increases the frequency of both spontaneous and miniature EPSCs and results in higher synaptic density, evidenced by an increase in GluA1, synapsin I and PSD95 in OHSC, highlighting a role for microglia for normal synaptic functioning. This was echoed in a more recent study which showed that microglia suppress neuronal activity by detecting neuronal-derived extracellular ATP, with microglial removal resulting in increased synchronous firing of neurons and seizures in mice (Badimon et al., 2020).

Altogether, the above studies demonstrate that microglia are not merely passive observers but are active players in the central nervous system. They are able to continuously adapt to their changing environment and respond appropriately to different signals to regulate the integrity of neuronal networks and synaptic activity, to ultimately assure its normal functioning.

1.5.2 Microglia in AD

In addition to amyloid plaques, neurofibrillary tangles and neuronal loss, inflammation has also been pinpointed as important for AD pathogenesis. This was noted for the first time in 1907 in the report of Alois Alzheimer himself, with a number of studies demonstrating alterations in activation and distribution of glia, as well as increased expression of inflammatory markers in the brains of AD patients (Beach et al., 1989; Itagaki et al., 1989). Indeed, given that several variants of microglial genes, including *CD33* (Hollingworth et al., 2011) and *TREM2* (Jonsson et al., 2013), have been associated with an increased risk of developing AD, the immune cells of the brain have been positioned as key regulators of disease pathogenesis. In fact, microglia have been shown to rapidly cluster around newly formed amyloid plaques in both post-mortem tissue from AD patients and mouse models, which is accompanied with profound changes in their morphology and gene expression (Baron et al., 2014; Condello et al., 2015; Matarin et al., 2015; Meyer-Luehmann et al., 2008; Serrano-Pozo et al., 2013; Town et al., 2005; Yuan et al., 2016). This is believed to be an early phenomenon, occurring shortly after plaque accumulation (Henstridge et al., 2019). It is unknown what the exact role of these microglia is – whether they have a role in separating plaques from surrounding regions (Condello et al., 2015), or whether microglia become dysfunctional in such contexts (Krabbe et al., 2013). A transcriptional study in 5xFAD mice showed that these microglia constitute a completely different subset of microglia, upregulating genes associated with microglial activation and which have also been highlighted as AD risk factors, such as *Trem2* (Guerreiro et al., 2013b; Jonsson et al., 2013), *Apoe* (Corder et al., 1993), and *Tyrobp* (Pottier et al., 2016), and downregulating homeostatic genes including the purinergic receptors *P2ry12/13*, *Cx3cr1*, and *Tmem119* (Butovsky et al., 2014; Keren-Shaul et al., 2017). The existence of these DAMs has also been confirmed in other models of AD (Ajami et al., 2018; Friedman et al., 2018; Krasemann et al., 2017),

indicating a potentially important role for these plaque-associated microglia in an AD context. Some DAM markers have also been reported in AD post-mortem brains (Friedman et al., 2018; Keren-Shaul et al., 2017), illustrating a common microglial signature in response to an AD environment.

The DAM signature is a two-step process, with currently unknown signals triggering the change from homeostatic microglia to stage I DAM microglia, and TREM2 signalling required for stage II induction (see Figure 1.5). The latter was confirmed in studies showing that TREM2 deficient mice are unable to produce stage II DAM, with the majority of microglia constituting stage I DAM (Keren-Shaul et al., 2017). The dependency of the DAM profile on TREM2 signalling demonstrates the importance of normal functioning of TREM2 for an appropriate microglial response, positioning it as an essential regulator of the immune response to amyloid pathology. Interestingly, a more recent transcriptional study in AD human tissue identified a number of different populations of microglia. However, several of these, rather than one cluster specifically, were shown to express some of the genes associated with the DAM signature found in mice (Olah et al., 2020). This illustrates that although there is no specific cluster expressing the murine DAM signature, thereby raising questions into the relevance of mouse models for recapitulating human AD, the fact that multiple populations differentially up- and down-regulate genes similarly as DAMs shows that mouse models could provide a general overview for understanding the microglial response in AD.

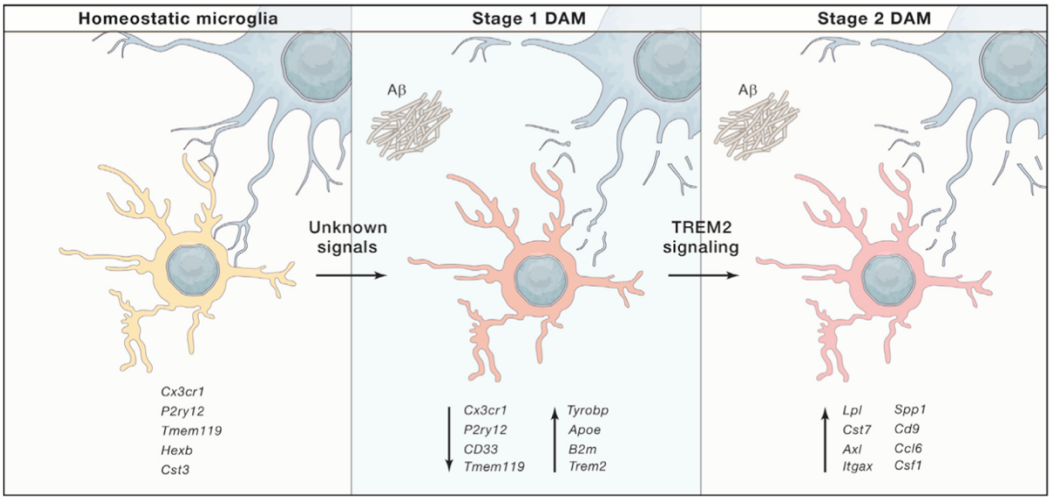

Figure 1.5. Induction of microglia to disease-associated microglia (DAM).
The induction of a homeostatic microglia to a stage I DAM is triggered by unknown signals, while TREM2 signalling is required for stage II induction. Microglia at both stages exhibit specific transcriptional signatures. Figure taken from Deczkowska et al. (2018).

1.5.3 Microglia and Aβ

Previous studies have suggested that DAMs are recruited to plaque regions in order to limit plaque formation and expansion. There have been indications of microglial binding and engulfment of Aβ species (Lee and Landreth, 2010; Yu and Ye, 2015), suggesting their potential role in phagocytosing Aβ and hence regulating plaque growth. Indeed, microglia have been shown to secrete an Aβ-degrading enzyme which potentially aids their role in removing Aβ in a CR3-dependent manner, with CR3 ablation promoting Aβ phagocytosis (Czirr et al., 2017; Fu et al., 2012). In comparison, another study by Baik et al. (2016) demonstrated that microglial engulfment of Aβ in the 5xFAD model induces microglial cell death and subsequent release of engulfed Aβ into the extracellular space, contributing to plaque growth. However, studies in which microglia are ablated either using a colony-stimulating factor 1 receptor (CSF1R) blocker (PLX5622 or PLX3397) – as CSF1R signalling is necessary for microglial development and survival (Chitu et al., 2016; Elmore et al., 2014) – or genetic manipulation are contradictory. Some studies report increased plaque growth and particularly increased size and number, as well as reduced circularity when microglia are removed (Clayton et al., 2021; Zhao et al., 2017), some find no changes in plaque number or maintenance (Dagher et al., 2015; Grathwohl et al., 2009; Spangenberg et al., 2016), while others show reduced plaque formation

(Benitez et al., 2021; Sosna et al., 2018; Spangenberg et al., 2019), arguing that microglia are instrumental in plaque formation.

The discrepancies of the above findings could be attributed to the different mouse models used in these studies, the timing of microglial ablation, as well as its duration. In particular, the studies implementing microglial depletion prior to or at very early plaque deposition (Sosna et al., 2018; Spangenberg et al., 2019) found reduced amyloid burden evidenced by reduction in both size and number of plaques with microglial removal. Some of these studies also found reduced intraneuronal and extracellular soluble Aβ in the cortex and hippocampus, a reduction of dense-core plaques, and the appearance of diffuse-like plaques in 5xFAD mice, while others have reported a reduction of small plaques upon microglial ablation in *App*$^{NL\text{-}G\text{-}F}$ mice (Benitez et al., 2021). These results suggest that microglia have a role in depositing soluble Aβ into plaques and compartmentalising those plaques into dense-core plaques, potentially limiting the spread of Aβ toxicity.

In comparison, those studies implementing the depletion paradigm later (i.e. at 4 months in *App*$^{NL\text{-}G\text{-}F}$ mice in (Clayton et al., 2021) when there is already advanced plaque load), see the opposite effect and report enhanced plaque burden upon microglial ablation. However, some studies (Casali et al., 2020; Son et al., 2020) also found reduced plaque size upon microglial removal despite beginning depletion at more advanced stages of pathology. Yet, both of these studies achieved partial microglial depletion (50-70%), making the effects observed heterogeneous and so it is hard to reach concrete conclusions. Nonetheless, the study by Casali et al. (2020), similarly to the above studies, observed a reduced proportion of compact plaques and an increased trend for filamentous plaques in the cortex, hippocampus, and subiculum upon microglial depletion, as evidenced by an increase in 6E10-positive plaques. This echoes the findings by Clayton et al. (2021) who similarly demonstrated reduced plaque compartmentalisation. Therefore, altogether these studies demonstrate that microglia may play an important state-dependent role in AD, wherein early in pathology they might be involved in depositing soluble Aβ into plaques, thereby potentially limiting the toxicity associated with oAβ, while later in pathology their role might be more focused on keeping the plaques themselves more compact, limiting the spread of damage.

The idea that the role of microglia is to keep plaques compact has been supported by one study which showed that microglia constitute a physical barrier around plaques, preventing the accumulation of more soluble Aβ and limiting the spread of damage of the plaque itself (Condello et al., 2015). Hence, upon microglial removal, this function is no longer achieved, resulting in more diffuse plaques and toxicity spread. This has further been supported by a recent study by Huang et al. (2021) which demonstrated an essential function for microglia and their TAM receptor tyrosine kinases – Axl and MerTK – for Aβ phagocytosis and the formation of dense-core Aβ plaques. As previous work has also shown an essential role of microglia in the formation of these plaques (Baik et al., 2016), the authors argued that dense-cored plaques are a confinement mechanism, which allows microglia to keep the toxicity of oAβ compact, limiting its spread to the rest of the tissue. This idea is in accordance with previous work which has shown that these receptors are involved in microglial clearance of dead cells (Fourgeaud et al., 2016). A protective mechanism for these DAMs has also been suggested in recent work in 5xFAD/P301S mice in which tau seeds were also injected to accelerate the tau pathology and neurodegeneration seen in this model (Lodder et al., 2021). This study demonstrated that activated plaque-associated microglia are preferentially preserved upon microglial depletion, similarly to what our lab showed recently in *App* knock-in models (Benitez et al., 2021), while non-plaque associated microglia are ablated, and this is accompanied with attenuated tau pathology and neurodegeneration. These results thus demonstrate that plaque-associated microglia and hence, DAMs, are functionally relevant, play an important protective role in early AD, and importantly, do not contribute to disease pathology. Therefore, it is clear that microglia are instrumental to disease mechanisms in the AD brain, highlighting the necessity of understanding in what ways they contribute or protect against disease progression.

A recent study by Grubman et al. (2021) demonstrated that microglia which phagocytose plaques, evidenced by the presence of Methoxy-XO4-positive inclusions in microglia, have a different transcriptional profile compared to microglia with no plaque deposits. This transcriptional profile was shown to have some overlap with the previously identified DAM profile, such as upregulation of *Apoe* and *Trem2,* although microglia also showed upregulation of genes related to the Hif-1 signalling pathway (involved in hypoxia regulation) and mitophagy. In this work, the authors also showed

that simply introducing microglia from wild-type mice into OHSC made from 5xFAD mice is enough to encourage the transition of microglia to a profile similar to Methoxy-XO4-positive microglia (Grubman et al., 2021). This demonstrates that the amyloid-containing environment is sufficient to prime microglia and change their transcriptional profile to an 'activated' one. Interestingly, the same study further indicated that those microglia which contain amyloid deposits are more likely to phagocytose synapses, creating an interesting link between microglial phagocytosis and amyloid plaques.

1.5.4 Microglia and synapses

In addition to their interaction with amyloid plaques, the function of microglia in synaptic pruning has also been suggested to be reactivated in disease contexts. In fact, a ground-breaking study by Hong et al. (2016) was the first to show that in the J20 mouse model of AD, which overexpresses *App* with the Swedish and Indiana mutations under the platelet-derived growth factor-β (PDGF-β) promoter, microglia contribute to early synaptic loss. Similarly to under homeostatic conditions, this process was again driven by the complement pathway, with C1q and C3 tagging synapses for engulfment by microglia (Bie et al., 2019; Hong et al., 2016). The same study further demonstrated that the addition of oAβ to wild-type mice was sufficient to trigger synaptic engulfment by microglia, suggesting that amyloid toxicity primes microglia to switch to this phagocytic phenotype (Hong et al., 2016). Interestingly, microglial ablation using the CSF1R inhibitor PLX3397 in 5xFAD mice prevented the reduction in spine density observed in the CA1 region of the hippocampus in this model (Spangenberg et al., 2016). The same effect was also reported in another study in APP/PS1 mice using the GW2580 compound for microglial ablation (Olmos-Alonso et al., 2016). In accordance with this, microglial removal has also been shown to prevent the downregulation of synaptic genes observed in the hippocampus in the 5xFAD model (Spangenberg et al., 2019). Altogether, these studies illustrate a clear link between microglia and synaptic pruning in AD conditions, raising questions as to whether this is normal functioning of microglia aiming to remove damaged synapses to keep toxicity contained, or an aberrant response whereby microglia excessively prune synapses in AD.

Increased C1q and C3 gene expression has been reported in PS2APP mice, which express the N141I mutation in *Psen2* and the *App* Swedish mutation, as well as in the transgenic tau model TauP301S (Wu et al., 2019). Although only the TauP301S model exhibited increased C1q protein accumulation in the hippocampus when compared to wild-types, both models showed reduced plaque-associated synapse loss when C3 is knocked out, indicating a role for complement in synapse loss in AD contexts. One interesting finding of this work is that increased complement protein expression was primarily observed in astrocytes although was also found in microglia, indicating that both glial cell types are important players in AD. Furthermore, inhibition or deletion of C3 has also been shown to enhance plaque accumulation and neurodegeneration in a J20 model (Maier et al., 2008; Wyss-Coray et al., 2002), suggesting that C3 signalling serves an important role in protecting against AD-related toxicity. Other studies have further reported reduced microglial association with plaques and rescued synapse loss in the APP/PS1 model upon C3 knock-out (Shi et al., 2017), highlighting an important role for the complement pathway in the microglial response in an AD environment.

Accumulation of C1q and C3 specifically in synapses has further been observed in Tau-P301S mice, as well as in AD post-mortem tissue, with C1q-blocking antibodies in the former inhibiting microglial engulfment of synapses (Dejanovic et al., 2018; Wu et al., 2019). Interestingly, by setting out to explore if microglia engulf functioning synapses or debris through the use of neuron-microglia co-cultures, Dejanovic et al. (2018) also demonstrated that microglia are able to phagocytose excitatory synapses without any evident damage, illustrating that this microglial phagocytosis of synapses is a physiological function which might be exacerbated in the presence of Aβ. This idea is supported by the finding that microglia in post-mortem tissue from healthy individuals co-localise with synaptic proteins (i.e. synapsin-1), though those from AD patients contain significantly more synaptic proteins (Tzioras et al., 2019). In addition, one study demonstrated that C1q expression is dramatically increased in close proximity to synapses in the cortex and hippocampus during healthy aging in both mouse and human brain, with C1q deletion resulting in enhanced synaptic potentiation and better performance on memory tasks (Stephan et al., 2013). These exact effects were echoed in another study exploring C3-knock-out mice, which also showed reduced age-dependent synapse loss upon C3 removal, evidenced by an increased

density of spines, as well as enhanced expression of the synaptic markers vesicular glutamate transporter-2 (VGLUT2), Homer1, PSD95, and synaptophysin (Shi et al., 2015). Although these studies did not specifically explore if microglia are involved in these mechanisms, they nonetheless showed that C1q and C3 accumulation in synapses is a normal process of ageing and is essential for the age-related modulation of synaptic activity, and this process might become exacerbated under disease conditions.

Similarly to the reactivation of C1q- and C3-mediated tagging of synapses, the "don't eat me" signal CD47 and the microglial receptor SIRPα, known for their role in synapse protection during development, have also been shown to be important in an AD context. In particular, a recent study by Ding et al. (2021) demonstrated that microglia-specific deletion of SIRPα in APP/PS1 mice results in reduced synaptic density and reduced memory performance. Interestingly, the same study also showed that SIRPα levels are downregulated in both AD mice (specifically in microglia) and AD patients with disease progression, demonstrating that SIRPα is essential for protecting against synaptopathology and aberrant microglial synaptic elimination in AD.

1.5.5 TREM2

Triggering receptor expressed on myeloid cells-2 (TREM2) is a cell-surface transmembrane glycoprotein which is expressed on macrophages and dendritic cells, while in the brain it has been reported to be exclusively expressed on microglia (Forabosco et al., 2013; Kiialainen et al., 2005). However, more recent evidence from the Barres database (Brain RNA-Seq, 2021) and from our lab does show its expression, although in small amounts, in astrocytes. The main signalling pathway through which TREM2 acts is by binding to the intracellular adaptor DNAX-activation protein 12 (DAP12), which leads to the tyrosine phosphorylation of its intracellular-immunoreceptor tyrosine-based activation motif (ITAM) by the Src family kinases. This in turns creates a docking site for molecules with SH2 domains which can trigger the initiation of intracellular cascades, with one of the main ones being the phosphatidylinositol 3-kinase (PI3K)/Akt signalling pathway (Sun et al.,

2013; Takahashi et al., 2005). In particular, PI3K activated via Syc leads to the transformation of phosphatidylinositol-4,5-biphosphate (PIP2) to phosphatidylinositol -3,4,5-triphosphate (PIP3), the recruitment of phospholipase-3-γ (PLCγ) kinases from the TEC family and Vav, ultimately resulting in the activation of Akt. Some of the binding partners of TREM2 include high-density lipoproteins, low-density lipoproteins, as well as several apolipoproteins such as ApoA1, ApoA2, clusterin, and ApoE (Atagi et al., 2015; Song et al., 2017; Yeh et al., 2016). Interestingly, *Clusterin*, *APOE*, and *TREM2* have all been suggested to be central genetic risk factors for AD, highlighting their interaction as important in driving AD pathogenesis. In fact, a recent study demonstrated that TREM2 is able to bind Aβ directly with specific preference for its oligomeric form, showcasing an important role of these receptors in disease mechanisms (Kim et al., 2017; Zhao et al., 2018).

TREM2 has been shown to be involved in a number of processes including in the regulation of phagocytosis, inflammatory signalling, as well as myeloid proliferation, migration, and survival. Indeed, several studies have demonstrated that microglia are less able to phagocytose apoptotic neurons upon TREM2 knock out, with TREM2 overexpression exerting the opposite effects (Hsieh et al., 2009; Takahashi et al., 2005). Furthermore, another study reported similar effects in a model of ischemic stroke, wherein the number of phagocytic microglia which associated with apoptotic cells was significantly reduced upon TREM2 deficiency (Kawabori et al., 2015). Furthermore, one study also showed that during development, TREM2 deletion leads to impaired microglia-dependent synaptic elimination, evidenced by a decreased number of PSD95-positive puncta in $CD68^+$ microglia, as well as enhanced excitatory transmission, as demonstrated by an increased frequency of mEPSCs (Filipello et al., 2018). Therefore, the role of TREM2 signalling in regulating phagocytosis by microglia adds to that of C1q shown previously (Schafer et al., 2012; Stevens et al., 2007), raising questions as to how this could be affected under AD conditions. With regards to inflammatory signalling, it is a general consensus that TREM2 has anti-inflammatory properties. In particular, upon toll-like receptor (TLR) stimulation, microglia lacking TREM2 are more likely to release more pro-inflammatory cytokines, including TNFα and interleukin-6 (IL6) (Liu et al., 2020; Takahashi et al., 2005; Turnbull et al., 2006). However, the fact that TREM2 signalling is essential for the switch of microglia to a more activated phenotype seen in AD contexts (i.e. into

the DAMs discussed above) (Keren-Shaul et al., 2017; Krasemann et al., 2017), suggests that the function of TREM2 in inflammatory signalling is much more complex than previously believed. Furthermore, as mentioned above, TREM2 has also been shown to have a role in microglial migration and proliferation. One study showed that upon TREM2 removal, microglia show reduced expression of genes related to chemotaxis and are less able to migrate or extend their processes towards apoptotic neurons or sites of injury (Mazaheri et al., 2017), illustrating impaired microglial chemotactic response in the absence of TREM2.

1.5.6 TREM2 and Aβ

The role of TREM2 in disease was first demonstrated when homozygous loss of function mutations in TREM2/DAP12 were shown to cause Nasu-Hakola disease, which is characterised by a severe form of dementia and multiple bone cysts (Dardiotis et al., 2017; Paloneva et al., 2000; Paloneva et al., 2003). Although the mechanism through which TREM2 leads to this disease is currently unknown, this finding illustrated the importance of TREM2 for maintaining homeostatic functions. In 2013, two independent GWAS identified that the rare variant rs75932628-T on exon 2 on the TREM2 gene, which causes an Arginine-to-Histidine substitution at amino acid position 47 (R47H), increases the risk of developing AD by 2- to 4-fold (Guerreiro et al., 2013b; Jonsson et al., 2013), similar to the risk conferred when carrying one copy of the APOE4 allele. This association was further confirmed by a number of other studies (Benitez et al., 2013; Finelli et al., 2015; Ruiz et al., 2014; Sims et al., 2017), which prompted research to explore how the variant impairs TREM2 function. Interestingly, several other variants of TREM2 have also been identified as risk factors for AD, including R62H, D87N, H157Y, T96K, and R136Q (Guerreiro et al., 2013b; Jin et al., 2014; Sims et al., 2017; Song et al., 2017), illustrating an important role for TREM2 in disease pathogenesis. There is no specific consensus on how the variants affect TREM2 function, although some studies have suggested that the R47H and R62H variants impair the interaction between TREM2 and some of its ligands including APOE and clusterin (Atagi et al., 2015; Bailey et al., 2015; Kober et al., 2016; Yeh et al., 2016), suggesting a loss-of-function of TREM2 in the presence of these variants.

A number of studies in transgenic models have demonstrated that TREM2 becomes upregulated with disease progression and amyloid accumulation (Frank et al., 2008; Jay et al., 2015; Matarin et al., 2015), making them useful models for examining the role of TREM2 in AD. Studies aiming to explore the link between TREM2 and AD pathogenesis have employed these different AD mouse models combined with partial and total depletion of TREM2. One study demonstrated that TREM2 deletion leads to impaired microglial clustering around amyloid plaques and lowered amyloid accumulation, evidenced by reduced plaque area and number in APP/PS1xTREM2$^{-/-}$ mice early in pathology (at 4 months of age) (Jay et al., 2015). Interestingly, the opposite effect was found at later stages of pathology when TREM2 depletion resulted in enhanced amyloid load. In particular, in their study, Wang et al. (2016) reported no change in plaque load at moderate stages of pathology in 5xFADxTrem2$^{-/-}$ mice, while they observed increased accumulation of amyloid at advanced stages. Interestingly, partial deletion of TREM2 in 5xFADxTREM2$^{+/-}$ resulted in an intermediate phenotype, confirming that TREM2 levels directly impact on amyloid burden late in pathology (Wang et al., 2015). These findings were echoed in the APPPS1-21 model by Jay et al. (2017) who further showed that at 2 months, when there is limited plaque load, TREM2 depletion leads to reduced plaque size and area, while at the more advanced stage of 8 months, its knock out has the opposite effect. From these studies it could be argued that TREM2 has stage-dependent effects on amyloid burden, where it contributes to greater Aβ deposition early in pathology, while resulting in ameliorated Aβ in later stages. In fact, this stage-dependent effect on amyloid pathology is similar to the one observed in microglial depletion studies as discussed above, which suggests that TREM2 was likely one of the drivers for the effects observed in these studies.

1.5.7 TREM2 and the microglial response in AD

It has previously been demonstrated that AD patients with the *TREM2*^{R47H} mutation exhibit defective microglial transcriptional activation (Zhou et al., 2020), which demonstrates the requirement for TREM2 for a switch to a reactive phenotype. Although the same study also showed the very different signatures of activated microglia in mice when compared to humans, it is interesting to note that both are reliant on TREM2 signalling, suggesting that studies on TREM2 are able to elucidate

some of the mechanisms involved in human AD. Importantly, TREM2 has been suggested to act as an immune sensor for microglia to detect surrounding damage and in line with this, a number of studies in AD models have indicated that microglia with dysfunctional TREM2 are unable to sense and become attracted to amyloid plaques, thus impairing their ability to cluster around and form a potential protective barrier to limit the spread of Aβ toxicity (Ulrich et al., 2014; Wang et al., 2015; Yuan et al., 2016). Interestingly, in their study Yuan et al. (2016) showed that the microglial processes which specifically envelop amyloid deposits are enriched in TREM2 and that TREM2 deficiency disrupts this process, as well as microglial clustering around plaques, in turn resulting in enlarged amyloid plaque area and increased axonal dystrophy. More recently, Lee et al. (2018) demonstrated that when TREM2 levels are increased in 5xFAD mice expressing human TREM2, both soluble and insoluble Aβ levels are reduced, plaque burden is ameliorated, and plaques appear more compact, illustrating an important role of TREM2 in maintaining the barrier formation function of microglia. The same study also reported that with increased TREM2 expression, microglia are more likely to express disease-associated genes, upregulate phagocytic markers such as CD68 and Lgasl3, and exhibit phagocytic activity, creating an interesting link between TREM2 and microglia phagocytosis in an AD context (Lee et al., 2018).

Taking this a step further, with the hope of elucidating the specific role of the AD-associated TREM2 variants in disease progression, research groups have recently generated mice expressing *Trem2* with the R47H variant. The first study to use such a model *in vivo* was the study by Song et al. (2018) who created 5xFAD mice expressing human *Trem2*^{R47H} using bacterial artificial chromosome (BAC) transgenes. They reported that the R47H variant confers a loss of function in microglia, as it was shown to impair microglial recruitment to amyloid plaques and reduce microgliosis. The authors observed reduced microglial density in both the cortex and hippocampus, as well as reduced expression of cortical activation markers (i.e. Cst7, Spp1, and Gpmnb) and inflammatory cytokines (i.e. TNFα and IL6) in the presence of the R47H variant (Song et al., 2018). The same study also demonstrated that soluble human TREM2 co-localises with neurons and plaques in mice carrying the common variant of human TREM2, suggesting that TREM2 might be used for recognising damaged neurons. Interestingly, this ability is impaired in *Trem2*^{R47H} mice, illustrating an important

interaction between Aβ and soluble TREM2 (Zhong et al., 2018), which appears to be impaired in R47H carriers. Following this, using CRISPR/Cas9, Cheng-Hathaway et al. (2018) knocked in the R47H variant in murine TREM2 and crossed these mice with the APP/PS1 model. They reported similar effects to Song et al. and specifically, a reduced number of plaque-associated microglia and that of compact plaques in APP/PS1x*Trem2*$^{R47H+/-}$ mice, illustrating that the R47H confers a loss of function for TREM2, significantly affecting the normal functioning of microglia (Cheng-Hathaway et al., 2018). Interestingly, they also demonstrated that in mice, but not in humans (Ma et al., 2016), the R47H variant leads to reduced *Trem2* mRNA levels due to altered splicing, suggesting that the observed effects in the study by Cheng-Hathaway et al. could be due to the partial reduction in TREM2 levels in addition to the variant itself. Similar findings, including reduced microglial density and downregulated *Trem2* expression, were also found in another *Trem*^{R47H} model (*Trem2*^{R47H} knock-in mice carrying the R47H point mutation) (Liu et al., 2020; Xiang et al., 2018), raising questions as to what the driving factor for the effects observed in these studies is.

More recently, to avoid the above problems, *Trem*^{R47H} knock-in rats were created (Ren et al., 2020b; Tambini and D'Adamio, 2020), which do not exhibit reduced *Trem2* levels and produce human Aβ under the endogenous rat *App* promoter, and hence, constitute a good model for exploring the specific effects of the R47H variant. In the presence of the R47H variant, rats exhibit enhanced TNFα levels in the brain, reduced LTP, and augmented glutamatergic transmission, evidenced by increased frequency and amplitude of mEPSCs (Ren et al., 2020b). Interestingly, these effects were reversed upon the addition of neutralising TNFα antibodies, suggesting that the effects of TREM2^{R47H} on transmission are primarily driven by its effects on increased TNFα concentrations and potentially by the increased AMPAR exocytosis previously shown to be caused by increased TNFα (Beattie et al., 2002; Stellwagen and Malenka, 2006). Furthermore, the change in mEPSC frequency was accompanied by no change in paired-pulse facilitation, but also by an enhanced AMPAR-mediated response (Ren et al., 2020b), suggesting that it might be driven by postsynaptic effects and specifically, by insertion of AMPARs and hence enhanced postsynaptic densities. As previous work has also shown that TREM2 deletion can increase the frequency of mEPSCs (Filipello et al., 2018), the R47H-mediated effects on transmission might also be

driven by a loss of function of TREM2 and specifically, by the impaired synapse elimination by microglia.

1.5.8 TREM2 and tau

In addition to exploring the effects of TREM2 on amyloid, previous work has tried to elucidate a mechanism which links TREM2 and its variants to amyloid pathology and tau aggregation. In fact, a recent study in APP/PS1 mice, which were additionally injected with human tau and made to express human TREM2, showed that tau pathology is accelerated and microglial recruitment to plaques is impaired when the R47H variant is introduced (Leyns et al., 2019). This effect is similar when human *Trem2* is knocked out, indicating that R47H might confer a loss of function for TREM2 (Leyns et al., 2019). Accelerated tau pathology in these models is also mimicked by microglial ablation (Gratuze et al., 2021), suggesting that TREM2-dependent activation of the DAM phenotype is key for delaying Aβ-induced tau spreading. These results are in line with recent work showing that tau propagation is accelerated upon TREM2 deletion but, interestingly, this effect is only observed when amyloid pathology is present in TauPS2APP mice and not in the tau model P301L (Lee et al., 2021). This showcases the important interaction between TREM2-expressing microglia, amyloid and tau, and indicates that TREM2 slows down disease progression by restricting the degree to which amyloid facilitates the spread of tau (Hardy and Salih, 2021). Therefore, microglia are suggested to play a crucial role in mitigating against amyloid-induced tau pathology, with TREM2 being an important sensor regulating this function. However, one study in P301Sx*Trem2*^{R47H} mice reported attenuated brain atrophy, reduced synapse loss, as well as microgliosis, arguing that TREM2^{R47H} has the opposite effect to the one argued previously (Gratuze et al., 2020). Moreover, these effects were accompanied with reduced C1q levels in synapses, suggesting that the R47H variant in this case appears to have reduced microglial phagocytosis in turn reducing brain atrophy (Gratuze et al., 2020). The authors argue that at this stage of AD pathology, the R47H variant is protective as its loss-of-function effects on TREM2 make microglia less able to eliminate aberrant synapses, limiting the damage to neighbouring neurons. This is plausible given that although phagocytosis could be protective against spread of toxicity, when it is excessive it could be damaging to neuronal networks.

Altogether, the above studies demonstrate a crucial role for microglia and normal TREM2 functioning in AD pathogenesis. It could be hypothesized that microglial activation early in pathology might be protective as it regulates the toxicity of Aβ through the formation of a protective barrier and the compartmentalisation of plaques, and it also allows for the elimination of dystrophic synapses, keeping the damage associated with Aβ local and not allowing its spread to the rest of the network (see Figure 1.6). In comparison, later in pathology their inflammatory signals might become dysregulated, leading to the enhanced release of inflammatory cytokines such as TNFα and IL6, and their synaptic elimination might become extensive or insufficient, in turn resulting in exacerbated neuronal loss, contributing to plaque toxicity and degeneration in AD contexts (Edwards, 2019; Hansen et al., 2018).

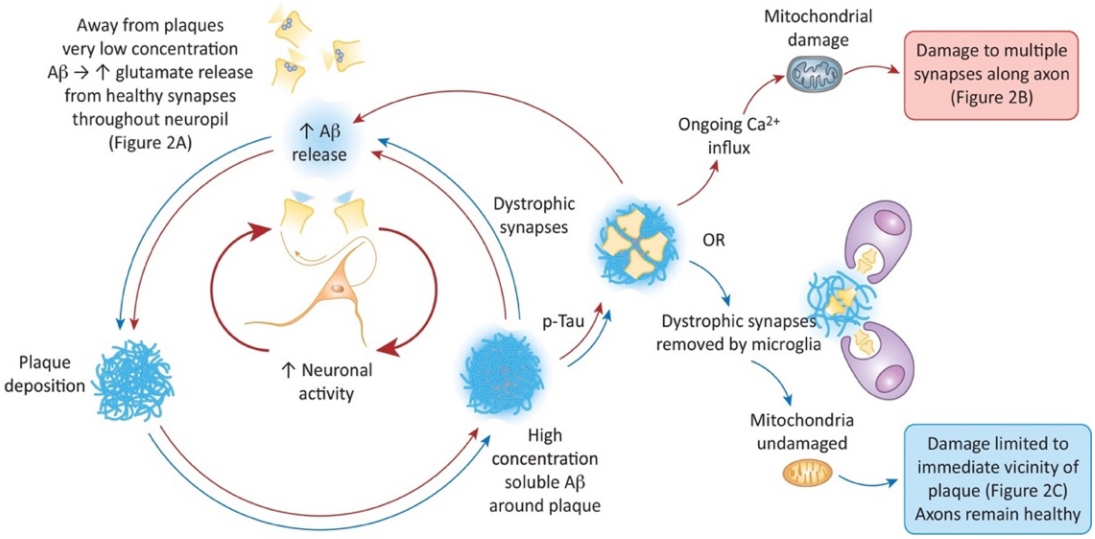

Figure 1.6. Early effects of Aβ release on microglia and synapses in AD.
Aβ is released in an activity-dependent manner during normal neuronal activity and results in an increased glutamate release and further release of Aβ. In AD, as plaques begin to grow and deposited Aβ forms a cloud around plaques, synapses in the vicinity of plaques begin to get damaged. As a result, microglia are recruited to the pathological plaques and phagocytose synapses in their vicinity in order to limit the spread of damage to other synapses. Figure taken from Edwards (2019).

1.5.9 Astrocytes in the healthy brain

Astrocytes are the most abundant glial cell type in the brain and they have a number of physiological functions within the central nervous system, including ion

homeostasis, neurotransmitter reuptake, gliotransmission, inflammation, and maintenance of the blood brain barrier (Iglesias et al., 2017; Magistretti and Allaman, 2015; Parpura et al., 1994; Pascual et al., 2005; Porter and McCarthy, 1996). Similar to neurons and microglia, astrocytes are functionally and morphologically diverse across neuronal networks (Ben Haim and Rowitch, 2017; Khakh and Sofroniew, 2015), illustrating their ability to sense and continuously adapt to their environment. In recent years, it has been widely accepted in the literature that astrocytes are not solely passive players in the nervous system but have an active role at the synapse, forming the so-called tri-partite synapse, consisting of the pre- and post-synaptic neuron, as well as surrounding astrocytes. The perisynaptic astrocytic processes of astrocytes tightly ensheath the synapse and express functionally relevant membrane proteins, including the glutamate transporters GLT-1 and GLAST for the reuptake of glutamate released at the synapse, but also cannabinoid receptors (CB1R), purinergic P2Y1 receptors, β_2 adenoreceptors, α7 nicotinic acetylcholine receptors (α7nAChRs), AMPARs, NMDARs, and metabotropic glutamate receptors (mGLURs) (MacVicar et al., 1989; Seifert et al., 1997; Teaktong et al., 2003; Ziak et al., 1998). Through these they can actively sense synaptic activity evidenced by astrocytic Ca^{2+} elevations in response to neuronal activity. In turn, astrocytes can release a number of gliotransmitters, such as glutamate and D-serine, to modulate synaptic activity. Furthermore, astrocytes are also able to release neurotrophic factors, such as transforming growth factor-β (TGFβ), which can regulate synaptogenesis, neuronal survival and neuronal differentiation. Interestingly, in the retina, the release of TGFβ from astrocytes results in the upregulation of C1q in neighbouring synapses, illustrating a role for astrocytes in regulating microglia-mediated phagocytosis (Bialas and Stevens, 2013). It is clear that astrocytes are important players regulating normal neuronal activity which raises the question as to how they can be affected under disease conditions.

1.5.10 Astrocytes in AD

Astrocytes are also known to go into an activation state in response to inflammation in disease contexts. Specifically, they become reactive, which has traditionally been characterised by increased glial fibrillary acidic protein (GFAP) expression, and undergo astrogliosis (Sofroniew, 2009; Wilhelmsson et al., 2006). Astrocyte

activation can result in different phenotypes which classically have been characterised into A1/A2, or neurotoxic/neuroprotective, although recent work suggests the existence of more than two types of astrocytes, making this classification particularly limiting in explaining the different astrocytic signatures (Escartin et al., 2021). Nonetheless, pro-inflammatory astrocytes upregulate classical complement cascade genes, such as *C3*, and *Serpina3n*. During CNS inflammation, astrocytes become attracted to the site of damage and their pro-inflammatory response is initiated through the activation of their nuclear factor κ-light-chain-enhancer of activated B cells (NFκB) heterodimer triggered by the release of cytokines, such as IL-1β, C1q, and TNFα, from microglia, as well as other cell types (Linnerbauer et al., 2020). The above interaction between microglia and astrocytes during inflammation has also recently been illustrated in one study which showed that the LPS (lipopolysaccharide)-induced activation of microglia is necessary and sufficient to induce astrocytic activation (Liddelow et al., 2017). These astrocytes release a neurotoxin which is detrimental to surrounding neurons and oligodendrocytes, while they also lose their ability to support synapses and perform their homeostatic functions. More recently, activated microglia were shown to play a similarly important role for astrocyte activation during normal ageing (Clarke et al., 2018), raising questions as to how this is affected in an AD context.

Similarly to microglia, astrocytes cluster around amyloid plaques in both post-mortem tissue from AD patients, as well as AD mice (Henstridge et al., 2019; Sofroniew, 2005, 2009; Wegiel, 2001; Wyss-Coray et al., 2003). In the APP/PS1 model, astrocytes also exhibit a global elevation in intracellular Ca^{2+} (Kuchibhotla et al., 2009), suggesting that the AD environment can induce a global phenotypic change in astrocytes which is independent of plaque location. However, more recent work has demonstrated that the Ca^{2+} elevations in astrocytes are in fact exacerbated in the vicinity of plaques and are triggered by the activation of their P2Y1 receptors, suggesting that purinergic signalling is essential for astrocyte activation in AD conditions (Delekate et al., 2014; Wilhelmsson et al., 2006). Yet, whether the role of astrocytes in these regions is beneficial remains to be explored.

Under inflammatory conditions, astrocytes are able to express components which are required for Aβ production, including APP, BACE-1, and γ-secretase, suggesting that

they might be involved in Aβ generation (Grolla et al., 2013; Zhao et al., 2011). However, there have also been suggestions that astrocytes are responsible for clearing Aβ deposits as both the incubation of astrocytes with $A\beta_{1-42}$ in primary cultures and the addition of astrocytes to brain slice cultures resulted in reduced Aβ area (Wyss-Coray et al., 2003). In APP/PS1 mice, genetic depletion of GFAP and vimentin, both of which are necessary for astrocyte activation, was shown to reduce the number of plaque-associated astrocytes, increase plaque load, and exacerbate neuritic dystrophy (Kraft et al., 2013). Although two subsequent studies found no effect of astrocyte removal on plaque load (Kamphuis et al., 2015; Katsouri et al., 2020), through the ablation of GFAP-expressing reactive astrocytes only, the latter study found reduced synaptic and neuronal density, as well as an increase in Aβ monomers in the APP23 model, which was argued to be due to reduced degradation and clearance of Aβ. This idea is plausible as astrocytes can produce the Aβ-degrading enzymes neprisylin, insulin-degrading enzyme (IDE), and endothelin-converting enzyme, as well as the chaperons APOE and clusterin, thereby suggesting that they might be directly involved in Aβ clearance (Ries and Sastre, 2016). This has been further supported by a recent study which showed that the removal of astrocytes in OHSCs from 5xFAD mice using the L-AAA compound, which binds to the cysteine glutamate antiporter solely expressed in astrocytes, results in increased levels of $A\beta_{40}$ and $A\beta_{42}$ and reduced levels of the Aβ-degrading enzymes neprisylin and IDE (Davis et al., 2021). Interestingly, the same study also found reduced spine number, alterations in microglial morphology, as well as an increase in IL-6 levels in both wild-type and AD mice upon astrocyte reduction, suggesting that astrocyte removal might have an effect on synaptic activity and also increase the proinflammatory profile of other cell types in organotypic slices independent of the Aβ environment (Davis et al., 2021).

The above link between astrocytes and synapses has also been reported in another study in astrocyte-neuron co-cultures which showed that disinhibition of NFκB signalling in astrocytes triggers the release of C3 which in turn reduces dendritic and spine morphology, as well as spine number by binding to neuronal C3a receptors (Lian et al., 2015). This was also shown to have an effect on excitatory synaptic activity, evidenced by reduced LTP, greater calcium elevations in neurons, and enhanced mEPSC amplitudes, all of which are rescued upon the addition of a C3aR antagonist

(Lian et al., 2015). Given that NFκB activation and C3 expression in astrocytes is a well-known process shown to occur in AD conditions, this study provides some interesting insight as to how astrocytic activation, in addition to microglia, can affect synaptic function during disease progression. Alternatively, it has also been reported that the addition of Aβ to hippocampal slices can activate astrocytic α7nAChRs (to which Aβ has been shown to bind (Wang et al., 2000)) and trigger the release of astrocytic glutamate (Talantova et al., 2013). This in turn binds to extrasynaptic NMDARs on neurons and results in reduced frequency of mEPSCs, synaptic depression, and spine loss, suggesting presynaptic changes and an additional mechanism through which astrocytic activation can lead to some of the synaptic alterations seen in AD.

Altogether the above studies demonstrate that astrocytes play an important role in AD progression, although whether their role is protective or detrimental to neurons and synapses remains to be established due to the particularly limited research in this area. Yet, similarly to microglia, astrocytes seem to have a key function in regulating plaque load and synaptic activity which could be accomplished through the release of pro-inflammatory mediators or gliotransmitters, or through their potential role in degrading Aβ.

1.6 Mouse models of AD

The discovery of mutations which directly lead to the production of amyloid plaques and tau tangles has led to the development of animal models which are able to recapitulate AD pathology at different stages of the disease. In fact, there are currently more than 190 mouse models used in Alzheimer's research (Alzforum, 2021). Although none of these are able to fully recapitulate AD and each has their limitations, they have still provided valuable insight into the mechanisms involved in AD.

1.6.1 Transgenic mouse models

AD transgenic mouse models aim to recapitulate AD pathology through the overexpression of proteins which are associated with the disease, such as mutant APP, PSEN-1 and -2, APOE, and TREM2 (Hall and Roberson, 2012). Most of the mouse models overexpressing APP exhibit plaque accumulation at early ages, for instance by

11-13 months in Tg2576 mice (carrying the APP Swedish mutation) (Hsiao et al., 1996) and by 5-7 months in the commonly used J20 mice (carrying the Swedish and Indiana APP mutations) (Mucke et al., 2000). Although these models reproduce the pathology seen in humans as they show noticeable amyloid plaque accumulation, they do have several limitations which are worth noting, with one of them being the overexpression paradigm. In order to get the desired Aβ pathology in mice, random insertions of the gene are automatically performed, and the number of gene copies of *App* is drastically increased. In turn, this leads to the accumulation of peptides derived from the *App* sequence which are different from Aβ, and the functions of these, as well as that of APP, such as its role in synaptic function (Kamenetz et al., 2003), become affected in addition to the Aβ peptide. Therefore, conclusions reached in such models end up being particularly varied, uncertain, and hard to interpret (Sasaguri et al., 2017). Furthermore, in addition to increased Aβ accumulation, it has been suggested that Aβ degradation can also be affected in sporadic AD cases (Hellstrom-Lindahl et al., 2008; Iwata et al., 2002; Mawuenyega et al., 2010). This is not well addressed in the aggressive overexpression mouse models, highlighting the necessity to find a model which also recapitulates the preclinical phase leading up to LOAD development.

Perhaps the biggest caveat of the above models is that mice transgenic for *App* only address a part of AD pathology and although show limited tau phosphorylation and modest cell loss at later ages, they do not exhibit NFT formation or extensive neuronal loss – two pathologies which are crucial for AD pathogenesis with the former being very closely linked to cognitive impairment in humans (Arriagada et al., 1992; Bejanin et al., 2017). Efforts to recapitulate this pathology have been made by combining models, for instance, by creating the widely used APP/PS1 (carrying the APP Swedish and a PSEN-1 mutations) and 5xFAD (carrying the APP Swedish, London and Florida and two PSEN-1 mutations) models which begin Aβ accumulation at 6 weeks and 2 months respectively (Oakley et al., 2006; Radde et al., 2006). Despite prominent cognitive deficits, synapse loss, electrophysiological changes, and gliosis observed at early ages in these mice (Bittner et al., 2012; Gengler et al., 2010; Oakley et al., 2006), they do not exhibit hyperphosphorylated tau deposition, again demonstrating a limitation of using such models. To address this problem, models which include a mutation in tau in addition to *App* were developed, for instance the Tg2576/Tau(P301L) model (Lewis et al., 2001) and the 3xTg model, which

overexpresses APP, PSEN-1 and MAPT (which encodes for tau) (Oddo et al., 2003), and these mice do show tau pathology, amyloid plaques, and some neurodegeneration. Furthermore, models which aim to mimic tau spread in the human brain have also been developed, with one example being the TgtauEC model, in which mutant tau is preferentially expressed in the entorhinal cortex and spreads to neighbouring brain regions (de Calignon et al., 2012), illustrating how tau can be transmitted through different circuits in the human brain. However, one big limitation of these tau models is the fact that no mutations in tau have been associated with AD, with tau pathology believed to be occurring as a result of Aβ accumulation rather than independently as it does in these models. Therefore, efforts have been made to recapitulate how human tau acts in AD, with some studies using AD models in which endogenous mouse tau is knocked out and replaced with human tau (Pickett et al., 2019; Tulloch et al., 2021). These mice exhibit a hyperactive phenotype and a downregulation of synaptic genes, both of which are suggested to be triggered by the interaction between Aβ and tau in these models (Pickett et al., 2019). Altogether these models provide good mechanistic insight into the interaction between Aβ and tau in the AD brain, yet their conclusions should be taken with caution as they could be caused by the overexpression paradigm employed in the generation of transgenic mice.

1.6.2 *App* knock-in models

To address the issues associated with transgenic models, the *App* knock-in mice were developed. In these mice, the murine Aβ sequence is humanized by altering three amino acids which differ between mice and humans (Saito et al., 2014). This second generation of mice harbour primarily either two or three mutations in the *App* gene. The line carrying two mutations in the Aβ sequence, the $App^{NL\text{-}F}$ mice, carries the Swedish (NL) and Iberian/Beyreuther (F) mutations which increase the production of $Aβ_{40}$ and $Aβ_{42}$ and the ratio between $Aβ_{42}/Aβ_{40}$ levels respectively, together resulting in increased levels of $Aβ_{42}$ (Saito et al., 2014). These $App^{NL\text{-}F}$ mice first begin to show plaque accumulation at about 9 months of age, making them a good model for examining changes which occur early in AD pathology. This model also exhibits microgliosis at 24 months of age, when there is an advanced plaque load (Benitez et al., 2021).

The Saido group developed a second line, the *App*$^{NL-G-F}$ mice, which in addition to the above mutations also harbour the Arctic mutation (G) that induces a conformational change in the Aβ sequence, thereby leading to an increased Aβ oligomerization and fibrillation. As a result, these mice show a more accelerated and aggressive AD phenotype, developing plaques around 2 months of age (see Figure 1.7 below). Hence, the *App*$^{NL-G-F}$ mice serve as a good model for examining later, post-plaque changes occurring in the mouse brain. Similarly to *App*$^{NL-F}$ mice, this model exhibits microgliosis at more advanced stages of pathology, with the earliest increases in the area occupied by astrocytes (visualised using GFAP) and microglia (visualised using IBA1 – ionized calcium binding adaptor molecule 1) observed at 6 months of age in the cortex and at 9 months in the hippocampus (Benitez et al., 2021; Masuda et al., 2016; Mehla et al., 2019).

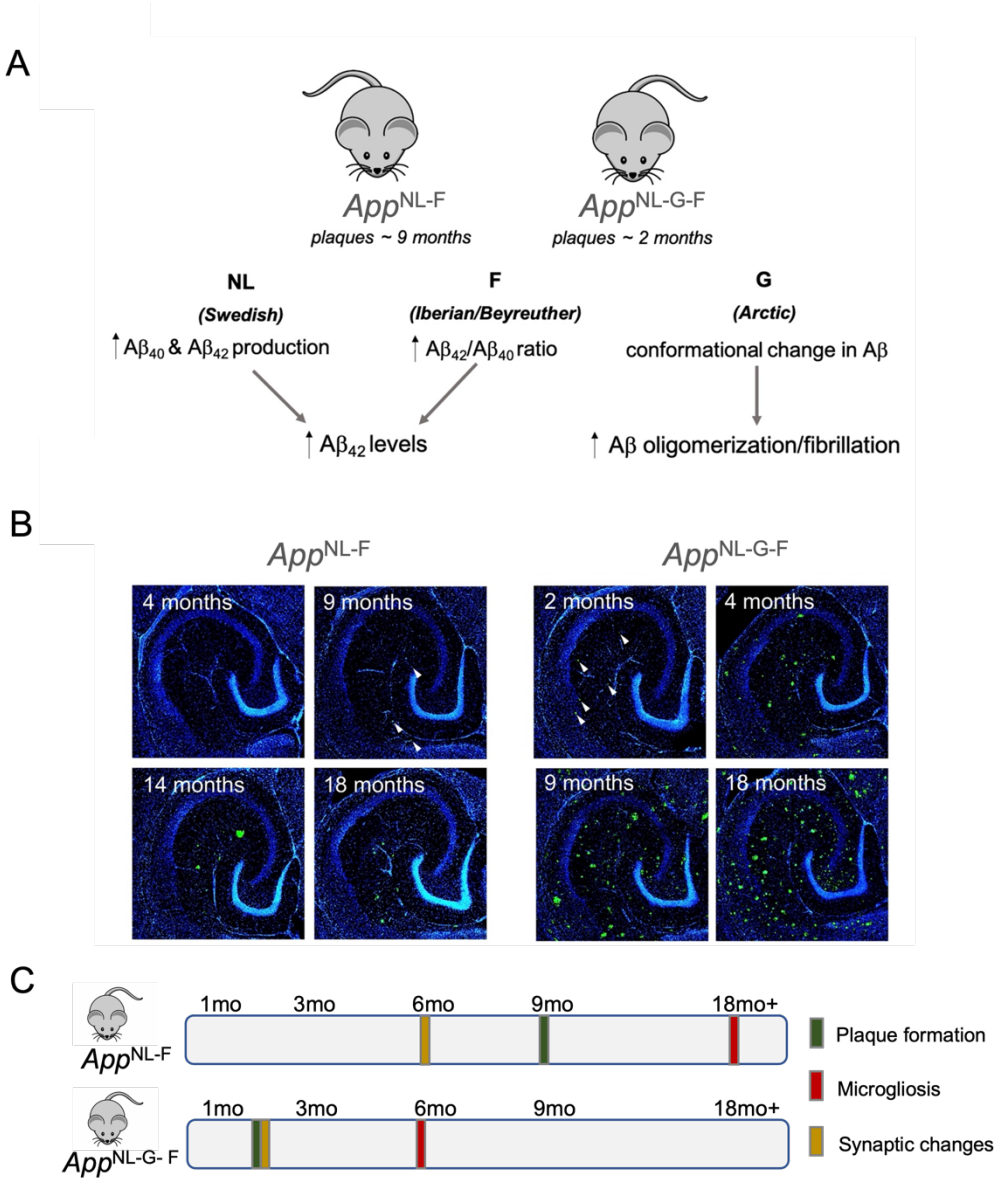

Figure 1.7. *App* knock-in models of AD.
(A) The Swedish (NL) mutation is adjacent to the β-secretase cleavage site of APP and results in the increased production of $A\beta_{40}$ and $A\beta_{42}$. The Iberian/Beyreuther (F) mutation instead affects the γ-secretase cleavage site on APP, thereby resulting in increased $A\beta_{42}/A\beta_{40}$ ratio. Together these two mutations lead to the increased levels of overall $A\beta_{42}$. The Arctic (G) mutation additionally confers a conformational change in the Aβ sequence, leading to its increased propensity for oligomerization and fibrillation and the generation of the more aggressive *App*$^{NL\text{-}G\text{-}F}$ model. **(B)** Representative images showing the progression of plaque accumulation (green) in the hippocampus of *App*$^{NL\text{-}F}$ at 4, 9, 14, and 18 months and *App*$^{NL\text{-}G\text{-}F}$ mice at 2, 4, 9, and 18 months. Arrows point at plaques at first stages of pathology. Figure adapted from Benitez et al. (2021). **(C)** Summary of the age at which plaque pathology, microgliosis and synaptic changes first occur in *App* knock-in mice

The *App*$^{NL-G-F}$ mice exhibit a somewhat abnormal behavioural phenotype, with studies pinpointing only subtle changes in social and anxiety-related performance at 3 months of age before prominent plaque pathology is observed in these mice (Latif-Hernandez et al., 2019). The emergence of cognitive deficits and anxiotic-like behaviour has been reported to occur around 6 months of age (Masuda et al., 2016; Mehla et al., 2019; Sakakibara et al., 2018), and these are accompanied with deficits in exploratory behaviour and reduced memory for familiar objects (Pauls et al., 2021; Whyte et al., 2018). This suggests that Aβ accumulation leads to alterations in synaptic circuitry which can have a direct effect on behaviour. At 9 months of age, these mice also exhibit impaired motivation in a progressive ratio task which was suggested to be caused, at least in part, by the reduced dopamine transporter levels observed in these mice (Hamaguchi et al., 2019). On the other hand, *App*$^{NL-F}$ mice exhibit a more modest behavioural phenotype, most likely due to the less accelerated Aβ pathology. However, one study did observe impaired Morris water maze performance at the age of 3 months, 6 months before plaque pathology is observed in this model, suggesting that there are some early alterations in neuronal connectivity arising from increases in soluble Aβ (Shah et al., 2018). This is in accordance with the findings from another study which showed that at 3 months of age, the proteome and proteins specifically involved in synaptic function are altered in *App*$^{NL-F}$ mice (Schedin-Weiss et al., 2020).

In terms of synaptic changes, recent work from our lab has demonstrated that in both the *App*$^{NL-F}$ and *App*$^{NL-G-F}$ models, changes in the frequency of sEPSCs arise during moderate and even advanced plaque pathology and specifically, at 9 and 20 months for the *App*$^{NL-G-F}$ and *App*$^{NL-F}$ model respectively (Benitez et al., 2021). In contrast, alterations in paired-pulse ratios are also observed prior to or at early stages of pathology, suggesting increased probability of glutamate release potentially (see Figure 1.7C) triggered by increases of soluble Aβ occurring at that stage (Latif-Hernandez et al., 2020). While no changes in LTP were observed in the same work, another study by Latif-Hernandez et al. (2020) found impaired LTP induction at 6-8 months in *App*$^{NL-G-F}$ mice. This discrepancy between the two studies could have arisen from the *App*^{NL} model, which also exhibits elevated soluble and insoluble Aβ levels compared to wild types, used as a control in the latter study, or because of the use of a different LTP induction paradigm. The same study also found increased frequency of both mIPSCs and mEPSCs in *App*$^{NL-G-F}$ mice at 6-8 months, suggesting altered

presynaptic activity at advanced stages of pathology (Latif-Hernandez et al., 2020). Some of the observed changes in these studies could be explained by the alterations in presynaptic proteins observed in a recent study. Both *App*$^{NL-F}$ and *App*$^{NL-G-F}$ mice exhibit impaired presynaptic protein turnover at 6 months of age compared to *App*^{NL} mice, illustrating the presynapse as particularly vulnerable at these early stages, providing more support for the findings of previous studies (Benitez et al., 2021; Hark et al., 2021). Interestingly, these changes in presynaptic proteins were no longer observed at 12 months of age, which the authors argued to be due to the loss of synapses at this age. Another study also found increased density of dendritic but reduced number of mushroom spines in *App*$^{NL-F}$ mice at 6 months of age (Zhang et al., 2015). The authors argued that this effect was caused by the binding of extracellular $A\beta_{42}$ to mGluR5 receptors in *App* knock-in mice, which triggers a series events ultimately leading to reduced CaMKII (Ca^{2+}/calmodulin-dependent protein kinase II) activity, destabilisation and loss of mushroom spines (Zhang et al., 2015).

The table below (Table 1.1) provides a summary of the main phenotypes observed in these *App* knock-in mice as elucidating the early gliosis and synaptic changes occurring in response to the AD pathology found in these mice was a primary focus of the present study. The table also provides a summary of the *Trem2*^{R47H} model which was additionally used in the present work in order to understand how a perturbed microglial response affects any of the observed changes in *App* knock-in mice. As mentioned above, although these models avoid the problems associated with the *App* overexpression found in transgenic mice, it is important to highlight that they do have their limitations. In particular, these models are not able to develop tau tangles, similarly to transgenic mice, making them useful models for2 understanding only the early processes in human AD which occur prior to tau tangles. However, it is important to note that more than two decades are required for tau pathology to form in humans (Bateman et al., 2012), and hence the age until which mice live could be the main constraint for observing this pathology. Furthermore, although the $A\beta_{42}/A\beta_{40}$ ratio in these mice is much higher than the ratio found in humans (Baiardi et al., 2019; Hellstrom-Lindahl et al., 2009; Karran et al., 2011; Saito et al., 2014; Steinerman et al., 2008), likely because of the presence of several mutations within the *App* sequence rather than just one as it is usually found in the brain of patients with familial AD. The fact that these models possess two or three mutations within the *App* sequence

additionally makes them particularly different from the human brain as there are no reports of humans carrying these mutations together. Lastly, the *App*$^{NL-G-F}$ model develops plaque pathology much faster than what is expected in humans, with plaque pathology appearing as early as 2 months of age (Saito et al., 2014). This is likely caused by the Artic mutation found in these mice which makes Aβ particularly prone to aggregate. Although using such an aggressive model reduces the costs associated with studies, the quick accumulation of plaques might not allow for processes dependent solely on soluble Aβ oligomers to take place, thereby questioning the relevance of using such a model. Nonetheless, exploring *App*$^{NL-G-F}$ mice can still provide important and direct insights into how the formation of plaques affects glial responses and synaptic transmission, making it a more relevant model than transgenic models. Altogether these *App* knock-in models are useful to suggest early, preclinical changes that occur in AD which are dependent on soluble Aβ oligomers and plaque formation, making them good models for the present work.

Table 1.1. Summary of key findings in *App* knock-in models and *Trem2*^{R47H} mice.

	***App*$^{NL-F}$**	***App*$^{NL-G-F}$**	***Trem2*^{R47H}**
Plaque pathology	*Benitez et al. (2021); Saito et al. (2014)* • Mice begin forming plaques around 9 months of age with moderate plaque accumulation at 18 months • Plaque formation begins in the cortex with plaques primarily made up of $A\beta_{42}$ species • Higher levels of soluble and insoluble Aβ than *App*$^{NL-G-F}$ mice even at 2 months of age	*Benitez et al. (2021); Saito et al. (2014)* • Mice begin forming plaques around 2 months of age with moderate plaque accumulation at 4 months and heavy plaque accumulation at 9 months of age *Michno et al. (2021); Saito et al. (2014)* • Plaque formation begins in the cortex; the plaque core which is made up of $A\beta_{40}$ is formed first, followed by $A\beta_{42}$ accumulation around that core *Latif-Hernandez et al. (2020)* • Increased soluble $A\beta_{42}/A\beta_{40}$ ratio before plaque formation at 1 months; insoluble $A\beta_{40}$ increases drastically at 6 months, while insoluble $A\beta_{42}$ increase in an age-dependent manner starting from 1 month	*Liu et al. (2020)* • No plaque pathology
Gliosis	*Benitez et al. (2021)* • Increased number of microglia compared to wild-types at 24 months of age; no change in *Trem2* expression even at that stage *Saito et al. (2014)* • Increased microglial area ($Iba1^+$) at 18 months	*Benitez et al. (2021)* • Increased number of microglia and *Trem2* expression per microglia compared to wild-types at 9 months *Saito et al. (2014)* • Increased microglial area (Iba^+) at 6 months of age *Mehla et al. (2019)* • Increased astrogliosis (GFAP area) with age, starting at 6 months in the cortex and 9 months in the hippocampus	*Liu et al. (2020); Xiang et al. (2018)* • Reduced mRNA and protein expression of *Trem2* in primary neurons from young mice • Reduced number of phagocytic ($CD68^+$) microglia compared to wild-types

Synaptic changes	*Hark et al. (2021)* • Reduced turnover of presynaptic proteins including SNAP25, VAMP1 and STX1B compared to *App*^{NL} mice before plaque accumulation (6 months) and reduced accumulation of these at 12 months *Benitez et al. (2021)* • Reduced sEPSC frequency compared to wild-types at 20 months • Reduced paired-pulse ratio compared to wild-types at 7 months which continues until 20 months • Reduced paired-pulse ratio during LTP, suggesting a shift to a presynaptic locus of LTP expression *Shah et al. (2018)* • Hypersynchrony between telencephalic neural networks at 3 months of age (6 months before plaque pathology), as measured using fMRI	*Hark et al. (2021)* • Reduced turnover of presynaptic proteins including SNAP25, VAMP1 and STX1B compared to *App*^{NL} mice before plaque accumulation (6 months) and reduced accumulation of these at 12 months *Benitez et al. (2021)* • Reduced sEPSC frequency compared to wild-types at 9 months • Reduced paired-pulse ratio at 2 months compared to wild-types, which is lost at 4 months and observed again at 9 and 20 months • No change in LTP but reduced paired-pulse ratio during LTP, suggesting a shift to a presynaptic locus of LTP expression *Latif-Hernandez et al. (2020)* • Reduced hippocampal LTP formation at 6-8 months (advanced plaque accumulation) when compared to *App*$^{NL-F}$ mice • Increased frequency of mEPSC and mIPSC at 6-8 months compared to *App*$^{NL-F}$ mice

1.7 Summary and present study

It is clear that Alzheimer's disease and the complex mechanisms leading to its development have made it particularly hard for research to discern the specific timeline in which AD events occur. Nonetheless, there is a general consensus about the major players involved in these and specifically, soluble and insoluble Aβ, tau tangles, synapse and neuronal loss, and gliosis, however how these different processes interact remains to be determined. Given that alterations in synaptic activity have on numerous occasions been shown to be one of the earliest noticeable changes in AD, and that microglia could be involved in the phagocytosis of synapses in AD conditions, the present study aimed to explore the link between synaptic activity, Aβ, and microglia using the *App* knock-in models. It specifically aimed to explore the hypothesis that plaque-associated microglia constitute a protective mechanism in AD, wherein they phagocytose damaged synapses around plaques, thereby limiting neuronal dysfunction to keep toxicity local and allowing the normal functioning of intact synapses.

The current study initially aimed to characterise plaque pathology, gliosis, and synaptic transmission changes in the hippocampus of $App^{NL\text{-}G\text{-}F}$ mice at moderate (4-5 months) and advanced stages (7-9 months) of pathology. Here, both male and female mice were examined as several studies have shown sex differences in AD progression. Specifically, it is known that the prevalence of AD is higher in women than in men (Ferretti et al., 2018), with a recent single-cell transcriptomic study revealing large differences in the transcriptional responses between the two genders (Mathys et al., 2019).

$App^{NL\text{-}G\text{-}F}$ mice showed a larger number of smaller-sized plaques with age, suggesting that small plaques are the main driver for the heavier plaque pathology seen at 7-9 months of age. Furthermore, $App^{NL\text{-}G\text{-}F}$ mice also showed similar increases in microglial density compared to wild-type mice at both ages, though no prominent changes were observed in astrocytic density. Examining synaptic transmission changes revealed longer decay times in $App^{NL\text{-}G\text{-}F}$ mice at 7-9 months, illustrating differences in receptor kinetics. Furthermore, to explore how local Aβ specifically affects synaptic transmission, the activity of individual CA3 axons which pass near a plaque was explored in $App^{NL\text{-}G\text{-}F}$ mice by recording from postsynaptic CA1 cells, and

this was compared to that of axons from non-plaque associated regions. Understanding how individual plaques affect the transmission of selected axons in these preparations will provide us with an idea as to whether effects of Aβ on activity is only local and is potentially modulated by microglia in these regions. This study found trends for lower postsynaptic amplitudes only at plaque conditions at 4-5 months of age, indicating that there are plaque-specific effects on postsynaptic activity.

To further examine the specific role of microglia in these regions, 18-month-old *App*$^{NL-F}$/*Trem2*^{R47H} mice, which exhibit a perturbed microglial response, were similarly explored. Results demonstrated that *App*$^{NL-F}$/*Trem2*^{R47H} mice exhibit a larger number of plaques and particularly smaller-sized plaques than *App*$^{NL-F}$ mice. Furthermore, increases in astrocyte density which were observed in *App*$^{NL-F}$ mice were no longer observed in the presence of *Trem*2^{R47H}. Examining spontaneous synaptic activity revealed reductions in the sIPSC amplitude in *App*$^{NL-F}$/*Trem2*^{R47H} compared to *Trem2*^{R47H} mice and a loss of the increased sEPSC frequency found in *App*$^{NL-F}$ mice in the presence of *Trem2*^{R47H}, suggesting altered excitatory/inhibitory balance in *App*$^{NL-F}$ mice in the presence of *Trem2*^{R47H}. Additionally, both *App*$^{NL-F}$ and *App*$^{NL-F}$/*Trem2*^{R47H} mice displayed increased glutamate release in plaque compared to no-plaque conditions, suggesting that these changes are primarily due to surrounding Aβ rather than microglia. Further reductions in postsynaptic amplitudes in plaque conditions were also found only in *App*$^{NL-F}$ mice, showing the necessity for microglia to observe these effects on synaptic activity. Altogether, the results in this work illustrate the dual effects of plaque presence around axons, which are driven by the effects of soluble Aβ on presynaptic release but are also mediated by potential effects of microglia on the postsynapse.

Chapter 2: Methods

All experimental methods were performed in agreement with the United Kingdom Animals (Scientific Procedures) Act 1986, and were under the approval of the Animal Welfare and Ethics Review Board of UCL under the project licence 70/8999.

2.1 Animals

The mice used for experiments were bred and housed in same-sex groups of 2-5 in individually ventilated cages in the Central and Cruciform Biological Services Units at UCL. They were housed under a 12-hour light/dark photoperiod and were kept at a controlled temperature and humidity, with food and water available *ad libitum*. All mice were provided with a shelter made out of cardboard, tubes, and nesting material.

Mice used for the experiments in this work were male and female homozygous *App* knock-in mice (App^{NL-F} or App^{NL-G-F}), homozygous knock-in mice expressing the $Trem2^{R47H}$ mutation, mice homozygous for both App^{NL-F} and $Trem2^{R47H}$ ($App^{NL-F}/Trem2^{R47H}$), or age-matched wild-type C57BL/6J (WT) controls. $Trem2^{R47H}$ knock-in mice were obtained from the Jackson Laboratory (C57BL/6J-Trem2^{em1Adiuj}/J; stock number: 027918, RRID: IMSR_JAX:027918), while *App* knock-in mice were a gift from the Saido group which developed the model (Saito et al., 2014). All knock-in mice were bred on a C57BL/6J background. The age groups used throughout this work are 4-5 months and 7-9 months for experiments involving App^{NL-G-F} mice, and 18 months for experiments involving App^{NL-F} and $App^{NL-F}/Trem2^{R47H}$ mice.

Mice were killed by decapitation and the brain was rapidly extracted. One hemisphere was dropped-fixed in 10% formalin solution and kept at 4°C overnight. This was washed three times using 0.01 M phosphate buffered saline (PBS) and then stored at 4°C in a PBS solution containing 30% sucrose and 0.03% sodium azide until immunohistochemical experiments. The other hemisphere was used for electrophysiological experiments.

2.2 Brain slice preparation for electrophysiology

Acute brain slices were prepared as previously described (Cummings et al., 2015; Medawar et al., 2019). Briefly, following decapitation, the brain was quickly removed from the skull and placed in ice-cold dissection artificial cerebrospinal fluid (aCSF), made up of (in mM): 125 NaCl, 2.4 KCl, 26 $NaHCO_3$, 1.4 NaH_2PO_4, 20 D-glucose, 3 $MgCl_2$, 0.5 $CaCl_2$, with a pH of 7.4 and osmolarity of ~315 mOsm/l. The high concentration of magnesium and low concentration of calcium, as well as the ice-cold nature of the aCSF, were used to reduce the probability of neurotransmitter release and block NMDA receptors, thereby minimizing potential excitotoxicity. After around two minutes, the brain was transferred to a dish, the olfactory bulbs and cerebellum removed, and the forebrain hemisected into two hemispheres. One hemisphere was drop-fixed in 10% formalin for subsequent immunohistochemistry experiments (as described above), whereas the other was cut at the dorsal side at 110 degrees from the midline surface in order to produce slices transverse to the longitudinal axis of the hippocampus. The hemisphere was then glued with superglue to a vibrating microtome stage (Integraslice model 7550 MM, Campden Instruments, Loughborough, UK), submerged in almost frozen dissection aCSF, and transverse slices were cut at 300 μm thickness at a speed of around 15 mm/s.

Following slicing, the hippocampus and a portion of the entorhinal cortex were carefully dissected out from the rest of the tissue using 19G needles and the slices were placed in a chamber perfused with dissection aCSF (bubbled with 95% O_2 and 5% CO_2, BOC Medical) at room temperature (~21°C). On average, 7 hippocampal slices were obtained during this process. After 5 minutes, the slices were warmed up in a heated chamber to 36°C. Slices were then subsequently transferred at 5-minute intervals to chambers filled with aCSF containing (in mM): i) 1 Mg^+, 0.5 Ca^{2+}; ii) 1 Mg^+, 1 Ca^{2+}; iii) 1 Mg^+, 2 Ca^{2+}, all at 36°C. The gradual movement of slices to an increasing concentration of Ca^{2+} and a decreasing concentration of Mg^+ allows for the release probability to return slowly back to normal conditions, without inducing excitotoxicity. This is a critical step for obtaining healthy slices from aged animals. Once slices were transferred to the last chamber containing aCSF with 1 mM Mg^+ and 2 mM Ca^{2+}, they were left to recover for around 40 minutes.

2.3 DiI preparation

In order to allow for the visualisation of individual axons of CA3 pyramidal cells and track back the recorded synapse for plaque presence in *App* knock-in mice, the lipophilic dye DiI (1,1'-dioctadecyl-3,3,3',3'-tetramethyllindocarbocyanine perchlorate) was used. Glass electrodes (1B150F-3 1·5 mm outer diameter × 0·84 mm inner diameter, World Precision Instruments) were pulled using an electrode puller (Model PP-830 Narishige, Japan), achieving electrode resistance of 4-6 MΩ. The lipophilic dye DiI (Biotium, Catalogue number: 60010) was used for axonal labelling and a stock solution containing 2% DiI made up in 100% ethanol was prepared and stored at 4°C. Two drops of this solution were carefully pipetted onto a glass coverslip which was then kept in a slide box at 4°C to prevent dye bleaching. On the day of the experiment, DiI crystals were carefully picked up using a glass electrode. This method allowed for a controlled collection of DiI crystals and made attachment to the electrode easier. The prepared electrodes were used immediately for axonal labelling.

After around 20 minutes in the last chamber filled with aCSF containing 2 mM Ca^{2+} and 1 mM Mg^{+}, each slice was transferred to a patch-clamp rig chamber filled with the same solution. Using infrared-differential interference contrast microscopy on an upright microscope (Olympus BX50WI) with an Olympus 40x infinity corrected 0.9NA water objective and a camera (Hitachi Denshi, Ltd. or C7500-51 Hamamatsu), each side of the slice was examined to determine the health of CA1 pyramidal neurons and hence, the optimal side for dye placement and subsequent patch-clamp recordings. The slice was then placed on a coverslip under an Olympus 5x infinity corrected 0.1 NA air objective to allow for dye loading and 1-2 drops of aCSF were pipetted on top of the slice to prevent slice dehydration and hypoxia. Using a micromanipulator (uMP micromanipulator, Sensapex, Finland or ACCi UI, Scientifica, Clarksburg, NJ), a glass electrode dipped in DiI was directed towards the CA3 area of the hippocampus and the Schaffer collaterals. Two crystals were placed on each slice (see Figure 2.1A) allowing for labelling of CA3 axons along the whole slice area. Slices were then transferred back to the heated chamber, with the side that the dye was placed facing upwards, where the dye was left to spread for ~1.5 hours. After this period, the chamber was positioned at room temperature for around 40 minutes for preparation for patch-clamp recordings.

2.4 Patch-clamp recordings and data acquisition

Following the incubation period, an individual slice was transferred to the patch-clamp rig chamber which was continuously perfused with recording aCSF (flow rate ~2 ml/min) containing (in mM): 125 NaCl, 2.4, KCl, 26 NaHCO3, 1.4 NaH2PO4, 20 D-glucose, 1 $MgCl_2$, 2 $CaCl_2$; equilibrated with 95% CO_2 and 5% O_2, at room temperature (~22°C). Slices were held down using a harp lined with dental floss fibres.

Using a mercury lamp (Olympus, Japan) and a filter (excitation emission: 530-550; detection emission: 570; U-MNG, Olympus, Japan) under a 40x objective, dye spread was initially examined and regions where CA3 axons could be clearly visualised were targeted for placement of the stimulating electrode. Electrodes (model GC150F-7.5, 1.5 mm outer diameter × 0.86 mm inner diameter, Harvard Apparatus Ltd, Edenbridge, UK; or model 1B150F-3 1.5 mm outer diameter × 0.84 mm inner diameter, World Precision Instruments) with a resistance between 4-6.5 MΩ were pulled using an electrode puller (Model PP-830, Narishige, Japan) for electrophysiological recordings.

A stimulating electrode was filled with recording aCSF and was carefully directed towards a clearly visualised axon in the Schaffer collateral region in the *stratum radiatum* using a micromanipulator. Following this, a recording electrode was filled with CsCl-based internal solution containing (in mM): 140 CsCl, 5 HEPES (4-(2-hydroxyethyl)-1-piperazineethanesulfonic acid), 10 EGTA (ethylene glycol-bis(β-aminoethyl ether)-N,N,N′,N′-tetraacetic acid), 2 Mg-ATP, pH 7.4, ~290 mOsm and Alexa Fluor 488 (AF488; 0.2 mg/ml, Invitrogen), used for filling the cells during recordings (see Figure 2.1A). Here, CsCl was used as an internal solution as Cs blocks potassium channels, allowing for little ion leakage and hence good space clamp when patching, and Cl^- allows for the detection of both inhibitory and excitatory events at the holding potential of –70mV. The recording electrode was directed towards the CA1 area of the hippocampus and in close vicinity to the stimulating electrode to allow for minimal stimulation recordings.

Whole-cell patch-clamp recordings of CA1 pyramidal neurons were performed using either an Axopatch 1D (Molecular Devices, Sunnyvale, CA, USA) or MultiClamp 700B (Molecular Devices, Sunnyvale, Cam USA) patch-clamp amplifiers. These were filtered through a low-pass filter at 10kHz followed by 2kHz. Recordings were further

digitized with a sampling rate of either 8.3kHZ or 10kHz (Digidata 1322A, Axon Instruments, CA, USA) and were recorded using the WinEDR and WinWCP softwares (John Dempster, Strathclyde University, UK). Access (<50 MΩ) and membrane resistances (>166 MΩ) were repeatedly monitored throughout the recording by applying –5mV test pulses. Spontaneous currents were recorded using WinEDR version 3.7.2 and evoked postsynaptic currents were acquired using WinWCP version 4.6.1.

2.5 Spontaneous inhibitory and excitatory currents

Continuous recordings were performed at a holding potential of –70mV. Spontaneous inhibitory currents were recorded in aCSF for around 3-5 minutes. Following this, 6μM SR 95531 (HelloBio, Bristol UK), a $GABA_A$ receptor antagonist was washed in the aCSF for the remainder of the experiment. Spontaneous excitatory postsynaptic currents (sEPSCs) were then recorded for around 15 minutes.

2.6 Evoked currents

Minimal stimulation recordings were performed in the presence of 6μM SR 95531 to allow for the recording of unitary excitatory postsynaptic currents (uEPSC). These evoked EPSCs are hereby referred to as uEPSC as they are driven by the activation of single synapses as a result of minimal stimulation. A pair of currents were applied once every 10 seconds via the stimulating electrode using a constant voltage (100 μs) stimulator (DS2A-MkII; Digitimer Ltd, UK) triggered by the WinWCP software. The stimulation intensity for uEPSC recordings was determined as the intensity halfway between that which just evokes a response and that which evokes a response double the amplitude of the postulated minimal response (Figure 2.1C). For most experiments, 80 recordings at inter-stimulus intervals of 25 and 50ms were performed. After recording, the stimulation electrode was moved in order to make a small hole in the tissue to allow for easier tracking of the stimulated axon during *post-hoc* imaging.

2.7 Analysis of electrophysiological recordings

All analyses were performed by the experimenter blinded to genotype or plaque presence around the stimulated axon. Spontaneous currents were detected using the WinEDR software and only those responses which had a rise time shorter than 4 ms

and remained at an amplitude above 3 pA for longer than 2 ms were detected as currents. In all conditions, the dead time and the running mean period for the baseline were both set at 10 ms. Once responses were detected using the WinEDR software (version 3.9.1), they were all visually inspected to assure that the rise time was faster than the decay. The inter-event interval was used to determine the instantaneous frequency (1/interval). Responses were then further analysed using the WinWCP software to determine their amplitude which was measured as the magnitude from the average baseline to the maximal negative deflection (an average of 5 digitised points was taken). The amplitude for each recording was then considered as the median of the amplitudes of all events as previous work has demonstrated that the amplitudes of synaptic currents at central synapses do not follow a Gaussian distribution (Edwards, 1995). Then, any complex currents were excluded, and an average trace of the leftover responses was produced. A single exponential curve was fitted to determine the decay time τ (time to decay by $(1 - e^{-1})$ times the peak current).

Evoked responses were analysed using WinWCP (version 5.5.5) The amplitudes of all first and second successful responses were acquired by taking the average of 5 digitised points at the maximal deflection. Failures were considered responses with a deflection of less than 3 pA from baseline at the expected time of EPSC peak and these were considered to have an amplitude of 0. To determine the paired-pulse ratio (PPR), which is an indicator of presynaptic neurotransmitter release, all first and second responses (including failures) were averaged and the PPR was considered as the average amplitude of all 2^{nd} responses over that of all 1^{st} responses. the

2.8 *Post-hoc* analysis of slices from electrophysiological recordings

After patch-clamp experiments, slices were transferred to 2% PFA, in which they were left overnight at 4°C. The next day, slices were washed 3 times in PBS for 5 minutes each, after which they were placed in a PBS solution with 0.03% sodium azide and 30% sucrose. Slices were left in a 24-well plate at 4°C until imaging. In order to visualize Aβ plaques in the slices on which patch-clamp recordings were performed, fixed slices were transferred to a solution containing the amyloid dyes luminescent conjugated oligothiophenes (LCOs) or the commercially-available equivalent Amytracker 520 (1:1000, EBBA Biotech AB, Sweden). In the current work, these will be referred to as LCOs. The two LCO variants, q-FTAA and h-FTAA, were used at

2.4 μM and 0.77 μM concentrations respectively (Nystrom et al., 2013). The former stains the core, whereas the latter stains the diffuse part of the amyloid-beta plaque. Slices were initially washed 3 times in PBS for 5 minutes and were then incubated in the LCO or Amytracker solution for 30 minutes at room temperature. After this, slices were washed twice and were prepared for mounting.

Nail varnish was used to make a well on SuperFrost Plus slides (Fisher) to prevent the dye and the slice from being crushed during coverslip placement. Slices were then mounted using mounting media (ProLong Diamond Antifade Mountant with DAPI, Invitrogen), they were cover-slipped and were left to dry until imaging.

Imaging of slices was usually performed on the day of mounting, in the same week in which electrophysiological experiments were performed. Imaging on 300μm slices following electrophysiological experiments was performed using a BioRad confocal microscope (Olympus BX50WI). The pixel to μm ratio was established to be 6.492 px/1 μm. Stimulated axons visualised using DiI (maximal emission at a wavelength of 568 nm) and recorded cells visualised using Alexa 488 (maximal emission at a wavelength of 488 nm) were tracked and imaged using an Olympus 60x infinity corrected 0.9NA water objective. Subsequent Z-stacks of the stimulated area were scanned using the Lasersharp 2000 (Version 6.0) software. Z-stacks were obtained at 50 lines per second (lps) speed, using a 1.5x optical zoom with 512x512 lines at a z-interval of 0.5 μm. Imaging allowed to determine if the stimulated axon during electrophysiological recordings passed near a plaque in *App* knock-in mice. Axons passing within a 30 μm radius of a plaque were considered plaque-associated axons due to previous work highlighting that this is the area within which the plaque is most toxic (Jackson et al., 2019b; Koffie et al., 2009; Sauerbeck et al., 2020; Spires et al., 2005) (see Figure 2.1A, B).

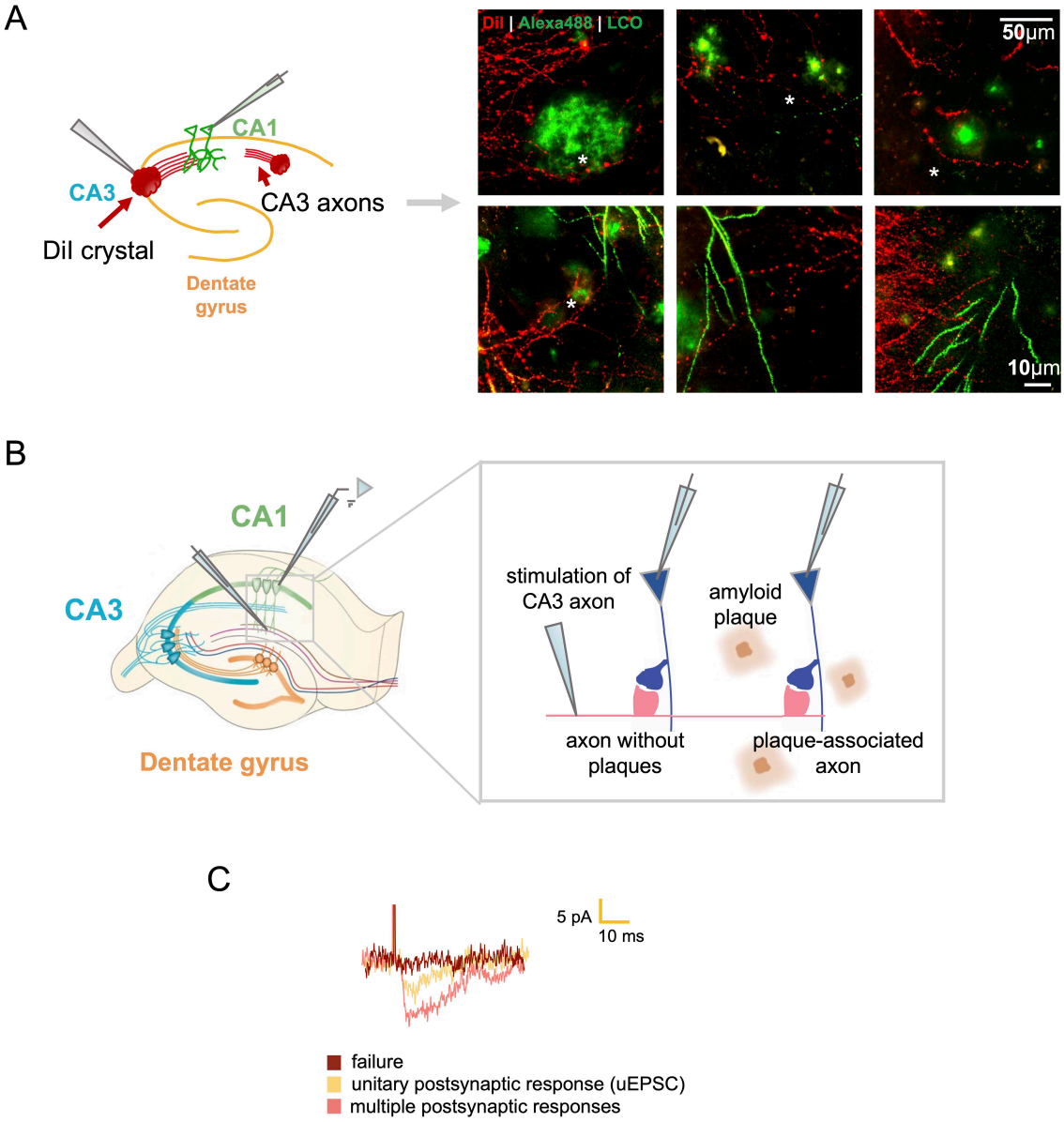

Figure 2.1. Illustration of the main methods employed in this work.
(A) A schematic of DiI placement in acute hippocampal slices prior to electrophysiological recordings. Two DiI crystals were placed in the hippocampus to label Schaffer collaterals – one in the CA3 pyramidal layer and one in the *stratum radiatum*. During patch-clamp recordings, the patch electrode was filled with Alexa Fluor 488 to allow for the subsequent visualisation of the recorded cell. Images on the right are maximal projections of representative Z-stacks from 300µm thick acute hippocampal slices taken at 60x on a confocal microscope. Images illustrate axons of CA3 pyramidal cells labelled in red (using DiI), dendrites of CA1 pyramidal cells labelled in green (using Alexa Fluor 488), and plaques labelled in green again (using LCOs). Asterisks indicate axons labelled as "plaque-associated" due to their vicinity to plaques on the way to the recorded cell**. (B)** A schematic illustrating the experimental setup of a patch-clamp experiment. In most cases, two recordings per an individual axon were made: (1) a plaque was present around the CA3 axon on its way to the recorded CA1 cell; (2) a plaque was not present around the CA3 axon on its way to the recorded CA1 cell. **(C)** Electrophysiological traces from paired-pulse recordings indicating the different amplitudes of the postsynaptic response upon stimulation. The yellow trace represents the response to a minimal stimulation which was the experimental paradigm employed in this work.

2.9 Immunohistochemistry

The drop-fixed hemisphere of each mouse was sectioned transverse to the long axis of the hippocampus at 30 μm using a frozen sledge microtome (SM 2000-R, Leica). Serial sections from each hemisphere were collected in 24-well plates until the hippocampus was no longer visible (~4/well) and these were stored in PBS containing 0.03% sodium azide until immunohistochemical experiments. Sections were washed once in PBS and then three times for 10 minutes each in a solution containing 0.3% Triton X-100 in PBS (PBST). After this, sections were incubated for 1 hour in blocking solution (3% goat serum – Novex, Catalogue number: PCN5000 – in 0.3% PBST). Sections were then incubated overnight at 4°C with the primary antibody prepared in the blocking solution (rabbit anti-Iba1, 1:1000, Wako, Catalogue number 019-19741; mouse anti-GFAP, 1:1000, Sigma, Catalogue number: G3893). The next day, sections were again washed three times in 0.3% PBST and were incubated in secondary antibodies prepared in blocking solution for 2 hours in the dark at room temperature (goat anti-rabbit Alexa Fluor 647, 1:1000, Invitrogen, Catalogue number: a-21244; goat anti-mouse Alexa Fluor 594, 1:1000, Invitrogen, Catalogue number: a-11032). After this, slices were washed once with PBS for 10 minutes and were incubated with either LCOs (1:1000) for 30 minutes (Table 2.1). Slices were washed again, incubated for 5 minutes in DAPI (1:10,000, Abcam, Catalogue number: ab228549) to allow for nuclei staining, and were then mounted onto Superfrost Plus glass slides (Fisher) by floating on PBS. Fluoromount-G medium (SouthernBiotech, Alabama, USA) was then applied and coverslips placed.

Table 2.1. Antibodies, dyes, and their respective dilutions used for immunohistochemistry.

Antibodies	Dilution	Catalogue number
Rabbit anti-Iba1	1:1000	Wako, 019-19741
Mouse anti-GFAP	1:1000	Sigma, G3893
Goat anti-rabbit Alexa Fluor 647	1:1000	Invitrogen, a-21244
Goat anti-rabbit Alexa Fluor 594	1:1000	Invitrogen, a-11032
Luminescent conjugated oligothiopene (LCO) or Amytracker 520	1:1000	LCO donated by the Jörg Hanrieder lab at the University of Gothenburg; Amytracker bought from EBBA Biotech
4′,6-diamidino-2-phenylindole (DAPI), 405	1:10,000	Abcam, ab228549

2.10 Imaging

Following immunohistochemistry of 30µm slices, photomicrographs of the whole hippocampal area were obtained using a 20x objective on an epifluorescent microscope – EVOS FL Auto Cell Imaging microscope (Life Technologies). The pixel to µm ratio at this magnification was established as 2.64 px/1 µm, illustrating that both individual plaques and glia could be visualised with these settings. DAPI was detected at a wavelength of 356 nm, Amytracker/LCO at 520 nm, GFAP at 594 nm, and Iba1 at 647 nm. Constant light intensity, gain, and exposure were used for image acquisition. A minimum of 3 sections were imaged and used as a mean for each animal.

2.11 Image analysis

Fiji (or ImageJ) (Schindelin et al., 2012) was used to determine plaque size and number. Briefly, the hippocampus was initially outlined on the DAPI channel. The

green channel image (representing plaque staining visualised with LCOs) was then converted to an 8-bit image and a thresholded value was determined for each slice to take into consideration each image's individual background staining. The number of particles within each hippocampal area and their respective areas were obtained for each slice using the Analyze Particles function. The range of particles was set between 10 μm^2 and infinity as previous work in our lab has shown that particles smaller than 10 μm^2 are likely to be noise rather than real signal (Medawar et al., 2019), and even if plaques of areas smaller than 10 μm^2 are present, their exclusion has little effect on the overall plaque coverage.

Adobe Photoshop 2020 was used for counts of microglia and astrocytes. For these, several regions of interest from the hippocampus were selected: the CA3 layer subfields, *stratum pyramidale, stratum lucidum*, *stratum radiatum* (SR), and *stratum lacunosum moleculare* (SLM); the CA1 layer subfields, *stratum pyramidale,* SR, and SLM; and the dentate gyrus subfields, the *stratum moleculare, stratum granulare*, and the hilus (see Figure 2.2). Cells which were both $DAPI^+$ and Iba^+ or $DAPI^+$ and $GFAP^+$ were counted as microglia or astrocytes, respectively. To calculate the overall distribution of microglia and astrocyte for the whole hippocampus for each slice, an average of their distribution/mm^2 in these areas was taken. For all image analysis, three slices were obtained and averaged to obtain the value for each mouse.

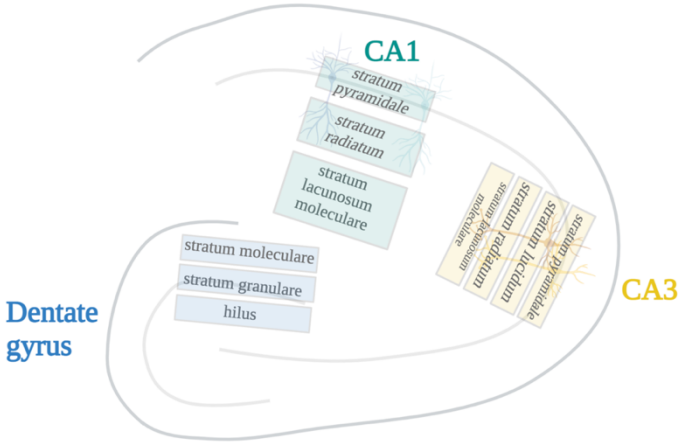

Figure 2.2. Illustration of the regions of interest used for image analysis.
Ten different regions were used for quantification of astrocytes and microglia. Four areas in the CA3 region were explored: *stratum pyramidale, stratum lucidum, stratrum radiatum,* and *stratum lacunosum moleculare*. Three different areas in the CA1 region were explored: *stratum pyramidale, stratum radiatum,* and *stratum lacunosum moleculare*. In the dentate gyrus region, the *stratum moleculare* and *stratum granulare*, and the hilus were explored.

2.12 Statistical analysis

All data analyses were performed blinded to sex, genotype, or condition. Statistical analyses were performed using GraphPad Prism 9 (La Jolla, California, USA). Where multiple slices/recordings were obtained from one animal, these were averaged to obtain a mean for that animal which was then used for subsequent analysis. In cases when from one mouse one electrophysiological recording was considered as "no-plaque" (there were no plaques around the stimulated axon) and the other as "plaque" condition (there was a plaque present around the stimulated axon), these recordings were considered as separate samples. If multiple cells were recorded from slices from one mouse and these were in the same condition, averages across cells for each animal were calculated for statistical analyses. Data points which were greater than 2x standard deviations from the mean were considered outliers and were excluded from further analysis. When comparisons between different genotypes were made, data from *App* knock-in mice were combined, regardless of plaque presence around the stimulated axon. For the 4-5 and 7-9-month groups, males and females were analysed separately, while they were grouped for the 18 months group due to insufficient number of animals at that age for statistical analyses. Data were analysed using one- and two-way ANOVAs, with Holm-Sidak used for *post-hoc* analyses. Cumulative probabilities were assessed using Kolmogorov-Smirnov tests. Data was assessed for normality using Shapiro-Wilk tests. Power analyses were performed using G*Power v3.1 to determine the required sample sizes for the analysis performed in this work. Importantly, despite the small sample sizes in some cases in the present thesis, post-hoc power analysis revealed that the lowest power reached is 0.75, indicating that the sample sizes used in this work were large enough for examining statistical differences. Graphs show Mean ± SEM. All diagrams in this work are created either using Biorender.com or Microsoft PowerPoint.

Chapter 3: *App*$^{NL-G-F}$ mice exhibit some plaque-dependent differences in synaptic transmission, as well as gliosis in response to plaque pathology

3.1 Introduction

Alterations in synaptic activity are one of the earliest hallmarks observed in AD (Scheff and Price, 2006). These synaptic changes have been shown to occur before any noticeable cognitive decline, highlighting the importance of understanding the driving factors behind them. Numerous studies have demonstrated that Aβ can have profound effects on synaptic activity through its effects on both the pre- and post-synaptic compartments. Specifically, soluble Aβ is able to increase presynaptic glutamate release by increasing Ca^{2+} in presynaptic terminals in physiological conditions (Abramov et al., 2009), and this has been suggested to be exacerbated in an AD environment. Aβ can directly interact with proteins involved in the SNARE complex in the presynaptic space, including syntaxin-1 and synapthophysin-1 (Russell et al., 2012; Yang et al., 2015), and there have also been reports of a reduced transcription of genes related to synaptic activity in AD (Yao et al., 2003). Additionally, soluble Aβ can also bind to glutamate transporters, in turn inhibiting glutamate reuptake and hence influencing excitability (Li et al., 2009; Zott et al., 2019), and can additionally impair the insertion of AMPARs and NMDARs in the postsynaptic space, thereby altering postsynaptic activity.

Several reports from our lab have shown that the above changes in presynaptic release probability occur before any noticeable Aβ plaque pathology (Benitez et al., 2021; Cummings et al., 2015), arguing that soluble Aβ rather than the plaques are the driving factor for synaptic changes. This has also been confirmed *in vivo,* with studies showing that prior to plaque formation, neurons in the CA1 region of the hippocampus of AD mice exhibit hyperactivity (Busche et al., 2012). Therefore, there is now consensus among the literature that soluble Aβ has a key role in synaptic dysfunction (Barry et al., 2011; Cleary et al., 2005; Edwards, 2019). The specific mechanisms through which Aβ results in increased release probability could be by inhibiting the interaction between VAMP2 and synaptophysin or by inhibiting glutamate reuptake, resulting in

mGluR activation, Ca^{2+}-induced Ca^{2+} release and synapsin phosphorylation (Ovsepian et al., 2017; Russell et al., 2012; Zott et al., 2019). Both of these processes increase the number of primed vesicles for exocytosis, providing one explanation as how Aβ can increase the release probability at these synapses.

However, it is still unclear how the deposition of soluble Aβ into plaques alters these effects of Aβ on synaptic activity. For instance, one study showed that the Aβ halo around plaques is the main driver of synaptic toxicity in these regions (Koffie et al., 2009), however how the extent of these effects compares to regions solely containing soluble Aβ remains to be determined. Some light has been shed on this mechanism by a recent study from our lab which explored the *App*$^{NL-G-F}$ model that contains the Arctic mutation, which makes Aβ particularly prone to aggregate and hence deposit into plaques rather than flowing through the neuropil (Benitez et al., 2021; Saito et al., 2014). This study found increased release probability in earlier stages of pathology (2 months), which disappears at moderate stages (4 months) and reappears at more advanced stages of pathology (9 months onwards). This is argued to be due to the fact that at earlier stages there are a very small number of plaques formed, yet high levels of soluble Aβ are found in both the cortex and hippocampus (Latif-Hernandez et al., 2020). Hence, the effects on release probability are very likely to be caused by soluble Aβ acting on the SNARE complex in presynaptic regions. When there is moderate plaque pathology, because of the Arctic mutation within the Aβ sequence, there is likely a shift towards deposition of Aβ into plaques, decreasing soluble Aβ in the neuropil and so no longer allowing for Aβ to exert its effects on release probability. These reappear at advanced stages of pathology potentially because most of the synapses examined are likely to be in the vicinity of plaques and the soluble Aβ surrounding them (Benitez et al., 2021). However, whether this is in fact the mechanism explaining this phenomenon remains to be established. Furthermore, it is important to note that findings from these mice should be taken with caution as it is hard to discern whether soluble Aβ is freely present in the neuropil in this model due to the high propensity of Aβ for fibrillation due to the Arctic mutation (Saito et al., 2014).

In this chapter, I aimed to explore the above mechanism at two different stages of pathology by examining the activity at CA3-CA1 synapses in the hippocampus of

App^{NL-G-F} mice. The hippocampus is a useful structure to explore specific alterations in synaptic activity due to its clear organisation and well-defined connectivity which has been thoroughly examined throughout the years (Andersen et al., 2007). I initially explored the plaque pathology, as well as gliosis, in these mice in order to understand what processes accompany some of the potential changes in synaptic transmission. I then explored electrophysiological changes in acute hippocampal slices to understand how synaptic activity is altered in these mice with pathology progression. These acute hippocampal slices can survive up to 8 hours in an oxygenated aCSF solution and hence allow for the examination of alterations in excitatory synaptic activity. The hippocampus is particularly vulnerable in the AD brain (Desikan et al., 2010), with studies in AD post-mortem tissue showing substantial loss of CA3 and CA1 neurons (Padurariu et al., 2012), as well as loss of dendritic spines (Spires et al., 2005) and altered morphology of CA1 neurons (Merino-Serrais et al., 2013). Therefore, this thesis aimed to examine the activity of CA1 neurons upon the stimulation of CA3 axons as this would provide good insight into how synaptic transmission at CA1 neurons is altered in *App* knock-in mice compared to wild-type animals. Importantly, here unitary excitatory postsynaptic currents (uEPSCs) which result from the activation of single synapses were recorded from these mice.

However, although this would help understand how the presence of plaques and other toxic processes associated with AD affect the transmission of individual synapses, it would not answer the question as to whether soluble Aβ oligomers present all over the hippocampus, or soluble Aβ oligomers associated with plaque regions are the driving factor for the observed effects in these mice. Therefore, here, the effects of plaques on the transmission of individual axons were also examined to determine if axons in the vicinity of plaques exhibit differential activity compared to those away from plaques.

3.2 *App*$^{NL-G-F}$ mice develop robust plaque pathology and more smaller-sized plaques at later ages

In order to understand the pathology found in *App*$^{NL-G-F}$ mice at two different stages of pathology – moderate and heavy plaque load – mice at 4-5 and 7-9 months of age were examined. I initially stained hippocampal slices with either luminescent conjugated oligothiophenes (LCOs) or the commercially-available substitute Amytracker 520 to determine plaque load in the hippocampus of *App*$^{NL-G-F}$ mice at

these two different pathology stages. These compounds bind to protein aggregates containing amyloid fibrils and protofibrils and hence are useful for the detection of Aβ plaques (Nystrom et al., 2013; Rasmussen et al., 2017). Following immunohistochemistry, these slices were imaged using an epifluorescent microscope to examine plaque pathology. As mentioned in Chapter 2, the pixel to μm resolution (2.64/1) was low enough to allow for the visualisation of even the smallest plaques.

The focus of this work was two-fold: to explore any genotype-related differences and also examine sex-related differences. This is an important, yet understudied avenue as previous AD research has primarily examined either only male or female mice, without taking into account the effects of sex. Interestingly, it has been demonstrated that female APP/PS1 mice exhibit higher plaque accumulation at more advanced stages of pathology than males (Wang et al., 2003). This suggests that there might be some differences in the brain response to pathology between the two sexes, highlighting the importance of exploring both pathology and synaptic differences between males and females. It has also been shown that microglia from females are distinct from those from males in both AD mice and human post-mortem tissue, with microglia from female mice upregulating genes associated with activation much more prominently (Guillot-Sestier et al., 2021; Zhao et al., 2020). The former study suggested that this can impair the phagocytic ability of female microglia, raising questions as to how this translates to AD mechanisms and compares to brain responses in males. Therefore, here both male and female *App*$^{NL\text{-}G\text{-}F}$ mice were explored at both stages of pathology.

In males, wild-types clearly demonstrated no amyloid staining at both ages, while *App*$^{NL\text{-}G\text{-}F}$ mice exhibited robust hippocampal plaque pathology at 4-5 months, which becomes more pronounced at 7-9 months (Figure 3.1A). This is confirmed when the number of plaques was explored which showed that 7-9 month-old *App*$^{NL\text{-}G\text{-}F}$ mice have more plaques than 4-5 month-old mice ($p<0.01$; unpaired t-test) (Figure 3.1B). Interestingly, the percentage of plaque coverage was not different between the two ages ($p>0.05$; Figure 3.1B). Further analysis of plaque area revealed a significant interaction between plaque size and age ($p<0.0001$; two-way ANOVA), with Sidak-corrected *post-hoc* tests revealing that *App*$^{NL\text{-}G\text{-}F}$ mice from the 7-9 month group exhibit a larger number of smaller-sized plaques (between 10 and 50 μm^2), but not of

plaques bigger than 50 μm^2, compared to 4-5-month old mice ($p<0.0001$; Figure 3.1C).

The above effects in males were replicated in females. Specifically, while wild-types exhibited no plaque pathology, *App*$^{NL-G-F}$ mice demonstrated increasingly more plaques in the hippocampus with age (Figure 3.1D). This was confirmed through statistical analysis which found a significantly greater number of plaques in 7-9 month-old compared to 4-5-month-old female *App*$^{NL-G-F}$ mice ($p<0.01$; unpaired t-test; Figure 3.1E). Similarly to males, no difference in the percentage of plaque coverage was found in females ($p>0.05$), which likewise could be explained by the observation of a greater number of smaller-sized plaques, in older mice (Figure 3.1E, right panel). In particular, analysis of plaque area revealed a significant interaction between plaque area and age ($p<0.0001$). Replicating the findings in males, *post-hoc* analysis revealed that 7-9 month-old female *App*$^{NL-G-F}$ mice exhibit a larger number of small plaques (between 10 and 50 μm^2) than 4-5 month old mice ($p<0.0001$), while no differences were found in the number of larger plaques (Figure 3.1F).

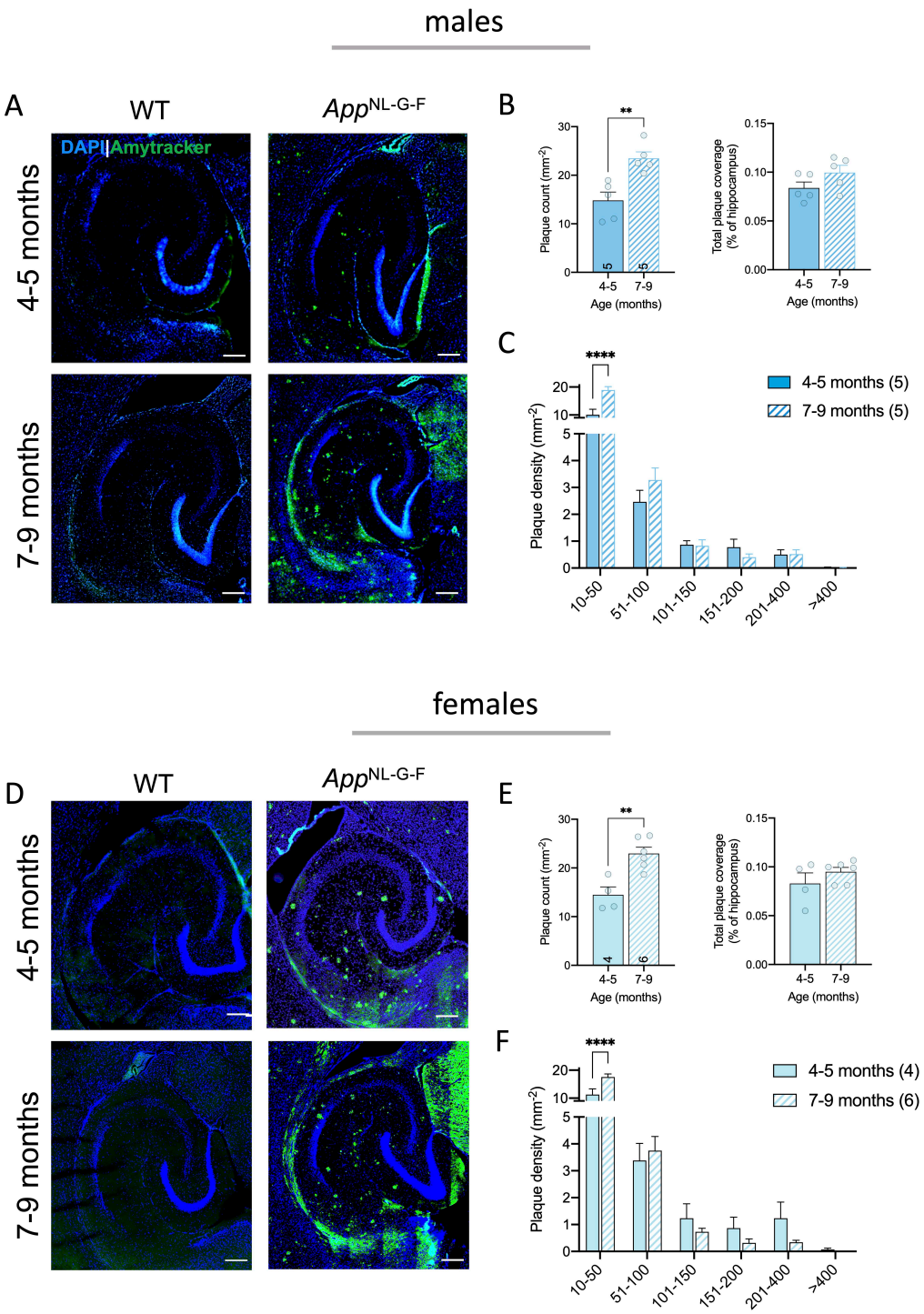

Figure 3.1. Deposition of Aβ plaques in male and female *App*$^{NL-G-F}$ mice at 4-5 and 7-9 months. **(A) & (D)** Representative images of epifluorescent micrographs of the hippocampi of male and female wild-type (WT) and *App*$^{NL-G-F}$ mice stained with Amytracker (green) for Aβ plaque labelling and DAPI (blue) for nuclei labelling. Scale bar: 200µm. Pixel/µm=2.64. **(B) & (E)** Plaque number and coverage in *App*$^{NL-G-F}$ mice. Males and females: differences between the ages in plaque number ($p<0.01$). **(C) & (F)** Frequency-size distribution of plaques in male and female *App*$^{NL-G-F}$ mice. Males and females: age x plaque size interactions ($p<0.0001$). Columns indicate mean ± SEM. Sample sizes are marked within bars. Individual points represent individual animals and the mean of three slices from each. T-tests and two-way ANOVAs followed by Sidak-corrected *post-hoc* comparisons if there was an interaction are indicated by: **p<0.01, ****p<0.0001. Asterisks between columns indicate *post-hoc* comparisons.

3.3 Changes in microgliosis and astrogliosis in *App*$^{NL-G-F}$ mice

3.3.1 Microglial density changes in *App*$^{NL-G-F}$ mice

In addition to the more advanced plaque pathology observed with disease progression in *App*$^{NL-G-F}$ mice, gliosis is another factor that is a feature of AD. Previous work on AD transgenic animals has demonstrated microglial and astrocytic activation in response to plaques, with both microglia and astrocytes responding to plaque presence by clustering around the Aβ aggregates (Henstridge et al., 2019; Keren-Shaul et al., 2017; Krasemann et al., 2017; Medawar et al., 2019; Sofroniew, 2005; Wyss-Coray et al., 2003). In *App*$^{NL-G-F}$ mice, microgliosis, evidenced by an increased number of Iba1^{+} microglia and increased *Trem2* expression per microglia, has been reported in the hippocampus at 9 months of age, when *App*$^{NL-G-F}$ mice already exhibit advanced pathology (Benitez et al., 2021; Saito et al., 2014). However, whether there are any specific changes in the different regions of the hippocampus and whether these changes are accompanied with changes in astrogliosis have not specifically been examined. Therefore, here, the density of microglia and astrocytes was explored using Iba1 and GFAP immunostaining respectively to determine any differences between male and female *App*$^{NL-G-F}$ mice at 4-5 and 7-9 months and age-matched controls.

In order to confirm previous reports of increased microglial density at advanced stages of pathology in *App*$^{NL-G-F}$ mice, the number of Iba1^{+} microglia which co-localised with a DAPI^{+} nucleus was quantified in both wild-types and *App* knock in mice. As demonstrated in Figure 3.2A below and as expected, microglia from 4-5 month-old male and female *App* knock-in mice tended to cluster around plaques, with their density clearly increased in plaque-associated regions (Figure 3.2Aii). The increased density was confirmed using a two-way ANOVA which found a main effect of genotype ($p<0.05$; Figure 3.2B), indicating that the density of microglia in *App*$^{NL-G-F}$ mice is higher than that of wild-type microglia. When examining if there are any specific regional differences in microglial density in the hippocampus, main effects of region and genotypes were revealed for males ($p<0.05$), indicating that microglial densities differ by region and that, irrespective of region, male microglial densities are higher in *App*$^{NL-G-F}$ mice. In females, a two-way ANOVA revealed a significant interaction between region and genotype,

indicating that different regions exhibit different microglial density depending on the genotype ($p<0.05$) (see Figure 3.2C). *Post-hoc* tests revealed that in both *App*$^{NL-G-F}$ and wild-type mice, the *stratum lacunosum moleculare* (SLM) region in the CA1 subfield has more microglia compared to the CA3 cell layer and the *stratum radiatum* (SR) in the CA1 subfield ($p<0.05$). Additionally, in *App*$^{NL-G-F}$ mice, the SLM also had more microglia than the CA1 cell layer ($p<0.05$).

Similarly to 4-5 months, 7-9 month-old mice demonstrated robust microglial accumulation, particularly around plaques (Figure 3.2D), illustrating a typical for AD microglial response to the Aβ aggregates. When this was quantified, an identical effect to the one observed at earlier ages was found and specifically, a higher microglial density in *App*$^{NL-G-F}$ mice compared to wild-types, irrespective of sex ($p<0.05$; two-way ANOVA; Figure 3.2E). Interestingly, in comparison to the 4–5-month-old group, there was no difference between the microglial density of the two genotypes in the different regions examined in this work ($p>0.05$; Figure 3.2F). This might suggest that, although microglia in the regions examined here show alterations in density depending on the genotype at earlier stages of pathology, these differences disappear at 7-9 months, likely because of the more spread-out plaque formation. Alternatively, in light of the high variability of microglial density in all regions at this age, the sample size might not have been large enough to elucidate these changes as *App*$^{NL-G-F}$ mice still showed a trend for larger microglial density in all regions compared to wild-types.

The similar microglial densities in both male and female *App*$^{NL-G-F}$ mice at the ages examined here, despite clear increases in plaque number with age, suggests that small plaques, which are the driving factor for the observed increase in plaque number in 7–9-month-old *App*$^{NL-G-F}$ mice, might be less able to elicit changes in microglial density compared to larger plaques. Alternatively, it might be that after early proliferation in response to the AD environment, microglial changes in the AD environment are primarily reflected in movement towards plaques and damaged regions.

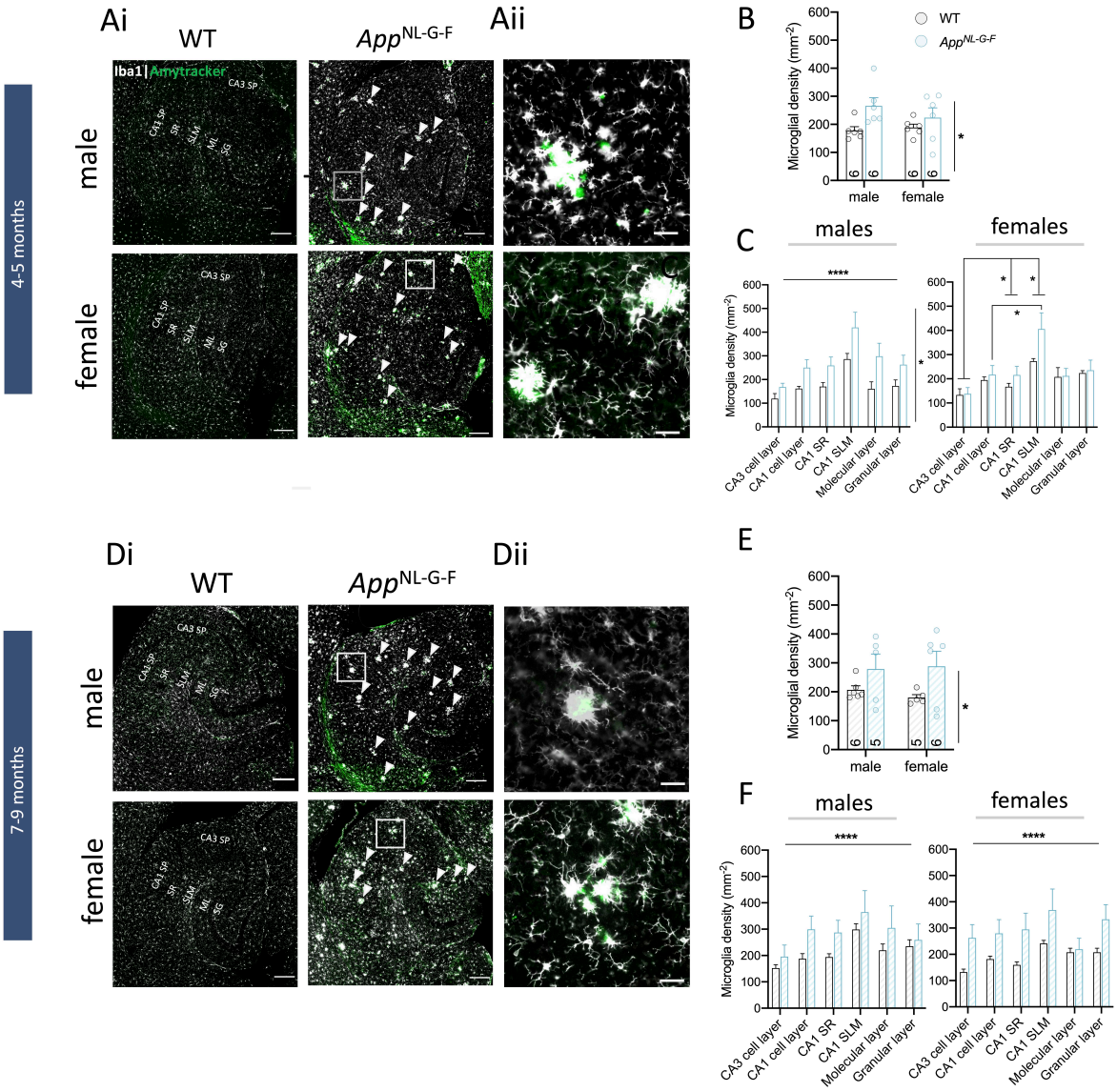

Figure 3.2. Microglial density and distribution in the hippocampus of male and female *App*$^{NL-G-F}$ and wild-type mice at 4-5 and 7-9 months of age.

(Ai) & (Di) Representative epifluorescent images of Iba^{+} microglia (white) and Aβ plaques (green) at 4-5 and 7-9 months. Arrows point at individual Aβ plaques. The different hippocampal regions examined in this analysis are also marked. Scale bar: 200µm. Pixel/µm=2.64. **(Aii) & (Dii)** Zoomed-in images of the squares indicated in (Ai) and (Di), showing microglial clustering around plaques at the ages indicated above. Scale bar: 50µm **(B) & (E)** Microglial density in *App*$^{NL-G-F}$ and wild-type mice. 4-5 months and 7-9 months: main effects of genotype ($p<0.05$). **(C) & (F)** Microglial distribution in the different hippocampal regions marked in (A) and (D). Columns indicate mean ± SEM. Sample sizes are marked within bars. Individual points represent individual animals and the mean of three slices from each. Two-way ANOVA followed by Sidak-corrected *post-hoc* comparisons if there was an interaction are indicated by: *$p<0.05$, **$p<0.01$, ****$p<0.0001$. Asterisks above columns indicate main effect of region. Asterisks beside columns indicate main effect of genotype. Asterisks between columns indicate *post-hoc* comparisons.

3.3.2 Changes in astrocytic density in *App*$^{NL-G-F}$ mice

Having established microglial density changes in *App*$^{NL-G-F}$ mice, the density of astrocytes was also explored. This was done by quantifying the number of astrocytes, identified using GFAP staining, in the hippocampus of male and female *App* knock-in mice and age-matched wild-type controls. Similarly to microglia and as expected, GFAP^{+} astrocytes from both male and female *App*$^{NL-G-F}$ mice at the two ages examined appeared to cluster around amyloid plaques, although not as tightly as microglia, with mostly their processes ensheathing plaque regions (see Figure 3.3A, D). In addition to this, the GFAP intensity appeared stronger overall in the hippocampus of *App*$^{NL-G-F}$ mice compared to wild-types (Figure 3.3Ai, Di), with clear increases in astrocytes in the vicinity of plaques (Figure 3.3Aii, Dii). This is observed in the two sexes from both age groups and is indicative of an increased astrocytic activation in the presence of plaque pathology.

At 4-5 months, when quantifying the astrocyte density in the hippocampus, a two-way ANOVA revealed no difference between the two genotypes or sexes ($p>0.05$; Figure 3.3B). To see if this difference is not hidden in a difference between hippocampal regions, the astrocyte density in the above hippocampal regions was also explored. Although a two-way ANOVA revealed no differences between the two genotypes, it showed a significant effect of region ($p<0.0001$; Figure 3.3C) for both sexes, showing that astrocytic density differs in the different hippocampal regions explored here, regardless of genotype.

Similarly to 4-5 months, female 7-9 month-old mice exhibited no differences in astrocyte number in the whole hippocampus ($p>0.05$; two-way ANOVA; Figure 3.3E), nor in the different regions examined in this work ($p>0.05$; two-way ANOVA; Figure 3.3F). In comparison, males demonstrated a significant region x genotype interaction at that age ($p=0.0012$; two-way ANOVA; Figure 3.3F), suggesting that different regions show differential up or downregulation of astrocyte numbers depending on the genotype. *Post-hoc* tests showed that the CA3 cell layer exhibits the lowest astrocytic density compared to all other regions, regardless of genotype. This finding hints at potential differences between male and female *App*$^{NL-G-F}$ mice and specifically, in their ability to trigger changes in astrocytic density at that age.

However, it is important to note that the measurements performed here do not directly correlate to astrogliosis as changes in astrocytic number might not reflect changes in the astrocytic transcriptional profile, which, however, was outside the scope of the current study.

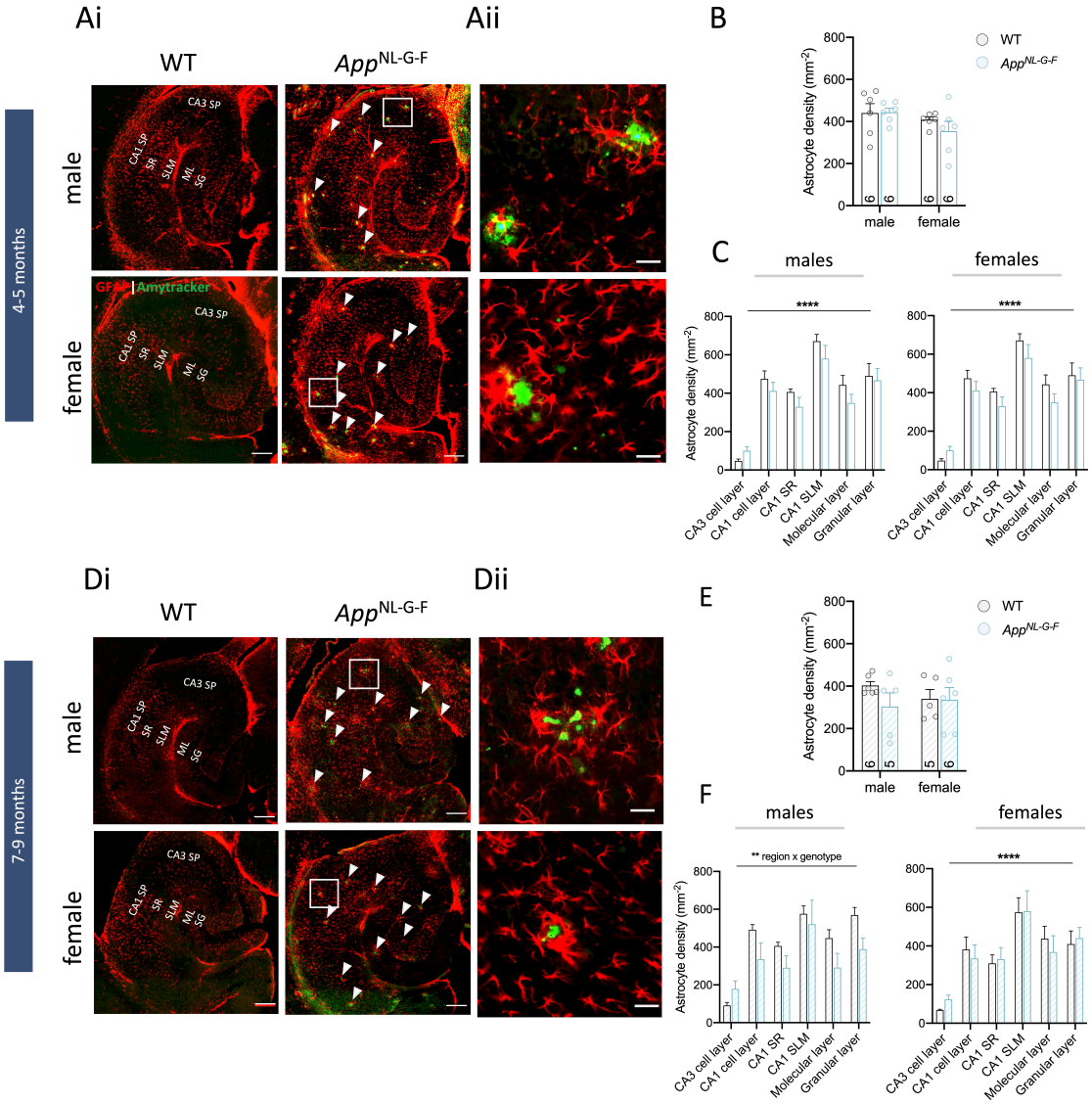

Figure 3.3. Astrocyte density and distribution in the hippocampus of male and female *App*$^{NL-G-F}$ and wild-type mice at 4-5 and 7-9 months of age.

(Ai) & (Di) Representative epifluorescent images of GFAP^{+} astrocytes (white) and Aβ plaques (green) at 4-5 and 7-9 months. Arrows point at individual Aβ plaques. The different hippocampal regions examined in this analysis are also marked. Scale bar: 200µm. Pixel/µm=2.64. **(Aii) & (Dii)** Zoomed-in image of the squares indicated in (Ai) and (Di), showing astrocytic clustering around plaques at the ages indicated above. Scale bar: 50µm **(B) & (E)** Astrocytic density in *App*$^{NL-G-F}$ and wild-type mice. **(C) & (F)** Astrocytic distribution in the different hippocampal regions marked in (A) and (D). Columns indicate mean ± SEM. Sample sizes are marked within bars. Individual points represent individual animals and the mean of three slices from each. Two-way ANOVA followed by Sidak-corrected *post-hoc* comparisons if there was an interaction. Asterisks above columns indicate main effect of region.

3.4 The minimal stimulation paradigm recruited single synapses

In order to determine if there are any changes in synaptic transmission between *App* knock-in animals and wild-types, wild-type and *App*$^{NL-G-F}$ mice at the same stages of pathology as above were explored. Here, unitary excitatory postsynaptic currents (uEPSCs) were recorded from CA1 pyramidal cells in the presence of a $GABA_A$ receptor blocker using a patch-clamp setup following the stimulation of a single, identified axon of a CA3 cell. To direct the stimulation electrode towards single CA3 axons during recordings, the lipophilic dye DiI was placed in the CA3 region prior to electrophysiological recordings.

To assure the stimulation of an individual axon, or at least the recruitment of only a small number of neighbouring axons around the stimulation site, a minimal stimulation paradigm was employed in this work. The use of minimal stimulation was important as it assured that only the axon visualised using DiI, or at least a small proportion of axons around it, were the ones stimulated during patch-clamp experiments, allowing for the examination of the properties of single synapses. Therefore, to ensure that this stimulation was truly minimal and resulted in uEPSCs (see Figure 2.1C), the recorded amplitudes of the successful first responses of male *App*$^{NL-G-F}$ and wild-type mice were compared to those of miniature excitatory postsynaptic currents (mEPSCs) previously recorded in our lab by Dr Damian Cummings and which are also published in Benitez et al. (2021). Indeed, no differences in the postsynaptic amplitude of the previously recorded mEPSCs and the uEPSCs recorded in this work (Figure 3.4A) were observed at both ages and both genotypes examined in this chapter ($p>0.05$; two way-ANOVAs) (Figure 3.4B, C), supporting the idea that one or two release sites on only one axon, or that only a few axons were recruited during the minimal stimulation paradigm employed here.

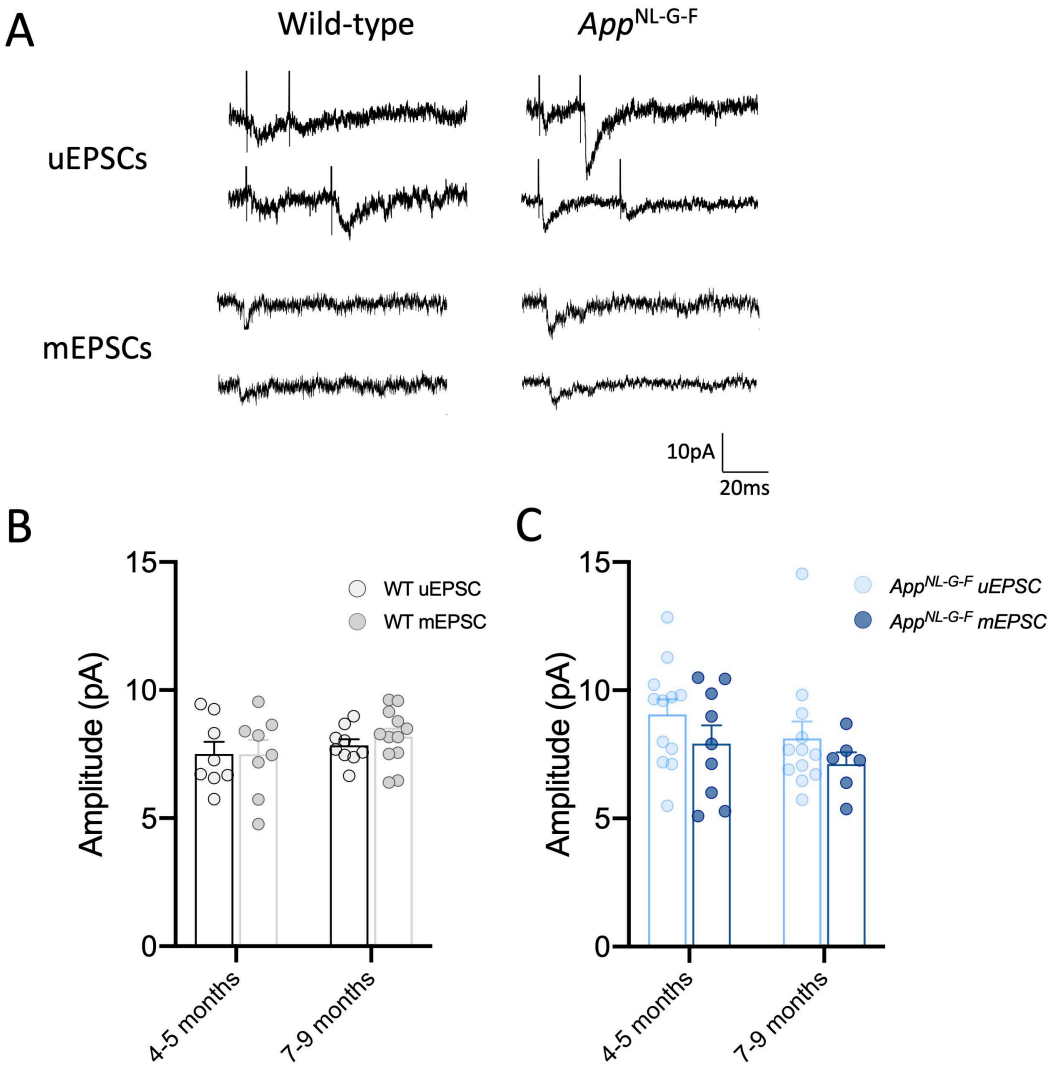

Figure 3.4. Comparison of uEPSC and mEPSC amplitudes in wild-type and *App*$^{NL-G-F}$ mice at 4-5 months and 7-9 months of age.
(A) Representative uEPSC and mEPSC traces from 4–5-month-old wild-type and *App*$^{NL-G-F}$ mice. mEPSC data represents data collected in Benitez et al. (2021) **(B)** & **(C)** There is no difference between the amplitudes at either age or genotype. Columns indicate mean ± SEM. Individual points represent the mean of all recordings taken from individual animals.

3.5 *App*$^{NL-G-F}$ mice exhibit some differences in synaptic activity compared to wild-type mice

Having confirmed the feasibility of using minimal stimulation to recruit individual axons, the postsynaptic activity of CA1 cells of both male and female *App*$^{NL-G-F}$ mice and age-matched wild-type controls were examined. Although previous work has examined if *App*$^{NL-G-F}$ mice exhibit alterations in synaptic transmission compared to

wild-types at different ages (Benitez et al., 2021; Latif-Hernandez et al., 2020), they have not explored what differences sex introduces to the observed changes. Furthermore, previous experiments were not performed at minimal stimulation intensities and hence did not examine the activity of single synapses, showing that the present study could elucidate some differences at the synaptic level which could have been masked in previous work.

3.5.1 Changes in postsynaptic compartments in *App*$^{NL-G-F}$ mice

No differences in the uEPSC amplitude of the first response were found either between the two genotypes, or between the two sexes at 4-5 months of age ($p>0.05$ for both main effects and interaction; two-way ANOVA; Figure 3.5B). Importantly, there was no difference in the stimulation voltages required to evoke the uEPSCs ($p>0.05$; two-way ANOVA; Figure 3.5C). The similar uEPSC amplitudes found between the two genotypes is consistent with the findings of previous work from our lab showing no differences in the amplitude of mEPSCs between male *App*$^{NL-G-F}$ and wild-type mice at that age (Benitez et al., 2021). Furthermore, there were no differences in the decay time ($p>0.05$; two-way ANOVA; Figure 3.5D), suggesting similar receptor kinetics between the two groups. Altogether these results suggest that there are no alterations in the postsynaptic compartments in *App*$^{NL-G-F}$ mice at that age.

The same properties of uEPSCs were also explored in 7–9-month-old *App*$^{NL-G-F}$ mice. Similarly to earlier stages of pathology, *App*$^{NL-G-F}$ mice did not exhibit altered postsynaptic amplitudes compared to age-matched wild-types ($p>0.05$; two-way ANOVA; Figure 3.5E). This was also accompanied by no differences between the two genotypes and sexes in the stimulation voltage ($p>0.05$; two-way ANOVA; Figure 3.5F). Interestingly, examining the decay times revealed a significant main effect of genotype ($p<0.05$; two-way ANOVA), with *App*$^{NL-G-F}$ mice exhibiting longer decay times than wild-types (Figure 3.5G). Altogether these results suggest that *App*$^{NL-G-F}$ mice exhibit altered properties of the postsynaptic receptors and specifically, their closing kinetics. This could be arising from different subunit composition of postsynaptic AMPARs, leading to changes in their unbinding kinetics or desensitisation. This is plausible as previous work has demonstrated that oligomeric forms of Aβ which are found in these mice can increase and decrease the number of GluA2- and GluA1- expressing AMPARs, respectively AMPARs (Reinders et al.,

2016; Whitcomb et al., 2015). Alternatively, the different decay times could be driven by a difference in the diffusion of glutamate out of the synaptic cleft in *App* knock-in mice.

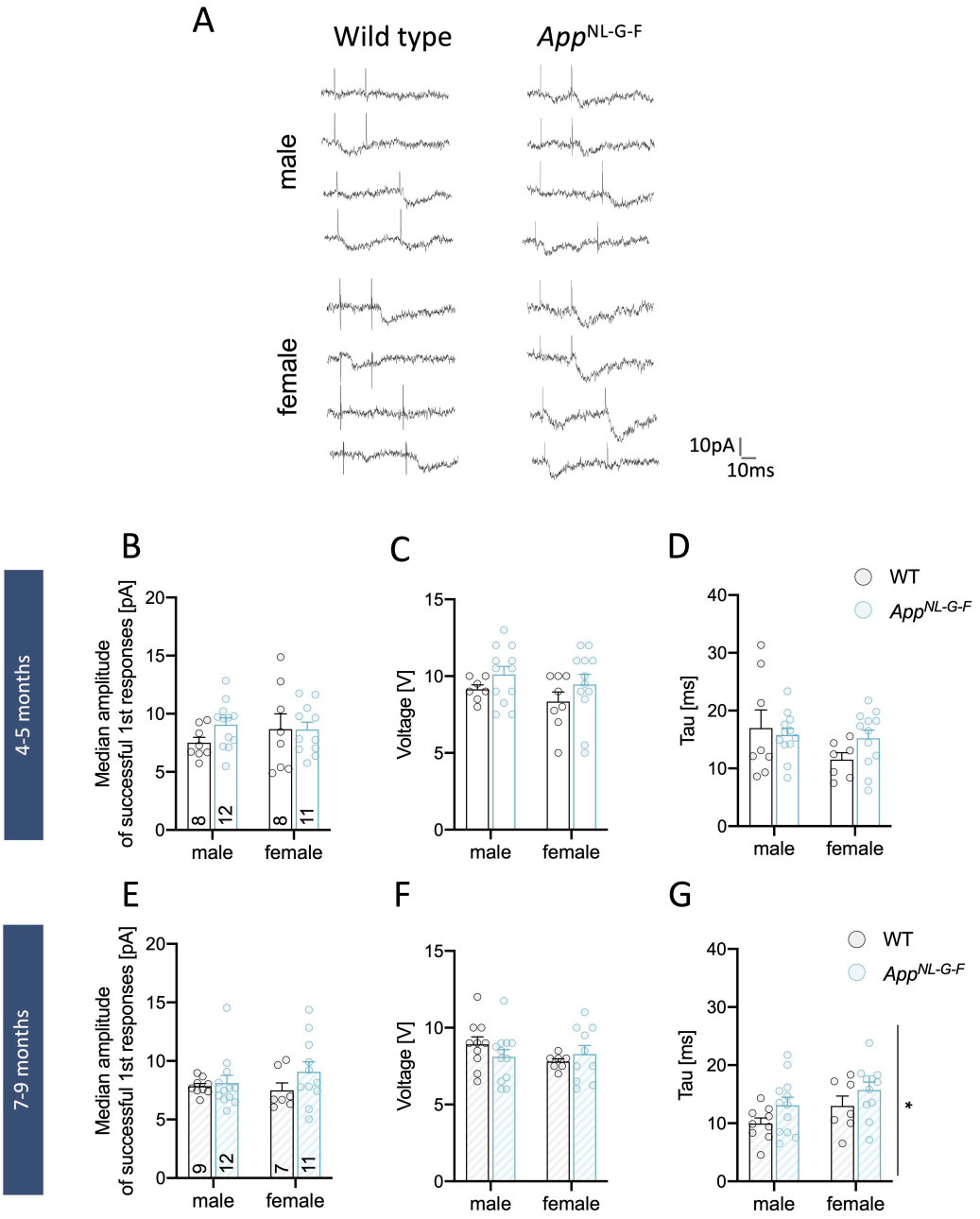

Figure 3.5. Properties of uEPSCs recorded from male and female *App*$^{NL-G-F}$ and wild-type mice at 4-5 and 7-9 months of age.

(A) Example uEPSC traces from male and female wild-type and *App*$^{NL-G-F}$ mice at 4-5 months of age following a pair of stimuli 25 and 50 ms apart. **(B) & (E)** Median postsynaptic amplitudes of the successful first responses between male and female *App*$^{NL-G-F}$ and wild-type mice in the ages indicated above. **(C) & (F)** The stimulation voltage used for recordings for all groups. **(D) & (G)** The mean decay time in both genotypes at the ages marked above. 7-9 months: main effect of genotype, with longer decay times in *App*$^{NL-G-F}$ mice compared to wild-types ($p<0.05$). Columns indicate mean ± SEM. Sample sizes are marked within bars. Individual points represent the mean of all recordings taken from individual animals. Two-way ANOVAs indicated by: *$p<0.05$. Asterisks beside comparisons indicate main effect of genotype.

3.5.2 Release probability alterations in *App*$^{NL-G-F}$ mice

Two pairs of stimuli were applied in the experiments performed here, with these being either 25ms or 50ms apart (see Figure 3.6A). Exploring differences in the ratio between the median amplitude of the second responses to that of the first response, which is called the paired-pulse ratio (PPR), can give an idea of the release probability of the examined synapses. The PPR is inversely proportional to the initial probability of release (Pr), with a facilitation of the second response (termed paired-pulse facilitation (PPF)) indicating low Pr and a reduction (termed paired-pulse depression (PPD)) indicating high Pr. After the first stimulation at synapses with low Pr, there is residual Ca^{2+} in the presynaptic space. This is additive to the Ca^{2+} influx triggered by the second stimulation, in turn leading to an enhanced vesicle release upon its arrival and a larger postsynaptic current. On the other hand, this residual Ca^{2+} is not able to enhance the release at synapses with high Pr due to a depletion of synaptic vesicles at the arrival of the first stimulation, resulting in a smaller postsynaptic current at subsequent stimulations (Regehr, 2012; Zucker and Regehr, 2002).

CA3-CA1 synapses typically exhibit low release probability, however how this is altered in *App*$^{NL-G-F}$ mice in comparison to wild-types, as well as between male and female mice, remains to be determined. Previous work from our lab found reduced PPR of *App*$^{NL-G-F}$ mice at 2 months, no change in the PPR at 4 months, and a decreased PPR and hence increased release probability at 9 months where there is more advanced plaque pathology (Benitez et al., 2021). Therefore, as expected, a two-way ANOVA found no differences in the PPR at either interval at 4-5 months ($p>0.05$; Figure 3.6Bi,ii). Further examination of the failure rate of the first responses revealed no differences between the two sexes and genotypes ($p>0.05$; two-way ANOVA), suggesting that the release probability is unaffected at this stage of pathology (Figure 3.6C).

In comparison to previous work, here no change in the PPR at either 25ms or 50ms was found at 7-9 months of age according to a two-way ANOVA ($p>0.05$; Figure 3.6Di,ii). This finding is not entirely consistent with previous results which found increased release probability at more advanced stages of pathology (Benitez et al., 2021). Interestingly, when the failure rate was examined, a two-way ANOVA revealed

a significant effect of genotype ($p<0.05$; Figure 3.6E), with *App*$^{NL-G-F}$ mice showing lower failure rates than wild-types. The lack of changes in the PPR despite reduced failure rates might suggest that *App*$^{NL-G-F}$ axons were more likely than wild-types' to respond to the stimulation intensities used in this work, hinting at differences in axonal excitability in AD conditions. Additionally, it is possible that receptor desensitization had masked any changes in the PPR, despite there being potential alterations in release probability in *App* knock-in mice. This idea, however, warrants further investigation into neurotransmitter vesicle dynamics.

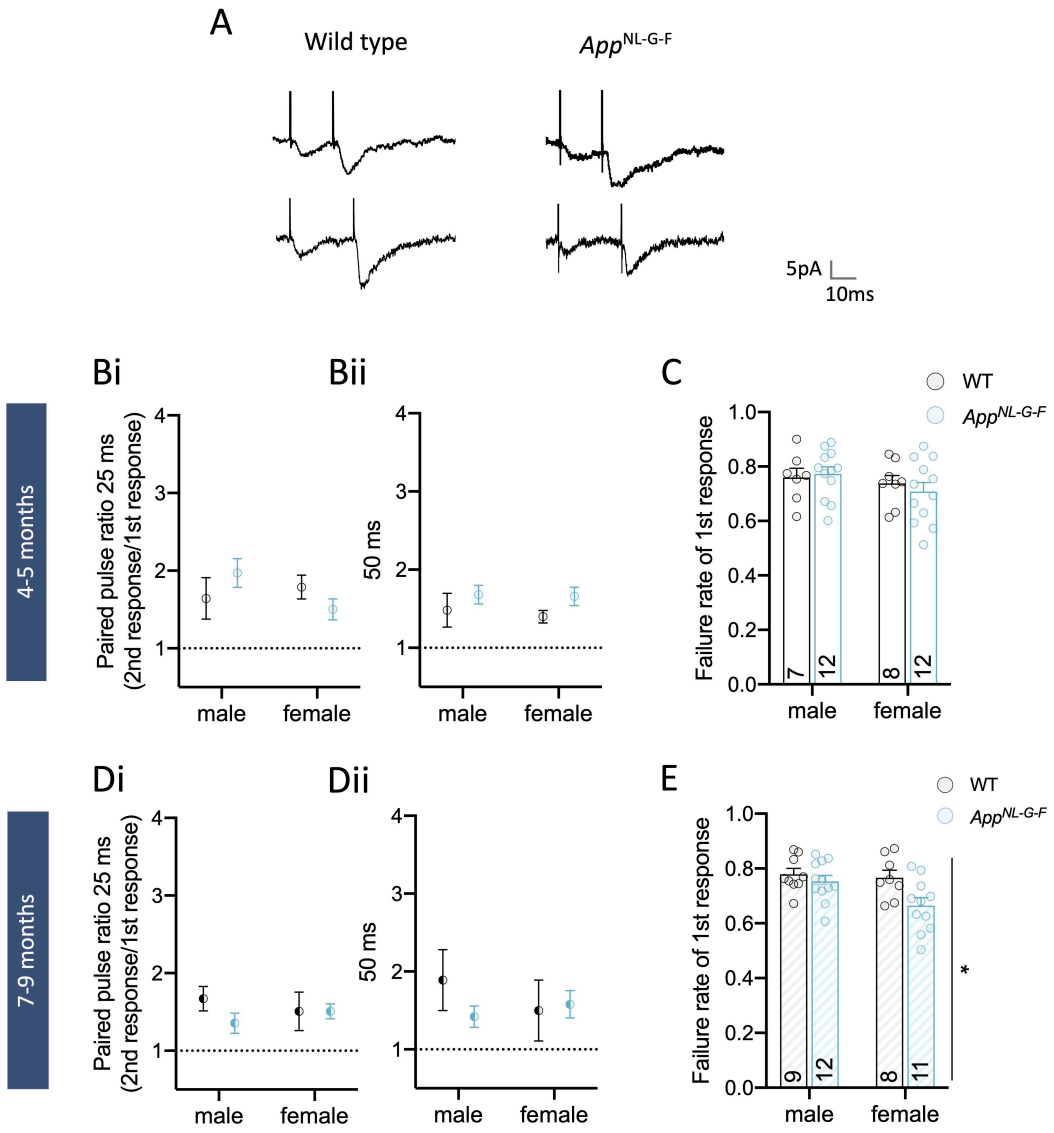

Figure 3.6. Release probability in male and female *App*$^{NL-G-F}$ and wild-type mice at 4-5 and 7-9 months of age.

(A) Representative averaged traces from *App*$^{NL-G-F}$ and wild-type mice at 4-5 months. **(B) & (D)** The paired pulse ratio (PPR) (amplitude of the 2nd response/amplitude of the 1st response) at an inter-stimulus interval of **(Bi) & (Di)** 25 and **(Bii) & (Dii)** 50 ms. **(C) & (E)** Failure rate of the 1st response at the ages indicated above. 7-9 months: main effect of genotype ($p<0.05$), with *App*$^{NL-G-F}$ mice displaying lower failure rates than wild-types. Columns indicate mean ± SEM. Sample sizes are marked within bars. Individual points represent the mean of all recordings taken from individual animals. Two-way ANOVA indicated by: *$p<0.05$. Asterisks beside comparisons indicate main effect of genotype.

3.6 Plaque presence has some effects on synaptic efficacy at postsynaptic compartments

As mentioned above, in addition to examining differences in synaptic transmission between wild-type and *App* knock-in mice, the present work also aimed to explore how the synaptic activity in *App* knock-in mice themselves is altered depending on the presence of a plaque around the stimulated axon. This would provide an idea as to whether the plaque, or even the plaque environment itself, has an effect on transmission. Therefore, here, $App^{NL\text{-}G\text{-}F}$ mice were further divided into two groups – "plaque" and "no plaque" condition – depending on whether the CA3 axon on which the stimulating electrode was placed was passing near a plaque on its way to the recorded CA1 cell during voltage-clamp experiments. This was determined through *post-hoc* immunohistochemical staining of amyloid-β plaques using LCOs on the same slices used for electrophysiological experiments. Therefore, subsequent confocal imaging allowed the visualisation of the stimulated axon (using DiI placed prior to electrophysiological experiments), the recorded cell (which was filled with AF488 during recordings), and the amyloid plaque (using LCOs following electrophysiological experiments). As this work used minimal stimulation during experiments, *post-hoc* tracing of the axon and the estimate of plaque presence around the stimulated axon in $App^{NL\text{-}G\text{-}F}$ mice could be considered an accurate representation of the plaque load during transmission and could provide insight into how plaque presence affects synaptic activity. An axon was deemed "plaque-associated" in cases when a plaque was present within 30 μm of the stimulated axon, and "non-plaque-associated" when plaques were outside of that region (Figure 3.7A). This distinction was based on previous studies which have demonstrated extensive synapse loss and axonal dystrophy within this radius (Koffie et al., 2012; Koffie et al., 2009; Sadleir et al., 2016). Thus, in cases when two recordings were made from the same animal and each belonged to a different condition, these were considered as separate samples in the present analysis. If, however, these recordings were both categorised in the same condition, an average for these was obtained to determine the average value for that animal.

3.6.1 Plaque presence effects on postsynaptic activity in *App*$^{NL-G-F}$ mice

Initially, the median of the amplitudes of the successful first responses was examined in plaque- and non-plaque associated recordings in male and female *App*$^{NL-G-F}$ mice. Here, similarly to before, analysis was done separately for the two age groups, although differences between the two stages of pathology will also be discussed. At 4-5 months of age, there was a trend for a significant main effect of plaque presence on the median amplitude ($p=0.06$; two-way ANOVA), as demonstrated in Figure 3.7B below. This suggests that the median amplitude is reduced in recordings when a plaque was present around the stimulated axon in comparison to recordings when no plaque was present. Interestingly, when comparing how many synapses were activated in both conditions by taking into account the mEPSC recorded previously from male *App*$^{NL-G-F}$ mice at that age, it appears that while at plaque conditions the number of synapses activated were on average 0.87 (calculated as uEPSC/mEPSC), for no-plaque conditions it was 1.27, suggesting that there might be fewer active synapses at plaque conditions. Despite differences in the postsynaptic amplitudes, no differences were observed in the stimulation voltage used in these conditions according to a two-way ANOVA ($p>0.05$; Figure 3.7C). Lastly, no difference in the decay time was observed at that age ($p>0.05$; two-way ANOVA; Figure 3.7D).

At 7-9 months, there was no difference in the postsynaptic amplitudes, stimulation voltage, or decay times ($p>0.05$; two-way ANOVAs; Figure 3.7E, F, G). This suggests that the differences in postsynaptic amplitudes between the two conditions which were observed at 4-5 months are lost at more advanced stages of pathology. This might be because the levels of soluble Aβ oligomers at this age are more similar in plaque and no-plaque conditions due to the high density of plaques and hence soluble Aβ oligomers at that stage. These findings also demonstrate that the longer decay times observed in the earlier comparisons between *App*$^{NL-G-F}$ and wild-type mice at that age are dependent on the AD environment itself rather than the presence of a plaque near the synapse.

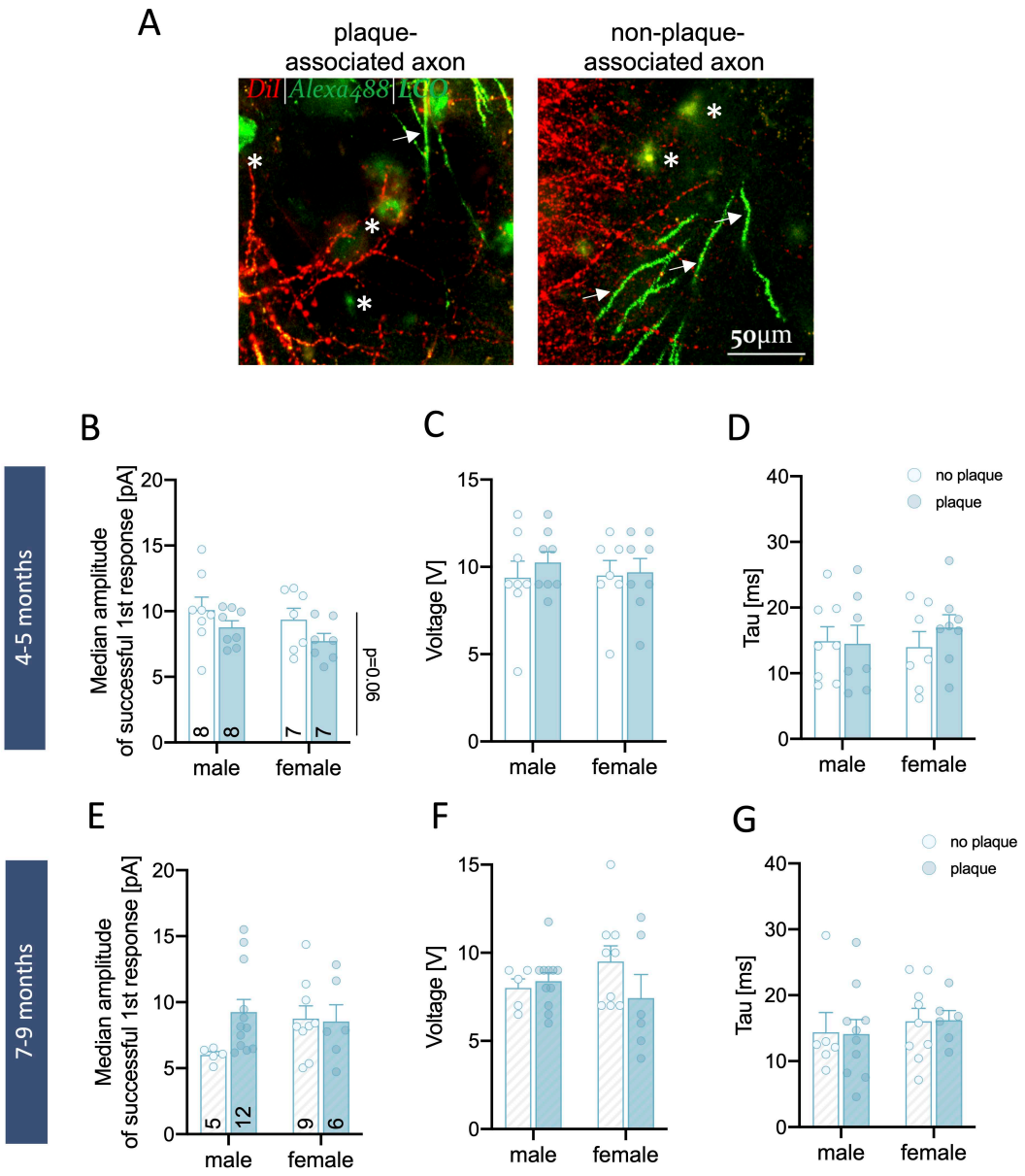

Figure 3.7. Properties of uEPSCs in response to the stimulation of axons near and away from plaques in male and female 4-5- and 7–9-month-old *App*$^{NL-G-F}$ mice.
(A) Representative images illustrating CA3 axons (red) passing near and away from a plaque (green; indicated with asterisks) on its way to a CA1 cell (green; dendrites indicated with arrows). Scale bar: 50µm. **(B) & (E)** Median uEPSC amplitude of successful first responses of CA1 cells in response to the stimulation of CA3 axons at the ages indicated above. 4-5 months: trend for main effect of genotype (p=0.06). **(C) & (F)** Mean voltage used for stimulation for all recordings. **(D) & (G)** Decay time of uEPSC recorded from all groups. Columns indicate mean ± SEM. Sample sizes are marked within bars. Individual points represent the mean of all recordings taken from individual animals. Two-way ANOVAs. P-values beside comparisons indicate main effect of plaque presence.

3.6.2 Release probability alterations at plaque-associated axons

According to the two-way ANOVA, there were no differences in the PPR at 4-5 months at either 25 ms or 50 ms ($p>0.05$; Figure 3.8Ai,ii), suggesting that the release probability is not differentially affected by the presence of a plaque. In accordance with this, no difference in the failure rate of the first response was observed at that age (two-way ANOVA; $p>0.05$; Figure 3.8B). Altogether these results show that soluble Aβ oligomers around plaques do not increase the number of vesicles primed for exocytosis at that age in this model, as it has previously been demonstrated in other AD models. This suggests that either plaques in *App*$^{NL-G-F}$ mice do not contain the same cloud of soluble Aβ previously reported around plaques in transgenic models, or the Aβ species found in plaque regions in this model might be different and exert different effects at synaptic regions.

At 7-9 months, there were no changes in the PPR at either 25 ms or 50 ms (two-way ANOVA; $p>0.05$; Figure 3.8Ci,ii). Interestingly, when the failure rate of the first response was examined, a two-way ANOVA found a significant main effect of sex ($p<0.01$; Figure 3.8D). These results indicate that the earlier observation of lower failure rates in *App*$^{NL-G-F}$ mice compared to wild-types was likely driven by the lower failure rates observed in female *App*$^{NL-G-F}$ mice. Altogether, these results suggest that female axons are more likely to be activated than male axons, suggesting that the mechanisms occurring in this AD model exhibit some interesting sex-specific differences which affect axonal activation and which warrant further investigation.

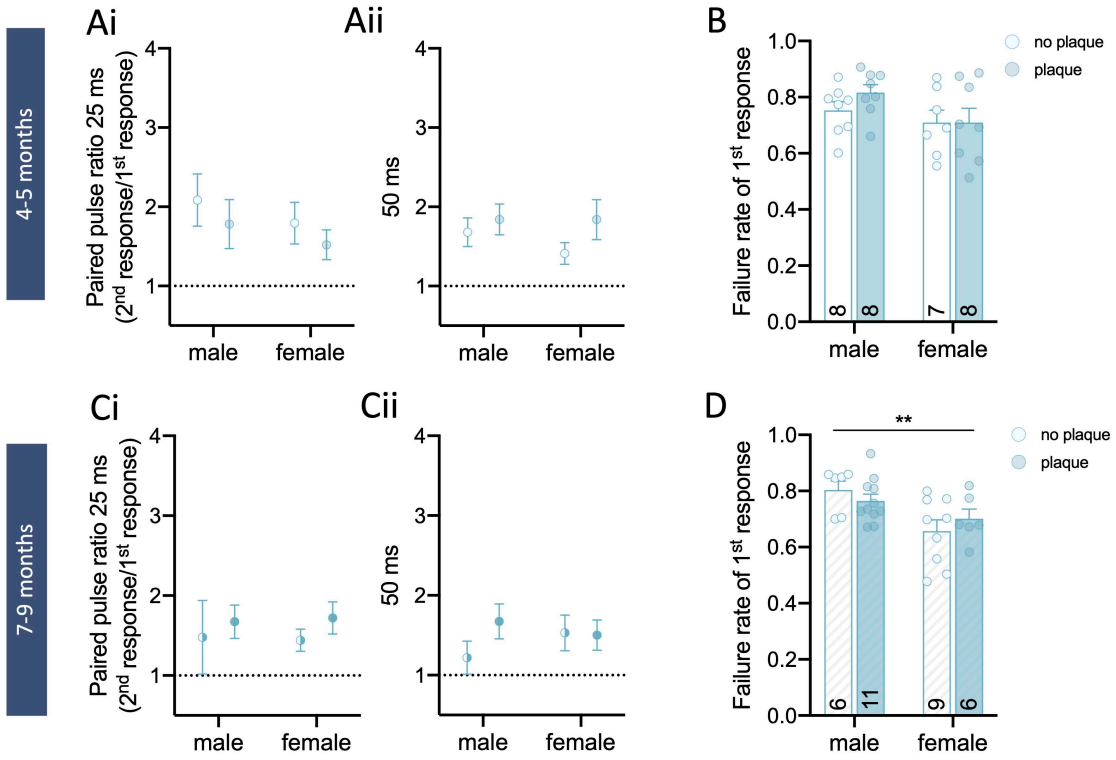

Figure 3.8. Release probability at axons near and away from plaques in male and female *App*$^{NL-G-F}$ mice at 4-5 and 7-9 months.

(A) & (C) The paired pulse ratio (PPR) (amplitude of the 2nd response/amplitude of the 1st response) at an inter-stimulus interval of **(Ai) & (Ci)** 25 and **(Aii) & (Cii)** 50 ms. **(B) & (D)** Failure rate of the first response at the ages indicated above. 7-9 months: main effect of sex ($p<0.05$). Columns indicate mean ± SEM. Sample sizes are marked within bars. Individual points represent the mean of all recordings taken from individual animals. Two-way ANOVA indicated by: **$p<0.01$. Asterisks above comparisons indicate main effect of sex.

3.7 Summary

This chapter explored the plaque pathology of *App*$^{NL-G-F}$ mice at 4-5 months and 7-9 months, as well as changes in microglial and astrocytic density to understand the effects of the AD environment in these mice. Furthermore, I also examined synaptic changes at CA3-CA1 synapses caused by the AD environment itself in *App*$^{NL-G-F}$ mice and how this transmission is altered when taking into account plaque presence around CA3 axons.

With regards to plaque load, both male and female 7–9-month-old *App*$^{NL-G-F}$ mice exhibited a larger number of plaques compared to 4-5-month-old mice, with this difference largely restricted to small plaques sized 10-50 μm^2. Microglial density was higher in *App*$^{NL-G-F}$ mice compared to wild-types at both sexes and ages, with some hippocampal regions showing higher microglial density at 4-5 months. Interestingly, the increased microglial density compared to wild-types was similar across the two ages, suggesting that after an initial increase in density in response to plaque pathology, microglia do not exhibit any further alterations in number. Therefore, one explanation for the heavier plaque load and larger number of smaller-sized plaques observed with age in *App*$^{NL-G-F}$ mice could be that after an initial response to plaques at 4-5 months, microglia are no longer able to regulate the number of plaques as pathology progresses, ultimately leading to an accelerated formation of smaller plaques. However, it is important to note that the present work did not examine any gene expression changes in microglia and it is possible that although microglial numbers did not increase further with age, their signature could have changed, an idea which in need of further investigation. In comparison to microglia, no clear differences were observed in astrocytic density, with results showing different distribution in the hippocampal regions examined regardless of genotypes or age.

I also found that merely exploring synaptic transmission changes brought about by the AD pathology seen in *App*$^{NL-G-F}$ mice reveals subtle differences in comparison to wild-type mice, with no changes in the postsynaptic amplitude, stimulation voltage used, or the paired-pulse ratio at either age examined here. However, *App*$^{NL-G-F}$ mice did exhibit longer decay times at advanced stages of pathology (7-9 months) regardless of sex, suggesting altered receptor kinetics at this stage which could potentially be driven by different AMPAR subunits at the postsynapse previously reported in AD models.

Furthermore, potential differences in axonal excitability or receptor desensitisation were also highlighted as *App*$^{NL-G-F}$ mice exhibited lower failure rates than age-matched wild-types at 7-9 months, while no changes in the PPR were observed. These results suggest that axons in *App*$^{NL-G-F}$ mice might be more easily excitable than those of wild-types, potentially illustrating interesting differences which occur in response to AD-associated mechanisms.

Examining how these properties are altered when the plaque presence around the stimulated axon is taken into account revealed a tendency for lower amplitudes of the first response at plaque- compared to non-plaque-associated synapses at 4-5 months, illustrating plaque-dependent alterations in postsynaptic compartments at this stage. These could be driven by either the soluble Aβ oligomers which are tightly associated with plaques, or by surrounding microglia which many studies have shown tend to cluster around the toxic aggregates. Interestingly, no differences were observed for the stimulation voltage, decay times, PPR, and failure rates at 4-5 months. Furthermore, at 7-9 months, there were no differences between plaque and no-plaque conditions, with no changes in the postsynaptic amplitude, stimulation voltage, decay times or the paired-pulse ratio. However, lower failure rates were observed in females compared to males, suggesting that there are potential sex differences in axonal activation or release in *App*$^{NL-G-F}$ mice which are independent of plaque presence.

Chapter 4: The effects of perturbed microglial functioning on the plaque pathology and glial distribution in *App*$^{NL-F}$ mice

4.1 Introduction

Neuroinflammation in response to Aβ pathology is a well-known feature of both the human AD brain and AD mouse models. A number of studies have demonstrated alterations in inflammatory markers and glial activation and distribution in the AD brain (Benitez et al., 2021; Medawar et al., 2019; Yuan et al., 2016). This has been confirmed by several GWAS which have further indicated that variants of inflammation-related genes, including *CD33*, *TREM2*, *APOE*, and *clusterin*, increase the risk of developing AD (Guerreiro et al., 2013c; Jansen et al., 2019; Ulland et al., 2017). The first three of these factors are highly expressed in microglia and particularly in disease-associated microglia (DAM) (Keren-Shaul et al., 2017), whereas TREM2, APOEε4, and clusterin show elevated levels in astrocytes. This highlights that microglia and astrocytes play a key role in the early response of the brain to the AD environment and, interestingly, both of these cell types have been demonstrated to cluster around amyloid plaques (Henstridge et al., 2019). Although this demonstrates their active response to Aβ pathology, their precise role in these regions is unclear.

Microglial accumulation around Aβ plaques has been suggested to serve several functions, including Aβ phagocytosis (Baik et al., 2016; Fu et al., 2012), the formation of a protective barrier to limit Aβ-associated toxicity (Yuan et al., 2016), the compartmentalisation of plaques (Clayton et al., 2021), as well as the phagocytosis of neighbouring synapses both as a protective and a detrimental mechanism (Edwards, 2019; Hong et al., 2016). The possibility that microglia can carry all of these functions suggests that microglia might have a different role depending on the disease stage and this has been confirmed by more recent work which demonstrated disease-stage-dependent effects of the microglial receptor TREM2 (Jay et al., 2017). This study demonstrated that although *Trem2* knockout ameliorates plaque pathology early in disease, it has the opposite effects in later stages (Jay et al., 2017), indicating that the

microglial phenotypes over the course of the disease can have opposing effects on the properties of Aβ plaques. Interestingly, previous work has also demonstrated that microglial association with amyloid plaques is reduced when *Trem2* levels are lower and/or when the R47H variant of *Trem2* is present, which is associated with an increased risk of developing AD (Song et al., 2018; Ulrich et al., 2014; Yuan et al., 2016). This suggests that microglial association with plaques in the first stages of the disease is important and is likely to have a function in limiting plaque spread, while in later stages, there is a switch to another unknown function.

In addition to microglia, astrocytes also show robust activation in AD conditions. This is classically characterized by the increased expression of GFAP, which recently has been shown to be a useful marker for the detection of people at increased AD risk (Chatterjee et al., 2021) and has even been shown to correlate with cognitive impairment in AD patients (Oeckl et al., 2019). Similarly to microglia, astrocytes also cluster around Aβ plaques, with their role in these regions suggested to be Aβ degradation owing to the fact that they can express two key Aβ degrading enzymes, neprilysin and IDE, as well as several well-known Aβ chaperones, including APOE and clusterin (Ries and Sastre, 2016). However, astrocytes in these regions might also have other roles, including the regulation of plaque-associated synapses through the release of the "eat-me" signal C3 or through the release of glutamate which has been shown to modulate synaptic activity (Lian et al., 2015; Talantova et al., 2013).

It is therefore clear that both microglia and astrocytes play an important function in AD, however their precise role in pathogenesis is still uncertain. The previous chapter elucidated some changes in gliosis and pathology, however because the *App*$^{NL-G-F}$ model exhibits a much faster plaque accumulation because of the Arctic mutation, it is possible that this did not allow for the sufficient build-up of processes dependent solely on soluble Aβ. As *App*$^{NL-F}$ mice begin exhibiting plaque formation around the age of 9 months of age, the much slower accumulation of Aβ observed in this model gives enough time for processes which are solely dependent on soluble Aβ oligomers to take place. Furthermore, it is still relatively unclear which of the mechanisms observed in AD mouse models are driven by soluble Aβ oligomers, or by secondary processes such as microglial activation in response to plaque pathology. To understand this, the present chapter will explore *App*$^{NL-F}$ and *App*$^{NL-F}$/*Trem2*^{R47H} mice, the latter

of which exhibits perturbed microglial functioning. As both of these models display moderate plaque pathology at 18 months of age., it would be interesting to examine how glial responses and plaque pathology are altered when microglial functioning is perturbed during robust plaque accumulation. Importantly, as the *App*$^{NL-F}$/*Trem2*^{R47H} model has previously been shown to exhibit a perturbed microglial response due to the R47H variant of *Trem2*, as well as reduced levels of *Trem2* (see Figure 4.1), examining this model will also provide interesting insight into how *Trem2*^{R47H} affects plaque pathology, as well as the response of both glial cell types (Cheng-Hathaway et al., 2018; Liu et al., 2020; Xiang et al., 2018). The *App*$^{NL-F}$/*Trem2*^{R47H} model has not been characterised previously, making the present work one of the first to understand how microglial disruption introduced by *Trem2*^{R47H}, a mutation associated with an increased risk of developing AD in humans, affects the progression of plaque pathology and glial responses to that pathology.

To accomplish the above, the present chapter quantified the number of Aβ plaques, microglia, and astrocytes in the two models. Alterations in specific hippocampal regions were also explored to elucidate if specific areas are more susceptible to AD-associated toxicity. Previous work has demonstrated that most of the changes in microglial density in the hippocampus of *App*$^{NL-F}$ mice occur around 24 months of age (Benitez et al., 2021), yet it is unclear whether specific hippocampal regions exhibit these changes earlier and whether astrogliosis is a prominent feature in these mice. Furthermore, if any of this is altered in the presence of the *Trem2*^{R47H} mutation also remains to be determined.

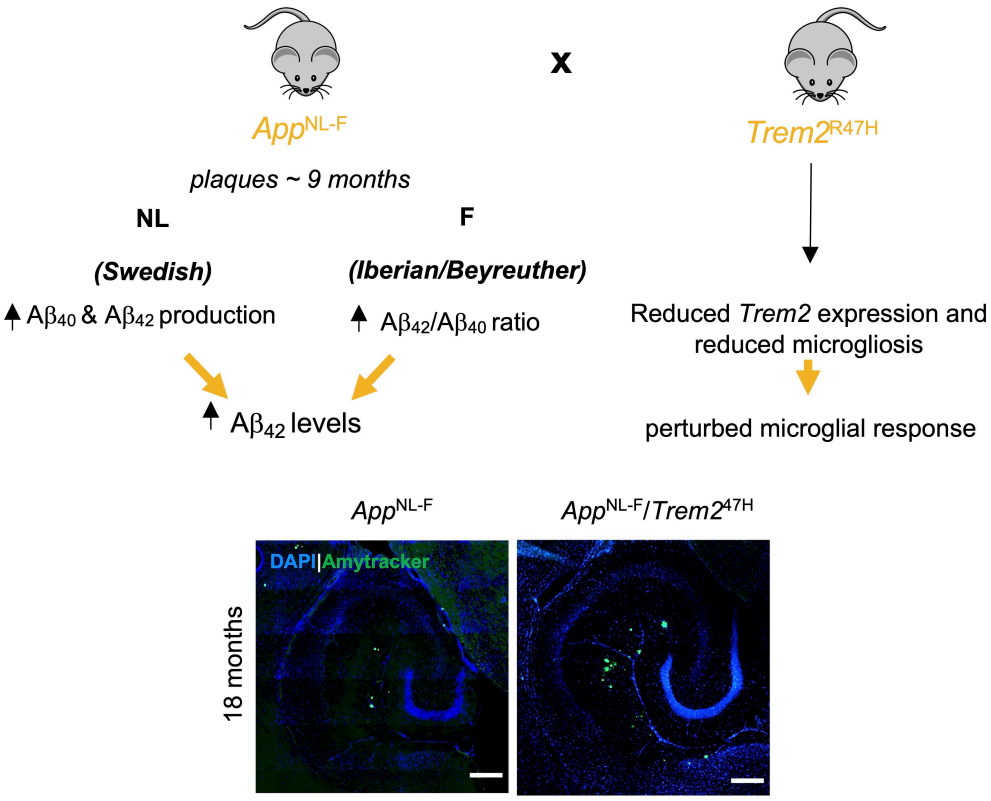

Figure 4.1. Schematic demonstrating the mouse models used in this chapter.
Top panel: *App*$^{NL-F}$ mice contain the Swedish and Iberian/Beyreuther mutations which together lead to increased Aβ$_{42}$ levels. The *Trem2*^{R47H} model carries the AD risk variant and also exhibits reduced *Trem2* expression and microgliosis, together resulting in a perturbed microglial response. Crossing these models results in the *App*$^{NL-F}$/*Trem2*^{R47H} model which similarly to *App*$^{NL-F}$ mice has robust plaque pathology at 18 months, but also exhibits an altered microglial response. Bottom panel: Plaque distribution (labelled with Amytracker in green) in the hippocampus of *App*$^{NL-F}$ and *App*$^{NL-F}$/*Trem2*^{R47H} mice at 18 months. Scale bar: 200μm.

4.2 Perturbed microglial functioning has some effects on plaque density and the number of small plaques

Similarly to in Chapter 3, slices were stained with LCOs to determine the plaque load in the hippocampus of APP^{NL-F} and $App^{NL-F}/Trem2^{R47H}$ mice at 18 months of age. While sample sizes for the individual sexes are sometime small, the data from both male and female mice were distributed across the full range of the combined samples, suggesting that sex differences were unlikely. Hence, the data from the two sexes was combined for each genotype and this was used for analysis. However, as there could be some sex differences which could have arisen at larger sample sizes, as well as because previous work on AD has demonstrated that sex can have an effect on the microglial response and how AD pathology progresses (Guillot-Sestier et al., 2021; Wang et al., 2003), individual points for each genotype are also presented and each sex is indicated with a different symbol.

As demonstrated in Figure 4.2A below, neither wild-type nor $Trem2^{R47H}$ mice exhibited any plaques, while both App^{NL-F} and $App^{NL-F}/Trem2^{R47H}$ mice demonstrated robust plaque pathology, particularly in the SR and SLM regions in the CA1 subfield. When the plaque density was compared between *App* knock-in mice and knock-in mice with perturbed microglial response, an unpaired t-test revealed that $App^{NL-F}/Trem2^{R47H}$ mice exhibit a higher density of plaques in the hippocampus than App^{NL-F} mice ($p<0.01$; Figure 4.2Bi). Exploring different-sized plaques revealed that this is driven by a larger number of smaller-sized plaques (10-50 μm^2) in $App^{NL-F}/Trem2^{R47H}$ compared to App^{NL-F} mice ($p<0.0001$; two-way ANOVA; Figure 4.2Bii). This suggests that a perturbed microglial response in $App^{NL-F}/Trem2^{R47H}$ mice results in a larger number of smaller sized plaques, indicating that microglia might be essential for the clearance of smaller plaques while they do not have much of an effect on larger plaques. Alternatively, it is possible that that the previously shown barrier formation function of microglia (Condello et al., 2015) is lost in $Trem2^{R47H}$-expressing mice, as previously demonstrated in mice lacking *Trem2* (Yuan et al., 2016), resulting in an enhanced breaking off of smaller plaques from bigger plaques in $App^{NL-F}/Trem2^{R47H}$ mice. Furthermore, u101nsurprisingly, given that only the number of smaller plaques was changed, the hippocampal plaque coverage was also found to be similar between the two genotypes (Figure 4.2C).

Previous work has also shown that microglia are important in compartmentalising plaques, with their ablation contributing to the formation of more diffuse plaques (Clayton et al., 2021; Spangenberg et al., 2019; Yuan et al., 2016). However, here when the plaque circularity was explored, no differences were found between the two genotypes ($p>0.05$; Figure 4.2D), suggesting that microglia might not be involved in keeping plaques compact in these models or at that stage of pathology.

As mentioned above, in both *App*$^{NL-F}$ and *App*$^{NL-F}$/*Trem2*^{R47H} mice, plaques seemed to be mainly located primarily in the SLM, although also in the SR region. To determine if one region is more susceptible to plaque formation than the other, the plaque density in these regions was examined. Unsurprisingly, significant main effects of region ($p<0.0001$) and genotype ($p<0.05$) were found for both plaque density and plaque coverage using two-way ANOVAs (Figure 4.2Ei,ii). This suggests that in the *App* knock-in model examined here, plaques are preferentially formed in the SLM region, suggesting that the synapses there are likely to be particularly affected in this model. It is interesting to determine what makes that region susceptible for the formation of plaques. One possibility might be that microglia are differentially affected in this region, or that the synapses in the SLM, which are primarily inputs from layer III in the entorhinal cortex to CA1 pyramidal neurons, are particularly vulnerable in AD.

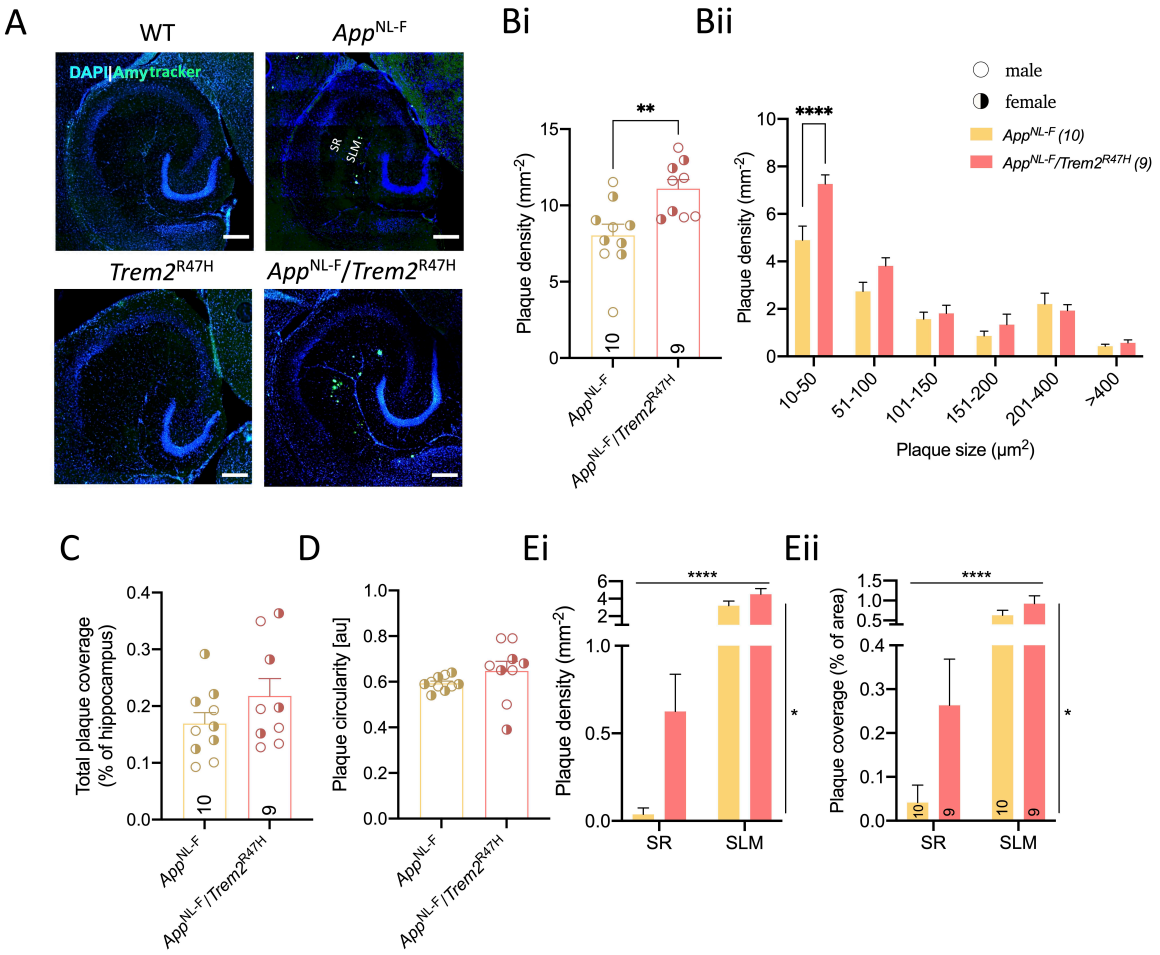

Figure 4.2. Deposition of Aβ plaques in 18-month-old *App*$^{NL-F}$ and *App*$^{NL-F}$/*Trem2*^{R47H} mice. **(A)** Representative images of hippocampi from wild-type, *App*$^{NL-F}$, *Trem2*^{R47H}, and *App*$^{NL-F}$/*Trem2*^{R47H} mice stained with Amytracker (green) for Aβ plaque labelling and DAPI (blue) for nuclei labelling. Scale bar: 200μm. **(Bi)** Plaque density for the two genotypes. Difference between genotypes, with *App*$^{NL-F}$/*Trem2*^{R47H} mice displaying more plaques than *App*$^{NL-F}$ mice ($p<0.01$) **(Bii)** Frequency-size distribution of plaques. Plaque size x genotype interaction ($p<0.0001$), with a larger number of smaller-sized plaques (10-50μm^2 in *App*$^{NL-F}$/*Trem2*^{R47H} mice. **(C)** Total plaque coverage in the hippocampus for the two genotypes. **(D)** Plaque circularity for the two genotypes. **(Ei)** Plaque density and **(Eii)** plaque coverage in the SR and SLM in the CA1 subfield. Main effects of region ($p<0.0001$) and genotype ($p<0.05$). Columns indicate mean ± SEM. Sample sizes are marked within bars. Individual points represent the mean of three slices taken from individual animals. Empty circles refer to males, while filled circles refer to females. Unpaired t-tests and two-way ANOVA followed by Sidak-corrected *post-hoc* comparisons when there was an interaction are indicated by: *$p<0.05$, **$p<0.01$, ****$p<0.0001$. Asterisks beside comparisons indicate main effect of genotype, while asterisks above comparisons indicate main effect of region.

4.3 Changes in microgliosis and astrogliosis

In order to determine if any of the above Aβ plaque load changes are accompanied with changes in either microgliosis or astrogliosis, the density and distribution of glia were examined. Previous work has demonstrated that microglia and astrocytes are attracted to and cluster around Aβ plaques (Henstridge et al., 2019) and this ability is impaired in the presence of the R47H variant of *Trem2* (Cheng-Hathaway et al., 2018; Song et al., 2018; Zhong et al., 2018). Recent work from our lab demonstrated that *App*$^{NL-F}$ mice only exhibit increased microglial density in the CA1 area of the hippocampus at 24 months of age and they do not demonstrate any increases in *Trem2* expression per microglia (Benitez et al., 2021). However, whether this is true for the different hippocampal regions or for astrocytic density, as well as for *App* knock-in mice with the *Trem2*^{47H} mutation remains to be determined.

4.3.1 Microglial density changes

Therefore, here the density and hippocampal distribution of microglia (Iba1^{+}) and astrocytes (GFAP^{+}) were examined. Slices were also stained with LCOs determine the relationship between glia and plaques in the hippocampus of these mice. The following analyses were performed using two-way ANOVAs with the *App* and *Trem2*^{R47H} mutations being the two factors as this can provide insight into how each affects the glial response in these models.

As expected, microglia from both *App*$^{NL-F}$ and *App*$^{NL-F}$/*Trem2*^{R47H} mice were clustered around amyloid plaques, although those from the latter mice did not seem as clustered as in *App*$^{NL-F}$ mice (see Figure 4.3Ai,ii). This is in accordance with previous studies which have shown abnormal microglial clustering around plaques in the presence of *Trem2*^{R47H} (Xiang et al., 2018). When the overall microglial density was quantified, a two-way ANOVA found no differences between the examined groups ($p>0.05$; Figure 4.3B). However, when the different hippocampal regions were examined, a significant genotype x region interaction was determined ($p=0.001$; two-way ANOVA), with *post-hoc* tests revealing that *App*$^{NL-F}$ mice exhibit higher microglial density in the SLM region in the CA1 subfield than all other genotypes ($p<0.05$; Figure 4.3C). It was also established that in the CA3 pyramidal layer, *App*$^{NL-F}$ mice exhibit higher microglial density than *App*$^{NL-F}$/*Trem2*^{R47H} mice ($p<0.01$). The fact that microglial density was

particularly increased in the SLM, a region the above analysis determined to exhibit robust plaque formation, suggests that microglia are more densely populated there because of plaque pathology. Furthermore, this increase in density was not evident in *App*$^{NL-F}$/*Trem2*^{R47H} mice, demonstrating that the R47H variant in these mice precludes microglial migration towards plaque regions, in accordance with previous work.

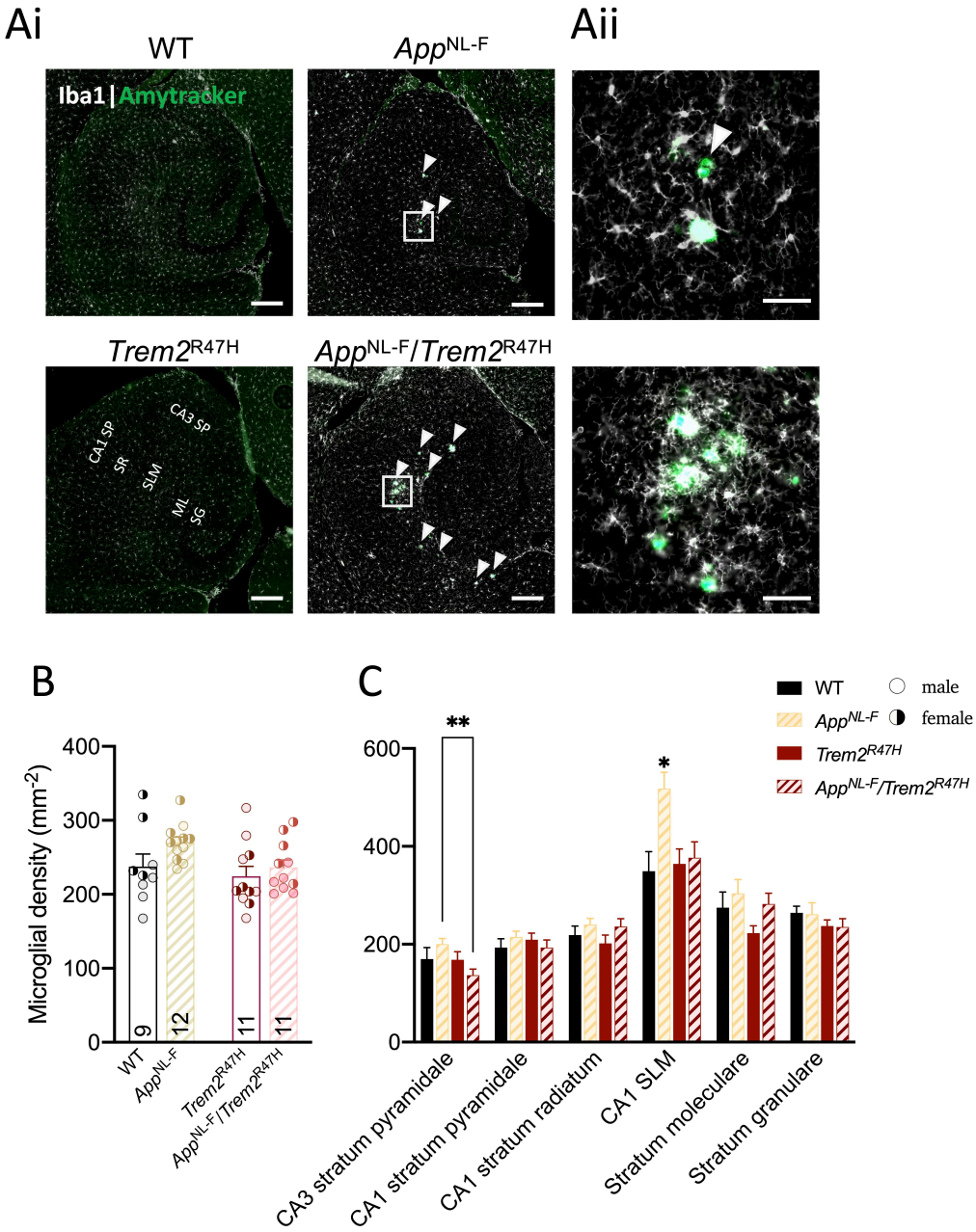

Figure 4.3. Microglial density and distribution in the hippocampus of *App*$^{NL-F}$ and *App*$^{NL-F}$/*Trem2*^{R47H} at 18 months in comparison to wild-type and *Trem2*^{R47H} controls.

(Ai) Representative images of Iba1^{+} microglia (white) and Aβ plaques (green) at 18 months. Arrows point at individual Aβ plaques. The different hippocampal regions examined in this analysis are also marked. Scale bar: 200μm **(Aii)** Zoomed-in images of the squares indicated in (Ai), showing microglial clustering around plaques. Scale bar: 50μm **(B)** Microglial density for all genotypes. **(C)** Microglial density in the different hippocampal regions. Genotype x region interaction (p=0.001). Columns indicate mean ± SEM. Sample sizes are marked within bars. Individual points represent the mean of three slices from individual animals. Empty circles refer to males, while filled circles refer to females. Two-way ANOVAs followed by Sidak-corrected *post-hoc* comparisons when there was an interaction indicated by: *p<0.05, **p<0.05.

4.3.2 Changes in astrocytic density

Having established microglial density changes in *App*$^{NL-F}$ and *App*$^{NL-F}$/*Trem2*^{R47H} mice, the density of astrocytes was also explored. Similarly to microglia and as expected, GFAP^{+} astrocytes from both *App*$^{NL-F}$ and *App*$^{NL-F}$/*Trem2*^{R47H} mice appeared to cluster around amyloid plaques, although not as tightly as microglia, with their processes mostly ensheathing plaques (Figure 4.4A). According to a two-way ANOVA, there was a significant *App* x *Trem2* interaction for astrocytic density ($p<0.05$; Figure 4.4B). This suggests that while *App*$^{NL-F}$ mice exhibit higher astrocytic density than wild-type controls, the addition of the *Trem2*^{R47H} mutation in *App*$^{NL-F}$/*Trem2*^{R47H} mice has the opposite effect on astrocytic density. This suggests that the overall astrocytic density is differentially affected in *App* knock-in mice in the presence of *Trem2*^{R47H}, demonstrating that perturbed microglial functioning can further affect the response of astrocytes to the AD-associated toxic processes. However, when the different hippocampal regions were examined, a two-way ANOVA only demonstrated a main effect of region on astrocytic density ($p<0.0001$; Figure 4.4C).

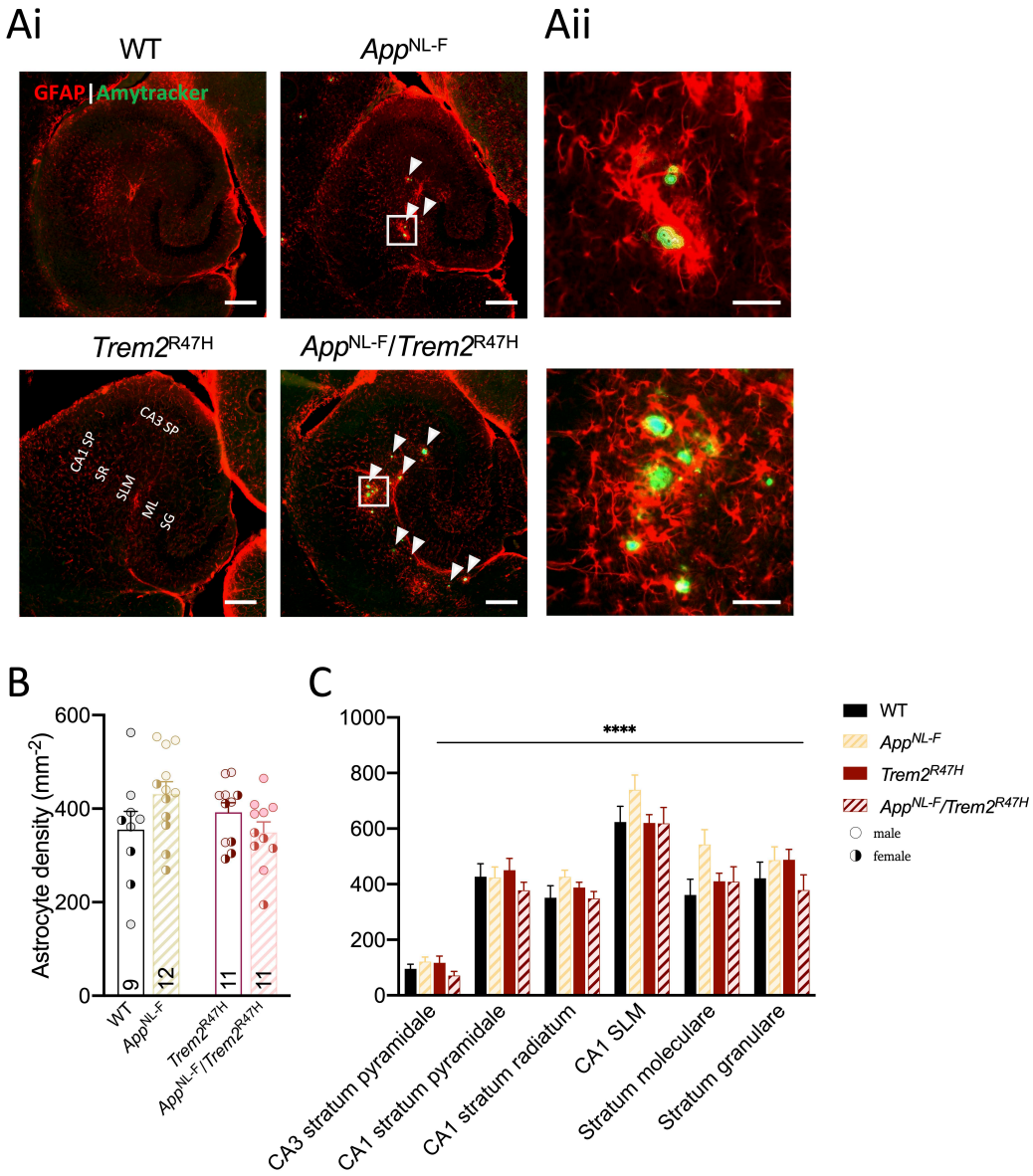

Figure 4.4. Astrocyte density and distribution in the hippocampus of *App*$^{NL-F}$ and *App*$^{NL-F}$/*Trem2*^{R47H} at 18 months in comparison to wild-type and *Trem2*^{R47H} controls. **(Ai)** Representative images of GFAP^{+} astrocytes (red) and Aβ plaques (green) at 18 months. Arrows point at individual Aβ plaques. The different hippocampal regions examined in this analysis are also marked. Scale bar: 200 µm **(Aii)** Zoomed-in images of the squares indicated in (Ai), showing astrocytic clustering around plaques. Scale bar: 50µm **(B)** Astrocytic density for all genotypes. *App* x *Trem2* interaction ($p<0.05$). **(C)** Astrocytic density in the different hippocampal regions. Main effect of region ($p<0.0001$). Columns indicate mean ± SEM. Sample sizes are marked within bars. Individual points represent the mean of three slices from individual animals. Empty circles refer to males, while filled circles refer to females. Main effect of region in a two-way ANOVA indicated by: ***$p<0.0001$. Asterisks above comparisons indicate main effect of region.

4.4 Summary

In this chapter I examined plaque pathology and glial density in *App*$^{NL-F}$ mice and whether these phenotypes are altered in the presence of the *Trem2*^{R47H} mutation. Plaque pathology was indeed different in the presence of the R47H variant of *Trem2*, with *App*$^{NL-F}$/*Trem2*^{R47H} mice exhibiting a larger number of plaques, and specifically smaller-sized plaques, than age-matched *App*$^{NL-F}$ mice. Interestingly, in both models the plaque pathology in the SLM region was much more prominent than in the SR, highlighting this region as particularly susceptible to AD pathology. In order to understand if any of these plaque changes are driven by changes in glial density, microglial and astrocytic distributions were also examined. Although overall hippocampal microglial density was unchanged, *App*$^{NL-F}$ exhibited higher microglial density in the SLM region in the CA1 subfield compared to wild-type, *Trem2*^{R47H} and *App*$^{NL-F}$/*Trem2*^{R47H} mice, suggesting impaired microglial migration to plaque-associated regions in *App*$^{NL-F}$ mice in the presence of the *Trem2*^{R47H} mutation. This shows an interesting interaction between plaques and microglia in the SLM which warrants further investigation of the processes occurring in this region. Lastly, exploring astrocytic density changes revealed a significant *App* x *Trem2* interaction, suggesting that the effects on astrocytic density of the *App* mutation are counteracted by the presence of the R47H variant of *Trem2*. Overall, these results provide an interesting insight into how perturbed microglial functioning can affect Aβ pathology, as well as microglial and astrocytic distribution.

Chapter 5: Synaptic changes in *App*$^{NL-F}$ mice and mice with perturbed microglial response

5.1 Introduction

Microglia have long been pinpointed as important players in AD pathogenesis. Even Alois Alzheimer himself noted their involvement in AD (Alzheimer, 1907), with more recent studies highlighting microgliosis as a key disease process in AD (Beach et al., 1989; Henstridge et al., 2019). Microglia are known for clustering around amyloid plaques in both AD post mortem tissue and AD mice (Condello et al., 2015; Meyer-Luehmann et al., 2008; Yuan and Grutzendler, 2016), and these microglia have been suggested to constitute a completely different subset of microglia based on their gene expression profile, known as DAMs (Keren-Shaul et al., 2017). Some studies have suggested that this mechanism allows microglia to form a protective barrier to keep plaque-associated toxicity local, while others have suggested that this allows for microglia to phagocytose Aβ species, thereby keep plaques more compact, reduce plaque burden, and protect surrounding neurons (Spangenberg et al., 2019; Yu and Ye, 2015). Yet, despite these suggestions, the precise role of microglia in these regions is still unclear.

In addition to their interaction with plaques, microglia have been suggested to have direct effects on neurons and synapses specifically in an AD environment. In particular, microglia from both AD mice and human post-mortem tissue have been shown to recognise and phagocytose synapses in a complement-dependent manner (Hong et al., 2016; Tzioras et al., 2019), a microglial process which has been well-established during development (Schafer et al., 2012; Stevens et al., 2007). This idea has been further supported by the fact that microglial ablation prevents the loss of spines seen in AD mice (Olmos-Alonso et al., 2016; Spangenberg et al., 2016), illustrating a clear link between microglia and synaptic changes in AD. However, it remains unclear whether this mechanism is detrimental to synapses, thereby impairing their function, or if it is a protective mechanism allowing microglia to phagocytose damaged synapses, in turn limiting the spread of toxicity and maintaining a relatively normal overall neuronal function (Edwards, 2019).

It is clear that the interaction between microglia, Aβ, and synapses is important in AD, however, in what ways these three key components drive disease progression remains to be determined. Chapter 3 explored how Aβ plaques and soluble Aβ in the neuropil affect synaptic transmission. However, it is important to note that the mouse model used there, the *App*$^{NL-G-F}$ model, has several limitations which might make it hard to discern what specific mechanisms drive the observed effects. The biggest limitation of this model is perhaps the inclusion of the Arctic mutation within the Aβ sequence which makes Aβ particularly prone to aggregate in non-physiological ways (Kamino et al., 1992; Nilsberth et al., 2001; Saito et al., 2014). This thus means that any changes observed in these mice could largely be attributed to Aβ plaques rather than the soluble Aβ species themselves, making it hard to discern which mechanism is the contributing factor to the observed effects on synaptic activity. Therefore, in this chapter, I aimed to explore how synaptic transmission is altered at single synapses in *App*$^{NL-F}$ mice which only contain the Swedish and Iberian/Beyreuther mutations, in order to understand the relationship between soluble Aβ and synaptic activity. Furthermore, here I also examined how this activity compares to that in *App*$^{NL-F}$/*Trem2*^{R47H} mice, which exhibit a perturbed microglial response, in order to understand in what ways microglia contribute to the altered synaptic activity observed in *App*$^{NL-F}$ mice. This will thus elucidate the specific role of microglia at individual synapses and provide some insight as to whether their role is protective or detrimental in moderate stages of pathology in AD mice, which is in fact considered early in terms of human disease.

In addition to exploring genotype differences, this chapter, similarly to Chapter 3, also aimed to examine plaque-dependent effects on synaptic transmission in both *App*$^{NL-F}$ and *App*$^{NL-F}$/*Trem2*^{R47H} mice. The *App*$^{NL-F}$ model is perhaps the more suitable knock-in model for examining this due to its much slower plaque formation. In addition, *App*$^{NL-F}$ mice also exhibit rapid accumulation of both $A\beta_{40}$ and $A\beta_{42}$ in the cortex between 6 and 24 months of age (Saito et al., 2014; Sato et al., 2021). This means that at 18 months, when there is a moderate plaque pathology in these mice (Benitez et al., 2021; Saito et al., 2014), there is a high proportion of both soluble and insoluble Aβ, allowing the examination of both plaque- and soluble Aβ-dependent changes on synaptic transmission. In comparison to *App*$^{NL-G-F}$ mice, *App*$^{NL-F}$ mice would allow for an easier distinction between plaque and non-plaque associated regions as in the

App^{NL-G-F} model even at the earliest age examined in the previous chapter (4 months), these mice already exhibited a heavy plaque load. Hence, it is possible that some recordings from regions without plaques could have actually been associated with plaques due to the potential presence of a plaque in a previous or subsequent hippocampal section serial to the one recorded from.

Therefore, it would be interesting to examine what synaptic transmission changes at single synapses are observed at 18 months in *App*$^{NL-F}$ mice and in mice with perturbed microglial response. This would allow the examination of plaque- and microglia-dependent effects on synaptic transmission. Therefore, here, unitary excitatory postsynaptic currents (uEPSCs), which are postsynaptic currents evoked from the activation of a single synapse upon stimulation, were recorded from CA1 pyramidal cells from 18-month-old *App*$^{NL-F}$ and *App*$^{NL-F}$/*Trem2*^{R47H} mice. These were elicited in the presence of a $GABA_A$ receptor blocker following the stimulation of a single, identified axon of a CA3 cell in the *stratum radiatum* using a patch-clamp setup. To direct the stimulation electrode towards single CA3 axons during recordings, similarly to in Chapter 3, the lipophilic dye DiI was placed in the CA3 region prior to electrophysiological recordings.

5.2 Minimal stimulation recruited single synapses

Similarly to Chapter 3, a minimal stimulation paradigm was employed in this work. To ensure that this stimulation was truly minimal and resulted in uEPSCs (see Figure 2.1C), the recorded amplitudes of the successful first responses of 18-month-old male *App*$^{NL-F}$ and wild-type mice were compared to those of mEPSCs from 20-month-old *App*$^{NL-F}$ mice previously recorded in our lab (Figure 5.1A) (Benitez et al., 2021). Indeed, no differences in the postsynaptic amplitude of the previously recorded mEPSCs and the uEPSCs recorded in this work were observed in either wild-types or *App*$^{NL-F}$ mice ($p>0.05$; two way-ANOVA; Figure 5.1B), supporting the idea that only one, or a few axons were recruited during minimal stimulation.

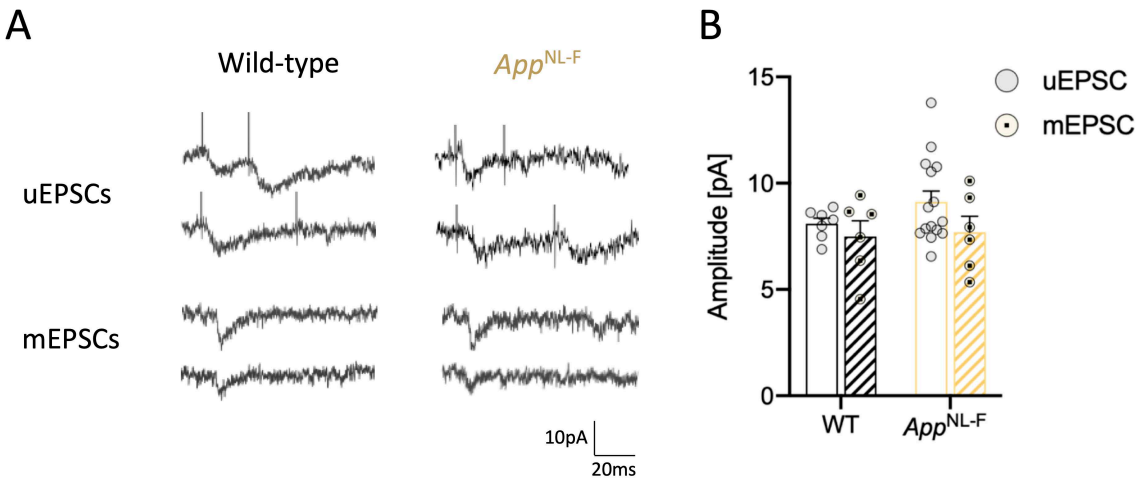

Figure 5.1. Amplitudes of uEPSCs and mEPSCs recorded from 18-20-month-old male wild-type and *App*$^{NL-F}$ mice.
(A) Representative uEPSC and mEPSC traces from wild-type and *App*$^{NL-F}$ mice at 18-20 months of age. **(B)** There are no differences in the postsynaptic amplitudes of the uEPSCs and mEPSCs of CA1 cells in the two genotypes examined. Columns indicate mean ± SEM. Individual points represent the mean of all recordings taken from individual animals.

5.3 Synaptic differences between *App*$^{NL-F}$ mice and mice with perturbed microglial response

5.3.1 Alterations in postsynaptic compartments

Having established that the minimal stimulation paradigm indeed resulted in the recruitment of individual synapses, the postsynaptic activity of male and female *App*$^{NL-F}$ and age-matched controls was examined. In addition to this, the activity of *App*$^{NL-F}$/*Trem2*^{R7H} mice was also examined in order to address the main aim of this chapter, that is to determine how a perturbed microglial response alters any of the synaptic transmission properties of AD mice. Similarly to Chapter 4, here male and female data were combined and presented as separate points in the subsequent graphs.

The first aim of this work was to determine if there were any differences in the postsynaptic response between the genotypes examined in this work. Hence, the following analyses were performed using two-way ANOVAs with the *App* and *Trem2*^{R47H} mutations being the two factors examined in the genotype comparisons.

There were subtle differences in the postsynaptic response of CA1 cells in the hippocampus upon the stimulation of individual CA3 axons. Specifically, the

amplitudes of the successful first responses were similar regardless of the presence of the *App* mutations or *Trem2*^{R47H} ($p>0.05$; two-way ANOVA; Figure 5.2B), suggesting that the postsynaptic compartment is very little affected in the AD environment or upon a perturbed microglial response. Alternatively, it could be that the postsynaptic compartment is affected but homeostatic processes have masked these effects. However, in accordance with the lack of change in the postsynaptic amplitude, the voltage used for stimulations was also comparable between the genotypes ($p>0.05$; two-way ANOVA; Figure 5.2C). Interestingly, when the decay time was examined, a two-way ANOVA revealed a tendency for faster decay times in *App* knock-in mice regardless of the microglial response ($p=0.07$; two-way ANOVA; Figure 5.2D). This suggests that *App* knock-in mice exhibit alterations in receptor kinetics which are dependent solely on AD-associated processes and are not driven by TREM2 signalling.

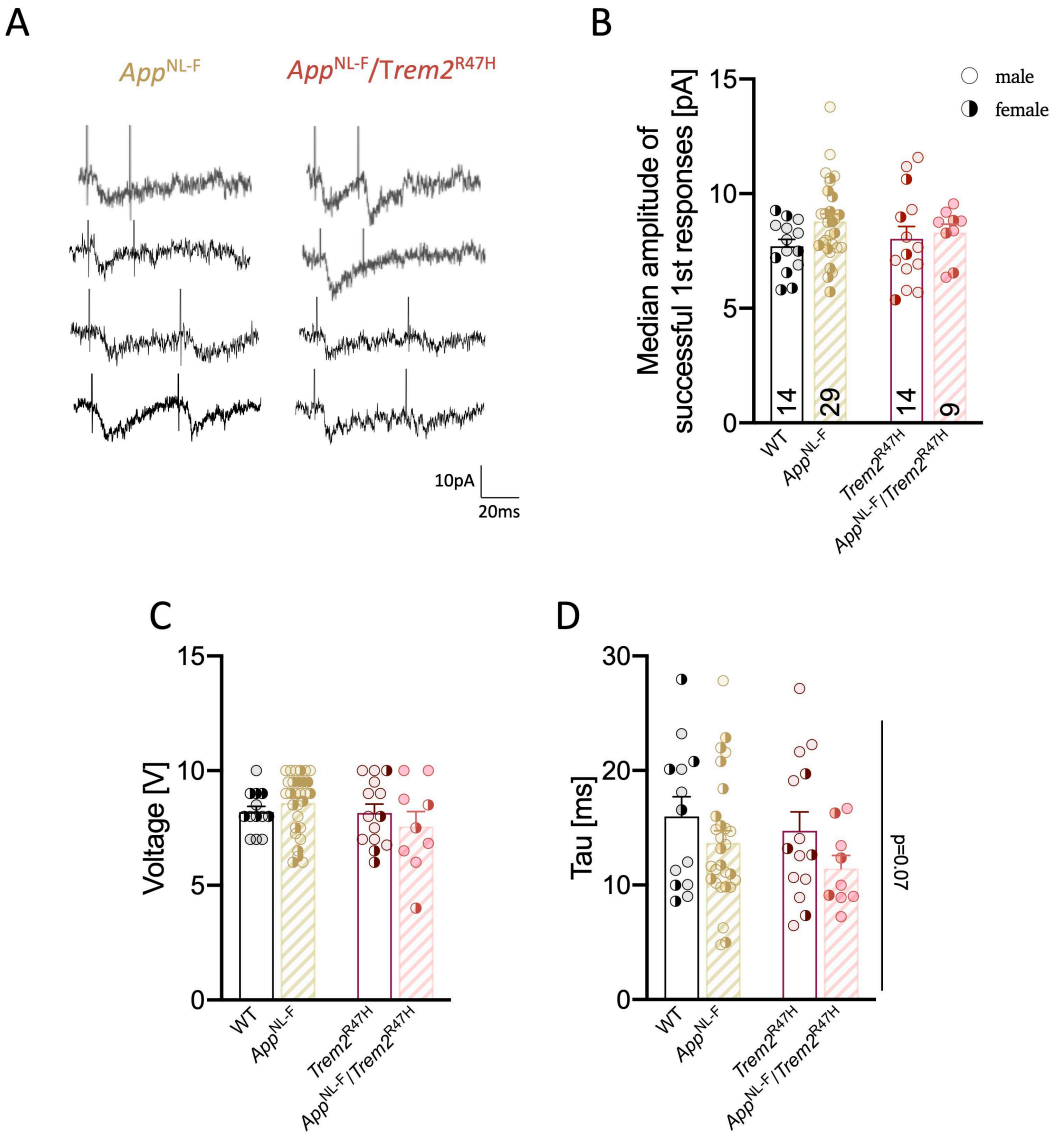

Figure 5.2. Properties of the uEPSCs recorded from male and female wild-type, *App*$^{NL-F}$, *Trem2*^{R47H}, and *App*$^{NL-F}$/*Trem2*^{R47H} mice at 18 months of age.

(A) Representative uEPSC traces from *App*$^{NL-F}$ and *App*$^{NL-F}$/*Trem2*^{47H} mice with inter-stimulus intervals of 25 and 50 ms. **(B)** The uEPSC amplitude of the successful first responses in all genotypes. **(C)** Voltage used for stimulations for recordings in all genotypes. **(D)** Decay time for all four genotypes. Trend for a main effect of the *App* mutation (p=0.07). Columns indicate mean ± SEM. Sample sizes are marked within bars. Individual points represent the mean of all recordings taken from individual animals. Empty circles refer to males, while filled circles refer to females. Two-way ANOVAs; p-values beside comparisons indicate main effects of the *App* mutations.

5.3.2 Release probability alterations in *App* knock-in mice

Two pairs of stimuli were applied in the experiments performed here, either at 25ms or 50ms intervals (see Figure 5.2A). The PPR is inversely proportional to the probability of release and how this is altered in App^{NL-F} and upon perturbed microglial response in $App^{NL-F}/Trem2^{R47H}$ mice remains to be determined. Previous work from our lab found reduced PPR and hence increased release probability in App^{NL-F} mice at 7 months, which is before any evident plaque pathology in these mice, thereby suggesting that soluble Aβ is the driving factor behind these effects (Benitez et al., 2021). These changes continue to the latest age examined in the work by Benitez et al. (2021) – 20 months – suggesting that the levels of soluble Aβ are likely continuing to rise and to exert their effects on release probability despite moderate plaque formation and increase in insoluble Aβ (Saito et al., 2014). However, whether this release probability is in any way affected when microglial responses are altered has not been explored.

Although two-way ANOVAs found no change in the PPR in either of the examined genotypes (Figure 5.3Ai,ii), *App* knock-in mice, regardless of the presence of the $Trem2^{R47H}$ variant, exhibited higher failure rates than their respective controls ($p<0.01$; two-way ANOVA; Figure 5.3B). This suggests that the effects on failure rates might be driven by factors other than reduced release probability, such as enhanced receptor desensitisation or reduced axonal excitability in *App* knock-in mice.

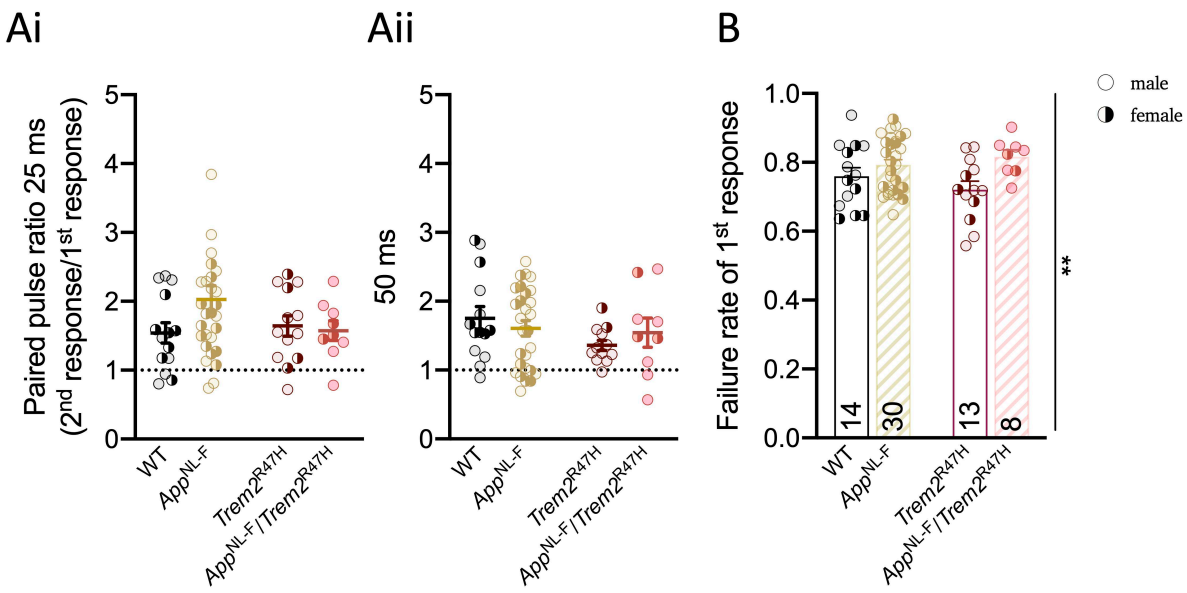

Figure 5.3. Paired-pulsed ratios of evoked unitary excitatory postsynaptic currents (uEPSCs) at CA3-CA1 synapses in 18-month-old mice.
(A) The paired-pulse ratio (PPR) at an inter-stimulus interval of **(Ai)** 25 ms and **(Aii)** 50 ms. **(B)** The failure rates of uEPSCs for all four genotypes. Main effect of the *App* mutation ($p<0.01$). Columns indicate mean ± SEM. Sample sizes are marked within bars. Individual points represent the mean of all recordings taken from individual animals. Empty circles indicate males, while filled circles indicate females. Significant main effects from two-way ANOVAs indicated by: **$p<0.01$. Asterisks beside comparisons indicate main effect of the *App* mutations.

5.3.3 Alterations in spontaneous activity

In addition to evoked responses, I also wanted to examine if postsynaptic currents in response to the spontaneous release of neurotransmitters have altered properties in the genotypes examined here. Spontaneous currents refer to currents which either result from the random fusion of a presynaptic vesicle with the presynaptic membrane, meaning that they are miniature postsynaptic currents, or from spontaneous action potentials (APs) in the presynaptic neuron which trigger the neurotransmitter release from one or multiple presynaptic sites of a single axon, making them spontaneous postsynaptic currents. Most of the spontaneous postsynaptic currents CA1 pyramidal neurons in the hippocampus produce are actually inhibitory as the addition of a $GABA_A$ receptor blocker (SR95531 or also known as gabazine) results in the removal of large portion (90-95%) of these (Benitez et al., 2021; Cummings et al., 2015). Hence, here the currents recorded without gabazine in the solution were considered spontaneous inhibitory postsynaptic currents (sIPSCs), while those recorded in the presence of gabazine were referred to spontaneous excitatory postsynaptic currents

(sEPSCs). Examining changes in the amplitude, frequency, and decay times of sIPSCs and sEPSCs can give an idea of how both pre- and postsynaptic properties are altered in different conditions.

5.3.3.1 Differential effects on sIPSC amplitudes in App^{NL-F} mice in the presence of Trem2^{R47H}

When the sIPSCs were examined (Figure 5.4A), there were no differences in the frequency nor in the decay times between the two groups ($p>0.05$; two-way ANOVA; Figure 5.4B, D). Interestingly, this was not the case for the postsynaptic amplitude of sIPSC as a two-way ANOVA found a significant *App* x *Trem2* interaction ($p=0.01$; Figure 5.4C). *Post-hoc* tests revealed that *App*$^{NL-F}$/*Trem2*^{R47H} mice exhibit a trend ($p=0.07$) for lower sIPSC amplitudes compared to *Trem2*^{R47H} controls, while this is not the case for *App*$^{NL-F}$ mice in comparison to their controls (Figure 5.4C). These findings suggest that although the release of inhibitory neurotransmitters is not altered in *App*$^{NL-F}$/*Trem2*^{R47H} mice as there is no change in the frequency of events, the AD environment might result in a smaller number of available inhibitory postsynaptic receptors when the microglial response is perturbed.

5.3.3.2 Differential effects on sEPSC frequencies in App^{NL-F} mice in the presence of Trem2^{R47H}

To isolate sEPSCs, gabazine was added to the solution and the same parameters as above were explored (see Figure 5.5A). A two-way ANOVA found a significant *App* x *Trem2* interaction on the frequency of sEPSCs ($p<0.05$; Figure 5.5B), with *post-hoc* tests showing that *App*$^{NL-F}$ mice have a higher uEPSC frequency than *App*$^{NL-F}$/*Trem2*^{R47H} mice ($p<0.05$). When the cumulative probability of the inter-event intervals was explored, a Kolmogorov-Smirnov test indicated that *App*$^{NL-F}$ mice have significantly shorter intervals than *App*$^{NL-F}$/*Trem2*^{R47H} mice across all events ($p<0.0001$; Figure 5.5C). This suggests that the presence of the *Trem2*^{R47H} variant counteracts the increased frequency seen in the presence of the *App* mutations. In comparison, two-way ANOVAs found no difference in the amplitude or decay times of sEPSCs between the four genotypes ($p>0.05$), suggesting that the AD environment, a perturbed microglial response, or the combination of the two have no effect on the excitatory postsynaptic compartments (Figure 5.5D, E). Together these findings

suggest that a perturbed microglial response might counteract the change in frequency of excitatory transmission seen in *App*$^{NL-F}$ mice. This hints at a change in the number of excitatory synapses available for spontaneous release which might be dependent on appropriate microglial function.

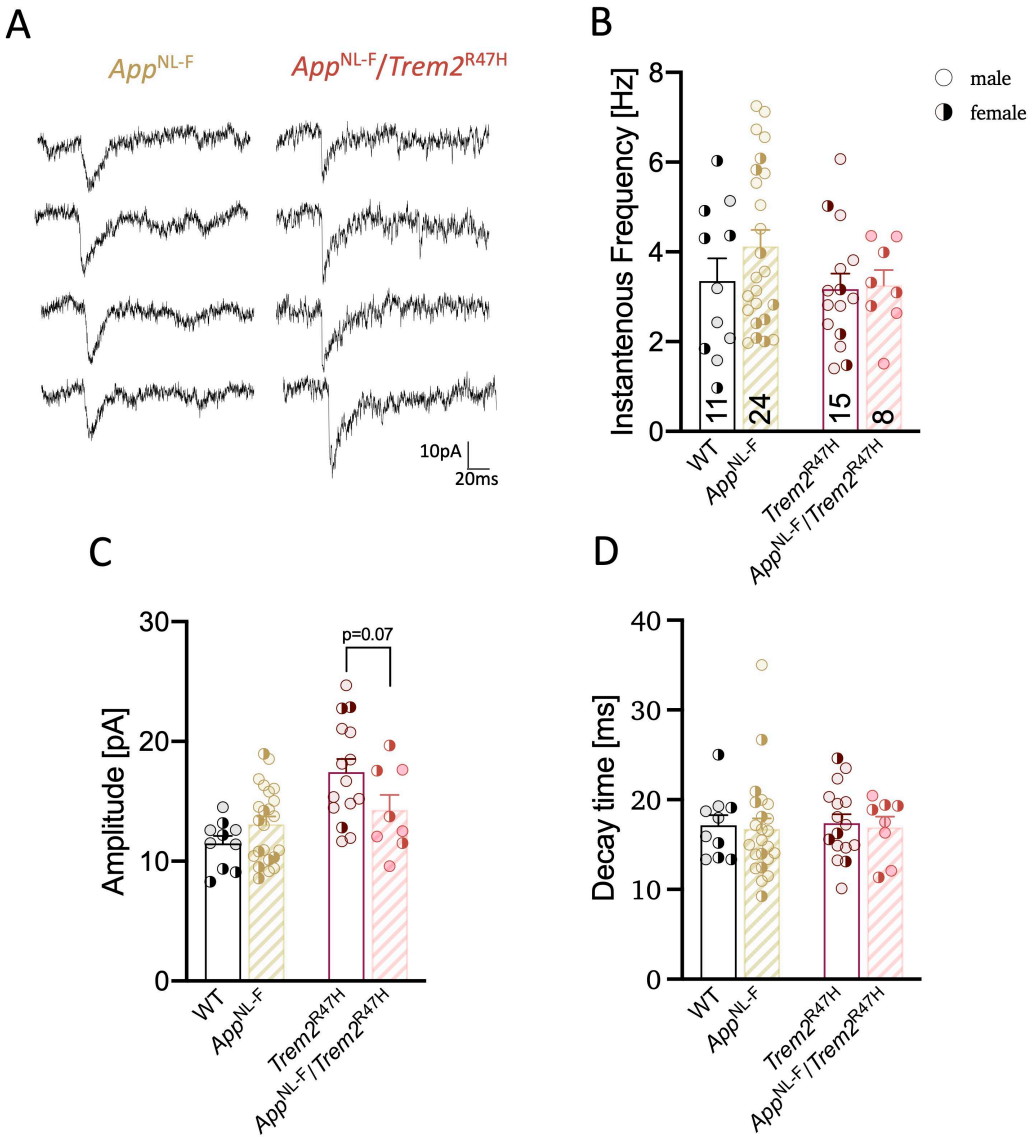

Figure 5.4. Properties of spontaneous inhibitory postsynaptic currents (sIPSCs) in hippocampal CA1 cells.
(A) Representative current traces recorded from *App*$^{NL-F}$ and *App*$^{NL-F}$/*Trem2*^{R47H} mice in aCSF. **(B)** The instantaneous frequency of sIPSCs for all four genotypes. **(C)** The median amplitude of sIPSCs. *App* x *Trem2* interaction (p=0.01). **(D)** The decay time of sIPSCs. Columns indicate mean ± SEM. Sample sizes are marked within bars. Individual points represent the mean of all recordings taken from individual animals. Empty circles indicate males, while filled circles indicate females. Two-way ANOVAs followed by Sidak-corrected *post-hoc* comparisons when there was an interaction indicated in graphs.

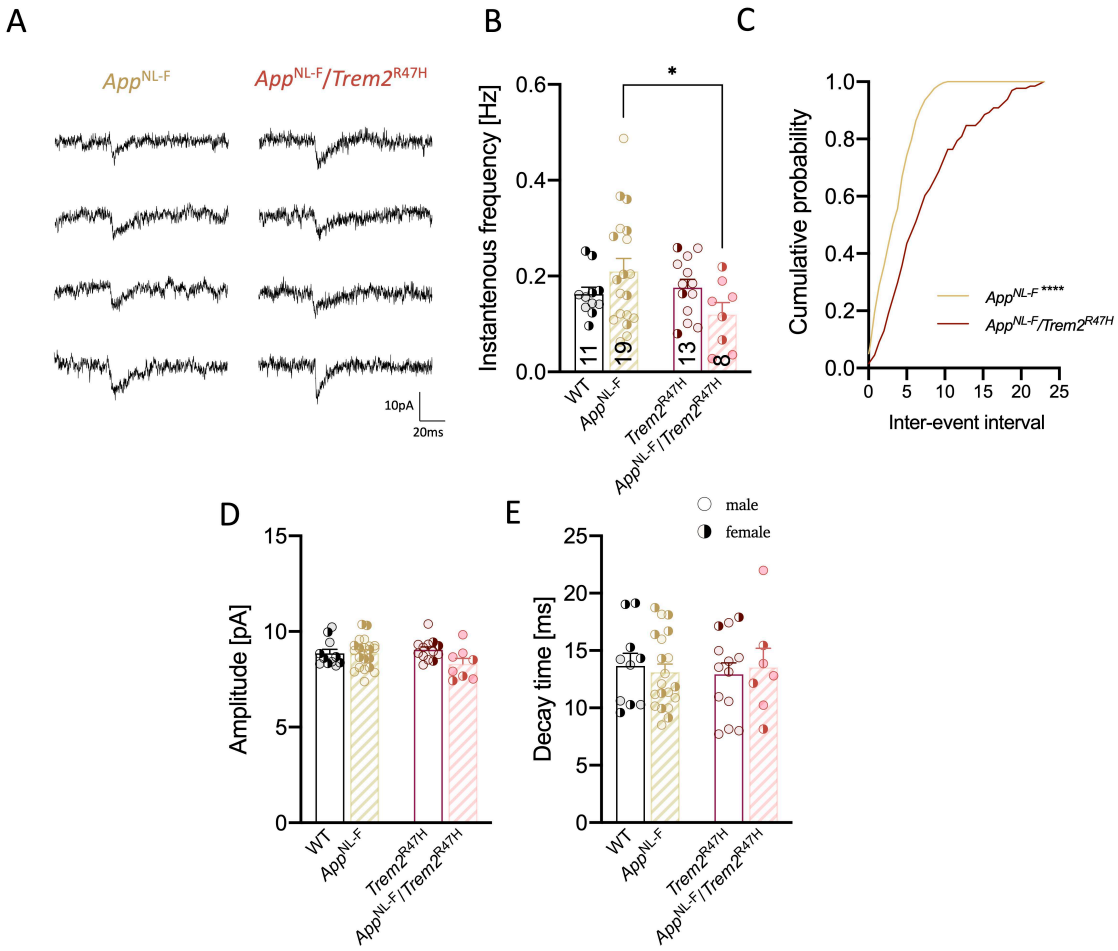

Figure 5.5. Properties of spontaneous excitatory postsynaptic currents (sEPSCs) in hippocampal CA1 cells.

(A) Representative current traces recorded from *App*$^{NL-F}$ and *App*$^{NL-F}$/*Trem2*^{R47H} mice in the presence of gabazine. **(B)** The instantaneous frequency of sEPSCs. *App* x *Trem2* interaction ($p<0.05$). **(C)** Cumulative probability of the inter-event interval. Difference between *App*$^{NL-F}$ and *App*$^{NL-F}$/*Trem2*^{R47H} mice ($p<0.0001$). The median amplitude of sEPSCs **(D)** The decay time of sEPSCs. Columns indicate mean ± SEM. Sample sizes are marked within bars. Individual points represent the mean of all recordings taken from individual animals. Empty circles indicate males, while filled circles indicate females. Two-way ANOVAs followed by Sidak-corrected *post-hoc* comparisons when there was an interaction indicated by *$p<0.05$. Kolmogorov-Smirnov test indicated by ****$p<0.0001$.

5.4 Effects of plaques and microglia on transmission

As mentioned above, in addition to examining differences in synaptic transmission between wild-type and *App* knock-in mice, the present work also aimed to explore how the synaptic activity in *App* knock-in mice themselves is altered depending on the presence of a plaque around the stimulated axon. This would provide an idea as to whether the plaque, or even the plaque environment itself, have an effect on transmission. Therefore, here, similarly to Chapter 3, $App^{NL\text{-}F}$ and $App^{NL\text{-}F}/Trem2^{R47H}$ mice were further divided into two groups – "plaque" and "no plaque" conditions – depending on whether the CA3 axon on which the stimulating electrode was placed was passing near a plaque on its way to the recorded CA1 cell during patch-clamp experiments (see Figure 5.6A). Similarly to Chapter 3, an axon was deemed "plaque-associated" in cases when a plaque was present within 30μm of the stimulated axon, and "non-plaque-associated" when plaques were outside of that region (Figure 5.6A). Here, plaque presence and genotype were considered the two factors in the comparisons exploring plaque effects.

5.4.1 The effects of plaque presence and perturbed microglial functioning on postsynaptic activity

Examining the properties of uEPSCs in plaque and non-plaque conditions in $App^{NL\text{-}F}$ and $App^{NL\text{-}F}/Trem2^{R47H}$ mice revealed interesting differences in the synaptic activity between the two models and these were dependent on normal microglial functioning. In particular, a two-way ANOVA revealed a significant genotype x plaque presence interaction when examining the uEPSC postsynaptic amplitude ($p<0.01$). Sidak-corrected *post-hoc* tests revealed that plaque-associated recordings in $App^{NL\text{-}F}$ mice have lower amplitudes than non-plaque-associated recordings ($p<0.05$), while this was not observed in $App^{NL\text{-}F}/Trem2^{R47H}$ mice ($p>0.05$; Figure 5.6B). Furthermore, non-plaque associated recordings in $App^{NL\text{-}F}$ mice also led to larger postsynaptic amplitudes than recordings from the same condition in $App^{NL\text{-}F}/Trem2^{R47H}$ mice ($p<0.05$). Altogether these results suggest that normal microglial activity in $App^{NL\text{-}F}$ mice is the driving factor for the observed reduction in postsynaptic amplitudes in plaque conditions, suggesting that microglia potentially have a role in removing active synapses in these mice.

To determine if the amplitudes in plaque and no-plaque conditions are more similar to those typically found at single synapses in *App*$^{NL-F}$ and wild-type mice, the uEPSC amplitudes of male *App*$^{NL-F}$ mice in both conditions were compared to that of mEPSCs previously recorded in male mice (Benitez et al., 2021). Interestingly, a one-way ANOVA found a significant difference between the examined conditions ($p<0.05$; Figure 5.6C). *Post-hoc* tests revealed that this was driven by higher uEPSC amplitudes recorded in no-plaque conditions compared to the mEPSC amplitudes from wild-type mice, as well as a tendency for higher uEPSC amplitudes in no-plaque conditions compared to mEPSCs recorded from *App*$^{NL-F}$ mice ($p=0.07$; Figure 5.6C). These results suggest that plaque-associated synapses have similar amplitudes to wild-type mice and the mEPSCs from plaque-associated axons are likely to be the main contributor to the mEPSC amplitudes previously recorded from *App*$^{NL-F}$ mice at that age. Interestingly, when comparing how many synapses were activated in both conditions by taking into account the mEPSC recorded previously from male *App*$^{NL-F}$ mice, it appears that while at plaque conditions the number of synapses activated were on average 1 (calculated as uEPSC/mEPSC), for non-plaque conditions it was 1.3, suggesting that there might be fewer active synapses in plaque conditions. Therefore, it might be that in *App*$^{NL-F}$ mice plaque-associated microglia phagocytose neighbouring synapses potentially as a way to reduce hyperactivity to normal levels.

The above changes in uEPSC amplitudes were not dependent on the stimulation voltage used, as a two-way ANOVA showed that it was similar between the four conditions ($p>0.05$; Figure 5.6D). Furthermore, no difference was observed when the decay time was explored ($p>0.05$; Figure 5.6E). This demonstrates that the above-mentioned tendency for faster decay times observed in *App* knock-in mice compared to their respective controls is driven by the AD environment rather than plaque presence specifically.

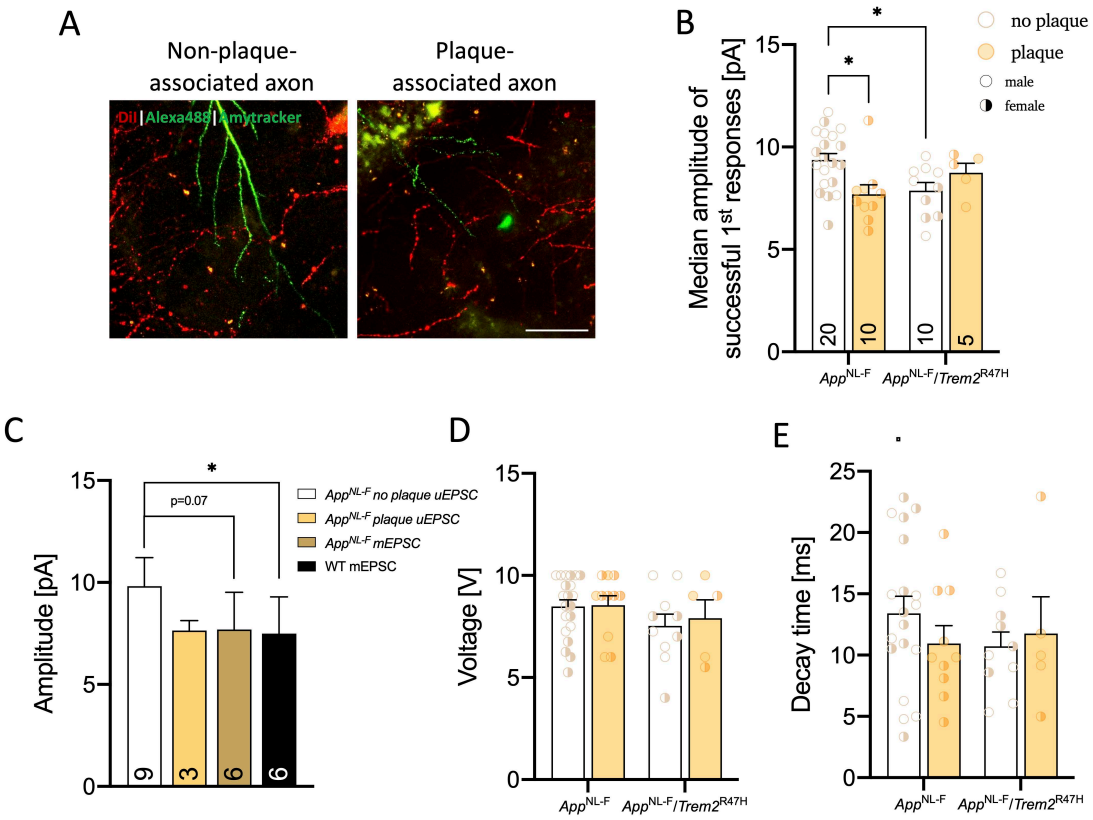

Figure 5.6. Differences in the properties of postsynaptic uEPSCs in response to the stimulation of axons near and away from plaques in 18-month-old *App*$^{NL-F}$ and *App*$^{NL-F}$/*Trem2*^{R47H} mice.

(A) Representative images illustrating CA3 axons (red) passing near (left panel – axon passes within 30µm of a plaque) and away (right panel) from a plaque (green) on its way to a CA1 cell (green). A stimulating electrode was placed on an individual CA3 axon visualised using DiI. A CA1 cell in close vicinity to the identified CA3 axon was voltage-clamped and synaptic currents as single synapses (uEPSC) in response to minimal stimulation were recorded using a patch-clamp setup. The cell was simultaneously filled with Alexa488. Following electrophysiological experiments, plaques were labelled using LCOs and recorded synapses were identified and imaged using a confocal microscope. Axons were deemed plaque- (plaque within 30µm) and non-plaque-associated post-hoc. **(B)** The uEPSC amplitude of all successful first responses of CA1 cells in response to the stimulation of CA3 axons. Genotype x plaque presence interaction ($p<0.01$) **(C)** A comparison of uEPSC amplitudes of male *App*$^{NL-F}$ in plaque- and non-plaque-associated conditions with mEPSC recorded from male *App*$^{NL-F}$ and wild-type mice. Difference between groups ($p<0.05$). **(D)** The stimulation voltage used for recordings. **(E)** The decay time of uEPSCs. Columns indicate mean ± SEM. Sample sizes are marked within bars. Individual points represent the mean of all recordings taken from individual animals. Empty circles indicate males, while filled circles indicate females. One- and two-way ANOVA followed by Sidak-corrected *post-hoc* comparisons if there was an interaction indicated by: *$p<0.05$.

5.4.2 Release probability at plaque-associated axons and its dependence on microglial functioning

In addition to the postsynaptic amplitude, here the PPR was also explored. When the two stimuli were 25 ms apart, there was no difference between the two genotypes ($p>0.05$; Figure 5.7Ai). However, at 50 ms, there was a trend for lower PPRs in plaque-associated recordings, regardless of genotype ($p=0.058$; Figure 5.7Aii), suggesting that axons passing in the vicinity of a plaque exhibit higher release probability than those away from plaques. This is in accordance with the idea that there is a halo of oligomeric Aβ around Aβ plaques which could exert its effects on neighbouring regions (Koffie et al., 2009), as well as the well-established role of Aβ in promoting presynaptic glutamate release (Abramov et al., 2009; Kamenetz et al., 2003). The fact that this is observed in both $App^{NL\text{-}F}$ and $App^{NL\text{-}F}/Trem2^{R47H}$ mice shows that this effect is independent of normal microglial functioning and is indeed likely to be driven by the effects on surrounding Aβ on the presynapse, for instance by increasing vesicle release probability by disrupting the VAMP2/Synaptophysin complex (Russell et al., 2012), or by impairing glutamate reuptake and activating presynaptic mGluRs (Marcaggi et al., 2009; Zott et al., 2019). Interestingly, however, this change in PPR was not accompanied with a change in the failure rate of the first response ($p>0.05$; Figure 5.7B), suggesting that processes other that changes in release probability such as impaired axonal activation might be contributing to the change in PPR.

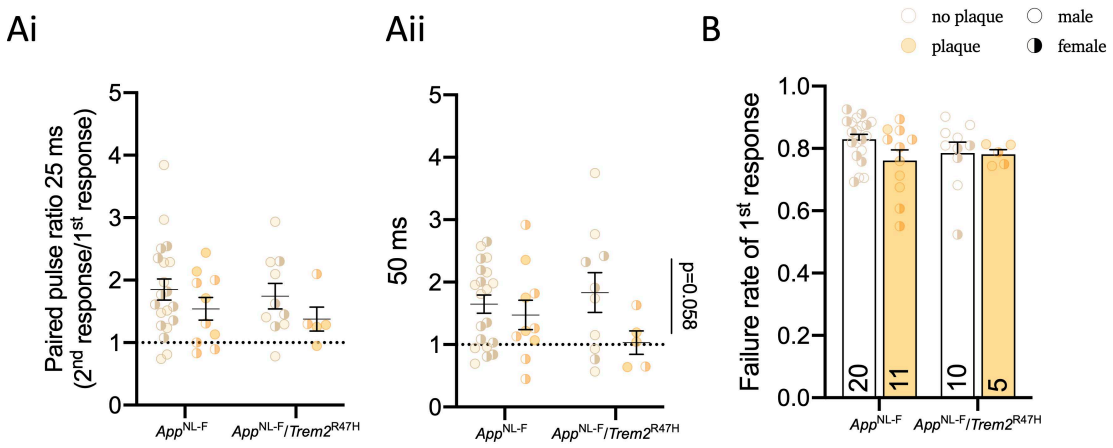

Figure 5.7. Release probability at axons near and away from plaques in 18-month-old *App*$^{NL-F}$ and *App*$^{NL-F}$/*Trem2*^{R47H} mice.
(A) The paired-pulse ratio (PPR) at an inter-stimulus interval of **(Ai)** 25 ms and **(Aii)** 50 ms. 50 ms: trend for main effect of plaque presence (p=0.058) **(B)** The failure rate of the first uEPSC response. Columns indicate mean ± SEM. Sample sizes are marked within bars. Individual points represent the mean of all recordings taken from individual animals. Empty circles indicate males, while filled circles indicate females. P-values beside comparisons indicate main effect of plaque presence.

5.5 Summary

In this chapter I explored synaptic changes at CA3-CA1 synapses in *App* knock-in mice to determine which of the synaptic alterations are dependent on an appropriate microglial response. Here I examined *App*$^{NL-F}$ mice, which harbour two mutations in a humanized Aβ sequence; *App*$^{NL-F}$/*Trem2*^{R47H} mice, which carry the AD risk variant *Trem2*^{R47H} and exhibit reduced levels of *Trem2;* as well as wild-type and *Trem2*^{R47H} controls.

There were no differences in the uEPSC amplitude or stimulation voltage between the examined genotypes, although both *App*$^{NL-F}$ and *App*$^{NL-F}$/*Trem2*^{R47H} mice exhibited a tendency for faster decay times. Furthermore, despite no changes in the PPR, *App*$^{NL-F}$ and *App*$^{NL-F}$/*Trem2*^{R47H} mice exhibited higher failure rates than their respective controls, suggesting that the *App* mutations might make axons less excitable or alter receptor responses. Examining sIPSCs revealed no differences in the frequency or decay times between the examined genotypes, although *App*$^{NL-F}$/*Trem2*^{R47H} mice exhibited a trend for lower sIPSC amplitudes than their *Trem2*^{R47H} controls. This was not observed in *App*$^{NL-F}$ mice, suggesting that a perturbed microglial response might enhance the amplitude of postsynaptic inhibitory currents and this is counteracted in

the presence of the *App* mutations. Examining the sEPSCs revealed no difference in the amplitude or decay time between the groups. In contrast, the frequency of sEPSCs was differentially affected depending on the *Trem2* variant, suggesting that the *Trem2*^{R47H} mutation counteracts the effects of the *App* knock-in mutations on increased sEPSC frequency observed in *App*$^{NL-F}$ mice.

Examining how the above is altered when the plaque presence around the stimulated axon is taken into account demonstrated that only *App*$^{NL-F}$ mice exhibit reductions in uEPSC amplitudes in plaque compared to no-plaque conditions despite no changes in the stimulation voltage. uEPSC amplitudes from *App*$^{NL-F}$ mice in plaque conditions were more similar to mEPSCs from age-matched wild-types, which suggests that plaque-associated microglia might be phagocytosing overly active synapses. In comparison, *App*$^{NL-F}$/*Trem2*^{R47H} mice demonstrated no differences in the uEPSC amplitudes, indicating that the above is driven by a perturbed microglial function around synapses. Examining the PPRs revealed a reduction in plaque conditions regardless of genotype, while no differences in the failure rates were observed. These results suggest that the alterations in synaptic activity in these mice are dependent on both Aβ and microglia, with the former primarily affecting presynaptic release and the latter having some effects on both the pre- and postsynapse.

Chapter 6: Discussion

Alzheimer's disease is the most common form of dementia and it has affected millions of people worldwide. AD impacts on different aspects of an individual's life and leads to extensive behavioural impairments, cognitive decline, and brain atrophy. Advances in our understanding of the molecular processes involved in AD development have highlighted some of the mechanisms which have a key role in disease pathology, including the activity of the non-neuronal cells in the brain. In particular, along with Aβ accumulation, synaptic alterations, subsequent synaptic loss and gliosis have all been pinpointed as key early processes in AD. Furthermore, GWAS in the last decade have additionally highlighted that variants of several microglial genes, including *TREM2, CD33* and *CLU,* are associated with an increased risk of developing AD (Guerreiro et al., 2013a; Jansen et al., 2019; Karch and Goate, 2015). Moreover, it has also recently been suggested that microglial activation is in fact a protective response to the synaptic alterations occurring early in disease and that mutations in these genes alter normal microglial function and exacerbate pathology (Edwards, 2019). This together suggests a potential beneficial role of these non-neuronal cells for normal brain functioning raising questions into their specific function in regions associated with heavy Aβ plaque load.

Therefore, in this thesis I aimed to explore in what ways Aβ and microglia contribute to the synaptic alterations observed in AD. To address the first part of this aim, I examined two knock-in mouse models – *App*$^{NL\text{-}G\text{-}F}$ and *App*$^{NL\text{-}F}$ (Saito et al., 2014) – and initially characterized synaptic alterations at single synapses driven by the presence of three or two mutations within the *App* sequence in both male and female mice. Although previous work from our lab has tried to characterize the synaptic properties of these mice (Benitez et al., 2021), by examining individual synapses and looking at the two sexes, this work aimed to explore if any specific properties have been masked upon the examination of multiple synapses and if any of these are dependent on sex. I used both *App* knock-in models as *App*$^{NL\text{-}G\text{-}F}$ mice exhibit specific alterations within the Aβ sequence itself, which makes Aβ much more likely to oligomerize and aggregate (Tsubuki et al., 2003). Hence, differences in the results between *App*$^{NL\text{-}G\text{-}F}$ and *App*$^{NL\text{-}F}$ mice could elucidate specific differences which are

driven by the potential lack of freely available soluble Aβ throughout the neuropil in the former model. Following the pathology characterisation of these models, Chapters 3 and 5 addressed the main aim of this work by examining how synaptic transmission is altered at synapses in the vicinity of plaques to further understand the specific effects of Aβ on synaptic activity. This was an important consideration as some of the synaptic differences between plaque- and non-plaque-associated regions could have been hidden in previous work, as these regions have not been examined separately. To address the second aim of this thesis, I also examined *App*$^{NL-F}$/*Trem2*^{R47H} mice which in addition to developing plaque pathology also exhibit a perturbed microglial response. Similarly to the other models, these were also explored for plaque-dependent synaptic changes and were compared to *App*$^{NL-F}$ mice, which allowed me to discern between the specific effects of Aβ and microglia on synaptic activity. Furthermore, examining changes in hippocampal plaque pathology and glial distribution between *App* knock-in mice and *App* knock-in mice with a perturbed microglial response also allowed me to understand in what ways microglia contribute to the hippocampal changes observed in the AD environment.

Overall, the results of this work demonstrated that with age, *App*$^{NL-G-F}$ mice exhibit a larger number of plaques and specifically, a larger number of smaller-sized plaques (plaques smaller than 50 μm^2), which was similar to the effects observed *App*$^{NL-F}$/*Trem2*^{R47H} when compared to *App*$^{NL-F}$ mice. The presence of the *Trem2*^{R47H} mutation in *App*$^{NL-F}$ mice also led to lower microglial density in the SLM region in the CA1 subfield, where these mice exhibited the largest number of plaques, and also reversed the increased astrocytic density which was observed in *App*$^{NL-F}$ mice. In terms of electrophysiological changes, I found alterations in the kinetics of the postsynaptic response, with longer decay times in 7-9-month old *App*$^{NL-G-F}$ mice and a tendency for shorter decay times in 18-month old *App*$^{NL-F}$ mice, regardless of the *Trem2*^{R47H} mutation. I also found that the *App* mutations lead to alterations in failure rates, with the three mutations in 7-9-month-old *App*$^{NL-G-F}$ mice leading to reduced failure rates, while the two mutations in 18-month-old *App*$^{NL-F}$ mice resulted in higher failure rates. These results suggest that either the presence of the Arctic mutation or age can have differential effects on the failure rates and the kinetics of the postsynaptic response, illustrating important differences between the two models. Examining spontaneous synaptic activity revealed reductions in the sIPSC amplitude in *App*$^{NL-F}$/*Trem2*^{R47H}

compared to *Trem2*^{R47H} mice and a loss of the increased sEPSC frequency found in *App*$^{NL-F}$ mice in the presence of *Trem2*^{R47H}, suggesting altered excitatory/inhibitory balance in *App*$^{NL-F}$ mice in the presence of *Trem2*^{R47H}. Exploring electrophysiological changes in plaque-associated regions revealed that both *App*$^{NL-G-F}$ and *App*$^{NL-F}$ mice exhibit lower amplitudes in plaque compared to no-plaque conditions, while this effect was lost in *App*$^{NL-F}$/*Trem2*^{R47H} mice, indicating its dependency on a functioning microglial response. Furthermore, both *App*$^{NL-F}$ and *App*$^{NL-F}$/*Trem2*^{R47H} mice showed reduced PPR indicating enhanced release probability in plaque conditions, illustrating that these effects were likely driven by the plaque-associated Aβ halo.

6.1 Alterations in plaque pathology and gliosis in *App* knock-in mice with age and in the face of the *Trem2*^{R47H} mutation

It is well established in AD mouse models and post-mortem tissue from AD patients that with age, plaque pathology becomes much more pronounced in the brain. This increase in pathology is accompanied with extensive gliosis, with a number of studies demonstrating that several variants of microglial genes increase the risk of developing AD (Guerreiro et al., 2013a; Hollingworth et al., 2011; Jonsson et al., 2013; Naj et al., 2011). This gliosis is characterized by the loss of homeostatic microglia and the switch to the so-called DAMs (Keren-Shaul et al., 2017), as well as astrocytic activation in the form of GFAP upregulation (Castillo et al., 2017; Liddelow et al., 2017), with both of these cells shown to cluster around amyloid plaques and in turn release cytokines and chemokines in these regions (Henstridge et al., 2019; Sofroniew, 2009; Wegiel, 2001; Yuan et al., 2016).

The present work made three main observations regarding plaque pathology and gliosis in the *App* knock-in mice examined here. First, with age *App*$^{NL-G-F}$ mice exhibited heavier plaque load and specifically a larger number of smaller-sized plaques which was also observed in *App*$^{NL-F}$/*Trem2*^{R47H} mice when compared to *App*$^{NL-F}$ mice. This was accompanied with increased microglial density compared to wild-types at both ages in *App*$^{NL-G-F}$ mice. Furthermore, *App*$^{NL-F}$ mice showed increased microglial density in the SLM region where plaques were present, and this effect was lost in the presence of the *Trem2*^{R47H} mutation. Second, the plaque

distribution between *App*$^{NL-G-F}$ and *App*$^{NL-F}$ mice was noticeably different, with the latter model showing plaque accumulation specifically in the SLM region in the CA1 subfield of the hippocampus. Third, the increase in astrocyte density in *App*$^{NL-F}$ mice was reversed in *App* knock-in mice with *Trem2*^{R47H}, illustrating a potential interaction between microglia and astrocytes in this model, or suggesting that *Trem2*^{R47H} also affects *Trem2* expression in astrocytes and the astrocytic response to the AD environment (Clarke et al., 2018).

6.1.1 Microglial density and plaque pathology changes in App knock-in mice

Previous work on *App*$^{NL-G-F}$ mice has demonstrated that mice exhibit pronounced amyloidopathy and microgliosis at 5 months of age, as measured using longitudinal positron emission tomography (Sacher et al., 2019). This was further confirmed in another study which demonstrated that at 5 months there are some gene expression changes in the cortex of *App*$^{NL-G-F}$ mice, including upregulation of *Gfap* and *S100b*, and pronounced microgliosis (Castillo et al., 2017). Additionally, an altered microglial proteome has also been reported in 6-month-old *App*$^{NL-G-F}$ mice, with upregulation of many of the markers associated with DAMs (Keren-Shaul et al., 2017; Sebastian Monasor et al., 2020). In accordance with the above, the present work found that at 4-5 months of age, *App*$^{NL-G-F}$ mice exhibited increased microglial density in the hippocampus compared to wild-types, with the same increased density observed in the 7-9 month-old group. This was reported for both males and females, suggesting that microgliosis in the form of proliferation is not sex dependent. These results are, to some extent, consistent with previous work from our lab which found increased microglial density, as well as increased *Trem2* per microglia in both males and females, though only in 9-month-old *App*$^{NL-G-F}$ mice (Benitez et al., 2021). However, it is important to note that the work by Benitez et al. (2021) did find a tendency for higher microglial density at 4 months of age and because here the sample size was slightly higher, that might have allowed to reach significance for microglial density. Furthermore, as the age group examined in this thesis was 4-5 months, this might mean that microglial density changes perhaps become prominent during this one-month period.

Interestingly, the above increase in microglial density compared to wild-types was similar in the two ages, despite the finding that at 7-9 months of age, *App*$^{NL-G-F}$ mice exhibit heavier plaque load and a larger number of smaller-sized plaques. This would suggest that microglia are less likely to react to smaller sized plaques and that only larger plaques are able to elicit changes in the microglial response. However, unpublished work from our lab done by a student I supervised – Ridwaan Joghee – showed that the microglial density is still increased even at the smallest-sized plaques in 18-month-old *App*$^{NL-F}$ mice. This, together with the data presented in this work, suggests that after an initial increase in density in response to plaque formation, microglia do not exhibit additional increases in number with pathology progression. However, it is important to note that the unaltered density does not necessarily mean that the signature of microglia is unchanged. This is supported by the finding that at early stages of pathology (2 months of age), *App*$^{NL-G-F}$ mice do not exhibit any alterations in *Trem2* expression, which only becomes noticeable at 9 months of age (Benitez et al., 2021), despite evident increases in microglial density at 4-5 months, as presented in the present work. This is similar to what was observed recently in the same model, with microglial transcriptomic changes appearing much later after initial plaque formation, that is, at the moderate stages of plaque pathology found at 6 months (Sebastian Monasor et al., 2020). Together this suggests that microglia increase their density in response to pathology, though only their signature might be altered after a certain point.

The change in microglial density could be limited to earlier stages of pathology because the protein makeup of the Aβ plaques at different pathology stages might be different. Therefore, it might be that microglia are particularly responsive to certain Aβ species which are found in plaques formed in early stages of pathology in *App*$^{NL-G-F}$ mice. Recent work using stable isotope labelling has demonstrated that Aβ plaques initially form a dense-core made up of $A\beta_{1-42}$, followed by the subsequent deposition of $A\beta_{1-38}$ around that core (Michno et al., 2021). Hence, the Aβ composition of different-sized plaques might be different and the microglial response might be highly dependent on this, an idea in need of further investigation. Although the idea that microglia are responsive to only initial plaque formations in AD mice is consistent with the present work, it is inconsistent with work on the 3xTg AD model which showed alterations in microglial density before plaque pathology and hence in

response to soluble Aβ species (Rodriguez et al., 2010). This discrepancy could be explained by the overexpression of *App* found in the transgenic mouse model used in the above study as this likely resulted in high levels of soluble Aβ to which microglia might react even before any plaque pathology. This suggestion is consistent with the findings of a recent study which showed that transgenic mice exhibit alterations in the microglial proteome at earlier stages of pathology when compared to $App^{NL\text{-}G\text{-}F}$ mice (Sebastian Monasor et al., 2020).

Some studies have argued that microglia are instrumental to the formation of plaques early in disease (Baik et al., 2016; Spangenberg et al., 2019), while others have proposed that microglia phagocytose Aβ species (Lee and Landreth, 2010; Yu and Ye, 2015), act as a physical barrier to compartmentalise Aβ-associated toxicity (Clayton et al., 2021; Condello et al., 2015; Yuan et al., 2016), or actively phagocytose plaque-associated synapses to limit the spread of damage (Edwards, 2019). The plaque-associated microglia, DAMs, have their own specific transcriptional signature which is highly dependent on appropriate TREM2 functioning (Keren-Shaul et al., 2017; Krasemann et al., 2017) and this is impaired in the presence of the $Trem2^{R47H}$ mutation (Cheng-Hathaway et al., 2018; Zhong et al., 2018). When examining the plaque load in both $App^{NL\text{-}F}$ and $App^{NL\text{-}F}/Trem2^{R47H}$ mice, I found that $App^{NL\text{-}F}/Trem2^{R47H}$ mice exhibit a larger number of plaques and particularly, smaller-sized plaques, similarly to what was observed with age in $App^{NL\text{-}G\text{-}F}$ mice. This finding is consistent with the idea that appropriate microglial functioning is required for regulating plaque pathology. For instance, one possible mechanism for the observed results could be that microglia are acting as a protective barrier which prevents the breaking off of smaller Aβ deposits from larger-sized plaques and this is impaired in the presence of $Trem2^{R47H}$, or with age. Interestingly, this effect on an increased number of smaller-sized plaques is in the opposite direction to what was previously observed in 10-month-old $App^{NL\text{-}F}$ and 4-month-old $App^{NL\text{-}G\text{-}F}$ mice upon microglial ablation (Benitez et al., 2021). However, it is important to note that in the study by Benitez et al. (2021), even the remaining microglia upon partial ablation were still functional. In comparison, the microglia from the $Trem2^{R47H}$ mice used in the present study exhibit a dysfunctional response in the form of reduced *Trem2* levels, the presence of the R47H variant in the remaining *Trem2*, altered microglial morphology, as well as a reduced number of $CD68^{+}$ microglia (Jadhav et al., 2020; Liu et al., 2020). Hence, it

is clear that a dysfunctional microglial response could be the main driver for the observed increase in smaller-sized plaques. It is also possible that the same perturbed microglial response is observed at the heavier plaque load found in 7-9-month-old *App*$^{NL-G-F}$ mice driven by the continuously increasing plaque burden, and this could have been instrumental to the observation of increased number of smaller-sized plaques in that model. Alternatively, it is also possible that microglia are only effective at phagocytosing small plaques and that once plaques grow past this size, microglia cannot remove them. Thus, it might be that although in 7-9-month-old *App*$^{NL-G-F}$ mice microglia are continuously phagocytosing small plaques, due to their enhanced production, it is more likely to observe their increased number, yet not an increased number of larger sized plaques.

In addition to forming a protective barrier, microglia have also been suggested to play an important role in compartmentalising Aβ plaques. Specifically, microglia have been suggested to keep plaques more compact by preventing the breaking off of Aβ deposits as their ablation in a number of studies has resulted in the formation of more diffuse-like plaques (Clayton et al., 2021; Spangenberg et al., 2019; Yuan et al., 2016). This role of microglia adds to their barrier function suggested in previous work as by reducing the surface area covered by the plaque, they are able to contain plaque-associated toxicity to specific regions. The results of the current thesis argue against this idea as no change in the circularity of plaques, a measure used in previous studies (Clayton et al., 2021), was observed in the presence of the *Trem2*^{R47H} mutation. However, in the work by Clayton et al., the authors showed that using different Aβ antibodies might mask the differences in plaque circularity. Hence, it is possible that the use of such specific antibodies did result in an artefact in the above work by staining only one conformation of the amyloid plaque and in fact not revealing the whole deposit. This is plausible given that LCOs, the amyloid plaque marker used in this work, binds to any β-sheet conformation and is therefore able to bind to both the core and diffuse part of the plaque (Nystrom et al., 2013), labelling all conformations within it. Alternatively, the observations in Clayton et al. (2021) were made at a more advanced stage of pathology than the *App*$^{NL-F}$ mice used in this work, suggesting that microglial compartmentalisation of plaques might be a process occurring at a later stage of pathology.

6.1.2 The SLM region is particularly vulnerable to plaque formation in *App*$^{NL-F}$ mice

During the course of the present study, I noticed that the plaque distribution in *App*$^{NL-F}$ mice was very different to that of *App*$^{NL-G-F}$ mice. In particular, in addition to a less pronounced plaque pathology, *App*$^{NL-F}$ mice seemed to exhibit an uneven plaque distribution across the hippocampus in comparison to *App*$^{NL-G-F}$ mice, with plaque pathology appearing much heavier in the central areas of the hippocampus and specifically the SR and the SLM in the CA1 subfield (see Figure 3.1 and Figure 4.2). When I quantified this, it was clear that the plaque load in the SLM was significantly more pronounced than in the SR region, which raised questions as to what causes the SLM region to be especially vulnerable to plaque formation. I performed the electrophysiological experiments of this work by stimulating the Schaffer collaterals in the SR region as previous studies had established specific differences at these CA3-CA1 synapses (Benitez et al., 2021; Cummings et al., 2015). However, it would be interesting to determine whether synapses in the SLM region, where CA1 cells receive inputs from layer III of the entorhinal cortex, exhibit alterations in synaptic transmission. One reason why the SLM region exhibits heavier pathology at that age could be the potential transfer of amyloid pathology from the entorhinal cortex, as previous work has shown that plaque formation first begins in the cortex (Latif-Hernandez et al., 2020; Michno et al., 2021). This is a well-established theory of tau pathology (de Calignon et al., 2012), and could be happening with soluble Aβ as well. This is idea supported by a study by Sheng et al. (2002) which showed that APP processed in the entorhinal cortex is the main source of Aβ in the hippocampus in transgenic mice. Furthermore, another study showed that restricting Aβ production to layers II and III of the EC results in the production of Aβ deposits in the dentate gyrus, suggesting a transfer of Aβ pathology through synaptically-connected regions (Harris et al., 2010).

Alternatively, because these synapses are so far away from the CA1 cell bodies, their maintenance might be harder, in turn making the postsynaptic compartments in SLM regions more likely to become dysfunctional in the face of oAβ. In accordance with

this idea, previous work on a transgenic mouse model has indicated that synapses in the SLM region exhibit alterations such as enhanced AMPAR expression and reduced synaptic boutons (Neuman et al., 2015). Lastly, it could be that EC (entorhinal cortex)-CA1 synapses are much more active synapses in the *in vivo* hippocampus than CA3-CA1 synapses, making them particularly vulnerable to Aβ, especially given that Aβ is released in an activity-dependent manner (Abramov et al., 2009; Dolev et al., 2013; Palop and Mucke, 2010). This idea is supported by the study of Kajiwara et al. (2008) who demonstrated that CA1 cells are more highly innervated by the perforant path and hence EC cells in comparison to neurons in the CA3 layer. Hence, it might be that that these synapses release the most Aβ and this distribution is not observed in other models because of *App* overexpression in transgenic models, or because of the high tendency of Aβ to deposit into plaques in $App^{NL\text{-}G\text{-}F}$ mice. Interestingly, work on AD postmortem tissue has shown the absence of plaques in the SLM region (Furcila et al., 2018), raising questions as to how relevant the pathology observed in the $App^{NL\text{-}F}$ model is to that found in human disease. However, it is important to note that this study only looked at the brains of four AD patients, suggesting that the lack of plaque formation in the SLM region might not be reflective of common AD pathology in humans.

The heavier plaque load in the SLM of $App^{NL\text{-}F}$ mice was also accompanied with higher overall microglial counts there compared to all regions, however this increase was observed in all of the examined genotypes, including wild-types. This suggests that microglia are particularly attracted to the SLM in the hippocampus and hence might be driving the plaque formation in these regions, providing one suggestion as to why plaque formation was specific to the SLM in $App^{NL\text{-}F}$ mice. Previous work has suggested that microglia are instrumental to the formation of initial plaques (Casali et al., 2020; Spangenberg et al., 2019). Hence their higher density in the SLM could inevitably result in a heavier plaque load in this region as a result of their potential role in depositing Aβ into plaques. Microglial density in the SLM was also found to be higher in $App^{NL\text{-}F}$ mice compared to both wild-types and $App^{NL\text{-}F}/Trem2^{R47H}$ mice. These alterations are likely driven by the increased accumulation of microglia around the plaques formed in the SLM region and it is clear that the $Trem2^{R47H}$ mutation impairs this ability of microglia in accordance with previous studies (Wang et al., 2015; Xiang et al., 2018).

6.1.3 *App* knock-in mice with *Trem2*^{R47H} exhibit altered astrocytic density

The present work also examined alterations in astrocytic density and found no differences between *App*$^{NL-G-F}$ mice and wild-types. Although this might suggest that astrogliosis is not observed in these mice, it is important to note that transcriptomic changes in specific astrocytic markers associated with astrogliosis were not specifically examined. This could also be extended to the microglia data as there only alterations in density were explored. Although density changes could provide some insight into how glial cells respond to the AD environment, they only examine one side of glial activation. For instance, it would be important to explore how astrocytic genes specifically associated with activation, such as *Gfap* and *C3* (Liddelow et al., 2017), as well as microglial markers, such as *Trem2* and *Cd68*, are altered in these mice and specifically in plaque regions. Interestingly, unpublished transcriptomic data from our lab has demonstrated clear increases in these markers in the hippocampus of 9-month-old *App*$^{NL-G-F}$ mice and a tendency for an increase in 18-month-old *App*$^{NL-F}$ mice (Figure 6.1). This shows that although there are no clear changes in the density of glial cells, there is in fact an increase in their inflammatory profile at these stages.

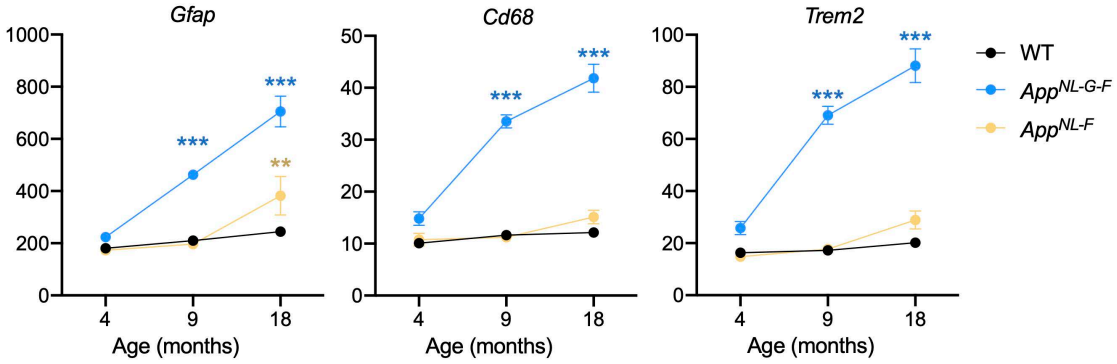

Figure 6.1. Gene expression changes in *App*$^{NL-F}$ and *App*$^{NL-G-F}$ mice at different ages. Alterations in the expression of astrocytic (*Gfap)* and microglial markers (*Cd68* and *Trem2*) associated with activation. Two-way ANOVAs revealed significant age x genotype interactions. Two-way ANOVA followed by Sidak-corrected *post-hoc* comparisons indicated by: **p<0.01, ***p<0.001.

Furthermore, it is well-established that the astrocytic processes are highly motile and although astrocytic density was unaltered in *App*$^{NL-G-F}$ mice, it might be that astrocytes had extended their processes towards toxic regions. Indeed, it was observed that astrocytic processes were ensheathing amyloid plaques, indicating that looking at changes in their movement might be a viable avenue for future studies. Furthermore, the lack of an effect on astrocytic density could also be driven by the fact that *App*$^{NL-G-F}$ mice exhibit rapid plaque accumulation, which could have not given enough time for the build-up of astrocytic changes dependent on soluble Aβ.

When examining *App*$^{NL-F}$ mice, I found increased astrocytic density in *App*$^{NL-F}$ mice compared to wild-types which was not observed in *App*$^{NL-F}$/*Trem2*^{R47H} mice. This finding introduces an interesting interaction between *Trem2*, microglia and astrocytes. It has previously been demonstrated that microglial activation is able to initiate astrogliosis (Liddelow et al., 2017), which suggests that the lack of microglial activation as a result of abnormal *Trem2* functioning not only contributed to plaque formation in *App*$^{NL-F}$/*Trem2*^{R47H} mice, but also impaired the appropriate response of astrocytes to the Aβ aggregates. This idea has been confirmed by recent unpublished work from our lab done by Ridwaan Joghee which demonstrated a clear difference in the area occupied by astrocytes in the vicinity of plaques between *App*$^{NL-F}$ and *App*$^{NL-F}$/*Trem2*^{R47H} mice, again suggesting that the *Trem2*^{R47H} mutation can affect the response of both glial cells (Figure 6.2).

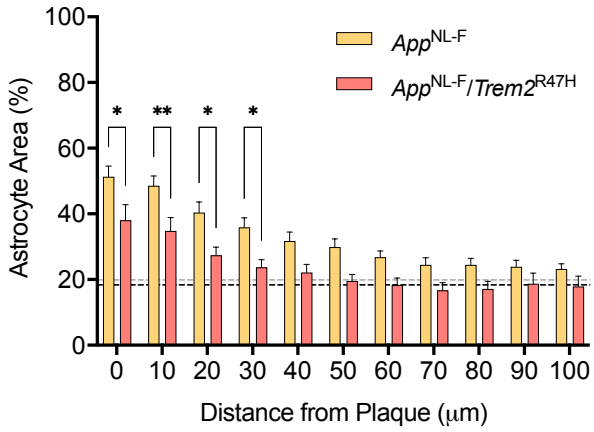

Figure 6.2. Astrocyte area at different distances from a plaque in 18-month-old *App*$^{NL-F}$ and *App*$^{NL-F}$/*Trem2*^{R47H} mice.
Near plaques (until 30 μm) the area occupied by astrocytes is higher in *App*$^{NL-F}$ compared to *App*$^{NL-F}$/*Trem2*^{R47H} mice. Two-way ANOVA followed by Sidak-corrected *post-hoc* comparisons indicated by: *p<0.05, **p<0.01. Dashed lines indicate the astrocyte area found in wild-type (black) and *Trem2*^{R47H} (grey) mice.

6.2 The addition of the Arctic mutation to the two *App* mutations reverses their effects on decay times

Alterations in the decay times can give an idea of the synchronicity of receptor closing in response to glutamate release. Here, 7-9 month-old *App*$^{NL-G-F}$ mice showed longer decay times than wild-types regardless of sex. Interestingly, the opposite effect was observed in 18-month-old *App*$^{NL-F}$ and *App*$^{NL-F}$/*Trem2*^{R47H} mice in which the *App* mutations instead led to faster decay times. Although the effects on decay time could be caused by dendritic filtering, a process whereby the signal is reduced and its time-course extended as it passes through the dendrite to the cell soma, there could be other mechanisms contributing to these.

AMPA receptors (AMPARs) are the main receptors responsible for the fast excitatory transmission at CA3-CA1 synapses (Lu et al., 2009; Tang et al., 1989) and these have been shown to exhibit alterations under AD conditions (Guntupalli et al., 2016; Hsieh et al., 2006; Sheng et al., 2012). Therefore, one possible mechanism for the above effects on the decay time could be driven by alterations in AMPAR subunits, which in turn affect neurotransmitter unbinding kinetics, receptor desensitization, as well as glutamate clearance mechanisms from the synaptic cleft. In 9 month-old *App*$^{NL-G-F}$ mice, the mRNA levels of almost all of the AMPAR subunits commonly found in the hippocampus are reduced in both males and females according to unpublished transcriptomic data from our lab, presumably due to loss of synapses around plaques (see Figure 6.3 below). This is not the case for *App*$^{NL-F}$ mice, suggesting that other mechanisms, such as changes in the receptor makeup of the postsynaptic membrane, could be contributing to the alterations in decay times observed in these mice. The idea that the AMPAR subunit composition could be altered in *App*$^{NL-G-F}$ mice is supported by work on acute hippocampal slices from rats which demonstrated that the intracellular injection of oligomeric Aβ can alter the AMPAR-mediated postsynaptic current through the insertion of GluA1-expressing AMPARs on the postsynaptic membrane (Whitcomb et al., 2015). On the other hand, oligomeric forms of Aβ can also bind to the GluA2 and GluA3 subunits of AMPARs (Reinders et al., 2016; Zhao et al., 2010), in turn triggering the internalisation of GluA2/3-containing AMPARs and AMPAR-bound Aβ. Hence, it might be that Aβ can affect response kinetics and

the waveform of the postsynaptic response by altering the receptor makeup at the postsynaptic space in *App* knock-in mice.

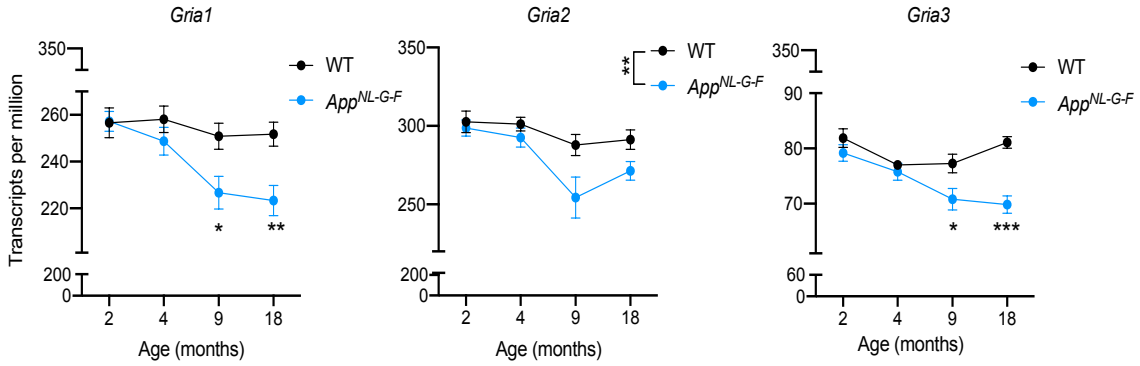

Figure 6.3. Gene expression changes in *App*$^{NL-G-F}$ mice at different ages.
The expression of *Gria1, Gria2,* and *Gria3* is altered in *App*$^{NL-G-F}$ mice. Two-way ANOVAs followed by Sidak-corrected *post-hoc* comparisons when there was an interaction indicated by: *p<0.05, **p<0.01, ***p<0.001. Asterisks between groups indicated a main effect of genotype.

Alternatively, the effects on decay time could be driven by alterations in astrocytic clearance of glutamate from the synaptic cleft. It is possible that the astrogliosis triggered by the AD environment makes astrocytes in *App* knock-in mice less able to perform their homeostatic function of clearing glutamate and instead switch to an activated phenotype. Thus, if the astrocytes were permanently impaired that would result in the background build-up of glutamate, in turn affecting receptor kinetics. Interestingly, previous work has demonstrated that Aβ can inhibit astrocytic glutamate reuptake by reducing the surface expression of the glutamate transporters GLT-1 and GLAST (Bicca et al., 2011; Scimemi et al., 2013), which have been shown to affect the time course of AMPA currents (Barbour et al., 1994). Furthermore, another study demonstrated that Aβ can alter the activity of both glutamate transporters in primary rat cultures through the activation of the mitogen-activated protein (MAP) kinases (Matos et al., 2008). This has more recently been also shown *in vivo* by the study of Zott et al. (2019) which found similar effects of exogenously applied Aβ and a glutamate transporter inhibitor on neuronal activity. Therefore, it is possible that the presence of Aβ in the neuropil at moderate and advanced stages of pathology in both *App* knock-in models could have affected glutamate transporter activity, in turn leading to alterations in the available glutamate in the synaptic cleft and affecting decay times. Interestingly, work in human post-mortem tissue has demonstrated that cognitively normal individuals with AD pathology exhibit higher GLT-1 expression

in astrocytes in comparison to AD patients (Kobayashi et al., 2018), suggesting the important role of glutamate transporter activity for protecting against AD mechanisms.

The different effects on the decay time between the two *App* knock-in models could be driven by a combination of the much later age at which *App*$^{NL-F}$ mice were examined, as well as the Arctic mutation present in *App*$^{NL-G-F}$ mice. Furthermore, at 18 months *App*$^{NL-F}$ mice exhibit much higher levels of both soluble and insoluble Aβ compared to 9-month-old *App*$^{NL-G-F}$ mice (Saito et al., 2014). This suggests that the faster decay times might be driven by the higher Aβ levels but also by the processes initiated by such high Aβ load.

6.3 The *App* mutations lead to alterations in failure rates

Although there were no differences in the PPR at either age in *App*$^{NL-G-F}$ mice, there was a reduced failure rate in *App*$^{NL-G-F}$ compared to wild-type mice at 7-9 months of age. Furthermore, I found that females exhibited lower failure rates compared to males and this was independent of plaque presence. Therefore, it appears that this reduced failure rate is a global effect to female CA1 cells in AD, raising questions as to what the contributing factor to the higher likelihood of a postsynaptic response found in females is. When examining *App*$^{NL-F}$ and *App*$^{NL-F}$/*Trem2*^{R47H} mice, I similarly found no alterations in the PPR, although I did find increased failure rates in the presence of the *App* mutations – an effect which was the opposite to what was observed in *App*$^{NL-G-F}$ mice at advanced stages of pathology.

The fact that the above changes in failure rates in both *App* knock-in models were not accompanied with a change in the PPR suggests that mechanisms other than release probability contributed to the observed effects. For instance, it could be that some axons are more readily excitable than others, with female *App*$^{NL-G-F}$ mice showing higher excitability than males, illustrating some sex differences in the axonal response. In the case of *App*$^{NL-F}$ mice, they could exhibit reduced excitability which could be driven by age- and AD-related effects. For instance, previous work has demonstrated that the axon initial segment of CA3 neurons in 18-month-old *App*$^{NL-F}$ mice is dystrophic (Sos et al., 2020), and if that dystrophy does spread along the axon, it could have led to changes in the likelihood of axonal activation. Alternatively, it is possible

that the number of silent synapses is higher in *App*$^{NL-F}$ mice. Silent synapses are synapses which do not express AMPARs but only NMDARs on the postsynaptic density, and hence only depolarisation can remove the Mg^{2+}-mediated blockage of these receptors and elicit a response (Kullmann, 1994). Thus, these synapses are essentially silent – that is not responsive – in normal stimulation scenarios. This idea is consistent with one study which demonstrated that rats injected with amyloid fibrils show impaired activation of silent synapses in CA1 cells (Bie et al., 2018). Hence, it could be because *App*$^{NL-F}$ mice exhibit much higher levels of both soluble and insoluble Aβ than *App*$^{NL-G-F}$ mice (Saito et al., 2014), the number of silent synapses is lower than in the latter model, leading to the observed differences in failure rates.

The lack of changes in the PPR in both models is not consistent with previous work in both transgenic and knock-in models. Specifically, it has previously been shown that the TASTPM model exhibits reduced PPR and hence increased release probability at 4 months of age (Cummings et al., 2015). This is before these mice develop any plaque pathology (Howlett et al., 2004) which is why the authors attributed this effect to soluble Aβ acting on presynaptic mechanisms rather than to plaques themselves (Cummings et al., 2015). Furthermore, recent work from our lab demonstrated that at 2 months of age, *App*$^{NL-G-F}$ mice exhibit reduced PPRs which is likely driven by soluble Aβ exerting its well-established effects on enhancing neurotransmitter release (Abramov et al., 2009; Benitez et al., 2021; Russell et al., 2012). This effect is lost at 4 months of age potentially due to the high deposition of Aβ into plaques, but reappears again in 9-month-old *App*$^{NL-G-F}$ mice, suggesting that rising levels of soluble Aβ might be continuously exerting their effects on presynaptic mechanisms. Additionally, the same work also demonstrated that 18-month *App*$^{NL-F}$ mice exhibit reduced PPR compared to wild-types, which similarly to *App*$^{NL-G-F}$ mice was argued to be driven by the effects of Aβ on enhancing presynaptic release (Benitez et al., 2021).

The discrepancy between the present findings and the study by Benitez et al. could be explained in several ways. First, the present work examined a much larger age range for *App*$^{NL-G-F}$ mice – 7-9 months – while the work by Benitez et al. (2021) focused only on 9-month-old mice. Hence, the point at which the effects on the PPR could re-emerge might be very specific to the end of the 7-9 month window, providing one

reason as to why they were not observed here. Second, the work by Benitez et al. (2021) did not explore female mice and hence although male *App*$^{NL-G-F}$ mice in the present thesis did show a trend towards increased probability of release compared to wild-types (see Figure 3.6D), this was not the case for females. Third, two different stimulation paradigms were used in the two studies. In particular, I used a minimal stimulation paradigm as individual synapses were my main focus, while the work by Benitez et al. (2021) employed near-minimal stimulation intensities which likely recruited several synapses during stimulation. Hence, it is possible that the recruitment of more synapses allowed for examining a much bigger sample, unmasking effects which would have not otherwise been observed at the single synapses recorded here. Alternatively, perhaps the use of higher stimulations in the work by Benitez et al. (2021) recruited even the less excitable axons which would not have been activated in the present work due to the smaller intensities used. Hence, it could be that although there might an effect on the PPR at that age, they could have been masked because these axons were not activated in the present work due to the high failure rate of axonal firing. This idea is supported by the finding that when plaque- and non-plaque-associated synapses were examined in *App*$^{NL-F}$ mice, a change in the PPR did indeed emerge, with plaque conditions showing reduced PPRs compared to no-plaque conditions.

6.4 *Trem2*^{R47H} affects the excitatory/inhibitory balance in *App*$^{NL-F}$ mice

In addition to evoked responses, I was also interested in examining alterations in spontaneous excitatory and inhibitory activity. Given that the *App*$^{NL-F}$/*Trem2*^{R47H} model is a new model which has not been characterised yet, examining alterations in the properties of excitatory and inhibitory transmission can provide important insight into whether microglial functioning has a global effect on such activity. Previous work on *Trem2*^{R47H} rats which also produce human Aβ demonstrated that the *Trem2* mutation results in reduced GABAergic transmission, evidenced by increased PPR and reduced postsynaptic amplitudes of inhibitory currents (Ren et al., 2020a). The authors argued that microglia from *Trem2*^{R47H} rats enhance the excitatory/inhibitory balance through the increased release of TNF-α which previously has been shown to promote the exocytosis of AMPARs, increase the spine size of dendritic branches, as

well as promote the endocytosis of GABA receptors (Barnes et al., 2017; Beattie et al., 2002; Ren et al., 2020a; Stellwagen et al., 2005). This has been supported by previous work which found enhanced excitatory synaptic transmission in the same model, with TNF-α inhibitors reversing these effects (Ren et al., 2020b).

Although I found no changes in the frequency or decay times of sIPSCs, I did observe an *App* x *Trem2* interaction on sIPSC amplitudes. In particular, while no changes were observed in *App*$^{NL-F}$ mice, *App*$^{NL-F}$/*Trem2*^{R47H} mice showed a trend for reduced sIPSC amplitudes compared to *Trem2*^{R47H} controls, thereby reaching amplitudes more similar to *App*$^{NL-F}$ and wild-type mice. Furthermore, when examining sEPSCs, I also found that the increased frequency observed in *App*$^{NL-F}$ mice is no longer present when *Trem2*^{R47H} is introduced. These results present an interesting insight into the effects of *App* and *Trem2* on the excitatory/inhibitory balance in mice.

The observed reduction in sIPSC amplitudes is somewhat contradictory to the findings presented by Ren et al. (2020a) as the opposite effect was expected. However, it is important to note that the reduction in the inhibitory currents found in the study by Ren and colleagues was also reported in the presence of human *App* and hence human Aβ, while the increased amplitude presented here is found in mice only expressing *Trem2*^{R47H}. Furthermore, these rats also exhibit normal *Trem2* splicing, meaning that the effects are most likely due to the presence of the R47H variant rather than reduced *Trem2* levels, which is characteristic of the *Trem2*^{R47H} mice used in the present work (Cheng-Hathaway et al., 2018; Liu et al., 2020; Xiang et al., 2018). Therefore, it could be that reduced *Trem2* levels rather than the presence of *Trem2*^{R47H} increase the number of GABA receptors in the postsynaptic membrane, in turn leading to enhanced amplitudes of sIPSCs. Furthermore, the work by Ren and colleagues also examined rats at 6-8 weeks of age, meaning that perhaps the effects would have been observed in younger mice to the ones examined in the present work. Interestingly, the *App* mutation which is introduced in *App*$^{NL-F}$ /*Trem2*^{R47H} mice, makes the neuronal environment slightly more similar to that found in the *Trem2*^{R47H} rats used in the work by Ren et al. (2020a) as these mice produce human Aβ, although at much higher levels, and also have *Trem2*^{R47H}. This can explain why the increase in inhibitory amplitudes is reversed in *App*$^{NL-F}$ /*Trem2*^{R47H} mice as microglia in these mice, similarly to the microglia in the rats examined by Ren et al. (2020a), might exhibit enhanced TNF-α

release which in turn enhances GABA receptor endocytosis. Additionally, given that enhanced production of TNF-α is a well-known feature of AD found in both AD mouse models (McAlpine and Tansey, 2008) and AD patients (Swardfager et al., 2010; Zhao et al., 2003), this might mean that its levels are even higher in *App*$^{NL-F}$/*Trem2*^{R47H} as a result of *Trem2*^{R47H}, further affecting inhibitory transmission.

As mentioned above, I also found that *App*$^{NL-F}$ mice exhibit enhanced frequency of sEPSCs which is no longer observed in the presence of *Trem2*^{R47H}. This suggests that microglia in the AD environment are able to enhance the activity at excitatory synapses and that this ability is lost with dysfunctional TREM2. Previous work has demonstrated that activated microglia release ATP which triggers astrocytic release of glutamate, which then enhances excitatory transmission by binding to presynaptic mGluR5 receptors (Pascual et al., 2012). Hence, it is possible that the AD environment initiated the activation of microglia, in turn increasing sEPSC frequency, while the presence of *Trem2*^{R47H} prevented microglial activation, thereby exerting no effects on excitatory transmission. Alternatively, it is well established that Aβ can increase the release probability (Abramov et al., 2009; Kamenetz et al., 2003) with previous work showing similar to this work's findings of increased sEPSC frequency in response to soluble Aβ (Wang et al., 2017). Although this might be a process also occurring in *App*$^{NL-F}$/*Trem2*^{R47H} mice, it has also been suggested that an impaired microglial response can reduce the release probability at excitatory synapses because of impaired microglia-neuron signalling (Basilico et al., 2019). Therefore, it might be that this latter process overrides the effects of Aβ, in turn resulting in reduced sEPSC frequency in the presence of *Trem2*^{R47H}. The present observations on increased frequency of sEPSCs in *App*$^{NL-F}$ mice have not been reported before in the work by Benitez et al. (2021). However, it should be noted that this is likely because the sample size here is much larger due to the combination of recordings from the two sexes, as well as because of the possibility that female *App*$^{NL-F}$ mice have potentially shifted the frequency towards an increase. Nonetheless, the above suggests an important role for microglia and TREM2 specifically in regulating the inhibitory/excitatory balance in the AD brain.

6.5 Plaque-specific effects on synaptic transmission

6.5.1 Plaque-associated regions exhibit reduced postsynaptic amplitudes, and this is dependent on normal microglial functioning

Although I found no effects on the postsynaptic amplitude when comparing *App*$^{NL-G-F}$ and *App*$^{NL-F}$ mice to wild-types, I did find changes in these parameters when the presence of a plaque around the stimulated axons was taken into account. In particular, the amplitude of the first uEPSC response showed a tendency for being lower in plaque compared to no-plaque conditions at 4-5 months of age, though these differences disappeared at the more advanced pathology stage of 7-9 months, suggesting the age- or pathology-dependency of these plaque-specific effects. Furthermore, 18-month-old *App*$^{NL-F}$ mice also exhibited similar to the 4-5-month-old *App*$^{NL-G-F}$ mice reductions in the uEPSC amplitude, and this effect was lost with the introduction of *Trem2*^{R47H}. The clear distinction between the synaptic effects observed at plaque and no-plaque regions at that age in the postsynaptic amplitude is consistent with previous work showing that the loss of synapses observed in 18-month-old *App*$^{NL-F}$ is limited to within 25 μm from the plaque region (Sauerbeck et al., 2020).

The above results in *App*$^{NL-G-F}$ mice are in keeping with previous work which has demonstrated extensive loss of synapses in the vicinity of plaques in both AD patients and AD mouse models (Koffie et al., 2012; Penzes et al., 2011; Sauerbeck et al., 2020; Spires et al., 2005). However, the reason behind this synapse loss remains unknown. It could be caused by the toxic effects on the postsynaptic density of oligomeric Aβ (oAβ) in these regions as it has been demonstrated that Aβ can alter the make-up of the postsynaptic density. For instance, one study showed that oAβ can specifically bind to GluA1-containing AMPARs and can thus inhibit their exocytosis (Tanaka et al., 2019). Furthermore, oAβ has also been shown to disrupt AMPAR trafficking by binding to GluA2-containing complexes or by interfering with CaMKII activity, in turn impairing phosphorylation-dependent trafficking (Gu et al., 2009; Zhao et al., 2010), potentially leading to alterations in uEPSC amplitudes.

Alternatively, however, it could be that mechanisms other than the activity of Aβ are contributing to the effects on uEPSC amplitudes observed in this study. For instance,

it is now very well-established that microglia rapidly cluster around Aβ plaques in both post-mortem tissue and AD mouse models (Baron et al., 2014; Condello et al., 2015; Matarin et al., 2015; Meyer-Luehmann et al., 2008; Serrano-Pozo et al., 2013; Town et al., 2005; Yuan et al., 2016). Therefore, it is possible that plaque-associated microglia are phagocytosing postsynaptic densities in this region, contributing to the reduced uEPSC amplitudes observed in this work in plaque regions. A role for this phagocytosis around that stage of pathology is supported by a study by Pauls et al. (2021) which demonstrated that genes associated with microglial phagocytosis are significantly upregulated at 6 months of age in *App*$^{NL-G-F}$ mice.

The above idea was further supported by the fact that *App*$^{NL-F}$ mice showed lower amplitudes in plaque compared to no-plaque conditions, while *App*$^{NL-F}$/*Trem2*^{R47H} mice exhibited no such differences. This suggests that these reductions in uEPSC amplitudes are dependent on the normal functioning of plaque-associated microglia rather than on Aβ. Interestingly, comparing both plaque- and non-plaque associated uEPSC amplitudes to mEPSCs previously recorded from wild-types revealed that this reduction of uEPSC amplitudes in plaque regions made them more similar to those of wild-type mice. Hence, it seems that plaque-associated microglia are indeed protective as they reduce the activity of overactive synapses to basal conditions potentially through phagocytosis. Phagocytosis of synapses is something which has been observed previously in work from both AD mice and AD patients (Hong et al., 2016; Tzioras et al., 2019). Microglial phagocytosis is accomplished in a complement-dependent manner, with C1q tagging synapses for engulfment and the microglial receptor C3R recognising these – a process similar to what has been observed during development (Stevens et al., 2007). Previous work has also demonstrated that the removal of microglia prevents the reduction of postsynaptic densities (Spangenberg et al., 2016) and the loss of synaptic genes observed in AD mice (Spangenberg et al., 2019). Therefore, the fact that the above effect on postsynaptic amplitudes is not observed in *App*$^{NL-F}$/*Trem2*^{R47H} mice suggests that introducing the R47H variant of *Trem2* results in similar effects on the postsynaptic density as microglial removal as it confers a loss of function for microglia (Song et al., 2018). This is consistent with the finding that *Trem2*^{R47H} mice exhibit reduced number of CD68^{+} microglia, indicating an impaired phagocytic ability of microglia in this model (Liu et al., 2020). This thesis has therefore provided valuable insight into the functional role of microglial

phagocytosis on the activity of neurons at moderate stages of pathology, illustrating that the role of microglia might indeed be protective to the hyperactivity driven by plaque-associated Aβ species (Figure 6.4) (Busche et al., 2012; Busche et al., 2008).

Interestingly, it has previously been demonstrated that if microglia become dysfunctional, astrocytes become activated and take over their phagocytic role (Konishi et al., 2020). This might suggest that astrocytic activity aims to compensate for the perturbed microglial functioning in *App*$^{NL-F}$/*Trem2*^{R47H} mice, providing one explanation as to why plaque and no-plaque regions exhibited similarly low postsynaptic amplitudes in these mice. Specifically, although astrocytes do cluster around plaques in AD (Henstridge et al., 2019), they do not migrate as closely as microglia, which means that the effects of their phagocytic ability might not be limited to the 30 μm used as a distinction between plaque and no-plaque regions in the present study. This compensatory role of astrocytes would be an interesting idea for future studies to focus on.

6.5.2 Increased release probability in plaque-associated regions in *App*$^{NL-F}$ mice

Although the present work found no changes in the PPR in *App*$^{NL-G-F}$ mice, it did find reduced PPR in plaque compared to no-plaque conditions in *App*$^{NL-F}$ mice which, however, was not accompanied with a change in the failure rates. The fact that this effect is in fact in the same direction as to what has previously been observed in *App*$^{NL-F}$ mice in comparison to wild-types (Benitez et al., 2021), suggests that previous experiments done at near-minimal stimulation conditions were likely made up primarily of recordings from synapses in the vicinity of plaques, or because of the higher stimulation intensities used, almost always resulted in the recruitment of plaque-associated axons. This is plausible since *App*$^{NL-F}$ mice have a moderate plaque pathology at that stage (Saito et al., 2014). These results could be attributed to the fact that in plaque-associated regions, the halo of soluble Aβ, which is tightly associated with insoluble Aβ and has also been shown to be damaging to the surrounding network (Koffie et al., 2012; Koffie et al., 2009; Yang et al., 2017), is able to exert its effects on the presynapse. In particular, numerous studies have demonstrated that Aβ is able to enhance synaptic activity (Abramov et al., 2009; Benitez et al., 2021; Busche et al.,

2008; Medawar et al., 2019; Ovsepian et al., 2017). This could be accomplished through the effects of Aβ on SNARE proteins which are involved in vesicle trafficking and release from the presynaptic site. For instance, Aβ has been shown to enhance Ca^{2+} influx in the presynaptic space which in turn could increase the phosphorylation of synapsin I, enhancing the availability of synaptic vesicles for neurotransmitter release (Marsh et al., 2017). Additionally, Aβ is also able to disrupt the interaction between synaptophysin and VAMP2, increasing the number of vesicles for exocytosis (Russell et al., 2012). In accordance with this idea, recent work by Hark et al. (2021) showed that the turnover of presynaptic proteins, including SNAP25, VAMP1 and STX1B, is impaired in the hippocampus of *App* knock-in mice at moderate stages of pathology. Alternatively, it has been shown that Aβ can also disrupt glutamate reuptake of astrocytes, leading to presynaptic mGLuR1 activation, again resulting in enhanced vesicle release probability (Ovsepian et al., 2017; Zott et al., 2019). This means that the presynaptic mechanisms are potentially enhanced, likely driven by the rapid increase of soluble Aβ at that age (Latif-Hernandez et al., 2020; Saito et al., 2014). Furthermore, unpublished transcriptional data from our lab has also demonstrated reduced *Vamp1* and *Stx1b* levels in the hippocampus of 9-month-old $App^{NL\text{-}G\text{-}F}$ mice, further supporting altered presynaptic mechanisms in this model.

However, although the above could explain the observed effects, it is unclear if the levels of soluble Aβ are in fact higher in plaque conditions in these mice, with future studies needed to examine this idea. Therefore, another mechanism for the observed increase in release probability in plaque conditions could be the influence of activated microglia in these regions. In particular, previous work from our lab has shown that partial microglial depletion leads to an increased release probability which is suggested to result from the activity of the remaining activated microglia ($CD68^{+}$) (Benitez, 2021). Hence, because activated microglia are likely to be primarily clustered around amyloid plaques, this could be another main contributor to the observed changes in the PPR, at least in $App^{NL\text{-}F}$ mice where microglia are functional.

The fact that the above effect was present in $App^{NL\text{-}F}$ but not in $App^{NL\text{-}G\text{-}F}$ mice could be explained by the presence of the Arctic mutation in the latter model which makes Aβ much more likely to oligomerise and shift towards deposition. In particular, at 4-5 months, Aβ in $App^{NL\text{-}G\text{-}F}$ mice is likely to be already incorporated into plaques,

leaving very little soluble Aβ in plaque regions to exert its effects on presynaptic release. In comparison, at 7-9 months, due to the extensive plaque pathology, it is likely that plaque- and no-plaque regions will be more similar to one another due to the possibility that even a non-plaque-associated region might contain a plaque in a previous or subsequent hippocampal section serial to the one recorded from. Hence, at both stages of pathology in *App*$^{NL-G-F}$ mice, the two regions are probably quite similar in terms of soluble Aβ levels, making it hard to see any changes in the release probability.

6.6 Limitations of the *App*$^{NL-G-F}$ model and relevance of the *App*$^{NL-F}$ model

Although the results from *App*$^{NL-G-F}$ mice provided some insight as to how the presence of a plaque affects synaptic activity, this model does have several limitations which are worth noting. First, the presence of the Arctic mutation in this model, which makes Aβ much more prone to aggregate (Tsubuki et al., 2003), means that the plaques found in these mice might not be representative of the plaques found in sporadic AD. Hence, it is unclear whether these plaques exhibit the halo of oligomeric Aβ which previous studies have highlighted as an important contributor to the toxicity observed in plaque regions, making it hard to interpret plaque-associated changes. Additionally, the rapid shift towards deposition into plaques found in these mice might not give enough time for the build-up of processes which are dependent on soluble Aβ accumulation. This is one explanation why, for example, *App*$^{NL-G-F}$ mice did not exhibit any of the alterations in astrocytic density which were observed in *App*$^{NL-F}$ mice. Finally, the heavy plaque load in these mice made it hard to discern between plaque- and non-plaque-associated regions, particularly in the 7-9 month group.

In sporadic AD, plaque development begins much earlier than the first signs of cognitive impairment, and only when the plaques are combined with other AD-associated processes such as inflammation, synaptic loss and network activity changes, do the clinical symptoms begin to emerge. Therefore, the rapid deposition of plaques observed in *App*$^{NL-G-F}$ mice might result in effects which are very different to those observed in human AD as they are not resultant from the slow build-up and gradual interaction of the above processes. Hence, to understand the above processes

better, I performed the second set of experiments in my thesis using the less aggressive *App* knock in model – $App^{NL\text{-}F}$ – which exhibits much higher soluble Aβ levels than the $App^{NL\text{-}G\text{-}F}$ model (Saito et al., 2014). Though this model still harbours two mutations within the *App* sequence, it is not as aggressive as the $App^{NL\text{-}G\text{-}F}$ model, with plaques beginning to form as late as 9 months of age, with mice at 24 months of age exhibiting just a moderate plaque pathology compared to $App^{NL\text{-}G\text{-}F}$ mice at 9 months of age (Benitez et al., 2021). This gradual increase in plaque number makes this model more relevant to the human AD brain as it allows for processes dependent on the slow accumulation of soluble Aβ oligomers to take place. Although this model does have a much higher $A\beta_{42}/A\beta_{40}$ ratio than the one found in humans (Karran et al., 2011; Saito et al., 2014), the fact that Aβ does not directly deposit into plaques means that processes which are dependent on soluble Aβ are likely to take place in this model. Furthermore, it is important to note that neither of the two *App* knock-in models produce tau tangles which are common to human AD. However, although this questions their relevance to all of the processes occurring in the human condition, they nonetheless serve as a good model for understanding the early mechanisms that happen in the AD brain which are only dependent on soluble Aβ and its downstream processes. Importantly, using the $App^{NL\text{-}F}$ model allowed for easier distinction between the mechanisms dependent on plaque presence, in turn shedding important light on which synaptic changes only occur in the vicinity of plaques, such as increased release proabibility and reduced postsynaptic amplitudes. Furthermore, the use of the $App^{NL\text{-}F}/Trem2^{R47H}$ model additionally provided insight into which of the alterations observed in $App^{NL\text{-}F}$ mice are due to the AD environment and plaque presence, and which are dependent on appropriate microglial functioning.

6.7 Proposed mechanisms occurring at synapses near and away from plaques in *App*$^{NL-F}$ mice

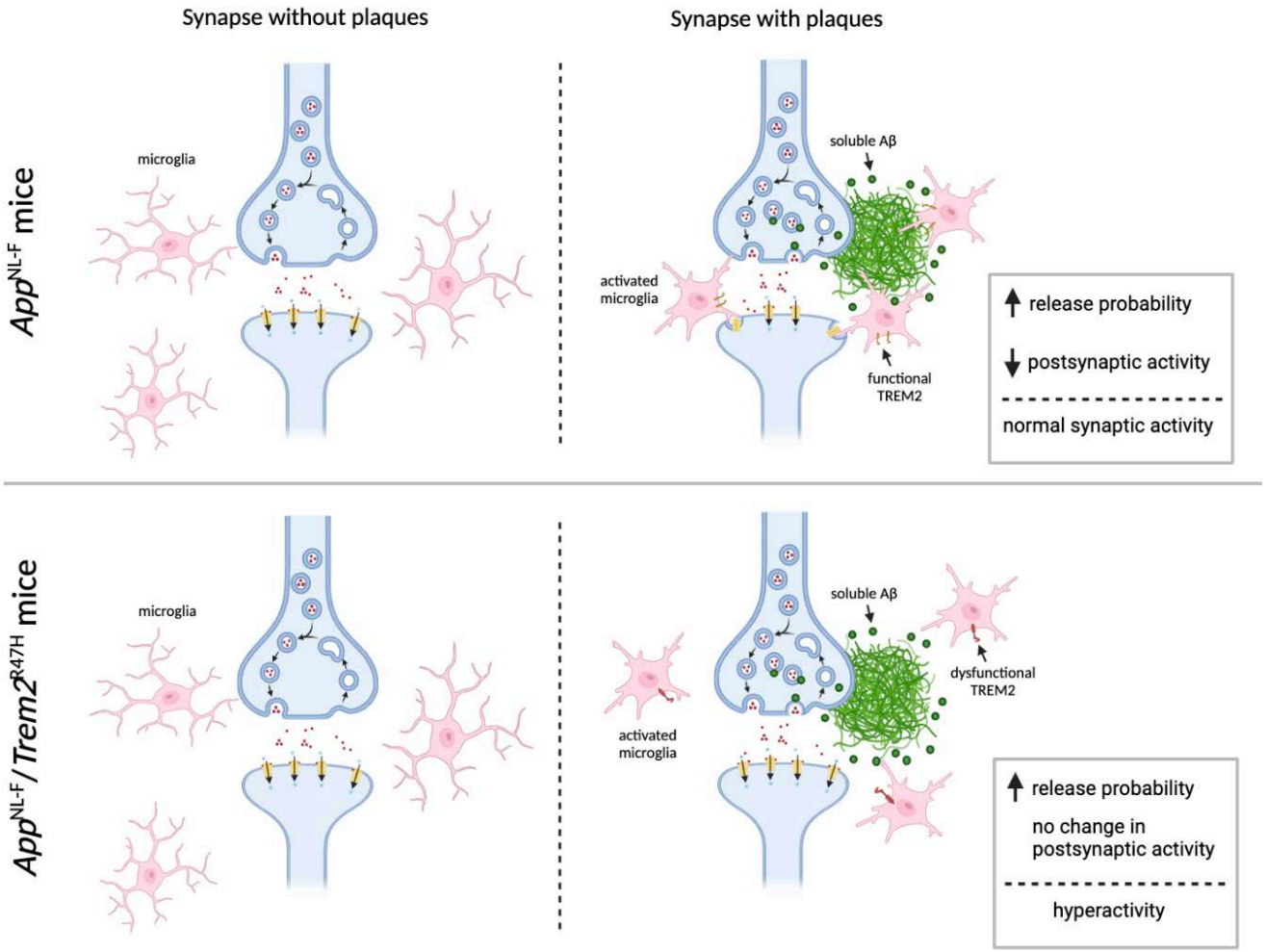

Figure 6.4. The effects of microglia and Aβ on the synaptic activity at plaque-associated regions in *App*$^{NL-F}$ and *App*$^{NL-F}$/*Trem*^{R47H} mice.

Schematic depicting the proposed mechanism of how microglia and Aβ affect the activity at synapses in the vicinity of plaques in both models. Amyloid plaques (green) have a halo of oligomeric Aβ which is able to enhance the presynaptic release of neurotransmitters at CA3-CA1 synapses potentially through its interaction with SNARE proteins, or by inhibiting astrocytic glutamate reuptake, in turn activating presynaptic mGluR1 and enhancing vesicle release. Microglia, on the other hand, primarily phagocytose parts of the postsynaptic densities as a protective mechanism in order to reduce the activity of the postsynaptic cell to basal levels. The ability of microglia to phagocytose the postsynaptic density in plaque-associated regions is lost in *App*$^{NL-F}$/*Trem*^{R47H} mice, while Aβ is still able to exert its effects on release probability, ultimately resulting in neuronal hyperactivity.

6.8 Conclusions

In this study I examined the effects of Aβ and microglia on the synaptic activity of CA1 hippocampal cells in *App* knock-in mice. Overall, the results of this thesis demonstrate an important role for both Aβ and microglia in synaptic transmission, providing valuable insight into how microglia can react to the AD environment. I found that Aβ primarily exerts its effects on the presynapse, while microglia have profound effects on the postsynaptic response and proposed a mechanism wherein, by phagocytosing postsynaptic densities, plaque-associated microglia are protective, at least at moderate stages of pathology, and balance the hyperactivity introduced by Aβ (see Figure 6.4 above and Table 6.1 below).

Although the models used in this work do have their limitations, including the fact that they only represent one aspect of AD pathology as they do not develop tau tangles, the results provide interesting insight into what is happening in the human brain in early AD. It appears that the activity of microglia in response to the early changes occurring in the disease could be in fact protective, postulating the immune cells of the brain as important therapeutic targets for future research. Until recently clinical trials were primarily focused on addressing one aspect of the disease, however it is clear from more recent work, including from the data presented in this thesis, that AD is a multifactorial disease involving multiple pathways, brain cells and synergistic interactions. In fact, recent work has indicated that microglia are important regulators of both amyloid and tau pathology, with the loss of this function conferred by the loss of *Trem2* contributing to an increased Aβ load, tau tangle formation and neuronal death (Hardy and Salih, 2021; Lee et al., 2021). Therefore, understanding the interaction between microglia, plaques and synapses will be invaluable to the early detection of AD and this can elucidate future therapeutic targets.

6.9 Future directions

It would be interesting for future work to examine transcriptional changes in both microglia and astrocytes in the App^{NLF} and $App^{NL\text{-}F}/Trem2^{R47H}$ models in order to understand in what ways their ability to respond to the AD environment is impaired in the presence of the $Trem2^{R47H}$ mutation. The present work did show that astrocytic

activation in the form of density changes is impaired in *Trem2*^{R47H}-expressing *App*$^{NL-F}$ mice, suggesting that examining markers such as *C3* and *Gfap* which are tightly associated with astrogliosis would be an interesting avenue for future work.

The present work also revealed that the SLM region in the hippocampus is particularly vulnerable to plaque formation in *App*$^{NL-F}$ mice, however the mechanism behind this susceptibility is unknown. Therefore, it would be interesting for future studies to examine how the EC-CA1 synapses are affected in this model and whether they exhibit hyperexcitability, which might make them more likely to produce excessive amounts of Aβ, in turn resulting in robust plaque accumulation. Given that at the age examined here – 18 months – plaque accumulation was particularly prominent in these regions, future work should focus on exploring these changes in synaptic activity at the earliest signs of or even before any plaque pathology is evident in these mice, as this could elucidate which synaptic changes are driven by the early accumulation of soluble Aβ.

Furthermore, there were some interesting differences between both *App* knock-in models in the decay times of the postsynaptic response, as well as the failure rates. Therefore, examining changes in the kinetics of the postsynaptic response at the dendrite specifically would provide interesting insight into how receptors are differentially affected by the two or three mutations in *App.*

The present work also revealed some interesting effects of plaque presence on synaptic activity. However, recording solely from the soma of CA1 cells did provide only limited insight into how plaques affect synaptic transmission. It is currently known that Aβ can increase release probability, however it is unknown how plaque-associated Aβ affects the ability of axons to transmit their signal. Hence, future work could use techniques like Ca^{2+} or voltage imaging to determine how the activity of axons is altered in the vicinity of plaques. This will provide a much better spatial resolution and help us understand whether axonal activity remains intact as it passes near a plaque, or if the signal is deteriorated as a result of the toxic cloud near plaques. This was something I planned to examine through a collaboration with a lab at the University of Oxford, but which the Covid-19 pandemic and the lockdown situation prevented me from doing.

Table 6.1. Summary of key findings of the present study

	App^{NL-G-F}	*App*$^{NL-F}$ and *App*$^{NL-F}$/*Trem2*^{R47H}
Plaque pathology	• Greater plaque density with age • Increased number of smaller plaques with age	• Greater plaque density in *App*$^{NL-F}$/*Trem2*^{R47H} than *App*$^{NL-F}$ mice • Increased number of smaller-sized plaques in *App*$^{NL-F}$/*Trem2*^{R47H} • Plaque formation is specific to SLM region in both models
Microgliosis	• Similar increases in microglial density in *App*$^{NL-G-F}$ compared to wild-types at both ages • No change in astrocyte density	• Increased microglial density in SLM and CA3 only in *App*$^{NL-F}$ mice • Increased astrocyte density in *App*$^{NL-F}$ mice is lost with the introduction of *Trem2*^{R47H}
Synaptic changes	• No change at 4-5 months • Longer uEPSC decay times and lower failure rates than wild-types at 7-9 months	• Higher uEPSC failure rates and trend for slower decay times than controls in both *App*$^{NL-F}$ and *App*$^{NL-F}$/*Trem2*^{R47H} mice • Higher sEPSC amplitude in *App*$^{NL-F}$ than *App*$^{NL-F}$/*Trem2*^{R47H} mice
Plaque-associated synaptic changes	• Reduced uEPSC amplitudes in plaque compared to no-plaque regions at 4-5 months • No change at 7-9 months	• Reduced uEPSC amplitudes in plaque compared to no-plaque regions only in *App*$^{NL-F}$ mice • Trend for lower PPRs in plaque regions in both models compared to no-plaque regions

References

Aarum, J., Sandberg, K., Haeberlein, S.L., and Persson, M.A. (2003). Migration and differentiation of neural precursor cells can be directed by microglia. Proc Natl Acad Sci U S A *100*, 15983-15988.

Abramov, E., Dolev, I., Fogel, H., Ciccotosto, G.D., Ruff, E., and Slutsky, I. (2009). Amyloid-beta as a positive endogenous regulator of release probability at hippocampal synapses. Nat Neurosci *12*, 1567-1576.

Aizenstein, H.J., Nebes, R.D., Saxton, J.A., Price, J.C., Mathis, C.A., Tsopelas, N.D., Ziolko, S.K., James, J.A., Snitz, B.E., Houck, P.R.*, et al.* (2008). Frequent amyloid deposition without significant cognitive impairment among the elderly. Arch Neurol *65*, 1509-1517.

Ajami, B., Samusik, N., Wieghofer, P., Ho, P.P., Crotti, A., Bjornson, Z., Prinz, M., Fantl, W.J., Nolan, G.P., and Steinman, L. (2018). Single-cell mass cytometry reveals distinct populations of brain myeloid cells in mouse neuroinflammation and neurodegeneration models. Nat Neurosci *21*, 541-551.

Albert, M.S., DeKosky, S.T., Dickson, D., Dubois, B., Feldman, H.H., Fox, N.C., Gamst, A., Holtzman, D.M., Jagust, W.J., Petersen, R.C.*, et al.* (2011). The diagnosis of mild cognitive impairment due to Alzheimer's disease: recommendations from the National Institute on Aging-Alzheimer's Association workgroups on diagnostic guidelines for Alzheimer's disease. Alzheimers Dement *7*, 270-279.

Alzheimer, A. (1907). About a peculiar disease of the cerebral cortex. (Translation by L. Jarvik and H. Greenson in 1987). Alzheimer Dis Assoc Disord *1*, 3-8.

Andersen, P., Morris, R., Amaral, D., Bliss, T., and O'Keefe, J. (2007). The hippocampus book (New York ; Oxford: Oxford University Press).

Arriagada, P.V., Growdon, J.H., Hedley-Whyte, E.T., and Hyman, B.T. (1992). Neurofibrillary tangles but not senile plaques parallel duration and severity of Alzheimer's disease. Neurology *42*, 631-639.

Atagi, Y., Liu, C.C., Painter, M.M., Chen, X.F., Verbeeck, C., Zheng, H., Li, X., Rademakers, R., Kang, S.S., Xu, H.*, et al.* (2015). Apolipoprotein E Is a Ligand for Triggering Receptor Expressed on Myeloid Cells 2 (TREM2). J Biol Chem *290*, 26043-26050.

Badimon, A., Strasburger, H.J., Ayata, P., Chen, X., Nair, A., Ikegami, A., Hwang, P., Chan, A.T., Graves, S.M., Uweru, J.O.*, et al.* (2020). Negative feedback control of neuronal activity by microglia. Nature *586*, 417-423.

Baiardi, S., Abu-Rumeileh, S., Rossi, M., Zenesini, C., Bartoletti-Stella, A., Polischi, B., Capellari, S., and Parchi, P. (2019). Antemortem CSF Abeta42/Abeta40 ratio predicts

Alzheimer's disease pathology better than Abeta42 in rapidly progressive dementias. Ann Clin Transl Neurol *6*, 263-273.

Baik, S.H., Kang, S., Son, S.M., and Mook-Jung, I. (2016). Microglia contributes to plaque growth by cell death due to uptake of amyloid beta in the brain of Alzheimer's disease mouse model. Glia *64*, 2274-2290.

Bailey, C.C., DeVaux, L.B., and Farzan, M. (2015). The Triggering Receptor Expressed on Myeloid Cells 2 Binds Apolipoprotein E. J Biol Chem *290*, 26033-26042.

Barbour, B., Keller, B.U., Llano, I., and Marty, A. (1994). Prolonged presence of glutamate during excitatory synaptic transmission to cerebellar Purkinje cells. Neuron *12*, 1331-1343.

Barnes, D.E., and Yaffe, K. (2011). The projected effect of risk factor reduction on Alzheimer's disease prevalence. Lancet Neurol *10*, 819-828.

Barnes, S.J., Franzoni, E., Jacobsen, R.I., Erdelyi, F., Szabo, G., Clopath, C., Keller, G.B., and Keck, T. (2017). Deprivation-Induced Homeostatic Spine Scaling In Vivo Is Localized to Dendritic Branches that Have Undergone Recent Spine Loss. Neuron *96*, 871-882 e875.

Baron, R., Babcock, A.A., Nemirovsky, A., Finsen, B., and Monsonego, A. (2014). Accelerated microglial pathology is associated with Abeta plaques in mouse models of Alzheimer's disease. Aging Cell *13*, 584-595.

Barry, A.E., Klyubin, I., Mc Donald, J.M., Mably, A.J., Farrell, M.A., Scott, M., Walsh, D.M., and Rowan, M.J. (2011). Alzheimer's disease brain-derived amyloid-beta-mediated inhibition of LTP in vivo is prevented by immunotargeting cellular prion protein. J Neurosci *31*, 7259-7263.

Basilico, B., Pagani, F., Grimaldi, A., Cortese, B., Di Angelantonio, S., Weinhard, L., Gross, C., Limatola, C., Maggi, L., and Ragozzino, D. (2019). Microglia shape presynaptic properties at developing glutamatergic synapses. Glia *67*, 53-67.

Bateman, R.J., Xiong, C., Benzinger, T.L., Fagan, A.M., Goate, A., Fox, N.C., Marcus, D.S., Cairns, N.J., Xie, X., Blazey, T.M.*, et al.* (2012). Clinical and biomarker changes in dominantly inherited Alzheimer's disease. N Engl J Med *367*, 795-804.

Beach, T.G., Walker, R., and McGeer, E.G. (1989). Patterns of gliosis in Alzheimer's disease and aging cerebrum. Glia *2*, 420-436.

Beattie, E.C., Stellwagen, D., Morishita, W., Bresnahan, J.C., Ha, B.K., Von Zastrow, M., Beattie, M.S., and Malenka, R.C. (2002). Control of synaptic strength by glial TNFalpha. Science *295*, 2282-2285.

Bejanin, A., Schonhaut, D.R., La Joie, R., Kramer, J.H., Baker, S.L., Sosa, N., Ayakta, N., Cantwell, A., Janabi, M., Lauriola, M.*, et al.* (2017). Tau pathology and

neurodegeneration contribute to cognitive impairment in Alzheimer's disease. Brain *140*, 3286-3300.

Ben Haim, L., and Rowitch, D.H. (2017). Functional diversity of astrocytes in neural circuit regulation. Nat Rev Neurosci *18*, 31-41.

Benitez, B.A., Cooper, B., Pastor, P., Jin, S.C., Lorenzo, E., Cervantes, S., and Cruchaga, C. (2013). TREM2 is associated with the risk of Alzheimer's disease in Spanish population. Neurobiol Aging *34*, 1711 e1715-1717.

Benitez, D. (2021). Assessment of microglia influence in synaptic transmission and early amiloid-B plaque deposition in knock-in mouse models for Alzheimer's disese. In Neuroscience, Physiology and Pharmacology (UCL).

Benitez, D.P., Jiang, S., Wood, J., Wang, R., Hall, C.M., Peerboom, C., Wong, N., Stringer, K.M., Vitanova, K.S., Smith, V.C.*, et al.* (2021). Knock-in models related to Alzheimer's disease: synaptic transmission, plaques and the role of microglia. Mol Neurodegener *16*, 47.

Berezovska, O., Lleo, A., Herl, L.D., Frosch, M.P., Stern, E.A., Bacskai, B.J., and Hyman, B.T. (2005). Familial Alzheimer's disease presenilin 1 mutations cause alterations in the conformation of presenilin and interactions with amyloid precursor protein. J Neurosci *25*, 3009-3017.

Bialas, A.R., and Stevens, B. (2013). TGF-beta signaling regulates neuronal C1q expression and developmental synaptic refinement. Nat Neurosci *16*, 1773-1782.

Bicca, M.A., Figueiredo, C.P., Piermartiri, T.C., Meotti, F.C., Bouzon, Z.L., Tasca, C.I., Medeiros, R., and Calixto, J.B. (2011). The selective and competitive N-methyl-D-aspartate receptor antagonist, (-)-6-phosphonomethyl-deca-hydroisoquinoline-3-carboxylic acid, prevents synaptic toxicity induced by amyloid-beta in mice. Neuroscience *192*, 631-641.

Bie, B., Wu, J., Foss, J.F., and Naguib, M. (2018). Amyloid fibrils induce dysfunction of hippocampal glutamatergic silent synapses. Hippocampus *28*, 549-556.

Bie, B., Wu, J., Foss, J.F., and Naguib, M. (2019). Activation of mGluR1 Mediates C1q-Dependent Microglial Phagocytosis of Glutamatergic Synapses in Alzheimer's Rodent Models. Mol Neurobiol *56*, 5568-5585.

Bittner, T., Burgold, S., Dorostkar, M.M., Fuhrmann, M., Wegenast-Braun, B.M., Schmidt, B., Kretzschmar, H., and Herms, J. (2012). Amyloid plaque formation precedes dendritic spine loss. Acta Neuropathol *124*, 797-807.

Bloodgood, B.L., and Sabatini, B.L. (2007). Nonlinear regulation of unitary synaptic signals by CaV(2.3) voltage-sensitive calcium channels located in dendritic spines. Neuron *53*, 249-260.

Bookheimer, S.Y., Strojwas, M.H., Cohen, M.S., Saunders, A.M., Pericak-Vance, M.A., Mazziotta, J.C., and Small, G.W. (2000). Patterns of brain activation in people at risk for Alzheimer's disease. N Engl J Med *343*, 450-456.

Borlikova, G.G., Trejo, M., Mably, A.J., Mc Donald, J.M., Sala Frigerio, C., Regan, C.M., Murphy, K.J., Masliah, E., and Walsh, D.M. (2013). Alzheimer brain-derived amyloid beta-protein impairs synaptic remodeling and memory consolidation. Neurobiol Aging *34*, 1315-1327.

Braak, E., and Braak, H. (1993). The New Monodendritic Neuronal Type within the Adult Human Cerebellar Granule Cell Layer Shows Calretinin-Immunoreactivity. Neuroscience Letters *154*, 199-202.

Braak, H., Alafuzoff, I., Arzberger, T., Kretzschmar, H., and Del Tredici, K. (2006). Staging of Alzheimer disease-associated neurofibrillary pathology using paraffin sections and immunocytochemistry. Acta Neuropathol *112*, 389-404.

Braak, H., and Braak, E. (1991). Neuropathological stageing of Alzheimer-related changes. Acta Neuropathol *82*, 239-259.

Braak, H., and Braak, E. (1995). Staging of Alzheimer's disease-related neurofibrillary changes. Neurobiol Aging *16*, 271-278; discussion 278-284.

Busche, M.A. (2018). In Vivo Two-Photon Calcium Imaging of Hippocampal Neurons in Alzheimer Mouse Models. Methods Mol Biol *1750*, 341-351.

Busche, M.A., Chen, X., Henning, H.A., Reichwald, J., Staufenbiel, M., Sakmann, B., and Konnerth, A. (2012). Critical role of soluble amyloid-β for early hippocampal hyperactivity in a mouse model of Alzheimer's disease. Proc Natl Acad Sci U S A *109*, 8740-8745.

Busche, M.A., Eichhoff, G., Adelsberger, H., Abramowski, D., Wiederhold, K.H., Haass, C., Staufenbiel, M., Konnerth, A., and Garaschuk, O. (2008). Clusters of hyperactive neurons near amyloid plaques in a mouse model of Alzheimer's disease. Science *321*, 1686-1689.

Busche, M.A., Grienberger, C., Keskin, A.D., Song, B., Neumann, U., Staufenbiel, M., Forstl, H., and Konnerth, A. (2015). Decreased amyloid-beta and increased neuronal hyperactivity by immunotherapy in Alzheimer's models. Nat Neurosci *18*, 1725-1727.

Busche, M.A., and Konnerth, A. (2016). Impairments of neural circuit function in Alzheimer's disease. Philos Trans R Soc Lond B Biol Sci *371*.

Butovsky, O., Jedrychowski, M.P., Moore, C.S., Cialic, R., Lanser, A.J., Gabriely, G., Koeglsperger, T., Dake, B., Wu, P.M., Doykan, C.E*., et al.* (2014). Identification of a unique TGF-beta-dependent molecular and functional signature in microglia. Nat Neurosci *17*, 131-143.

Cai, Q., and Tammineni, P. (2017). Mitochondrial Aspects of Synaptic Dysfunction in Alzheimer's Disease. J Alzheimers Dis *57*, 1087-1103.

Campion, D., Dumanchin, C., Hannequin, D., Dubois, B., Belliard, S., Puel, M., Thomas-Anterion, C., Michon, A., Martin, C., Charbonnier, F.*, et al.* (1999). Early-onset autosomal dominant Alzheimer disease: prevalence, genetic heterogeneity, and mutation spectrum. Am J Hum Genet *65*, 664-670.

Casali, B.T., MacPherson, K.P., Reed-Geaghan, E.G., and Landreth, G.E. (2020). Microglia depletion rapidly and reversibly alters amyloid pathology by modification of plaque compaction and morphologies. Neurobiol Dis *142*, 104956.

Castillo, E., Leon, J., Mazzei, G., Abolhassani, N., Haruyama, N., Saito, T., Saido, T., Hokama, M., Iwaki, T., Ohara, T.*, et al.* (2017). Comparative profiling of cortical gene expression in Alzheimer's disease patients and mouse models demonstrates a link between amyloidosis and neuroinflammation. Sci Rep *7*, 17762.

Cavedo, E., Lista, S., Houot, M., Vergallo, A., Grothe, M.J., Teipel, S., Zetterberg, H., Blennow, K., Habert, M.O., Potier, M.C.*, et al.* (2020). Plasma tau correlates with basal forebrain atrophy rates in people at risk for Alzheimer disease. Neurology *94*, e30-e41.

Chatterjee, P., Pedrini, S., Stoops, E., Goozee, K., Villemagne, V.L., Asih, P.R., Verberk, I.M.W., Dave, P., Taddei, K., Sohrabi, H.R.*, et al.* (2021). Plasma glial fibrillary acidic protein is elevated in cognitively normal older adults at risk of Alzheimer's disease. Transl Psychiatry *11*, 27.

Cheng-Hathaway, P.J., Reed-Geaghan, E.G., Jay, T.R., Casali, B.T., Bemiller, S.M., Puntambekar, S.S., von Saucken, V.E., Williams, R.Y., Karlo, J.C., Moutinho, M.*, et al.* (2018). The Trem2 R47H variant confers loss-of-function-like phenotypes in Alzheimer's disease. Mol Neurodegener *13*, 29.

Chin, J., Palop, J.J., Puolivali, J., Massaro, C., Bien-Ly, N., Gerstein, H., Scearce-Levie, K., Masliah, E., and Mucke, L. (2005). Fyn kinase induces synaptic and cognitive impairments in a transgenic mouse model of Alzheimer's disease. J Neurosci *25*, 9694-9703.

Chitu, V., Gokhan, S., Nandi, S., Mehler, M.F., and Stanley, E.R. (2016). Emerging Roles for CSF-1 Receptor and its Ligands in the Nervous System. Trends Neurosci *39*, 378-393.

Cirrito, J.R., Yamada, K.A., Finn, M.B., Sloviter, R.S., Bales, K.R., May, P.C., Schoepp, D.D., Paul, S.M., Mennerick, S., and Holtzman, D.M. (2005). Synaptic activity regulates interstitial fluid amyloid-beta levels in vivo. Neuron *48*, 913-922.

Clarke, L.E., Liddelow, S.A., Chakraborty, C., Munch, A.E., Heiman, M., and Barres, B.A. (2018). Normal aging induces A1-like astrocyte reactivity. Proc Natl Acad Sci U S A *115*, E1896-E1905.

Clayton, K., Delpech, J.C., Herron, S., Iwahara, N., Ericsson, M., Saito, T., Saido, T.C., Ikezu, S., and Ikezu, T. (2021). Plaque associated microglia hyper-secrete extracellular vesicles and accelerate tau propagation in a humanized APP mouse model. Mol Neurodegener *16*, 18.

Cleary, J.P., Walsh, D.M., Hofmeister, J.J., Shankar, G.M., Kuskowski, M.A., Selkoe, D.J., and Ashe, K.H. (2005). Natural oligomers of the amyloid-beta protein specifically disrupt cognitive function. Nat Neurosci *8*, 79-84.

Condello, C., Yuan, P., Schain, A., and Grutzendler, J. (2015). Microglia constitute a barrier that prevents neurotoxic protofibrillar Abeta42 hotspots around plaques. Nat Commun *6*, 6176.

Corder, E.H., Saunders, A.M., Strittmatter, W.J., Schmechel, D.E., Gaskell, P.C., Small, G.W., Roses, A.D., Haines, J.L., and Pericak-Vance, M.A. (1993). Gene dose of apolipoprotein E type 4 allele and the risk of Alzheimer's disease in late onset families. Science *261*, 921-923.

Cosenza-Nashat, M., Zhao, M.L., Suh, H.S., Morgan, J., Natividad, R., Morgello, S., and Lee, S.C. (2009). Expression of the translocator protein of 18 kDa by microglia, macrophages and astrocytes based on immunohistochemical localization in abnormal human brain. Neuropathol Appl Neurobiol *35*, 306-328.

Cserep, C., Posfai, B., Lenart, N., Fekete, R., Laszlo, Z.I., Lele, Z., Orsolits, B., Molnar, G., Heindl, S., Schwarcz, A.D.*, et al.* (2020). Microglia monitor and protect neuronal function through specialized somatic purinergic junctions. Science *367*, 528-537.

Cummings, D.M., Liu, W., Portelius, E., Bayram, S., Yasvoina, M., Ho, S.H., Smits, H., Ali, S.S., Steinberg, R., Pegasiou, C.M.*, et al.* (2015). First effects of rising amyloid-beta in transgenic mouse brain: synaptic transmission and gene expression. Brain *138*, 1992-2004.

Cunningham, C.L., Martinez-Cerdeno, V., and Noctor, S.C. (2013). Microglia regulate the number of neural precursor cells in the developing cerebral cortex. J Neurosci *33*, 4216-4233.

Czirr, E., Castello, N.A., Mosher, K.I., Castellano, J.M., Hinkson, I.V., Lucin, K.M., Baeza-Raja, B., Ryu, J.K., Li, L., Farina, S.N.*, et al.* (2017). Microglial complement receptor 3 regulates brain Abeta levels through secreted proteolytic activity. J Exp Med *214*, 1081-1092.

Dagher, N.N., Najafi, A.R., Kayala, K.M., Elmore, M.R., White, T.E., Medeiros, R., West, B.L., and Green, K.N. (2015). Colony-stimulating factor 1 receptor inhibition prevents microglial plaque association and improves cognition in 3xTg-AD mice. J Neuroinflammation *12*, 139.

Dardiotis, E., Siokas, V., Pantazi, E., Dardioti, M., Rikos, D., Xiromerisiou, G., Markou, A., Papadimitriou, D., Speletas, M., and Hadjigeorgiou, G.M. (2017). A novel mutation in TREM2 gene causing Nasu-Hakola disease and review of the literature. Neurobiol Aging *53*, 194 e113-194 e122.

Davis, N., Mota, B.C., Stead, L., Palmer, E.O.C., Lombardero, L., Rodriguez-Puertas, R., de Paola, V., Barnes, S.J., and Sastre, M. (2021). Pharmacological ablation of astrocytes reduces Abeta degradation and synaptic connectivity in an ex vivo model of Alzheimer's disease. J Neuroinflammation *18*, 73.

de Calignon, A., Polydoro, M., Suarez-Calvet, M., William, C., Adamowicz, D.H., Kopeikina, K.J., Pitstick, R., Sahara, N., Ashe, K.H., Carlson, G.A.*, et al.* (2012). Propagation of tau pathology in a model of early Alzheimer's disease. Neuron *73*, 685-697.

De Felice, F.G., Wu, D., Lambert, M.P., Fernandez, S.J., Velasco, P.T., Lacor, P.N., Bigio, E.H., Jerecic, J., Acton, P.J., Shughrue, P.J.*, et al.* (2008). Alzheimer's disease-type neuronal tau hyperphosphorylation induced by A beta oligomers. Neurobiol Aging *29*, 1334-1347.

Deczkowska, A., Keren-Shaul, H., Weiner, A., Colonna, M., Schwartz, M., and Amit, I. (2018). Disease-Associated Microglia: A Universal Immune Sensor of Neurodegeneration. Cell *173*, 1073-1081.

Dejanovic, B., Huntley, M.A., De Maziere, A., Meilandt, W.J., Wu, T., Srinivasan, K., Jiang, Z., Gandham, V., Friedman, B.A., Ngu, H.*, et al.* (2018). Changes in the Synaptic Proteome in Tauopathy and Rescue of Tau-Induced Synapse Loss by C1q Antibodies. Neuron *100*, 1322-1336 e1327.

DeKosky, S.T., and Scheff, S.W. (1990). Synapse loss in frontal cortex biopsies in Alzheimer's disease: correlation with cognitive severity. Ann Neurol *27*, 457-464.

Delekate, A., Fuchtemeier, M., Schumacher, T., Ulbrich, C., Foddis, M., and Petzold, G.C. (2014). Metabotropic P2Y1 receptor signalling mediates astrocytic hyperactivity in vivo in an Alzheimer's disease mouse model. Nat Commun *5*, 5422.

Desikan, R.S., Sabuncu, M.R., Schmansky, N.J., Reuter, M., Cabral, H.J., Hess, C.P., Weiner, M.W., Biffi, A., Anderson, C.D., Rosand, J.*, et al.* (2010). Selective disruption of the cerebral neocortex in Alzheimer's disease. PLoS One *5*, e12853.

Diaz-Aparicio, I., Paris, I., Sierra-Torre, V., Plaza-Zabala, A., Rodriguez-Iglesias, N., Marquez-Ropero, M., Beccari, S., Huguet, P., Abiega, O., Alberdi, E.*, et al.* (2020). Microglia Actively Remodel Adult Hippocampal Neurogenesis through the Phagocytosis Secretome. J Neurosci *40*, 1453-1482.

Dickerson, B.C., Salat, D.H., Greve, D.N., Chua, E.F., Rand-Giovannetti, E., Rentz, D.M., Bertram, L., Mullin, K., Tanzi, R.E., Blacker, D.*, et al.* (2005). Increased hippocampal activation in mild cognitive impairment compared to normal aging and AD. Neurology *65*, 404-411.

Ding, X., Wang, J., Huang, M., Chen, Z., Liu, J., Zhang, Q., Zhang, C., Xiang, Y., Zen, K., and Li, L. (2021). Loss of microglial SIRPalpha promotes synaptic pruning in preclinical models of neurodegeneration. Nat Commun *12*, 2030.

Dissing-Olesen, L., LeDue, J.M., Rungta, R.L., Hefendehl, J.K., Choi, H.B., and MacVicar, B.A. (2014). Activation of neuronal NMDA receptors triggers transient ATP-mediated microglial process outgrowth. J Neurosci *34*, 10511-10527.

Dolev, I., Fogel, H., Milshtein, H., Berdichevsky, Y., Lipstein, N., Brose, N., Gazit, N., and Slutsky, I. (2013). Spike bursts increase amyloid-beta 40/42 ratio by inducing a presenilin-1 conformational change. Nat Neurosci *16*, 587-595.

Domercq, M., Vazquez-Villoldo, N., and Matute, C. (2013). Neurotransmitter signaling in the pathophysiology of microglia. Front Cell Neurosci *7*, 49.

Du, A.T., Schuff, N., Amend, D., Laakso, M.P., Hsu, Y.Y., Jagust, W.J., Yaffe, K., Kramer, J.H., Reed, B., Norman, D.*, et al.* (2001). Magnetic resonance imaging of the entorhinal cortex and hippocampus in mild cognitive impairment and Alzheimer's disease. J Neurol Neurosurg Psychiatry *71*, 441-447.

Du, H., Guo, L., Fang, F., Chen, D., Sosunov, A.A., McKhann, G.M., Yan, Y., Wang, C., Zhang, H., Molkentin, J.D.*, et al.* (2008). Cyclophilin D deficiency attenuates mitochondrial and neuronal perturbation and ameliorates learning and memory in Alzheimer's disease. Nat Med *14*, 1097-1105.

Du, H., Guo, L., Yan, S., Sosunov, A.A., McKhann, G.M., and Yan, S.S. (2010). Early deficits in synaptic mitochondria in an Alzheimer's disease mouse model. Proc Natl Acad Sci U S A *107*, 18670-18675.

Dubois, B., Feldman, H.H., Jacova, C., Hampel, H., Molinuevo, J.L., Blennow, K., DeKosky, S.T., Gauthier, S., Selkoe, D., Bateman, R.*, et al.* (2014). Advancing research diagnostic criteria for Alzheimer's disease: the IWG-2 criteria. Lancet Neurol *13*, 614-629.

Edwards, F.A. (1995). Patch clamp recording in brain slices. In Brain slices in basic and clinical research, A. Schurr, and B.M. Rigor, eds. (CRC Press, Inc).

Edwards, F.A. (2019). A Unifying Hypothesis for Alzheimer's Disease: From Plaques to Neurodegeneration. Trends Neurosci *42*, 310-322.

Elmore, M.R., Najafi, A.R., Koike, M.A., Dagher, N.N., Spangenberg, E.E., Rice, R.A., Kitazawa, M., Matusow, B., Nguyen, H., West, B.L.*, et al.* (2014). Colony-stimulating factor 1 receptor signaling is necessary for microglia viability, unmasking a microglia progenitor cell in the adult brain. Neuron *82*, 380-397.

Escartin, C., Galea, E., Lakatos, A., O'Callaghan, J.P., Petzold, G.C., Serrano-Pozo, A., Steinhauser, C., Volterra, A., Carmignoto, G., Agarwal, A.*, et al.* (2021). Reactive astrocyte nomenclature, definitions, and future directions. Nat Neurosci *24*, 312-325.

Esch, F.S., Keim, P.S., Beattie, E.C., Blacher, R.W., Culwell, A.R., Oltersdorf, T., McClure, D., and Ward, P.J. (1990). Cleavage of amyloid beta peptide during constitutive processing of its precursor. Science *248*, 1122-1124.

Eyo, U.B., Peng, J., Swiatkowski, P., Mukherjee, A., Bispo, A., and Wu, L.J. (2014). Neuronal hyperactivity recruits microglial processes via neuronal NMDA receptors and microglial P2Y12 receptors after status epilepticus. J Neurosci *34*, 10528-10540.

Farias, S.T., Mungas, D., Reed, B.R., Harvey, D., and DeCarli, C. (2009). Progression of mild cognitive impairment to dementia in clinic- vs community-based cohorts. Arch Neurol *66*, 1151-1157.

Ferretti, M.T., Iulita, M.F., Cavedo, E., Chiesa, P.A., Schumacher Dimech, A., Santuccione Chadha, A., Baracchi, F., Girouard, H., Misoch, S., Giacobini, E.*, et al.* (2018). Sex differences in Alzheimer disease - the gateway to precision medicine. Nat Rev Neurol *14*, 457-469.

Fiala, J.C., Spacek, J., and Harris, K.M. (2002). Dendritic spine pathology: cause or consequence of neurological disorders? Brain Res Brain Res Rev *39*, 29-54.

Filipello, F., Morini, R., Corradini, I., Zerbi, V., Canzi, A., Michalski, B., Erreni, M., Markicevic, M., Starvaggi-Cucuzza, C., Otero, K.*, et al.* (2018). The Microglial Innate Immune Receptor TREM2 Is Required for Synapse Elimination and Normal Brain Connectivity. Immunity *48*, 979-991 e978.

Finelli, D., Rollinson, S., Harris, J., Jones, M., Richardson, A., Gerhard, A., Snowden, J., Mann, D., and Pickering-Brown, S. (2015). TREM2 analysis and increased risk of Alzheimer's disease. Neurobiol Aging *36*, 546 e549-513.

Fogel, H., Frere, S., Segev, O., Bharill, S., Shapira, I., Gazit, N., O'Malley, T., Slomowitz, E., Berdichevsky, Y., Walsh, D.M.*, et al.* (2014). APP homodimers transduce an amyloid-beta-mediated increase in release probability at excitatory synapses. Cell Rep *7*, 1560-1576.

Forabosco, P., Ramasamy, A., Trabzuni, D., Walker, R., Smith, C., Bras, J., Levine, A.P., Hardy, J., Pocock, J.M., Guerreiro, R.*, et al.* (2013). Insights into TREM2 biology by network analysis of human brain gene expression data. Neurobiol Aging *34*, 2699-2714.

Fourgeaud, L., Traves, P.G., Tufail, Y., Leal-Bailey, H., Lew, E.D., Burrola, P.G., Callaway, P., Zagorska, A., Rothlin, C.V., Nimmerjahn, A.*, et al.* (2016). TAM receptors regulate multiple features of microglial physiology. Nature *532*, 240-244.

Fox, N., Scahill, R., and Rossor, M. (1999). Correlation between rates of brain atrophy and cognitive decline in AD

. Neurology *52*.

Frank, S., Burbach, G.J., Bonin, M., Walter, M., Streit, W., Bechmann, I., and Deller, T. (2008). TREM2 is upregulated in amyloid plaque-associated microglia in aged APP23 transgenic mice. Glia *56*, 1438-1447.

Friedman, B.A., Srinivasan, K., Ayalon, G., Meilandt, W.J., Lin, H., Huntley, M.A., Cao, Y., Lee, S.H., Haddick, P.C.G., Ngu, H., *et al.* (2018). Diverse Brain Myeloid Expression Profiles Reveal Distinct Microglial Activation States and Aspects of Alzheimer's Disease Not Evident in Mouse Models. Cell Rep *22*, 832-847.

Frisoni, G.B., Boccardi, M., Barkhof, F., Blennow, K., Cappa, S., Chiotis, K., Demonet, J.F., Garibotto, V., Giannakopoulos, P., Gietl, A., *et al.* (2017). Strategic roadmap for an early diagnosis of Alzheimer's disease based on biomarkers. Lancet Neurol *16*, 661-676.

Fu, H., Liu, B., Frost, J.L., Hong, S., Jin, M., Ostaszewski, B., Shankar, G.M., Costantino, I.M., Carroll, M.C., Mayadas, T.N., *et al.* (2012). Complement component C3 and complement receptor type 3 contribute to the phagocytosis and clearance of fibrillar Abeta by microglia. Glia *60*, 993-1003.

Furcila, D., DeFelipe, J., and Alonso-Nanclares, L. (2018). A Study of Amyloid-beta and Phosphotau in Plaques and Neurons in the Hippocampus of Alzheimer's Disease Patients. J Alzheimers Dis *64*, 417-435.

Games, D., Adams, D., Alessandrini, R., Barbour, R., Berthelette, P., Blackwell, C., Carr, T., Clemens, J., Donaldson, T., Gillespie, F., *et al.* (1995). Alzheimer-type neuropathology in transgenic mice overexpressing V717F beta-amyloid precursor protein. Nature *373*, 523-527.

Gautier, E.L., Shay, T., Miller, J., Greter, M., Jakubzick, C., Ivanov, S., Helft, J., Chow, A., Elpek, K.G., Gordonov, S., *et al.* (2012). Gene-expression profiles and transcriptional regulatory pathways that underlie the identity and diversity of mouse tissue macrophages. Nat Immunol *13*, 1118-1128.

Gengler, S., Hamilton, A., and Holscher, C. (2010). Synaptic plasticity in the hippocampus of a APP/PS1 mouse model of Alzheimer's disease is impaired in old but not young mice. PLoS One *5*, e9764.

Ginhoux, F., Greter, M., Leboeuf, M., Nandi, S., See, P., Gokhan, S., Mehler, M.F., Conway, S.J., Ng, L.G., Stanley, E.R., *et al.* (2010). Fate mapping analysis reveals that adult microglia derive from primitive macrophages. Science *330*, 841-845.

Ginhoux, F., and Guilliams, M. (2016). Tissue-Resident Macrophage Ontogeny and Homeostasis. Immunity *44*, 439-449.

Gomes, C., Ferreira, R., George, J., Sanches, R., Rodrigues, D.I., Goncalves, N., and Cunha, R.A. (2013). Activation of microglial cells triggers a release of brain-derived neurotrophic factor (BDNF) inducing their proliferation in an adenosine A2A receptor-dependent manner: A2A receptor blockade prevents BDNF release and proliferation of microglia. J Neuroinflammation *10*, 16.

Gosselin, D., Link, V.M., Romanoski, C.E., Fonseca, G.J., Eichenfield, D.Z., Spann, N.J., Stender, J.D., Chun, H.B., Garner, H., Geissmann, F., *et al.* (2014). Environment drives selection and function of enhancers controlling tissue-specific macrophage identities. Cell *159*, 1327-1340.

Gosselin, D., Skola, D., Coufal, N.G., Holtman, I.R., Schlachetzki, J.C.M., Sajti, E., Jaeger, B.N., O'Connor, C., Fitzpatrick, C., Pasillas, M.P.*, et al.* (2017). An environment-dependent transcriptional network specifies human microglia identity. Science *356*.

Grathwohl, S.A., Kalin, R.E., Bolmont, T., Prokop, S., Winkelmann, G., Kaeser, S.A., Odenthal, J., Radde, R., Eldh, T., Gandy, S.*, et al.* (2009). Formation and maintenance of Alzheimer's disease beta-amyloid plaques in the absence of microglia. Nat Neurosci *12*, 1361-1363.

Gratuze, M., Chen, Y., Parhizkar, S., Jain, N., Strickland, M.R., Serrano, J.R., Colonna, M., Ulrich, J.D., and Holtzman, D.M. (2021). Activated microglia mitigate Abeta-associated tau seeding and spreading. J Exp Med *218*.

Gratuze, M., Leyns, C.E., Sauerbeck, A.D., St-Pierre, M.K., Xiong, M., Kim, N., Serrano, J.R., Tremblay, M.E., Kummer, T.T., Colonna, M.*, et al.* (2020). Impact of TREM2R47H variant on tau pathology-induced gliosis and neurodegeneration. J Clin Invest *130*, 4954-4968.

Grolla, A.A., Sim, J.A., Lim, D., Rodriguez, J.J., Genazzani, A.A., and Verkhratsky, A. (2013). Amyloid-beta and Alzheimer's disease type pathology differentially affects the calcium signalling toolkit in astrocytes from different brain regions. Cell Death Dis *4*, e623.

Grubman, A., Choo, X.Y., Chew, G., Ouyang, J.F., Sun, G., Croft, N.P., Rossello, F.J., Simmons, R., Buckberry, S., Landin, D.V.*, et al.* (2021). Transcriptional signature in microglia associated with Abeta plaque phagocytosis. Nat Commun *12*, 3015.

Gu, Z., Liu, W., and Yan, Z. (2009). {beta}-Amyloid impairs AMPA receptor trafficking and function by reducing Ca2+/calmodulin-dependent protein kinase II synaptic distribution. J Biol Chem *284*, 10639-10649.

Guerreiro, R., Bilgic, B., Guven, G., Bras, J., Rohrer, J., Lohmann, E., Hanagasi, H., Gurvit, H., and Emre, M. (2013a). Novel compound heterozygous mutation in TREM2 found in a Turkish frontotemporal dementia-like family. Neurobiol Aging *34*, 2890 e2891-2895.

Guerreiro, R., and Bras, J. (2015). The age factor in Alzheimer's disease. Genome Med *7*, 106.

Guerreiro, R., Wojtas, A., Bras, J., Carrasquillo, M., Rogaeva, E., Majounie, E., Cruchaga, C., Sassi, C., Kauwe, J.S., Younkin, S.*, et al.* (2013b). TREM2 variants in Alzheimer's disease. N Engl J Med *368*, 117-127.

Guerreiro, R.J., Lohmann, E., Bras, J.M., Gibbs, J.R., Rohrer, J.D., Gurunlian, N., Dursun, B., Bilgic, B., Hanagasi, H., Gurvit, H.*, et al.* (2013c). Using exome sequencing to reveal mutations in TREM2 presenting as a frontotemporal dementia-like syndrome without bone involvement. JAMA Neurol *70*, 78-84.

Guillot-Sestier, M.V., Araiz, A.R., Mela, V., Gaban, A.S., O'Neill, E., Joshi, L., Chouchani, E.T., Mills, E.L., and Lynch, M.A. (2021). Microglial metabolism is a pivotal factor in sexual dimorphism in Alzheimer's disease. Commun Biol *4*, 711.

Gulisano, W., Melone, M., Ripoli, C., Tropea, M.R., Li Puma, D.D., Giunta, S., Cocco, S., Marcotulli, D., Origlia, N., Palmeri, A.*, et al.* (2019). Neuromodulatory Action of Picomolar Extracellular Abeta42 Oligomers on Presynaptic and Postsynaptic Mechanisms Underlying Synaptic Function and Memory. J Neurosci *39*, 5986-6000.

Guntupalli, S., Widagdo, J., and Anggono, V. (2016). Amyloid-beta-Induced Dysregulation of AMPA Receptor Trafficking. Neural Plast *2016*, 3204519.

Hall, A.M., and Roberson, E.D. (2012). Mouse models of Alzheimer's disease. Brain Res Bull *88*, 3-12.

Hamaguchi, T., Tsutsui-Kimura, I., Mimura, M., Saito, T., Saido, T.C., and Tanaka, K.F. (2019). App(NL-G-F/NL-G-F) mice overall do not show impaired motivation, but cored amyloid plaques in the striatum are inversely correlated with motivation. Neurochem Int *129*, 104470.

Hamelin, L., Lagarde, J., Dorothee, G., Leroy, C., Labit, M., Comley, R.A., de Souza, L.C., Corne, H., Dauphinot, L., Bertoux, M.*, et al.* (2016). Early and protective microglial activation in Alzheimer's disease: a prospective study using 18F-DPA-714 PET imaging. Brain *139*, 1252-1264.

Hansen, D.V., Hanson, J.E., and Sheng, M. (2018). Microglia in Alzheimer's disease. J Cell Biol *217*, 459-472.

Hansson Petersen, C.A., Alikhani, N., Behbahani, H., Wiehager, B., Pavlov, P.F., Alafuzoff, I., Leinonen, V., Ito, A., Winblad, B., Glaser, E.*, et al.* (2008). The amyloid beta-peptide is imported into mitochondria via the TOM import machinery and localized to mitochondrial cristae. Proc Natl Acad Sci U S A *105*, 13145-13150.

Hardy, J., and Salih, D. (2021). TREM2-mediated activation of microglia breaks link between amyloid and tau. Lancet Neurology *20*, 416-417.

Hardy, J.A., and Higgins, G.A. (1992). Alzheimer's disease: the amyloid cascade hypothesis. Science *256*, 184-185.

Hark, T.J., Rao, N.R., Castillon, C., Basta, T., Smukowski, S., Bao, H., Upadhyay, A., Bomba-Warczak, E., Nomura, T., O'Toole, E.T.*, et al.* (2021). Pulse-Chase Proteomics of the App Knockin Mouse Models of Alzheimer's Disease Reveals that Synaptic Dysfunction Originates in Presynaptic Terminals. Cell Syst *12*, 141-158 e149.

Harris, J.A., Devidze, N., Verret, L., Ho, K., Halabisky, B., Thwin, M.T., Kim, D., Hamto, P., Lo, I., Yu, G.Q.*, et al.* (2010). Transsynaptic progression of amyloid-beta-induced neuronal dysfunction within the entorhinal-hippocampal network. Neuron *68*, 428-441.

Haynes, S.E., Hollopeter, G., Yang, G., Kurpius, D., Dailey, M.E., Gan, W.B., and Julius, D. (2006). The P2Y12 receptor regulates microglial activation by extracellular nucleotides. Nat Neurosci *9*, 1512-1519.

Hedskog, L., Pinho, C.M., Filadi, R., Ronnback, A., Hertwig, L., Wiehager, B., Larssen, P., Gellhaar, S., Sandebring, A., Westerlund, M.*, et al.* (2013). Modulation of the endoplasmic reticulum-mitochondria interface in Alzheimer's disease and related models. Proc Natl Acad Sci U S A *110*, 7916-7921.

Hellstrom-Lindahl, E., Ravid, R., and Nordberg, A. (2008). Age-dependent decline of neprilysin in Alzheimer's disease and normal brain: inverse correlation with A beta levels. Neurobiol Aging *29*, 210-221.

Hellstrom-Lindahl, E., Viitanen, M., and Marutle, A. (2009). Comparison of Abeta levels in the brain of familial and sporadic Alzheimer's disease. Neurochem Int *55*, 243-252.

Heneka, M.T., Carson, M.J., Khoury, J.E., Landreth, G.E., Brosseron, F., Feinstein, D.L., Jacobs, A.H., Wyss-Coray, T., Vitorica, J., Ransohoff, R.M.*, et al.* (2015). Neuroinflammation in Alzheimer's disease. The Lancet Neurology *14*, 388-405.

Henneman, W.J., Sluimer, J.D., Barnes, J., van der Flier, W.M., Sluimer, I.C., Fox, N.C., Scheltens, P., Vrenken, H., and Barkhof, F. (2009). Hippocampal atrophy rates in Alzheimer disease: added value over whole brain volume measures. Neurology *72*, 999-1007.

Henstridge, C.M., Hyman, B.T., and Spires-Jones, T.L. (2019). Beyond the neuron-cellular interactions early in Alzheimer disease pathogenesis. Nat Rev Neurosci.

Hickman, S.E., Kingery, N.D., Ohsumi, T.K., Borowsky, M.L., Wang, L.C., Means, T.K., and El Khoury, J. (2013). The microglial sensome revealed by direct RNA sequencing. Nat Neurosci *16*, 1896-1905.

Hoeffel, G., and Ginhoux, F. (2015). Ontogeny of Tissue-Resident Macrophages. Front Immunol *6*, 486.

Hollingworth, P., Harold, D., Sims, R., Gerrish, A., Lambert, J.C., Carrasquillo, M.M., Abraham, R., Hamshere, M.L., Pahwa, J.S., Moskvina, V.*, et al.* (2011). Common variants at ABCA7, MS4A6A/MS4A4E, EPHA1, CD33 and CD2AP are associated with Alzheimer's disease. Nat Genet *43*, 429-435.

Hong, S., Beja-Glasser, V.F., Nfonoyim, B.M., Frouin, A., Li, S., Ramakrishnan, S., Merry, K.M., Shi, Q., Rosenthal, A., Barres, B.A.*, et al.* (2016). Complement and microglia mediate early synapse loss in Alzheimer mouse models. Science *352*, 712-716.

Hoshiko, M., Arnoux, I., Avignone, E., Yamamoto, N., and Audinat, E. (2012). Deficiency of the microglial receptor CX3CR1 impairs postnatal functional development of thalamocortical synapses in the barrel cortex. J Neurosci *32*, 15106-15111.

Howlett, D.R., Richardson, J.C., Austin, A., Parsons, A.A., Bate, S.T., Davies, D.C., and Gonzalez, M.I. (2004). Cognitive correlates of Abeta deposition in male and female mice bearing amyloid precursor protein and presenilin-1 mutant transgenes. Brain Res *1017*, 130-136.

Hsiao, K., Chapman, P., Nilsen, S., Eckman, C., Harigaya, Y., Younkin, S., Yang, F., and Cole, G. (1996). Correlative memory deficits, Abeta elevation, and amyloid plaques in transgenic mice. Science *274*, 99-102.

Hsieh, C.L., Koike, M., Spusta, S.C., Niemi, E.C., Yenari, M., Nakamura, M.C., and Seaman, W.E. (2009). A role for TREM2 ligands in the phagocytosis of apoptotic neuronal cells by microglia. J Neurochem *109*, 1144-1156.

Hsieh, H., Boehm, J., Sato, C., Iwatsubo, T., Tomita, T., Sisodia, S., and Malinow, R. (2006). AMPAR removal underlies Abeta-induced synaptic depression and dendritic spine loss. Neuron *52*, 831-843.

Huang, Y., Happonen, K.E., Burrola, P.G., O'Connor, C., Hah, N., Huang, L., Nimmerjahn, A., and Lemke, G. (2021). Microglia use TAM receptors to detect and engulf amyloid β plaques. Nature Immunology *22*, 586-594.

Huang, Y.A., Zhou, B., Wernig, M., and Sudhof, T.C. (2017). ApoE2, ApoE3, and ApoE4 Differentially Stimulate APP Transcription and Abeta Secretion. Cell *168*, 427-441 e421.

Hyman, B.T., Phelps, C.H., Beach, T.G., Bigio, E.H., Cairns, N.J., Carrillo, M.C., Dickson, D.W., Duyckaerts, C., Frosch, M.P., Masliah, E.*, et al.* (2012). National Institute on Aging-Alzheimer's Association guidelines for the neuropathologic assessment of Alzheimer's disease. Alzheimers Dement *8*, 1-13.

Iglesias, J., Morales, L., and Barreto, G.E. (2017). Metabolic and Inflammatory Adaptation of Reactive Astrocytes: Role of PPARs. Mol Neurobiol *54*, 2518-2538.

Itagaki, S., McGeer, P.L., Akiyama, H., Zhu, S., and Selkoe, D. (1989). Relationship of microglia and astrocytes to amyloid deposits of Alzheimer disease. J Neuroimmunol *24*, 173-182.

Iwata, N., Takaki, Y., Fukami, S., Tsubuki, S., and Saido, T.C. (2002). Region-specific reduction of A beta-degrading endopeptidase, neprilysin, in mouse hippocampus upon aging. J Neurosci Res *70*, 493-500.

Jack, C.R., Jr., Knopman, D.S., Jagust, W.J., Petersen, R.C., Weiner, M.W., Aisen, P.S., Shaw, L.M., Vemuri, P., Wiste, H.J., Weigand, S.D.*, et al.* (2013). Tracking pathophysiological processes in Alzheimer's disease: an updated hypothetical model of dynamic biomarkers. Lancet Neurol *12*, 207-216.

Jack, C.R., Jr., Petersen, R.C., Xu, Y., O'Brien, P.C., Smith, G.E., Ivnik, R.J., Boeve, B.F., Tangalos, E.G., and Kokmen, E. (2000). Rates of hippocampal atrophy correlate with change in clinical status in aging and AD. Neurology *55*, 484-489.

Jack, C.R., Jr., Shiung, M.M., Gunter, J.L., O'Brien, P.C., Weigand, S.D., Knopman, D.S., Boeve, B.F., Ivnik, R.J., Smith, G.E., Cha, R.H.*, et al.* (2004). Comparison of different MRI brain atrophy rate measures with clinical disease progression in AD. Neurology *62*, 591-600.

Jackson, J., Jambrina, E., Li, J., Marston, H., Menzies, F., Phillips, K., and Gilmour, G. (2019a). Targeting the Synapse in Alzheimer's Disease. Front Neurosci *13*, 735.

Jackson, R.J., Rose, J., Tulloch, J., Henstridge, C., Smith, C., and Spires-Jones, T.L. (2019b). Clusterin accumulates in synapses in Alzheimer's disease and is increased in apolipoprotein E4 carriers. Brain Communications *1*, ID:fcz003.

Jadhav, V.S., Lin, P.B.C., Pennington, T., Di Prisco, G.V., Jannu, A.J., Xu, G., Moutinho, M., Zhang, J., Atwood, B.K., Puntambekar, S.S.*, et al.* (2020). Trem2 Y38C mutation and loss of Trem2 impairs neuronal synapses in adult mice. Molecular neurodegeneration *15*, 62-62.

Janelidze, S., Mattsson, N., Stomrud, E., Lindberg, O., Palmqvist, S., Zetterberg, H., Blennow, K., and Hansson, O. (2018). CSF biomarkers of neuroinflammation and cerebrovascular dysfunction in early Alzheimer disease. Neurology *91*, e867-e877.

Jansen, I.E., Savage, J.E., Watanabe, K., Bryois, J., Williams, D.M., Steinberg, S., Sealock, J., Karlsson, I.K., Hagg, S., Athanasiu, L.*, et al.* (2019). Genome-wide meta-analysis identifies new loci and functional pathways influencing Alzheimer's disease risk. Nat Genet *51*, 404-413.

Jarosz-Griffiths, H.H., Noble, E., Rushworth, J.V., and Hooper, N.M. (2016). Amyloid-beta Receptors: The Good, the Bad, and the Prion Protein. J Biol Chem *291*, 3174-3183.

Jay, T.R., Hirsch, A.M., Broihier, M.L., Miller, C.M., Neilson, L.E., Ransohoff, R.M., Lamb, B.T., and Landreth, G.E. (2017). Disease Progression-Dependent Effects of TREM2 Deficiency in a Mouse Model of Alzheimer's Disease. J Neurosci *37*, 637-647.

Jay, T.R., Miller, C.M., Cheng, P.J., Graham, L.C., Bemiller, S., Broihier, M.L., Xu, G., Margevicius, D., Karlo, J.C., Sousa, G.L.*, et al.* (2015). TREM2 deficiency eliminates TREM2+ inflammatory macrophages and ameliorates pathology in Alzheimer's disease mouse models. J Exp Med *212*, 287-295.

Ji, K., Akgul, G., Wollmuth, L.P., and Tsirka, S.E. (2013). Microglia actively regulate the number of functional synapses. PLoS One *8*, e56293.

Jin, S.C., Benitez, B.A., Karch, C.M., Cooper, B., Skorupa, T., Carrell, D., Norton, J.B., Hsu, S., Harari, O., Cai, Y.*, et al.* (2014). Coding variants in TREM2 increase risk for Alzheimer's disease. Hum Mol Genet *23*, 5838-5846.

Jonsson, T., Atwal, J.K., Steinberg, S., Snaedal, J., Jonsson, P.V., Bjornsson, S., Stefansson, H., Sulem, P., Gudbjartsson, D., Maloney, J.*, et al.* (2012). A mutation in APP protects against Alzheimer's disease and age-related cognitive decline. Nature *488*, 96-99.

Jonsson, T., Stefansson, H., Steinberg, S., Jonsdottir, I., Jonsson, P.V., Snaedal, J., Bjornsson, S., Huttenlocher, J., Levey, A.I., Lah, J.J., *et al.* (2013). Variant of TREM2 associated with the risk of Alzheimer's disease. N Engl J Med *368*, 107-116.

Josephs, K.A., Whitwell, J.L., Ahmed, Z., Shiung, M.M., Weigand, S.D., Knopman, D., Boeve, B., Parisi, J.E., Petersen, R.C., Dickson, D., *et al.* (2008). β-Amyloid Burden Is Not Associated withRates of Brain Atrophy. Annals of Neurology *63*, 204-212.

Kajiwara, R., Wouterlood, F.G., Sah, A., Boekel, A.J., Baks-te Bulte, L.T., and Witter, M.P. (2008). Convergence of entorhinal and CA3 inputs onto pyramidal neurons and interneurons in hippocampal area CA1--an anatomical study in the rat. Hippocampus *18*, 266-280.

Kamenetz, F., Tomita, T., Hsieh, H., Seabrook, G., Borchelt, D., Iwatsubo, T., Sisodia, S., and Malinow, R. (2003). APP processing and synaptic function. Neuron *37*, 925-937.

Kamino, K., Orr, H.T., Payami, H., Wijsman, E.M., Alonso, M.E., Pulst, S.M., Anderson, L., O'Dahl, S., Nemens, E., White, J.A., *et al.* (1992). Linkage and mutational analysis of familial Alzheimer disease kindreds for the APP gene region. Am J Hum Genet *51*, 998-1014.

Kamphuis, W., Kooijman, L., Orre, M., Stassen, O., Pekny, M., and Hol, E.M. (2015). GFAP and vimentin deficiency alters gene expression in astrocytes and microglia in wild-type mice and changes the transcriptional response of reactive glia in mouse model for Alzheimer's disease. Glia *63*, 1036-1056.

Karch, C.M., Cruchaga, C., and Goate, A.M. (2014). Alzheimer's disease genetics: from the bench to the clinic. Neuron *83*, 11-26.

Karch, C.M., and Goate, A.M. (2015). Alzheimer's disease risk genes and mechanisms of disease pathogenesis. Biol Psychiatry *77*, 43-51.

Karran, E., and De Strooper, B. (2016). The amyloid cascade hypothesis: are we poised for success or failure? J Neurochem *139 Suppl 2*, 237-252.

Karran, E., Mercken, M., and De Strooper, B. (2011). The amyloid cascade hypothesis for Alzheimer's disease: an appraisal for the development of therapeutics. Nat Rev Drug Discov *10*, 698-712.

Katsouri, L., Birch, A.M., Renziehausen, A.W.J., Zach, C., Aman, Y., Steeds, H., Bonsu, A., Palmer, E.O.C., Mirzaei, N., Ries, M., *et al.* (2020). Ablation of reactive astrocytes exacerbates disease pathology in a model of Alzheimer's disease. Glia *68*, 1017-1030.

Katzman, R., Terry, R., DeTeresa, R., Brown, T., Davies, P., Fuld, P., Renbing, X., and Peck, A. (1988). Clinical, pathological, and neurochemical changes in dementia: a subgroup with preserved mental status and numerous neocortical plaques. Ann Neurol *23*, 138-144.

Kawabori, M., Kacimi, R., Kauppinen, T., Calosing, C., Kim, J.Y., Hsieh, C.L., Nakamura, M.C., and Yenari, M.A. (2015). Triggering Receptor Expressed on Myeloid Cells 2 (TREM2) Deficiency Attenuates Phagocytic Activities of Microglia and Exacerbates Ischemic Damage in Experimental Stroke. J Neurosci *35*, 3384-3396.

Keren-Shaul, H., Spinrad, A., Weiner, A., Matcovitch-Natan, O., Dvir-Szternfeld, R., Ulland, T.K., David, E., Baruch, K., Lara-Astaiso, D., Toth, B.*, et al.* (2017). A Unique Microglia Type Associated with Restricting Development of Alzheimer's Disease. Cell *169*, 1276-1290 e1217.

Khakh, B.S., and Sofroniew, M.V. (2015). Diversity of astrocyte functions and phenotypes in neural circuits. Nat Neurosci *18*, 942-952.

Kiialainen, A., Hovanes, K., Paloneva, J., Kopra, O., and Peltonen, L. (2005). Dap12 and Trem2, molecules involved in innate immunity and neurodegeneration, are co-expressed in the CNS. Neurobiol Dis *18*, 314-322.

Killiany, R.J., Hyman, B.T., Gomez-Isla, T., Moss, M.B., Kikinis, R., Jolesz, F., Tanzi, R., Jones, K., and Albert, M.S. (2002). MRI measures of entorhinal cortex vs hippocampus in preclinical AD. Neurology *58*, 1188-1196.

Killin, L.O., Starr, J.M., Shiue, I.J., and Russ, T.C. (2016). Environmental risk factors for dementia: a systematic review. BMC Geriatr *16*, 175.

Kim, S.-M., Mun, B.-R., Lee, S.-J., Joh, Y., Lee, H.-Y., Ji, K.-Y., Choi, H.-R., Lee, E.-H., Kim, E.-M., Jang, J.-H.*, et al.* (2017). TREM2 promotes Aβ phagocytosis by upregulating C/EBPα-dependent CD36 expression in microglia. Scientific reports *7*, 11118-11118.

Klunk, W.E., Engler, H., Nordberg, A., Wang, Y., Blomqvist, G., Holt, D.P., Bergstrom, M., Savitcheva, I., Huang, G.F., Estrada, S.*, et al.* (2004). Imaging brain amyloid in Alzheimer's disease with Pittsburgh Compound-B. Ann Neurol *55*, 306-319.

Knobloch, M., and Mansuy, I.M. (2008). Dendritic spine loss and synaptic alterations in Alzheimer's disease. Mol Neurobiol *37*, 73-82.

Kobayashi, E., Nakano, M., Kubota, K., Himuro, N., Mizoguchi, S., Chikenji, T., Otani, M., Mizue, Y., Nagaishi, K., and Fujimiya, M. (2018). Activated forms of astrocytes with higher GLT-1 expression are associated with cognitive normal subjects with Alzheimer pathology in human brain. Sci Rep *8*, 1712.

Kober, D.L., Alexander-Brett, J.M., Karch, C.M., Cruchaga, C., Colonna, M., Holtzman, M.J., and Brett, T.J. (2016). Neurodegenerative disease mutations in TREM2 reveal a functional surface and distinct loss-of-function mechanisms. Elife *5*.

Koffie, R.M., Hashimoto, T., Tai, H.C., Kay, K.R., Serrano-Pozo, A., Joyner, D., Hou, S., Kopeikina, K.J., Frosch, M.P., Lee, V.M.*, et al.* (2012). Apolipoprotein E4 effects in Alzheimer's disease are mediated by synaptotoxic oligomeric amyloid-beta. Brain *135*, 2155-2168.

Koffie, R.M., Meyer-Luehmann, M., Hashimoto, T., Adams, K.W., Mielke, M.L., Garcia-Alloza, M., Micheva, K.D., Smith, S.J., Kim, M.L., Lee, V.M.*, et al.* (2009). Oligomeric amyloid beta associates with postsynaptic densities and correlates with excitatory synapse loss near senile plaques. Proc Natl Acad Sci U S A *106*, 4012-4017.

Konishi, H., Okamoto, T., Hara, Y., Komine, O., Tamada, H., Maeda, M., Osako, F., Kobayashi, M., Nishiyama, A., Kataoka, Y.*, et al.* (2020). Astrocytic phagocytosis is a compensatory mechanism for microglial dysfunction. EMBO J *39*, e104464.

Krabbe, G., Halle, A., Matyash, V., Rinnenthal, J.L., Eom, G.D., Bernhardt, U., Miller, K.R., Prokop, S., Kettenmann, H., and Heppner, F.L. (2013). Functional impairment of microglia coincides with Beta-amyloid deposition in mice with Alzheimer-like pathology. PLoS One *8*, e60921.

Kraft, A.W., Hu, X., Yoon, H., Yan, P., Xiao, Q., Wang, Y., Gil, S.C., Brown, J., Wilhelmsson, U., Restivo, J.L.*, et al.* (2013). Attenuating astrocyte activation accelerates plaque pathogenesis in APP/PS1 mice. FASEB J *27*, 187-198.

Krasemann, S., Madore, C., Cialic, R., Baufeld, C., Calcagno, N., El Fatimy, R., Beckers, L., O'Loughlin, E., Xu, Y., Fanek, Z.*, et al.* (2017). The TREM2-APOE Pathway Drives the Transcriptional Phenotype of Dysfunctional Microglia in Neurodegenerative Diseases. Immunity *47*, 566-581 e569.

Kuchibhotla, K.V., Lattarulo, C.R., Hyman, B.T., and Bacskai, B.J. (2009). Synchronous hyperactivity and intercellular calcium waves in astrocytes in Alzheimer mice. Science *323*, 1211-1215.

Kullmann, D.M. (1994). Amplitude fluctuations of dual-component EPSCs in hippocampal pyramidal cells: implications for long-term potentiation. Neuron *12*, 1111-1120.

Lambert, J.C., Ibrahim-Verbaas, C.A., Harold, D., Naj, A.C., Sims, R., Bellenguez, C., DeStafano, A.L., Bis, J.C., Beecham, G.W., Grenier-Boley, B.*, et al.* (2013). Meta-analysis of 74,046 individuals identifies 11 new susceptibility loci for Alzheimer's disease. Nat Genet *45*, 1452-1458.

Latif-Hernandez, A., Sabanov, V., Ahmed, T., Craessaerts, K., Saito, T., Saido, T., and Balschun, D. (2020). The two faces of synaptic failure in App(NL-G-F) knock-in mice. Alzheimers Res Ther *12*, 100.

Latif-Hernandez, A., Shah, D., Craessaerts, K., Saido, T., Saito, T., De Strooper, B., Van der Linden, A., and D'Hooge, R. (2019). Subtle behavioral changes and increased prefrontal-hippocampal network synchronicity in APP(NL-G-F) mice before prominent plaque deposition. Behav Brain Res *364*, 431-441.

Lavin, Y., Winter, D., Blecher-Gonen, R., David, E., Keren-Shaul, H., Merad, M., Jung, S., and Amit, I. (2014). Tissue-resident macrophage enhancer landscapes are shaped by the local microenvironment. Cell *159*, 1312-1326.

Lee, C.Y., and Landreth, G.E. (2010). The role of microglia in amyloid clearance from the AD brain. J Neural Transm (Vienna) *117*, 949-960.

Lee, C.Y.D., Daggett, A., Gu, X., Jiang, L.L., Langfelder, P., Li, X., Wang, N., Zhao, Y., Park, C.S., Cooper, Y.*, et al.* (2018). Elevated TREM2 Gene Dosage Reprograms Microglia Responsivity and Ameliorates Pathological Phenotypes in Alzheimer's Disease Models. Neuron *97*, 1032-1048 e1035.

Lee, S.H., Kang, J., Ho, A., Watanabe, H., Bolshakov, V.Y., and Shen, J. (2020). APP Family Regulates Neuronal Excitability and Synaptic Plasticity but Not Neuronal Survival. Neuron *108*, 676-690 e678.

Lee, S.H., Meilandt, W.J., Xie, L., Gandham, V.D., Ngu, H., Barck, K.H., Rezzonico, M.G., Imperio, J., Lalehzadeh, G., Huntley, M.A.*, et al.* (2021). Trem2 restrains the enhancement of tau accumulation and neurodegeneration by beta-amyloid pathology. Neuron *109*, 1283-1301 e1286.

Lehrman, E.K., Wilton, D.K., Litvina, E.Y., Welsh, C.A., Chang, S.T., Frouin, A., Walker, A.J., Heller, M.D., Umemori, H., Chen, C.*, et al.* (2018). CD47 Protects Synapses from Excess Microglia-Mediated Pruning during Development. Neuron *100*, 120-134 e126.

Lewis, J., Dickson, D.W., Lin, W.L., Chisholm, L., Corral, A., Jones, G., Yen, S.H., Sahara, N., Skipper, L., Yager, D.*, et al.* (2001). Enhanced neurofibrillary degeneration in transgenic mice expressing mutant tau and APP. Science *293*, 1487-1491.

Leyns, C.E.G., Gratuze, M., Narasimhan, S., Jain, N., Koscal, L.J., Jiang, H., Manis, M., Colonna, M., Lee, V.M.Y., Ulrich, J.D.*, et al.* (2019). TREM2 function impedes tau seeding in neuritic plaques. Nat Neurosci *22*, 1217-1222.

Li, Q., and Barres, B.A. (2018). Microglia and macrophages in brain homeostasis and disease. Nat Rev Immunol *18*, 225-242.

Li, Q., Cheng, Z., Zhou, L., Darmanis, S., Neff, N.F., Okamoto, J., Gulati, G., Bennett, M.L., Sun, L.O., Clarke, L.E.*, et al.* (2019). Developmental Heterogeneity of Microglia and Brain Myeloid Cells Revealed by Deep Single-Cell RNA Sequencing. Neuron *101*, 207-223 e210.

Li, S., Hong, S., Shepardson, N.E., Walsh, D.M., Shankar, G.M., and Selkoe, D. (2009). Soluble oligomers of amyloid Beta protein facilitate hippocampal long-term depression by disrupting neuronal glutamate uptake. Neuron *62*, 788-801.

Li, S., Jin, M., Koeglsperger, T., Shepardson, N.E., Shankar, G.M., and Selkoe, D.J. (2011). Soluble Abeta oligomers inhibit long-term potentiation through a mechanism involving excessive activation of extrasynaptic NR2B-containing NMDA receptors. J Neurosci *31*, 6627-6638.

Li, Y., Zhu, K., Li, N., Wang, X., Xiao, X., Li, L., He, Y., Zhang, J., Wo, J., Cui, Y.*, et al.* (2021). Reversible GABAergic dysfunction involved in hippocampal hyperactivity

predicts early-stage Alzheimer disease in a mouse model. Alzheimer's Research & Therapy *13*.

Lian, H., Yang, L., Cole, A., Sun, L., Chiang, A.C., Fowler, S.W., Shim, D.J., Rodriguez-Rivera, J., Taglialatela, G., Jankowsky, J.L.*, et al.* (2015). NFkappaB-activated astroglial release of complement C3 compromises neuronal morphology and function associated with Alzheimer's disease. Neuron *85*, 101-115.

Liddelow, S.A., Guttenplan, K.A., Clarke, L.E., Bennett, F.C., Bohlen, C.J., Schirmer, L., Bennett, M.L., Munch, A.E., Chung, W.S., Peterson, T.C.*, et al.* (2017). Neurotoxic reactive astrocytes are induced by activated microglia. Nature *541*, 481-487.

Lin, Y.T., Seo, J., Gao, F., Feldman, H.M., Wen, H.L., Penney, J., Cam, H.P., Gjoneska, E., Raja, W.K., Cheng, J.*, et al.* (2018). APOE4 Causes Widespread Molecular and Cellular Alterations Associated with Alzheimer's Disease Phenotypes in Human iPSC-Derived Brain Cell Types. Neuron *98*, 1141-1154 e1147.

Linnerbauer, M., Wheeler, M.A., and Quintana, F.J. (2020). Astrocyte Crosstalk in CNS Inflammation. Neuron *108*.

Liu, C.C., Liu, C.C., Kanekiyo, T., Xu, H., and Bu, G. (2013). Apolipoprotein E and Alzheimer disease: risk, mechanisms and therapy. Nat Rev Neurol *9*, 106-118.

Liu, W., Taso, O., Wang, R., Bayram, S., Graham, A.C., Garcia-Reitboeck, P., Mallach, A., Andrews, W.D., Piers, T.M., Botia, J.A.*, et al.* (2020). Trem2 promotes anti-inflammatory responses in microglia and is suppressed under pro-inflammatory conditions. Hum Mol Genet *29*, 3224-3248.

Liu, Y.U., Ying, Y., Li, Y., Eyo, U.B., Chen, T., Zheng, J., Umpierre, A.D., Zhu, J., Bosco, D.B., Dong, H.*, et al.* (2019). Neuronal network activity controls microglial process surveillance in awake mice via norepinephrine signaling. Nat Neurosci *22*, 1771-1781.

Llorens, F., Thune, K., Tahir, W., Kanata, E., Diaz-Lucena, D., Xanthopoulos, K., Kovatsi, E., Pleschka, C., Garcia-Esparcia, P., Schmitz, M.*, et al.* (2017). YKL-40 in the brain and cerebrospinal fluid of neurodegenerative dementias. Mol Neurodegener *12*, 83.

Lodder, C., Scheyltjens, I., Stancu, I.C., Botella Lucena, P., Gutierrez de Rave, M., Vanherle, S., Vanmierlo, T., Cremers, N., Vanrusselt, H., Brone, B.*, et al.* (2021). CSF1R inhibition rescues tau pathology and neurodegeneration in an A/T/N model with combined AD pathologies, while preserving plaque associated microglia. Acta Neuropathol Commun *9*, 108.

Long, J.M., and Holtzman, D.M. (2019). Alzheimer Disease: An Update on Pathobiology and Treatment Strategies. Cell *179*, 312-339.

Lu, W., Shi, Y., Jackson, A.C., Bjorgan, K., During, M.J., Sprengel, R., Seeburg, P.H., and Nicoll, R.A. (2009). Subunit composition of synaptic AMPA receptors revealed by a single-cell genetic approach. Neuron *62*, 254-268.

Lustbader, J.W., Cirilli, M., Lin, C., Xu, H.W., Takuma, K., Wang, N., Caspersen, C., Chen, X., Pollak, S., Chaney, M.*, et al.* (2004). ABAD directly links Abeta to mitochondrial toxicity in Alzheimer's disease. Science *304*, 448-452.

Ma, L., Allen, M., Sakae, N., Ertekin-Taner, N., Graff-Radford, N.R., Dickson, D.W., Younkin, S.G., and Sevlever, D. (2016). Expression and processing analyses of wild type and p.R47H TREM2 variant in Alzheimer's disease brains. Mol Neurodegener *11*, 72.

MacVicar, B.A., Tse, F.W., Crichton, S.A., and Kettenmann, H. (1989). GABA-activated Cl- channels in astrocytes of hippocampal slices. J Neurosci *9*, 3577-3583.

Magistretti, P.J., and Allaman, I. (2015). A cellular perspective on brain energy metabolism and functional imaging. Neuron *86*, 883-901.

Maier, M., Peng, Y., Jiang, L., Seabrook, T.J., Carroll, M.C., and Lemere, C.A. (2008). Complement C3 deficiency leads to accelerated amyloid beta plaque deposition and neurodegeneration and modulation of the microglia/macrophage phenotype in amyloid precursor protein transgenic mice. J Neurosci *28*, 6333-6341.

Marcaggi, P., Mutoh, H., Dimitrov, D., Beato, M., and Knopfel, T. (2009). Optical measurement of mGluR1 conformational changes reveals fast activation, slow deactivation, and sensitization. Proc Natl Acad Sci U S A *106*, 11388-11393.

Marsh, J., Bagol, S.H., Williams, R.S.B., Dickson, G., and Alifragis, P. (2017). Synapsin I phosphorylation is dysregulated by beta-amyloid oligomers and restored by valproic acid. Neurobiol Dis *106*, 63-75.

Masuda, A., Kobayashi, Y., Kogo, N., Saito, T., Saido, T.C., and Itohara, S. (2016). Cognitive deficits in single App knock-in mouse models. Neurobiol Learn Mem *135*, 73-82.

Matarin, M., Salih, D.A., Yasvoina, M., Cummings, D.M., Guelfi, S., Liu, W., Nahaboo Solim, M.A., Moens, T.G., Paublete, R.M., Ali, S.S.*, et al.* (2015). A genome-wide gene-expression analysis and database in transgenic mice during development of amyloid or tau pathology. Cell Rep *10*, 633-644.

Mathys, H., Davila-Velderrain, J., Peng, Z., Gao, F., Mohammadi, S., Young, J.Z., Menon, M., He, L., Abdurrob, F., Jiang, X.*, et al.* (2019). Single-cell transcriptomic analysis of Alzheimer's disease. Nature *570*, 332-337.

Matos, M., Augusto, E., Oliveira, C.R., and Agostinho, P. (2008). Amyloid-beta peptide decreases glutamate uptake in cultured astrocytes: involvement of oxidative stress and mitogen-activated protein kinase cascades. Neuroscience *156*, 898-910.

Mattson, M.P. (2004). Pathways towards and away from Alzheimer's disease. Nature *430*, 631-639.

Mattson, M.P., Barger, S.W., Cheng, B., Lieberburg, I., Smith-Swintosky, V.L., and Rydel, R.E. (1993). beta-Amyloid precursor protein metabolites and loss of neuronal Ca2+ homeostasis in Alzheimer's disease. Trends Neurosci *16*, 409-414.

Mattsson, N., Insel, P.S., Palmqvist, S., Portelius, E., Zetterberg, H., Weiner, M., Blennow, K., Hansson, O., and Alzheimer's Disease Neuroimaging, I. (2016a). Cerebrospinal fluid tau, neurogranin, and neurofilament light in Alzheimer's disease. EMBO Mol Med *8*, 1184-1196.

Mattsson, N., Zetterberg, H., Janelidze, S., Insel, P.S., Andreasson, U., Stomrud, E., Palmqvist, S., Baker, D., Tan Hehir, C.A., Jeromin, A.*, et al.* (2016b). Plasma tau in Alzheimer disease. Neurology *87*, 1827-1835.

Mawuenyega, K.G., Sigurdson, W., Ovod, V., Munsell, L., Kasten, T., Morris, J.C., Yarasheski, K.E., and Bateman, R.J. (2010). Decreased clearance of CNS beta-amyloid in Alzheimer's disease. Science *330*, 1774.

Mazaheri, F., Snaidero, N., Kleinberger, G., Madore, C., Daria, A., Werner, G., Krasemann, S., Capell, A., Trumbach, D., Wurst, W.*, et al.* (2017). TREM2 deficiency impairs chemotaxis and microglial responses to neuronal injury. EMBO Rep *18*, 1186-1198.

McAlpine, F.E., and Tansey, M.G. (2008). Neuroinflammation and tumor necrosis factor signaling in the pathophysiology of Alzheimer's disease. J Inflamm Res *1*, 29-39.

McKhann, G., Drachman, D., Folstein, M., Katzman, R., Price, D., and Stadlan, E.M. (1984). Clinical diagnosis of Alzheimer's disease: report of the NINCDS-ADRDA Work Group under the auspices of Department of Health and Human Services Task Force on Alzheimer's Disease. Neurology *34*, 939-944.

Medawar, E., Benway, T.A., Liu, W., Hanan, T.A., Haslehurst, P., James, O.T., Yap, K., Muessig, L., Moroni, F., Nahaboo Solim, M.A.*, et al.* (2019). Effects of rising amyloidbeta levels on hippocampal synaptic transmission, microglial response and cognition in APPSwe/PSEN1M146V transgenic mice. EBioMedicine *39*, 422-435.

Mehla, J., Lacoursiere, S.G., Lapointe, V., McNaughton, B.L., Sutherland, R.J., McDonald, R.J., and Mohajerani, M.H. (2019). Age-dependent behavioral and biochemical characterization of single APP knock-in mouse (APP(NL-G-F/NL-G-F)) model of Alzheimer's disease. Neurobiol Aging *75*, 25-37.

Merino-Serrais, P., Benavides-Piccione, R., Blazquez-Llorca, L., Kastanauskaite, A., Rabano, A., Avila, J., and DeFelipe, J. (2013). The influence of phospho-tau on dendritic spines of cortical pyramidal neurons in patients with Alzheimer's disease. Brain *136*, 1913-1928.

Meyer-Luehmann, M., Spires-Jones, T.L., Prada, C., Garcia-Alloza, M., de Calignon, A., Rozkalne, A., Koenigsknecht-Talboo, J., Holtzman, D.M., Bacskai, B.J., and Hyman, B.T. (2008). Rapid appearance and local toxicity of amyloid-beta plaques in a mouse model of Alzheimer's disease. Nature *451*, 720-724.

Michno, W., Stringer, K.M., Enzlein, T., Passarelli, M.K., Escrig, S., Vitanova, K., Wood, J., Blennow, K., Zetterberg, H., Meibom, A.*, et al.* (2021). Following spatial Abeta aggregation dynamics in evolving Alzheimer's disease pathology by imaging stable isotope labeling kinetics. Sci Adv *7*, eabg4855.

Mila-Aloma, M., Salvado, G., Gispert, J.D., Vilor-Tejedor, N., Grau-Rivera, O., Sala-Vila, A., Sanchez-Benavides, G., Arenaza-Urquijo, E.M., Crous-Bou, M., Gonzalez-de-Echavarri, J.M.*, et al.* (2020). Amyloid beta, tau, synaptic, neurodegeneration, and glial biomarkers in the preclinical stage of the Alzheimer's continuum. Alzheimers Dement.

Mirzaei, N., Tang, S.P., Ashworth, S., Coello, C., Plisson, C., Passchier, J., Selvaraj, V., Tyacke, R.J., Nutt, D.J., and Sastre, M. (2016). In vivo imaging of microglial activation by positron emission tomography with [(11)C]PBR28 in the 5XFAD model of Alzheimer's disease. Glia *64*, 993-1006.

Morris, G.P., Clark, I.A., and Vissel, B. (2014). Inconsistencies and controversies surrounding the amyloid hypothesis of Alzheimer's disease. Acta Neuropathol Commun *2*, 135.

Mucke, L., Masliah, E., Yu, G.Q., Mallory, M., Rockenstein, E.M., Tatsuno, G., Hu, K., Kholodenko, D., Johnson-Wood, K., and McConlogue, L. (2000). High-level neuronal expression of abeta 1-42 in wild-type human amyloid protein precursor transgenic mice: synaptotoxicity without plaque formation. J Neurosci *20*, 4050-4058.

Muller, M.K., Jacobi, E., Sakimura, K., Malinow, R., and von Engelhardt, J. (2018). NMDA receptors mediate synaptic depression, but not spine loss in the dentate gyrus of adult amyloid Beta (Abeta) overexpressing mice. Acta Neuropathol Commun *6*, 110.

Naj, A.C., Jun, G., Beecham, G.W., Wang, L.S., Vardarajan, B.N., Buros, J., Gallins, P.J., Buxbaum, J.D., Jarvik, G.P., Crane, P.K.*, et al.* (2011). Common variants at MS4A4/MS4A6E, CD2AP, CD33 and EPHA1 are associated with late-onset Alzheimer's disease. Nat Genet *43*, 436-441.

Neuman, K.M., Molina-Campos, E., Musial, T.F., Price, A.L., Oh, K.J., Wolke, M.L., Buss, E.W., Scheff, S.W., Mufson, E.J., and Nicholson, D.A. (2015). Evidence for Alzheimer's disease-linked synapse loss and compensation in mouse and human hippocampal CA1 pyramidal neurons. Brain Struct Funct *220*, 3143-3165.

Nilsberth, C., Westlind-Danielsson, A., Eckman, C.B., Condron, M.M., Axelman, K., Forsell, C., Stenh, C., Luthman, J., Teplow, D.B., Younkin, S.G.*, et al.* (2001). The 'Arctic' APP mutation (E693G) causes Alzheimer's disease by enhanced Abeta protofibril formation. Nat Neurosci *4*, 887-893.

Nimmerjahn, A., Kirchhoff, F., and Helmchen, F. (2005). Resting microglial cells are highly dynamic surveillants of brain parenchyma in vivo. Science *308*, 1314-1318.

Nimmrich, V., Grimm, C., Draguhn, A., Barghorn, S., Lehmann, A., Schoemaker, H., Hillen, H., Gross, G., Ebert, U., and Bruehl, C. (2008). Amyloid beta oligomers (A beta(1-42) globulomer) suppress spontaneous synaptic activity by inhibition of P/Q-type calcium currents. J Neurosci *28*, 788-797.

Norton, S., Matthews, F.E., Barnes, D.E., Yaffe, K., and Brayne, C. (2014). Potential for primary prevention of Alzheimer's disease: an analysis of population-based data. Lancet Neurol *13*, 788-794.

Nystrom, S., Psonka-Antonczyk, K.M., Ellingsen, P.G., Johansson, L.B., Reitan, N., Handrick, S., Prokop, S., Heppner, F.L., Wegenast-Braun, B.M., Jucker, M.*, et al.* (2013). Evidence for age-dependent in vivo conformational rearrangement within Abeta amyloid deposits. ACS Chem Biol *8*, 1128-1133.

O'Brien, J.L., O'Keefe, K.M., LaViolette, P.S., DeLuca, A.N., Blacker, D., Dickerson, B.C., and Sperling, R.A. (2010). Longitudinal fMRI in elderly reveals loss of hippocampal activation with clinical decline. Neurology *74*, 1969-1976.

Oakley, H., Cole, S.L., Logan, S., Maus, E., Shao, P., Craft, J., Guillozet-Bongaarts, A., Ohno, M., Disterhoft, J., Van Eldik, L.*, et al.* (2006). Intraneuronal beta-amyloid aggregates, neurodegeneration, and neuron loss in transgenic mice with five familial Alzheimer's disease mutations: potential factors in amyloid plaque formation. J Neurosci *26*, 10129-10140.

Oddo, S., Caccamo, A., Shepherd, J.D., Murphy, M.P., Golde, T.E., Kayed, R., Metherate, R., Mattson, M.P., Akbari, Y., and LaFerla, F.M. (2003). Triple-transgenic model of Alzheimer's disease with plaques and tangles: intracellular Abeta and synaptic dysfunction. Neuron *39*, 409-421.

Oeckl, P., Halbgebauer, S., Anderl-Straub, S., Steinacker, P., Huss, A.M., Neugebauer, H., von Arnim, C.A.F., Diehl-Schmid, J., Grimmer, T., Kornhuber, J.*, et al.* (2019). Glial Fibrillary Acidic Protein in Serum is Increased in Alzheimer's Disease and Correlates with Cognitive Impairment. J Alzheimers Dis *67*, 481-488.

Olah, M., Menon, V., Habib, N., Taga, M.F., Ma, Y., Yung, C.J., Cimpean, M., Khairallah, A., Coronas-Samano, G., Sankowski, R.*, et al.* (2020). Single cell RNA sequencing of human microglia uncovers a subset associated with Alzheimer's disease. Nat Commun *11*, 6129.

Olmos-Alonso, A., Schetters, S.T., Sri, S., Askew, K., Mancuso, R., Vargas-Caballero, M., Holscher, C., Perry, V.H., and Gomez-Nicola, D. (2016). Pharmacological targeting of CSF1R inhibits microglial proliferation and prevents the progression of Alzheimer's-like pathology. Brain *139*, 891-907.

Ovsepian, S.V., Blazquez-Llorca, L., Freitag, S.V., Rodrigues, E.F., and Herms, J. (2017). Ambient Glutamate Promotes Paroxysmal Hyperactivity in Cortical Pyramidal Neurons at Amyloid Plaques via Presynaptic mGluR1 Receptors. Cereb Cortex *27*, 4733-4749.

Padurariu, M., Ciobica, A., Mavroudis, I., Fotiou, D., and Baloyannis, S. (2012). Hippocampal neuronal loss in the CA1 and CA3 areas of Alzheimer's disease patients. Psychiatr Danub *24*, 152-158.

Paloneva, J., Kestila, M., Wu, J., Salminen, A., Bohling, T., Ruotsalainen, V., Hakola, P., Bakker, A.B., Phillips, J.H., Pekkarinen, P.*, et al.* (2000). Loss-of-function mutations in

TYROBP (DAP12) result in a presenile dementia with bone cysts. Nat Genet *25*, 357-361.

Paloneva, J., Mandelin, J., Kiialainen, A., Bohling, T., Prudlo, J., Hakola, P., Haltia, M., Konttinen, Y.T., and Peltonen, L. (2003). DAP12/TREM2 deficiency results in impaired osteoclast differentiation and osteoporotic features. J Exp Med *198*, 669-675.

Palop, J.J., and Mucke, L. (2010). Amyloid-beta-induced neuronal dysfunction in Alzheimer's disease: from synapses toward neural networks. Nat Neurosci *13*, 812-818.

Paolicelli, R.C., Bolasco, G., Pagani, F., Maggi, L., Scianni, M., Panzanelli, P., Giustetto, M., Ferreira, T.A., Guiducci, E., Dumas, L.*, et al.* (2011). Synaptic pruning by microglia is necessary for normal brain development. Science *333*, 1456-1458.

Parkhurst, C.N., Yang, G., Ninan, I., Savas, J.N., Yates, J.R., 3rd, Lafaille, J.J., Hempstead, B.L., Littman, D.R., and Gan, W.B. (2013). Microglia promote learning-dependent synapse formation through brain-derived neurotrophic factor. Cell *155*, 1596-1609.

Parpura, V., Basarsky, T.A., Liu, F., Jeftinija, K., Jeftinija, S., and Haydon, P.G. (1994). Glutamate-mediated astrocyte-neuron signalling. Nature *369*, 744-747.

Pascual, O., Ben Achour, S., Rostaing, P., Triller, A., and Bessis, A. (2012). Microglia activation triggers astrocyte-mediated modulation of excitatory neurotransmission. Proc Natl Acad Sci U S A *109*, E197-205.

Pascual, O., Casper, K.B., Kubera, C., Zhang, J., Revilla-Sanchez, R., Sul, J.Y., Takano, H., Moss, S.J., McCarthy, K., and Haydon, P.G. (2005). Astrocytic purinergic signaling coordinates synaptic networks. Science *310*, 113-116.

Patterson, C. (2018). The state of the art of dementia research: New frontiers. In World Alzheimer Report 2018 (London: Alzheimer's Disease International (ADI)).

Pauls, E., Bayod, S., Mateo, L., Alcalde, V., Juan-Blanco, T., Saido, T.C., Saito, T., Berrenguer-Llergo, A., Attolini, C.S.-O., Gay, M.*, et al.* (2021). Identification and drug-induced reversion of molecular signatures of Alzheimer's disease onset and progression in App^{NL-G-F}, App^{NL-F} and 3xTg-AD mouse models. bioRxiv, 2021.2003.2017.435753.

Penzes, P., Cahill, M.E., Jones, K.A., VanLeeuwen, J.E., and Woolfrey, K.M. (2011). Dendritic spine pathology in neuropsychiatric disorders. Nat Neurosci *14*, 285-293.

Pereira, J.B., Janelidze, S., Ossenkoppele, R., Kvartsberg, H., Brinkmalm, A., Mattsson-Carlgren, N., Stomrud, E., Smith, R., Zetterberg, H., Blennow, K.*, et al.* (2021). Untangling the association of amyloid-beta and tau with synaptic and axonal loss in Alzheimer's disease. Brain *144*, 310-324.

Peretti, D., Bastide, A., Radford, H., Verity, N., Molloy, C., Martin, M.G., Moreno, J.A., Steinert, J.R., Smith, T., Dinsdale, D.*, et al.* (2015). RBM3 mediates structural plasticity and protective effects of cooling in neurodegeneration. Nature *518*, 236-239.

Petrache, A.L., Rajulawalla, A., Shi, A., Wetzel, A., Saito, T., Saido, T.C., Harvey, K., and Ali, A.B. (2019). Aberrant Excitatory-Inhibitory Synaptic Mechanisms in Entorhinal Cortex Microcircuits During the Pathogenesis of Alzheimer's Disease. Cereb Cortex *29*, 1834-1850.

Petrella, J.R., Coleman, R.E., and Doraiswamy, P.M. (2003). Neuroimaging and early diagnosis of Alzheimer disease: a look to the future. Radiology *226*, 315-336.

Pickett, E.K., Herrmann, A.G., McQueen, J., Abt, K., Dando, O., Tulloch, J., Jain, P., Dunnett, S., Sohrabi, S., Fjeldstad, M.P.*, et al.* (2019). Amyloid Beta and Tau Cooperate to Cause Reversible Behavioral and Transcriptional Deficits in a Model of Alzheimer's Disease. Cell Rep *29*, 3592-3604 e3595.

Pont-Lezica, L., Beumer, W., Colasse, S., Drexhage, H., Versnel, M., and Bessis, A. (2014). Microglia shape corpus callosum axon tract fasciculation: functional impact of prenatal inflammation. Eur J Neurosci *39*, 1551-1557.

Porter, J.T., and McCarthy, K.D. (1996). Hippocampal astrocytes in situ respond to glutamate released from synaptic terminals. J Neurosci *16*, 5073-5081.

Pottier, C., Ravenscroft, T.A., Brown, P.H., Finch, N.A., Baker, M., Parsons, M., Asmann, Y.W., Ren, Y., Christopher, E., Levitch, D.*, et al.* (2016). TYROBP genetic variants in early-onset Alzheimer's disease. Neurobiol Aging *48*, 222 e229-222 e215.

Puzzo, D., Privitera, L., Fa, M., Staniszewski, A., Hashimoto, G., Aziz, F., Sakurai, M., Ribe, E.M., Troy, C.M., Mercken, M.*, et al.* (2011). Endogenous amyloid-beta is necessary for hippocampal synaptic plasticity and memory. Ann Neurol *69*, 819-830.

Quiroz, Y.T., Budson, A.E., Celone, K., Ruiz, A., Newmark, R., Castrillon, G., Lopera, F., and Stern, C.E. (2010). Hippocampal hyperactivation in presymptomatic familial Alzheimer's disease. Ann Neurol *68*, 865-875.

Radde, R., Bolmont, T., Kaeser, S.A., Coomaraswamy, J., Lindau, D., Stoltze, L., Calhoun, M.E., Jaggi, F., Wolburg, H., Gengler, S.*, et al.* (2006). Abeta42-driven cerebral amyloidosis in transgenic mice reveals early and robust pathology. EMBO Rep *7*, 940-946.

Rammes, G., Seeser, F., Mattusch, K., Zhu, K., Haas, L., Kummer, M., Heneka, M., Herms, J., and Parsons, C.G. (2018). The NMDA receptor antagonist Radiprodil reverses the synaptotoxic effects of different amyloid-beta (Abeta) species on long-term potentiation (LTP). Neuropharmacology *140*, 184-192.

Rasmussen, J., Mahler, J., Beschorner, N., Kaeser, S.A., Hasler, L.M., Baumann, F., Nystrom, S., Portelius, E., Blennow, K., Lashley, T.*, et al.* (2017). Amyloid polymorphisms constitute distinct clouds of conformational variants in different etiological subtypes of Alzheimer's disease. Proc Natl Acad Sci U S A *114*, 13018-13023.

Regehr, W.G. (2012). Short-term presynaptic plasticity. Cold Spring Harb Perspect Biol *4*, a005702.

Reiman, E.M., Arboleda-Velasquez, J.F., Quiroz, Y.T., Huentelman, M.J., Beach, T.G., Caselli, R.J., Chen, Y., Su, Y., Myers, A.J., Hardy, J.*, et al.* (2020). Exceptionally low likelihood of Alzheimer's dementia in APOE2 homozygotes from a 5,000-person neuropathological study. Nat Commun *11*, 667.

Reinders, N.R., Pao, Y., Renner, M.C., da Silva-Matos, C.M., Lodder, T.R., Malinow, R., and Kessels, H.W. (2016). Amyloid-beta effects on synapses and memory require AMPA receptor subunit GluA3. Proc Natl Acad Sci U S A *113*, E6526-E6534.

Ren, S., Breuillaud, L., Yao, W., Yin, T., Norris, K.A., Zehntner, S.P., and D'Adamio, L. (2020a). TNFalpha reduces inhibitory transmission in young Trem2R47H Sporadic Alzheimer rats before observable Ab and brain pathology. bioRxiv *2020.08.20.256099*, 1-24.

Ren, S., Yao, W., Tambini, M.D., Yin, T., Norris, K.A., and D'Adamio, L. (2020b). Microglia TREM2(R47H) Alzheimer-linked variant enhances excitatory transmission and reduces LTP via increased TNF-alpha levels. Elife *9*.

Ries, M., and Sastre, M. (2016). Mechanisms of Abeta Clearance and Degradation by Glial Cells. Front Aging Neurosci *8*, 160.

Rodriguez, J.J., Witton, J., Olabarria, M., Noristani, H.N., and Verkhratsky, A. (2010). Increase in the density of resting microglia precedes neuritic plaque formation and microglial activation in a transgenic model of Alzheimer's disease. Cell Death Dis *1*, e1.

Rogan, S., and Lippa, C.F. (2002). Alzheimer's disease and other dementias: a review. Am J Alzheimers Dis Other Demen *17*, 11-17.

Rowe, C.C., and Villemagne, V.L. (2013). Brain amyloid imaging. J Nucl Med Technol *41*, 11-18.

Ruiz, A., Dols-Icardo, O., Bullido, M.J., Pastor, P., Rodriguez-Rodriguez, E., Lopez de Munain, A., de Pancorbo, M.M., Perez-Tur, J., Alvarez, V., Antonell, A.*, et al.* (2014). Assessing the role of the TREM2 p.R47H variant as a risk factor for Alzheimer's disease and frontotemporal dementia. Neurobiol Aging *35*, 444 e441-444.

Russell, C.L., Semerdjieva, S., Empson, R.M., Austen, B.M., Beesley, P.W., and Alifragis, P. (2012). Amyloid-beta acts as a regulator of neurotransmitter release disrupting the interaction between synaptophysin and VAMP2. PLoS One *7*, e43201.

Sacher, C., Blume, T., Beyer, L., Peters, F., Eckenweber, F., Sgobio, C., Deussing, M., Albert, N.L., Unterrainer, M., Lindner, S.*, et al.* (2019). Longitudinal PET Monitoring of Amyloidosis and Microglial Activation in a Second-Generation Amyloid-beta Mouse Model. J Nucl Med *60*, 1787-1793.

Sadleir, K.R., Kandalepas, P.C., Buggia-Prevot, V., Nicholson, D.A., Thinakaran, G., and Vassar, R. (2016). Presynaptic dystrophic neurites surrounding amyloid plaques are sites of microtubule disruption, BACE1 elevation, and increased Abeta generation in Alzheimer's disease. Acta Neuropathol *132*, 235-256.

Saito, T., Matsuba, Y., Mihira, N., Takano, J., Nilsson, P., Itohara, S., Iwata, N., and Saido, T.C. (2014). Single App knock-in mouse models of Alzheimer's disease. Nat Neurosci *17*, 661-663.

Sakakibara, Y., Sekiya, M., Saito, T., Saido, T.C., and Iijima, K.M. (2018). Cognitive and emotional alterations in App knock-in mouse models of Abeta amyloidosis. BMC Neurosci *19*, 46.

Sanan, D.A., Weisgraber, K.H., Russell, S.J., Mahley, R.W., Huang, D., Saunders, A., Schmechel, D., Wisniewski, T., Frangione, B., Roses, A.D.*, et al.* (1994). Apolipoprotein E associates with beta amyloid peptide of Alzheimer's disease to form novel monofibrils. Isoform apoE4 associates more efficiently than apoE3. J Clin Invest *94*, 860-869.

Sasaguri, H., Nilsson, P., Hashimoto, S., Nagata, K., Saito, T., De Strooper, B., Hardy, J., Vassar, R., Winblad, B., and Saido, T.C. (2017). APP mouse models for Alzheimer's disease preclinical studies. EMBO J *36*, 2473-2487.

Sassi, C., Ridge, P.G., Nalls, M.A., Gibbs, R., Ding, J., Lupton, M.K., Troakes, C., Lunnon, K., Al-Sarraj, S., Brown, K.S.*, et al.* (2016). Influence of Coding Variability in APP-Abeta Metabolism Genes in Sporadic Alzheimer's Disease. PLoS One *11*, e0150079.

Sato, K., Watamura, N., Fujioka, R., Mihira, N., Sekiguchi, M., Nagata, K., Ohshima, T., Saito, T., Saido, T.C., and Sasaguri, H. (2021). New App knock-in mice that accumulate wild-type human Aβ as rapidly as AppNL-G-F mice exhibit intensive cored plaque pathology and neuroinflammation. bioRxiv, 2021.2004.2030.442122.

Sauerbeck, A.D., Gangolli, M., Reitz, S.J., Salyards, M.H., Kim, S.H., Hemingway, C., Gratuze, M., Makkapati, T., Kerschensteiner, M., Holtzman, D.M.*, et al.* (2020). SEQUIN Multiscale Imaging of Mammalian Central Synapses Reveals Loss of Synaptic Connectivity Resulting from Diffuse Traumatic Brain Injury. Neuron *107*, 257-273 e255.

Schafer, D.P., Lehrman, E.K., Kautzman, A.G., Koyama, R., Mardinly, A.R., Yamasaki, R., Ransohoff, R.M., Greenberg, M.E., Barres, B.A., and Stevens, B. (2012). Microglia sculpt postnatal neural circuits in an activity and complement-dependent manner. Neuron *74*, 691-705.

Schedin-Weiss, S., Nilsson, P., Sandebring-Matton, A., Axenhus, M., Sekiguchi, M., Saito, T., Winblad, B., Saido, T., and Tjernberg, L.O. (2020). Proteomics Time-Course Study of App Knock-In Mice Reveals Novel Presymptomatic Abeta42-Induced Pathways to Alzheimer's Disease Pathology. J Alzheimers Dis *75*, 321-335.

Scheff, S.W., and Price, D.A. (2006). Alzheimer's disease-related alterations in synaptic density: neocortex and hippocampus. J Alzheimers Dis *9*, 101-115.

Scheuner, D., Eckman, C., Jensen, M., Song, X., Citron, M., Suzuki, N., Bird, T.D., Hardy, J., Hutton, M., Kukull, W.*, et al.* (1996). Secreted amyloid beta-protein similar to that in the senile plaques of Alzheimer's disease is increased in vivo by the presenilin 1 and 2 and APP mutations linked to familial Alzheimer's disease. Nat Med *2*, 864-870.

Schindelin, J., Arganda-Carreras, I., Frise, E., Kaynig, V., Longair, M., Pietzsch, T., Preibisch, S., Rueden, C., Saalfeld, S., Schmid, B.*, et al.* (2012). Fiji: an open-source platform for biological-image analysis. Nat Methods *9*, 676-682.

Scimemi, A., Meabon, J.S., Woltjer, R.L., Sullivan, J.M., Diamond, J.S., and Cook, D.G. (2013). Amyloid-beta1-42 slows clearance of synaptically released glutamate by mislocalizing astrocytic GLT-1. J Neurosci *33*, 5312-5318.

Sebastian Monasor, L., Muller, S.A., Colombo, A.V., Tanrioever, G., Konig, J., Roth, S., Liesz, A., Berghofer, A., Piechotta, A., Prestel, M.*, et al.* (2020). Fibrillar Abeta triggers microglial proteome alterations and dysfunction in Alzheimer mouse models. Elife *9*.

Seifert, G., Zhou, M., and Steinhauser, C. (1997). Analysis of AMPA receptor properties during postnatal development of mouse hippocampal astrocytes. J Neurophysiol *78*, 2916-2923.

Selkoe, D.J. (2002). Alzheimer's disease is a synaptic failure. Science *298*, 789-791.

Selkoe, D.J. (2008). Soluble oligomers of the amyloid beta-protein impair synaptic plasticity and behavior. Behav Brain Res *192*, 106-113.

Selkoe, D.J., and Hardy, J. (2016). The amyloid hypothesis of Alzheimer's disease at 25 years. EMBO Mol Med *8*, 595-608.

Serrano-Pozo, A., Frosch, M.P., Masliah, E., and Hyman, B.T. (2011). Neuropathological alterations in Alzheimer disease. Cold Spring Harb Perspect Med *1*, a006189.

Serrano-Pozo, A., Muzikansky, A., Gomez-Isla, T., Growdon, J.H., Betensky, R.A., Frosch, M.P., and Hyman, B.T. (2013). Differential relationships of reactive astrocytes and microglia to fibrillar amyloid deposits in Alzheimer disease. J Neuropathol Exp Neurol *72*, 462-471.

Shah, D., Latif-Hernandez, A., De Strooper, B., Saito, T., Saido, T., Verhoye, M., D'Hooge, R., and Van der Linden, A. (2018). Spatial reversal learning defect coincides with hypersynchronous telencephalic BOLD functional connectivity in APP(NL-F/NL-F) knock-in mice. Sci Rep *8*, 6264.

Shankar, G.M., Bloodgood, B.L., Townsend, M., Walsh, D.M., Selkoe, D.J., and Sabatini, B.L. (2007). Natural oligomers of the Alzheimer amyloid-beta protein induce reversible synapse loss by modulating an NMDA-type glutamate receptor-dependent signaling pathway. J Neurosci *27*, 2866-2875.

Sheng, J.G., Price, D.L., and Koliatsos, V.E. (2002). Disruption of corticocortical connections ameliorates amyloid burden in terminal fields in a transgenic model of Abeta amyloidosis. J Neurosci *22*, 9794-9799.

Sheng, M., Sabatini, B.L., and Sudhof, T.C. (2012). Synapses and Alzheimer's disease. Cold Spring Harb Perspect Biol *4*.

Shi, Q., Chowdhury, S., Ma, R., Le, K.X., Hong, S., Caldarone, B.J., Stevens, B., and Lemere, C.A. (2017). Complement C3 deficiency protects against neurodegeneration in aged plaque-rich APP/PS1 mice. Sci Transl Med *9*.

Shi, Q., Colodner, K.J., Matousek, S.B., Merry, K., Hong, S., Kenison, J.E., Frost, J.L., Le, K.X., Li, S., Dodart, J.C.*, et al.* (2015). Complement C3-Deficient Mice Fail to Display Age-Related Hippocampal Decline. J Neurosci *35*, 13029-13042.

Sims, R., van der Lee, S.J., Naj, A.C., Bellenguez, C., Badarinarayan, N., Jakobsdottir, J., Kunkle, B.W., Boland, A., Raybould, R., Bis, J.C.*, et al.* (2017). Rare coding variants in PLCG2, ABI3, and TREM2 implicate microglial-mediated innate immunity in Alzheimer's disease. Nat Genet *49*, 1373-1384.

Snyder, E.M., Nong, Y., Almeida, C.G., Paul, S., Moran, T., Choi, E.Y., Nairn, A.C., Salter, M.W., Lombroso, P.J., Gouras, G.K.*, et al.* (2005). Regulation of NMDA receptor trafficking by amyloid-beta. Nat Neurosci *8*, 1051-1058.

Sofroniew, M.V. (2005). Reactive astrocytes in neural repair and protection. Neuroscientist *11*, 400-407.

Sofroniew, M.V. (2009). Molecular dissection of reactive astrogliosis and glial scar formation. Trends Neurosci *32*, 638-647.

Son, Y., Jeong, Y.J., Shin, N.R., Oh, S.J., Nam, K.R., Choi, H.D., Choi, J.Y., and Lee, H.J. (2020). Inhibition of Colony-Stimulating Factor 1 Receptor by PLX3397 Prevents Amyloid Beta Pathology and Rescues Dopaminergic Signaling in Aging 5xFAD Mice. Int J Mol Sci *21*.

Song, W., Hooli, B., Mullin, K., Jin, S.C., Cella, M., Ulland, T.K., Wang, Y., Tanzi, R.E., and Colonna, M. (2017). Alzheimer's disease-associated TREM2 variants exhibit either decreased or increased ligand-dependent activation. Alzheimers Dement *13*, 381-387.

Song, W.M., Joshita, S., Zhou, Y., Ulland, T.K., Gilfillan, S., and Colonna, M. (2018). Humanized TREM2 mice reveal microglia-intrinsic and -extrinsic effects of R47H polymorphism. J Exp Med *215*, 745-760.

Sos, K.E., Mayer, M.I., Takacs, V.T., Major, A., Bardoczi, Z., Beres, B.M., Szeles, T., Saito, T., Saido, T.C., Mody, I.*, et al.* (2020). Amyloid beta induces interneuron-specific changes in the hippocampus of APPNL-F mice. PLoS One *15*, e0233700.

Sosna, J., Philipp, S., Albay, R., 3rd, Reyes-Ruiz, J.M., Baglietto-Vargas, D., LaFerla, F.M., and Glabe, C.G. (2018). Early long-term administration of the CSF1R inhibitor PLX3397 ablates microglia and reduces accumulation of intraneuronal amyloid, neuritic plaque deposition and pre-fibrillar oligomers in 5XFAD mouse model of Alzheimer's disease. Mol Neurodegener *13*, 11.

Soudry, Y., Lemogne, C., Malinvaud, D., Consoli, S.M., and Bonfils, P. (2011). Olfactory system and emotion: common substrates. Eur Ann Otorhinolaryngol Head Neck Dis *128*, 18-23.

Spangenberg, E., Severson, P.L., Hohsfield, L.A., Crapser, J., Zhang, J., Burton, E.A., Zhang, Y., Spevak, W., Lin, J., Phan, N.Y., *et al.* (2019). Sustained microglial depletion with CSF1R inhibitor impairs parenchymal plaque development in an Alzheimer's disease model. Nat Commun *10*, 3758.

Spangenberg, E.E., Lee, R.J., Najafi, A.R., Rice, R.A., Elmore, M.R., Blurton-Jones, M., West, B.L., and Green, K.N. (2016). Eliminating microglia in Alzheimer's mice prevents neuronal loss without modulating amyloid-beta pathology. Brain *139*, 1265-1281.

Spires, T.L., Meyer-Luehmann, M., Stern, E.A., McLean, P.J., Skoch, J., Nguyen, P.T., Bacskai, B.J., and Hyman, B.T. (2005). Dendritic spine abnormalities in amyloid precursor protein transgenic mice demonstrated by gene transfer and intravital multiphoton microscopy. J Neurosci *25*, 7278-7287.

Steinerman, J.R., Irizarry, M., Scarmeas, N., Raju, S., Brandt, J., Albert, M., Blacker, D., Hyman, B., and Stern, Y. (2008). Distinct pools of beta-amyloid in Alzheimer disease-affected brain: a clinicopathologic study. Arch Neurol *65*, 906-912.

Stella, F., Cerasti, E., Si, B., Jezek, K., and Treves, A. (2012). Self-organization of multiple spatial and context memories in the hippocampus. Neurosci Biobehav Rev *36*, 1609-1625.

Stellwagen, D., Beattie, E.C., Seo, J.Y., and Malenka, R.C. (2005). Differential regulation of AMPA receptor and GABA receptor trafficking by tumor necrosis factor-alpha. J Neurosci *25*, 3219-3228.

Stellwagen, D., and Malenka, R.C. (2006). Synaptic scaling mediated by glial TNF-alpha. Nature *440*, 1054-1059.

Stephan, A.H., Madison, D.V., Mateos, J.M., Fraser, D.A., Lovelett, E.A., Coutellier, L., Kim, L., Tsai, H.H., Huang, E.J., Rowitch, D.H., *et al.* (2013). A dramatic increase of C1q protein in the CNS during normal aging. J Neurosci *33*, 13460-13474.

Stevens, B., Allen, N.J., Vazquez, L.E., Howell, G.R., Christopherson, K.S., Nouri, N., Micheva, K.D., Mehalow, A.K., Huberman, A.D., Stafford, B., *et al.* (2007). The classical complement cascade mediates CNS synapse elimination. Cell *131*, 1164-1178.

Stowell, R.D., Sipe, G.O., Dawes, R.P., Batchelor, H.N., Lordy, K.A., Whitelaw, B.S., Stoessel, M.B., Bidlack, J.M., Brown, E., Sur, M., *et al.* (2019). Noradrenergic signaling in the wakeful state inhibits microglial surveillance and synaptic plasticity in the mouse visual cortex. Nat Neurosci *22*, 1782-1792.

Sun, M., Zhu, M., Chen, K., Nie, X., Deng, Q., Hazlett, L.D., Wu, Y., Li, M., Wu, M., and Huang, X. (2013). TREM-2 promotes host resistance against Pseudomonas aeruginosa infection by suppressing corneal inflammation via a PI3K/Akt signaling pathway. Invest Ophthalmol Vis Sci *54*, 3451-3462.

Swardfager, W., Lanctot, K., Rothenburg, L., Wong, A., Cappell, J., and Herrmann, N. (2010). A meta-analysis of cytokines in Alzheimer's disease. Biol Psychiatry *68*, 930-941.

Takahashi, K., Rochford, C.D., and Neumann, H. (2005). Clearance of apoptotic neurons without inflammation by microglial triggering receptor expressed on myeloid cells-2. J Exp Med *201*, 647-657.

Talantova, M., Sanz-Blasco, S., Zhang, X., Xia, P., Akhtar, M.W., Okamoto, S., Dziewczapolski, G., Nakamura, T., Cao, G., Pratt, A.E.*, et al.* (2013). Abeta induces astrocytic glutamate release, extrasynaptic NMDA receptor activation, and synaptic loss. Proc Natl Acad Sci U S A *110*, E2518-2527.

Tambini, M.D., and D'Adamio, L. (2020). Trem2 Splicing and Expression are Preserved in a Human Abeta-producing, Rat Knock-in Model of Trem2-R47H Alzheimer's Risk Variant. Sci Rep *10*, 4122.

Tanaka, H., Sakaguchi, D., and Hirano, T. (2019). Amyloid-beta oligomers suppress subunit-specific glutamate receptor increase during LTP. Alzheimers Dement (N Y) *5*, 797-808.

Tang, C.M., Dichter, M., and Morad, M. (1989). Quisqualate activates a rapidly inactivating high conductance ionic channel in hippocampal neurons. Science *243*, 1474-1477.

Taylor, D.L., Diemel, L.T., Cuzner, M.L., and Pocock, J.M. (2002). Activation of group II metabotropic glutamate receptors underlies microglial reactivity and neurotoxicity following stimulation with chromogranin A, a peptide up-regulated in Alzheimer's disease. J Neurochem *82*, 1179-1191.

Taylor, D.L., Diemel, L.T., and Pocock, J.M. (2003). Activation of microglial group III metabotropic glutamate receptors protects neurons against microglial neurotoxicity. J Neurosci *23*, 2150-2160.

Teaktong, T., Graham, A., Court, J., Perry, R., Jaros, E., Johnson, M., Hall, R., and Perry, E. (2003). Alzheimer's disease is associated with a selective increase in alpha7 nicotinic acetylcholine receptor immunoreactivity in astrocytes. Glia *41*, 207-211.

Terry, R.D., Masliah, E., Salmon, D.P., Butters, N., DeTeresa, R., Hill, R., Hansen, L.A., and Katzman, R. (1991). Physical basis of cognitive alterations in Alzheimer's disease: synapse loss is the major correlate of cognitive impairment. Ann Neurol *30*, 572-580.

Tondo, G., Iaccarino, L., Caminiti, S.P., Presotto, L., Santangelo, R., Iannaccone, S., Magnani, G., and Perani, D. (2020). The combined effects of microglia activation and brain glucose hypometabolism in early-onset Alzheimer's disease. Alzheimers Res Ther *12*, 50.

Town, T., Nikolic, V., and Tan, J. (2005). The microglial "activation" continuum: from innate to adaptive responses. J Neuroinflammation *2*, 24.

Townsend, M., Shankar, G.M., Mehta, T., Walsh, D.M., and Selkoe, D.J. (2006). Effects of secreted oligomers of amyloid beta-protein on hippocampal synaptic plasticity: a potent role for trimers. J Physiol *572*, 477-492.

Toyoda, H., Li, X.Y., Wu, L.J., Zhao, M.G., Descalzi, G., Chen, T., Koga, K., and Zhuo, M. (2011). Interplay of amygdala and cingulate plasticity in emotional fear. Neural Plast *2011*, 813749.

Tsubuki, S., Takaki, Y., and Saido, T.C. (2003). Dutch, Flemish, Italian, and Arctic mutations of APP and resistance of Abeta to physiologically relevant proteolytic degradation. Lancet *361*, 1957-1958.

Tulloch, J., Netsyk, O., Pickett, E.K., Herrmann, A.G., Jain, P., Stevenson, A.J., Oren, I., Hardt, O., and Spires-Jones, T.L. (2021). Maintained memory and long-term potentiation in a mouse model of Alzheimer's disease with both amyloid pathology and human tau. Eur J Neurosci *53*, 637-648.

Turnbull, I.R., Gilfillan, S., Cella, M., Aoshi, T., Miller, M., Piccio, L., Hernandez, M., and Colonna, M. (2006). Cutting edge: TREM-2 attenuates macrophage activation. J Immunol *177*, 3520-3524.

Tzioras, M., Daniels, M.J.D., King, D., Popovic, K., Holloway, R.K., Stevenson, A.J., Tulloch, J., Kandasamy, J., Sokol, D., Latta, C.*, et al.* (2019). Altered synaptic ingestion by human microglia in Alzheimer's disease. bioRxiv *ID795930*, 1-25.

Ueno, M., Fujita, Y., Tanaka, T., Nakamura, Y., Kikuta, J., Ishii, M., and Yamashita, T. (2013). Layer V cortical neurons require microglial support for survival during postnatal development. Nat Neurosci *16*, 543-551.

Ulland, T.K., Song, W.M., Huang, S.C., Ulrich, J.D., Sergushichev, A., Beatty, W.L., Loboda, A.A., Zhou, Y., Cairns, N.J., Kambal, A.*, et al.* (2017). TREM2 Maintains Microglial Metabolic Fitness in Alzheimer's Disease. Cell *170*, 649-663 e613.

Ulrich, J.D., Finn, M.B., Wang, Y., Shen, A., Mahan, T.E., Jiang, H., Stewart, F.R., Piccio, L., Colonna, M., and Holtzman, D.M. (2014). Altered microglial response to Abeta plaques in APPPS1-21 mice heterozygous for TREM2. Mol Neurodegener *9*, 20.

van Groen, T., Miettinen, P., and Kadish, I. (2003). The entorhinal cortex of the mouse: organization of the projection to the hippocampal formation. Hippocampus *13*, 133-149.

Varatharajah, Y., Ramanan, V.K., Iyer, R., Vemuri, P., and Alzheimer's Disease Neuroimaging, I. (2019). Predicting Short-term MCI-to-AD Progression Using Imaging, CSF, Genetic Factors, Cognitive Resilience, and Demographics. Sci Rep *9*, 2235.

Verheijen, J., and Sleegers, K. (2018). Understanding Alzheimer Disease at the Interface between Genetics and Transcriptomics. Trends Genet *34*, 434-447.

Verret, L., Mann, E.O., Hang, G.B., Barth, A.M., Cobos, I., Ho, K., Devidze, N., Masliah, E., Kreitzer, A.C., Mody, I.*, et al.* (2012). Inhibitory interneuron deficit links altered network activity and cognitive dysfunction in Alzheimer model. Cell *149*, 708-721.

Vogel, J.W., Young, A.L., Oxtoby, N.P., Smith, R., Ossenkoppele, R., Strandberg, O.T., La Joie, R., Aksman, L.M., Grothe, M.J., Iturria-Medina, Y.*, et al.* (2021). Four distinct trajectories of tau deposition identified in Alzheimer's disease. Nat Med *27*, 871-881.

Wake, H., Moorhouse, A.J., Jinno, S., Kohsaka, S., and Nabekura, J. (2009). Resting microglia directly monitor the functional state of synapses in vivo and determine the fate of ischemic terminals. J Neurosci *29*, 3974-3980.

Wallace, J., Lord, J., Dissing-Olesen, L., Stevens, B., and Murthy, V. (2019). Microglia are necessary for normal functional development of adult-born neurons in the olfactory bulb. bioRxiv.

Walsh, D.M., Klyubin, I., Fadeeva, J.V., Cullen, W.K., Anwyl, R., Wolfe, M.S., Rowan, M.J., and Selkoe, D.J. (2002). Naturally secreted oligomers of amyloid beta protein potently inhibit hippocampal long-term potentiation in vivo. Nature *416*, 535-539.

Wang, C., Yue, H., Hu, Z., Shen, Y., Ma, J., Li, J., Wang, X.D., Wang, L., Sun, B., Shi, P.*, et al.* (2020). Microglia mediate forgetting via complement-dependent synaptic elimination. Science *367*, 688-694.

Wang, H.Y., Lee, D.H., D'Andrea, M.R., Peterson, P.A., Shank, R.P., and Reitz, A.B. (2000). beta-Amyloid(1-42) binds to alpha7 nicotinic acetylcholine receptor with high affinity. Implications for Alzheimer's disease pathology. J Biol Chem *275*, 5626-5632.

Wang, J., Tanila, H., Puolivali, J., Kadish, I., and van Groen, T. (2003). Gender differences in the amount and deposition of amyloidbeta in APPswe and PS1 double transgenic mice. Neurobiol Dis *14*, 318-327.

Wang, Y., Cella, M., Mallinson, K., Ulrich, J.D., Young, K.L., Robinette, M.L., Gilfillan, S., Krishnan, G.M., Sudhakar, S., Zinselmeyer, B.H.*, et al.* (2015). TREM2 lipid sensing sustains the microglial response in an Alzheimer's disease model. Cell *160*, 1061-1071.

Wang, Y., Ulland, T.K., Ulrich, J.D., Song, W., Tzaferis, J.A., Hole, J.T., Yuan, P., Mahan, T.E., Shi, Y., Gilfillan, S.*, et al.* (2016). TREM2-mediated early microglial response limits diffusion and toxicity of amyloid plaques. J Exp Med *213*, 667-675.

Wang, Z., Jackson, R.J., Hong, W., Taylor, W.M., Corbett, G.T., Moreno, A., Liu, W., Li, S., Frosch, M.P., Slutsky, I.*, et al.* (2017). Human Brain-Derived Abeta Oligomers Bind to Synapses and Disrupt Synaptic Activity in a Manner That Requires APP. J Neurosci *37*, 11947-11966.

Wegiel, J. (2001). The role of microglial cells and astrocytes in fibrillar plaque evolution in transgenic APPSW mice. Neurobiology of Aging *22*, 49-61.

Wei, W., Nguyen, L.N., Kessels, H.W., Hagiwara, H., Sisodia, S., and Malinow, R. (2010). Amyloid beta from axons and dendrites reduces local spine number and plasticity. Nat Neurosci *13*, 190-196.

Weinhard, L., di Bartolomei, G., Bolasco, G., Machado, P., Schieber, N.L., Neniskyte, U., Exiga, M., Vadisiute, A., Raggioli, A., Schertel, A.*, et al.* (2018). Microglia remodel synapses by presynaptic trogocytosis and spine head filopodia induction. Nat Commun *9*, 1228.

Whitcomb, D.J., Hogg, E.L., Regan, P., Piers, T., Narayan, P., Whitehead, G., Winters, B.L., Kim, D.H., Kim, E., St George-Hyslop, P.*, et al.* (2015). Intracellular oligomeric amyloid-beta rapidly regulates GluA1 subunit of AMPA receptor in the hippocampus. Sci Rep *5*, 10934.

Whitlock, J.R., Heynen, A.J., Shuler, M.G., and Bear, M.F. (2006). Learning induces long-term potentiation in the hippocampus. Science *313*, 1093-1097.

Whyte, L.S., Hemsley, K.M., Lau, A.A., Hassiotis, S., Saito, T., Saido, T.C., Hopwood, J.J., and Sargeant, T.J. (2018). Reduction in open field activity in the absence of memory deficits in the App(NL-G-F) knock-in mouse model of Alzheimer's disease. Behav Brain Res *336*, 177-181.

Wilhelmsson, U., Bushong, E.A., Price, D.L., Smarr, B.L., Phung, V., Terada, M., Ellisman, M.H., and Pekny, M. (2006). Redefining the concept of reactive astrocytes as cells that remain within their unique domains upon reaction to injury. Proceedings of the National Academy of Sciences *103*, 17513.

Wilton, D.K., Dissing-Olesen, L., and Stevens, B. (2019). Neuron-Glia Signaling in Synapse Elimination. Annu Rev Neurosci *42*, 107-127.

Wu, T., Dejanovic, B., Gandham, V.D., Gogineni, A., Edmonds, R., Schauer, S., Srinivasan, K., Huntley, M.A., Wang, Y., Wang, T.M.*, et al.* (2019). Complement C3 Is Activated in Human AD Brain and Is Required for Neurodegeneration in Mouse Models of Amyloidosis and Tauopathy. Cell Rep *28*, 2111-2123 e2116.

Wyss-Coray, T., Loike, J.D., Brionne, T.C., Lu, E., Anankov, R., Yan, F., Silverstein, S.C., and Husemann, J. (2003). Adult mouse astrocytes degrade amyloid-beta in vitro and in situ. Nat Med *9*, 453-457.

Wyss-Coray, T., Yan, F., Lin, A.H., Lambris, J.D., Alexander, J.J., Quigg, R.J., and Masliah, E. (2002). Prominent neurodegeneration and increased plaque formation in complement-inhibited Alzheimer's mice. Proc Natl Acad Sci U S A *99*, 10837-10842.

Xiang, X., Piers, T.M., Wefers, B., Zhu, K., Mallach, A., Brunner, B., Kleinberger, G., Song, W., Colonna, M., Herms, J.*, et al.* (2018). The Trem2 R47H Alzheimer's risk variant impairs splicing and reduces Trem2 mRNA and protein in mice but not in humans. Mol Neurodegener *13*, 49.

Yang, T., Li, S., Xu, H., Walsh, D.M., and Selkoe, D.J. (2017). Large Soluble Oligomers of Amyloid beta-Protein from Alzheimer Brain Are Far Less Neuroactive Than the Smaller Oligomers to Which They Dissociate. J Neurosci *37*, 152-163.

Yang, Y., Kim, J., Kim, H.Y., Ryoo, N., Lee, S., Kim, Y., Rhim, H., and Shin, Y.K. (2015). Amyloid-beta Oligomers May Impair SNARE-Mediated Exocytosis by Direct Binding to Syntaxin 1a. Cell Rep *12*, 1244-1251.

Yao, P.J., Zhu, M., Pyun, E.I., Brooks, A.I., Therianos, S., Meyers, V.E., and Coleman, P.D. (2003). Defects in expression of genes related to synaptic vesicle trafficking in frontal cortex of Alzheimer's disease. Neurobiol Dis *12*, 97-109.

Yeh, F.L., Wang, Y., Tom, I., Gonzalez, L.C., and Sheng, M. (2016). TREM2 Binds to Apolipoproteins, Including APOE and CLU/APOJ, and Thereby Facilitates Uptake of Amyloid-Beta by Microglia. Neuron *91*, 328-340.

York, E.M., Bernier, L.P., and MacVicar, B.A. (2018). Microglial modulation of neuronal activity in the healthy brain. Dev Neurobiol *78*, 593-603.

Yu, Y., and Ye, R.D. (2015). Microglial Abeta receptors in Alzheimer's disease. Cell Mol Neurobiol *35*, 71-83.

Yuan, P., Condello, C., Keene, C.D., Wang, Y., Bird, T.D., Paul, S.M., Luo, W., Colonna, M., Baddeley, D., and Grutzendler, J. (2016). TREM2 Haplodeficiency in Mice and Humans Impairs the Microglia Barrier Function Leading to Decreased Amyloid Compaction and Severe Axonal Dystrophy. Neuron *90*, 724-739.

Yuan, P., and Grutzendler, J. (2016). Attenuation of beta-Amyloid Deposition and Neurotoxicity by Chemogenetic Modulation of Neural Activity. J Neurosci *36*, 632-641.

Zhan, Y., Paolicelli, R.C., Sforazzini, F., Weinhard, L., Bolasco, G., Pagani, F., Vyssotski, A.L., Bifone, A., Gozzi, A., Ragozzino, D.*, et al.* (2014). Deficient neuron-microglia signaling results in impaired functional brain connectivity and social behavior. Nat Neurosci *17*, 400-406.

Zhang, H., Wu, L., Pchitskaya, E., Zakharova, O., Saito, T., Saido, T., and Bezprozvanny, I. (2015). Neuronal Store-Operated Calcium Entry and Mushroom Spine Loss in Amyloid Precursor Protein Knock-In Mouse Model of Alzheimer's Disease. J Neurosci *35*, 13275-13286.

Zhao, J., O'Connor, T., and Vassar, R. (2011). The contribution of activated astrocytes to Abeta production: implications for Alzheimer's disease pathogenesis. J Neuroinflammation *8*, 150.

Zhao, M., Cribbs, D.H., Anderson, A.J., Cummings, B.J., Su, J.H., Wasserman, A.J., and Cotman, C.W. (2003). The induction of the TNFalpha death domain signaling pathway in Alzheimer's disease brain. Neurochem Res *28*, 307-318.

Zhao, N., Ren, Y., Yamazaki, Y., Qiao, W., Li, F., Felton, L.M., Mahmoudiandehkordi, S., Kueider-Paisley, A., Sonoustoun, B., Arnold, M., *et al.* (2020). Alzheimer's Risk Factors Age, APOE Genotype, and Sex Drive Distinct Molecular Pathways. Neuron.

Zhao, R., Hu, W., Tsai, J., Li, W., and Gan, W.B. (2017). Microglia limit the expansion of beta-amyloid plaques in a mouse model of Alzheimer's disease. Mol Neurodegener *12*, 47.

Zhao, W.Q., Santini, F., Breese, R., Ross, D., Zhang, X.D., Stone, D.J., Ferrer, M., Townsend, M., Wolfe, A.L., Seager, M.A., *et al.* (2010). Inhibition of calcineurin-mediated endocytosis and alpha-amino-3-hydroxy-5-methyl-4-isoxazolepropionic acid (AMPA) receptors prevents amyloid beta oligomer-induced synaptic disruption. J Biol Chem *285*, 7619-7632.

Zhao, Y., Wu, X., Li, X., Jiang, L.L., Gui, X., Liu, Y., Sun, Y., Zhu, B., Pina-Crespo, J.C., Zhang, M., *et al.* (2018). TREM2 Is a Receptor for beta-Amyloid that Mediates Microglial Function. Neuron *97*, 1023-1031 e1027.

Zhong, L., Wang, Z., Wang, D., Wang, Z., Martens, Y.A., Wu, L., Xu, Y., Wang, K., Li, J., Huang, R., *et al.* (2018). Amyloid-beta modulates microglial responses by binding to the triggering receptor expressed on myeloid cells 2 (TREM2). Mol Neurodegener *13*, 15.

Zhou, Y., Song, W.M., Andhey, P.S., Swain, A., Levy, T., Miller, K.R., Poliani, P.L., Cominelli, M., Grover, S., Gilfillan, S., *et al.* (2020). Human and mouse single-nucleus transcriptomics reveal TREM2-dependent and TREM2-independent cellular responses in Alzheimer's disease. Nat Med *26*, 131-142.

Ziak, D., Chvatal, A., and Sykova, E. (1998). Glutamate-, kainate- and NMDA-evoked membrane currents in identified glial cells in rat spinal cord slice. Physiol Res *47*, 365-375.

Zott, B., Simon, M.M., Hong, W., Unger, F., Chen-Engerer, H.J., Frosch, M.P., Sakmann, B., Walsh, D.M., and Konnerth, A. (2019). A vicious cycle of beta amyloid-dependent neuronal hyperactivation. Science *365*, 559-565.

Zucker, R.S., and Regehr, W.G. (2002). Short-term synaptic plasticity. Annu Rev Physiol *64*, 355-405.